

Technical Report Documentation Page

1. REPORT No.

FHWA/CA/TL 96-02

2. GOVERNMENT ACCESSION No.**3. RECIPIENT'S CATALOG No.****4. TITLE AND SUBTITLE**

Decomposed Granite as an Embankment Fill Material:
Mechanical Properties and Influence of Particle Breakage.
Volume 1 of 3 Presenting Results of Research Project,

5. REPORT DATE

June 1993

6. PERFORMING ORGANIZATION

65-323-652014

7. AUTHOR(S)

Kashayapa A.S. Yapa, James K. Mitchell and Nicholas Sitar

8. PERFORMING ORGANIZATION REPORT No.

F92TL04C

9. PERFORMING ORGANIZATION NAME AND ADDRESS

California Department of Transportation
New Technology and Research, MS-83
P.O. Box 942873
Sacramento, CA 94273-0001

10. WORK UNIT No.**11. CONTRACT OR GRANT No.**

RTA-65T128

12. SPONSORING AGENCY NAME AND ADDRESS

California Department of Transportation
Sacramento, CA 95819

13. TYPE OF REPORT & PERIOD COVERED

Final, 06/01/92 - 06/30/93

14. SPONSORING AGENCY CODE**15. SUPPLEMENTARY NOTES**

This project was performed in cooperation with the U.S. Department of Transportation, Federal Highway Administration.

16. ABSTRACT

The suitability of decomposed granite as an embankment fill material has been investigated. Using a sample from the Shasta Ballay batholith in Northern California, important mechanical properties were studied in oedometer and triaxial tests. In addition, the feasibility of using geogrid reinforcements in decomposed granite embankments to enable steemening of side slopes was investigated through direct shear and pullout tests.

Experimental results show that breakage is primarily controlled by the applied strain level rather than the stress level. Shear-induced breakage under conventional triaxial conditions is greater than under oedometer conditions, because of the greater shear stress/strain component under triaxial conditions. The friction angle of compacted decomposed granite decreases significantly with increasing stress level. In dense triaxial specimens, under confinements ranging from 100 to 1500 kPa, the reduction in peak value was about 25 percent. The pullout coefficient of interaction of a geogrid embedded in dense decomposed granite decreased by more than 50 percent when normal pressure was increased from 70 to 700 kPa. In direct shear (decomposed granite-geogrid) interface strength test, residual values were nearly equal to those from direct shear tests of the soil alone. Settlement and hydrocompression in oedometer specimens were not large under axial pressures as high as 1600 kPa, probably because breakage in these specimens was small. However, decreasing the compaction water content significantly increased the hydrocompression.

17. KEYWORDS

Decomposed granite, shear strength, compaction, consolidation, reinforced soil, particle crushing

18. No. OF PAGES:

234

19. DRI WEBSITE LINK

<http://www.dot.ca.gov/hq/research/researchreports/1989-1996/96-02A.pdf>

20. FILE NAME

96-02A.pdf

96-02A

DECOMPOSED GRANITE AS AN EMBANKMENT FILL MATERIAL:
MECHANICAL PROPERTIES AND THE INFLUENCE
OF PARTICLE BREAKAGE

by

Kashayapa A.S. Yapa, James K. Mitchell and Nicholas Sitar

A report on research supported by the
California Department of Transportation
Award No. RTA-65T128

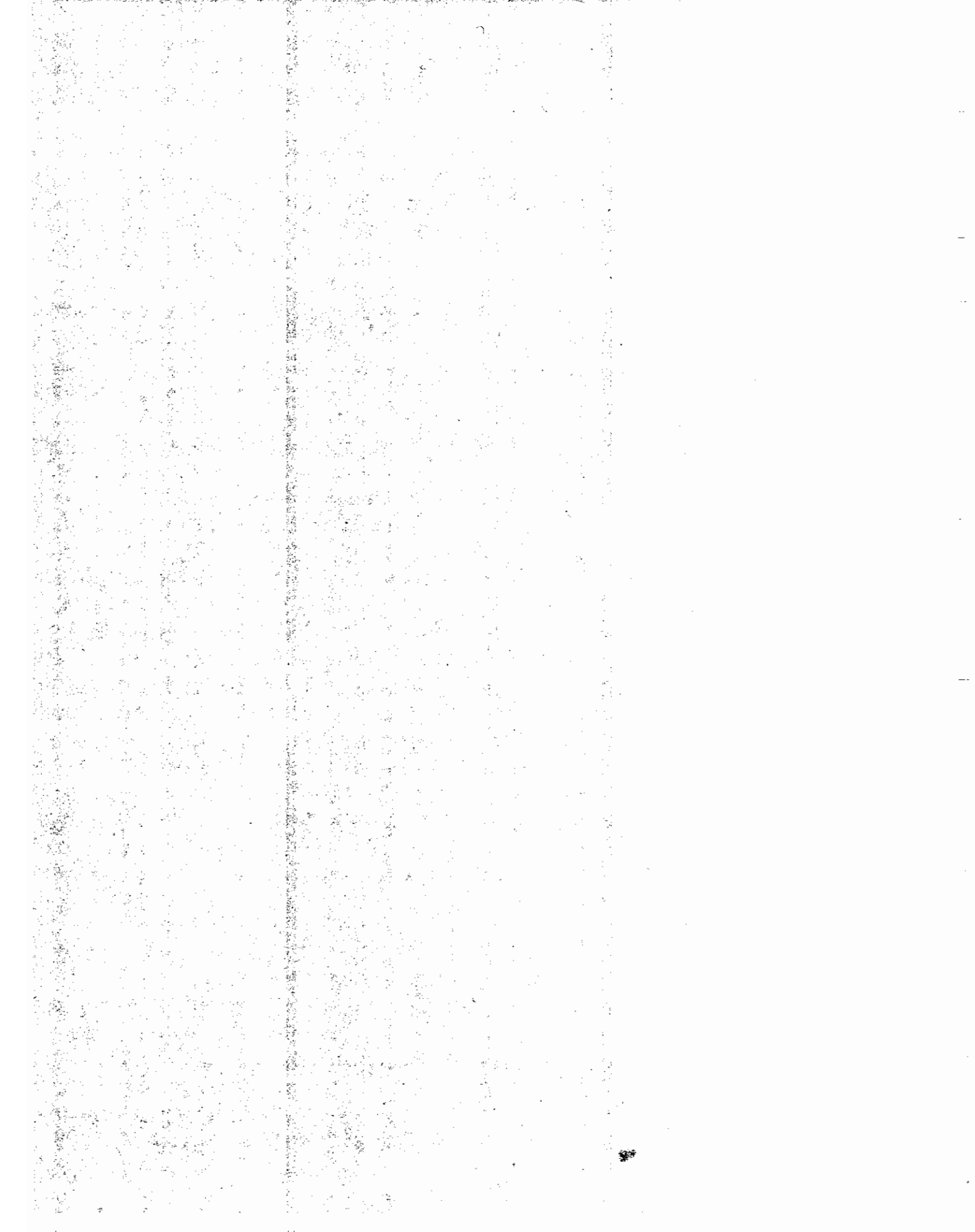
~~93-06~~

Geotechnical Engineering Report No. UCB/GT/93-06

June 1993
Corrected and reprinted December 1995



GEOTECHNICAL ENGINEERING
DEPARTMENT OF CIVIL AND ENVIRONMENTAL ENGINEERING
UNIVERSITY OF CALIFORNIA • BERKELEY



DECOMPOSED GRANITE AS AN EMBANKMENT FILL MATERIAL:

MECHANICAL PROPERTIES AND THE INFLUENCE
OF PARTICLE BREAKAGE

by

Kashayapa A.S. Yapa, James K. Mitchell and Nicholas Sitar

A report on research supported by the
California Department of Transportation
Award No. RTA-65T128

The conclusions and opinions presented in this report are those of the authors and do not necessarily represent the views of the California Department of Transportation or the University of California.

Geotechnical Engineering Report No. UCB/GT/93-06

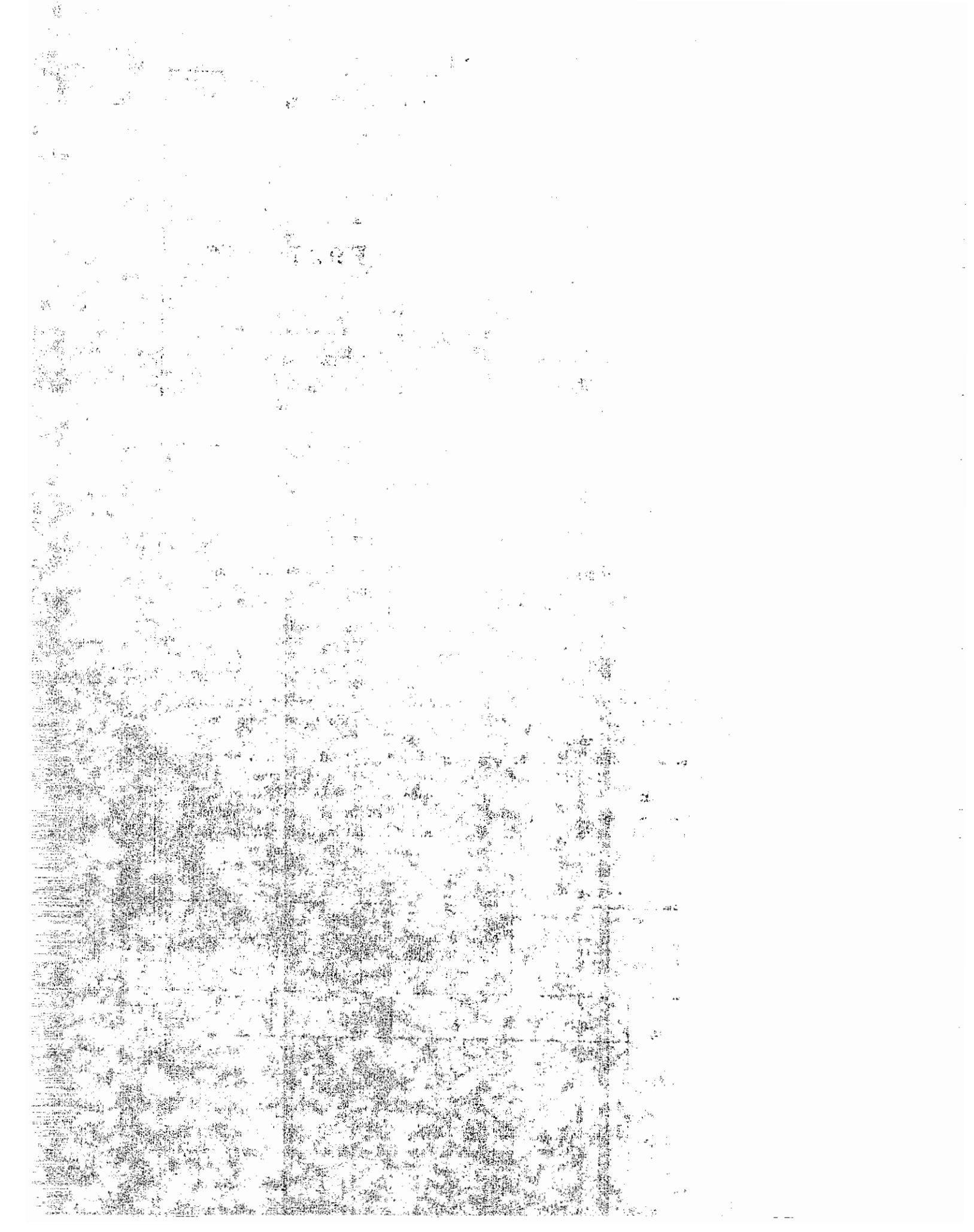
June 1993
Corrected and reprinted December 1995

1944

[The remainder of the page is extremely faint and illegible due to heavy noise and low contrast. It appears to contain several paragraphs of text.]

Technical Report Documentation Page

1. Report No. FHWA/CA/TL- 96-02		2. Government Accession No.		3. Recipient's Catalog No.	
4. Title and Subtitle Decomposed granite as an Embankment Fill Material: Mechanical Properties and Influence of Particle Breakage. Volume 1 of 3 presenting results of research project, entitled: "Evaluation of Properties of Decomposed Granite and Analysis of Performance of High Embankments of Decomposed Granite."				5. Report Date June 1993 Revised December 1995	
				6. Performing Organization Code 65-323-652014	
7. Authors Kashayapa A.S. Yapa, James K. Mitchell and Nicholas Sitar				8. Performing Organization Report No. F92TL04C	
9. Performing Organization Name and Address California Department of Transportation New Technology and Research, MS-83 P.O. Box 942873 Sacramento, CA 94273-0001				10. Work Unit No.	
				11. Contract or Grant No. RTA-65T128	
12. Sponsoring Agency Name and Address California Department of Transportation Sacramento, CA 95819				13. Type of Report and Period Covered Final, 06/01/92 - 06/30/93	
				14. Sponsoring Agency Code	
15. Supplementary Notes This project was performed in cooperation with the U.S. Department of Transportation, Federal Highway Administration.					
16. Abstract The suitability of decomposed granite as an embankment fill material has been investigated. Using a sample from the Shasta Bally batholith in Northern California, important mechanical properties were studied in oedometer and triaxial tests. In addition, the feasibility of using geogrid reinforcements in decomposed granite embankments to enable steepening of side slopes was investigated through direct shear and pullout tests. Experimental results show that breakage is primarily controlled by the applied strain level rather than the stress level. Shear-induced breakage under conventional triaxial conditions is greater than under oedometer conditions, because of the greater shear stress/strain component under triaxial conditions. The friction angle of compacted decomposed granite decreases significantly with increasing stress level. In dense triaxial specimens, under confinements ranging from 100 to 1500 kPa, the reduction in ϕ_{peak} value was about 25 percent. The pullout coefficient of interaction of a geogrid embedded in dense decomposed granite decreased by more than 50 percent when normal pressure was increased from 70 to 700 kPa. In direct shear (decomposed granite-geogrid) interface strength test, $\phi_{residual}$ values were nearly equal to those from direct shear tests of the soil alone. Settlement and hydrocompression in oedometer specimens were not large under axial pressures as high as 1600 kPa, probably because breakage in these specimens was small. However, decreasing the compaction water content significantly increased the hydrocompression.					
17. Key Words Decomposed granite, shear strength, , compaction, consolidation, reinforced soil, particle crushing.				18. Distribution Statement No restrictions. This document is available to the public through the National Technical Information Service, Springfield, VA 22161	
19. Security Classif. (of this report) Unclassified		20. Security Classif. (of this page) Unclassified		21. No. of Pages	22. Price



ABSTRACT

The suitability of decomposed granite as an embankment fill material has been investigated. The physical characteristics of several decomposed granites were examined through a review of literature on deposits worldwide. Using a sample from the Shasta Bally batholith in northern California, important mechanical properties were studied through oedometer and triaxial tests. In addition, the feasibility of using geogrid reinforcements in decomposed granite embankment fills to enable steepening of side slopes was investigated through direct shear and pullout tests.

The term "decomposed granite" is used to identify a broad range of materials, from slightly weathered but intact rocks and boulders, to sand and even clay. The in situ fabric of decomposed granite typically contains coarse grained aggregates of minerals, predominantly quartz, weathered feldspar and mica, and a relatively small proportion of fines. Decomposed granite particles undergo substantial breakage under relatively low loads.

Experimental results from this study showed that breakage is primarily controlled by the applied strain level rather than the stress level. Shear-induced breakage under conventional triaxial conditions is greater than under oedometer conditions, because of the greater shear stress/strain component under triaxial conditions.

The friction angle of compacted decomposed granite decreases significantly with increasing stress level. In dense triaxial specimens, under confinements ranging from 100 to 1500 kPa, the reduction in ϕ_{peak} value was about 25 percent. The pullout coefficient of interaction of a geogrid embedded in dense decomposed granite decreased by more than 50 percent when normal pressure was increased from 70 to 700 kPa. In direct shear (decomposed granite-geogrid) interface strength tests, ϕ_{residual} values were nearly equal to those from direct shear tests of the soil alone. Settlement and hydrocompression in oedometer specimens were not large under axial pressures as high as 1600 kPa, probably because breakage in

these specimens was small. However, decreasing the compaction water content significantly increased the hydrocompression.

Based on these findings, it is recommended that compaction water content in a fill be maintained near the optimum. Compaction density should be decided upon after comparing the economics of alternative designs that consider steepness of the slope, utility of geosynthetics and acceptable settlement.

ACKNOWLEDGEMENT

The California Department of Transportation personnel generously helped during various phases of this project. Mr. Gary Garofalo, the contract monitor, provided invaluable help throughout in procuring information and test samples. The geologists in the Sacramento office provided information on their investigation along the new alignment of SH299. Engineers at the District 2, Redding office also provided data on field operations at the site. In particular, Mr. Tom Graves personally helped in procuring bulk of the soil samples.

During laboratory testing, the assistants Larry Lekuang and Ramesh Gunathilake were of immense help. Fabrication of the laboratory equipment was completed fairly rapidly by the technicians of the Civil Engineering Department workshop. They were also very helpful in smoothing out the problems faced during equipment design.

Professor Takeaki Fukumoto of the Department of Civil Engineering, Ritsumeikan University, Japan, provided invaluable assistance in revising the Index of Crushing (IC) data as presented in this updated version of the report.

The funding has been provided by the California Department of Transportation, Award No. RTA-65T128.

TABLE OF CONTENTS

CHAPTER		PAGE
1	Introduction	1
2	A review of physical characteristics of decomposed granite	3
2.1	Stages of weathering of granitic rocks	3
2.2	Factors controlling granitic weathering	5
2.3	Decomposed granite of Shasta Bally batholith	10
2.3.1	Characteristics of parent rock	10
2.3.2	Climatic setting	13
2.3.3	Characteristics of the weathered product	14
2.4	Use of common physical properties to describe decomposed granite	16
2.4.1	Particle size distribution	16
2.4.2	Specific gravity	17
2.4.3	Atterberg Limits	20
2.5	A generalized classification system for decomposed granite ...	21
2.6	Range of variation of some physical properties of decomposed granite	23
3	Experimental program	25
3.1	Preliminary analyses and tests	26
3.1.1	Physical characteristics of the material	26
3.1.2	Material preparation	30
3.1.3	Compaction test	31

TABLE OF CONTENTS (Contd...)

CHAPTER		PAGE
	3.1.4	Material placement conditions 31
	3.1.5	Test parameters - general 34
3.2		Oedometer test program 34
	3.2.1	Specimen dimensions 34
	3.2.2	Specimen preparation 35
	3.2.3	Testing and measuring equipment 36
	3.2.4	Preliminary tests 36
	3.2.5	Test program 38
3.3		Triaxial test program 42
	3.3.1	Specimen dimensions 42
	3.3.2	Specimen preparation 44
	3.3.3	Testing and measuring equipment 44
	3.3.4	Test program 46
	3.3.5	Correction for membrane penetration 48
3.4		Direct shear and pullout test program 50
	3.4.1	Specimen dimensions 52
	3.4.2	Design and fabrication of testing equipment 53
	3.4.3	Specimen preparation 58
	3.4.4	Measuring devices 60
	3.4.5	Testing problems and preliminary tests 62

TABLE OF CONTENTS (Contd...)

CHAPTER		PAGE
	3.4.6 Test program	67
4	Factors governing particle breakage	72
4.1	Factors controlling the susceptibility to breakage	73
4.2	Quantifying breakage	75
4.3	Compaction-induced breakage	78
4.4	Load-induced breakage	84
4.4.1	Effect of stress level	84
4.4.2	Effect of strain level	96
4.5	Effect of soaking	101
5	Volume change characteristics and the influence of particle breakage	103
5.1	One-dimensional settlement	103
5.2	Hydrocompression	110
5.3	Time effects on settlement	116
5.4	Volume change in strength tests	123
5.4.1	Volumetric strain in consolidation phase	125
5.4.2	Volumetric strain in shearing phase	127
5.4.3	Total volumetric strain	132
5.4.4	The rate of volume change	135

TABLE OF CONTENTS (Contd...)

CHAPTER	PAGE
6 Shear strength characteristics and the influence of particle breakage	139
PART I - Triaxial test results	
6.1 Shear strength parameters of granular materials	139
6.2 Factors governing shear strength parameters	141
6.2.1 Effects of stress level	141
6.2.2 Effects of particle compressive strength	146
6.2.3 General trends of ϕ_f	148
6.2.4 Behavior of decomposed granite	151
6.2.4 Effects of other factors on shear strength of decomposed granite	163
PART II - Direct shear and pullout tests	
6.3 Direct shear tests	166
6.4 Pullout tests	170
6.5 Past practices in some decomposed granite embankments	186
7 Summary, conclusions and recommendations	188
References	194
Appendix A	205

LIST OF FIGURES

FIGURE	PAGE
2.1 A highly weathered granitic rock profile (after Ruxton and Berry, 1957)	4
2.2 Map of Shasta Bally and the vicinity	11
2.3 Schematic model of compacted soil mass	18
3.1 Effect of wet sieving on gradation curve	28
3.2 Initial gradation curves of decomposed granite samples used in laboratory testing	29
3.3 Compaction curve for decomposed granite from SH299 PM 0.6, Shasta County, CA (Modified AASHTO method)	32
3.4 Schematic diagram of oedometer test apparatus	37
3.5 Axial strain versus log time in oedometer specimen C105a, RC = 90%, $w_c = 8\%$	39
3.6 Axial strain versus log time in oedometer specimen C155a, RC = 95%, $w_c = 8\%$	40
3.7 Axial strain versus log axial pressure in oedometer specimen C103a, RC = 90%, $w_c = 8\%$	43
3.8 Test results of triaxial specimen T154a, RC = 95%, $\sigma_c = 400$ kPa	49
3.9 Typical direct shear and pullout test configurations	51
3.10 Pullout test clamping arrangement recommended by ASTM (1992 draft)	55
3.11 Schematic diagram of direct shear and pullout apparatus	56
3.12 Schematic diagram of the horizontal loading mechanism for pullout tests	57
3.13 Schematic diagram of the clamp used in pullout tests	59

LIST OF FIGURES (Contd...)

FIGURE	PAGE
3.14 Schematic diagram of the kneading compaction apparatus for direct shear and pullout tests	61
3.15 Effect of soil thickness on pullout force, RC = 95%, $\sigma_N = 200$ kPa	64
3.16 Comparison of two similar pullout tests, RC = 95%, $\sigma_N = 200$ kPa, soil thickness = 150 mm	65
3.17 Test results of direct shear specimen D103b, RC = 95%, $\sigma_N = 400$ kPa	70
3.18 Pullout force versus gage displacement in specimen P202b, RC = 95%, $\sigma_N = 200$ kPa	71
4.1 Calculation of Breakage Index - B_g (after Marsal, 1973)	76
4.2 Variation of breakage with compactive effort and weathering (after Fukumoto, 1979)	80
4.3 Variation of compaction-induced breakage with compaction water content under Modified Proctor compactive effort	81
4.4 Effect of compaction technique on breakage, RC = 90%, $w_c = 8\%$.	83
4.5 Variation of breakage with stress level (after Marsal, 1973)	85
4.6 Variation of breakage with stress level in triaxial tests on decomposed granite (after Fedá, 1977)	88
4.7 Variation of breakage with stress level in triaxial tests on decomposed granite (after Lee, 1991)	89
4.8 Variation of breakage (total) with stress level in triaxial tests on decomposed granite from SH299 PM 0.6, Shasta County, CA	92
4.9 Variation of breakage (post-compaction) with stress level in triaxial tests on decomposed granite from SH299 PM 0.6, Shasta County, CA	94
4.10 Variation of breakage (total) with stress level in oedometer tests on decomposed granite, $w_c = 8\%$	95

LIST OF FIGURES (Contd...)

FIGURE	PAGE
4.11 Variation of breakage (total) with stress level in direct shear tests on decomposed granite, RC = 95%	97
4.12 Variation of breakage (total) with stress level in pullout tests on decomposed granite, RC = 95%, pull = 50 mm	98
4.13 Variation of breakage (post-compaction) with axial strain in triaxial tests on decomposed granite, RC = 95%, specimens subjected to the same maximum principal stress	100
4.14 Effects of soaking on breakage (from Miura and others, 1983) ...	102
5.1 Compressibility of sand, rockfill and clay	104
5.2 Relationship between compressibility and particle breakage of granular materials (after Hagerty and others, 1993)	106
5.3 Settlement curves of decomposed granite from the Shasta Bally batholith, $w_c = 8\%$	108
5.4 Effect of compaction water content on settlement of decomposed granite, RC = 90%	109
5.5 Effect of the stage of soaking on hydrocompression of Pyramid rockfill (from Nobari, 1971)	112
5.6 Settlement of initially saturated and as-compacted decomposed granite specimens. $w_c = 8\%$	113
5.7 Effect of the soaking axial pressure on hydrocompression of decomposed granite, $w_c = 8\%$	115
5.8 Effect of compaction water content on hydrocompression and particle breakage in decomposed granite, RC = 90%	117
5.9 Time settlement curves in rockfill (after Marsal, 1973)	119
5.10 Effect of axial pressure on the secondary compression index in decomposed granite and in Goldisthal shale	121
5.11 Relationship between creep rate and time for some clays granular materials (from Feda, 1992)	122

LIST OF FIGURES (Contd...)

FIGURE	PAGE
5.12 Relationship between creep rate and time for decomposed granite	124
5.13 Effect of K_c value on compressibility of sands (from Lee and Farhoomand, 1967)	126
5.14 Variation of consolidation phase volumetric strain with σ_{1c} in decomposed granite triaxial specimens	128
5.15 Variation of shearing phase volumetric strain with $(\sigma_m)_f$ in Chattahoochee River sand triaxial specimens (after Vesic and Clough, 1968)	130
5.16 Variation of shearing phase volumetric strain with $(\sigma_m)_f$ in decomposed granite	131
5.17 Variation of volumetric strain (in shearing phase and total) at failure with confinement in Venato sandstone (after Becker, 1972)	133
5.18 Behavior of $(d\epsilon_V/d\epsilon_1)_f$ with confining pressure in sands (from Lo and Roy, 1973)	136
5.19 Variation of $(d\epsilon_V/d\epsilon_1)_f$ with σ_3 in decomposed granite triaxial specimens	138
6.1 Variation of components of ϕ_f with normal stress in sand (after Lee and Seed, 1967)	143
6.2 Effect of confining pressure on volume change and shear strength of Sacramento River sand (from Lee and Seed, 1967) ...	144
6.3 Effect of confining pressure on volume change and shear strength of Toyoura sand (from Miura & Yamanouchi, 1977)	145
6.4 Variation of ϕ_f with σ_m at failure in sand, rockfill, and minerals ..	147
6.5 A schematic of variation of components of ϕ_f with $(\sigma_m)_f$ (after Murphy, 1987)	150
6.6 Variation of ϕ_f with σ_3 in decomposed granite from southern Bohemia (after Fedá, 1977)	152

LIST OF FIGURES (Contd...)

FIGURE	PAGE
6.7 Effect of particle structure stability on stress-strain behavior in decomposed granite (from Feda, 1971)	152
6.8 Effect of confinement on σ_1/σ_3 and ϵ_v of triaxial specimens of decomposed granite from the Shasta Bally batholith, RC = 90% ..	156
6.9 Effect of confinement on σ_1/σ_3 and ϵ_v of triaxial specimens of decomposed granite from the Shasta Bally batholith, RC = 95% ..	157
6.10 Variation of ϕ_f with confining pressure in decomposed granite from the Shasta Bally batholith	158
6.11 Variation of ϕ_f and $(d\epsilon_v/d\epsilon_1)_f$ with $(\sigma_m)_f$ RC = 90%	160
6.12 Variation of ϕ_f and $(d\epsilon_v/d\epsilon_1)_f$ with $(\sigma_m)_f$ RC = 95%	161
6.13 A schematic diagram of a dilative triaxial specimen	162
6.14 Comparison of stress-strain behavior for dry, wet, and saturated samples of decomposed granite form South Korea (from Lee, 1991)	165
6.15 Three mechanisms resisting direct sliding over a geogrid (from Jewell and others, 1984)	167
6.16 Effect of particle size on direct sliding over a geogrid (from Jewell and others, 1984)	167
6.17 Results of direct shear interface strength tests on decomposed granite under different normal pressures	169
6.18 Variation of decomposed granite-geogrid interface shear strength with normal pressure	171
6.19 Results of direct shear tests on decomposed granite under different normal pressures	172
6.20 Variation of ϕ with normal pressure in direct shear tests on decomposed granite	173
6.21 Mechanisms of bond strength development between a grid and soil (from Jewell and others, 1984)	174

LIST OF FIGURES (Contd...)

FIGURE	PAGE
6.22 Variation of pullout force with normal pressure in decomposed granite, RC = 95%, soil thickness = 150 mm	177
6.23 Variation of C_i with normal pressure in pullout tests on decomposed granite, RC = 95%	179
6.24 Comparison of gage displacements with that of the clamp in a pullout test, RC = 90%, $\sigma_N = 200$ kPa, soil thickness = 150 mm .	180
6.25 The extent of shear zone in pullout tests	181
6.26 The extent of shear zone in direct shear tests	183
6.27 Variation of pullout force with relative compaction, $\sigma_N = 200$ kPa, soil thickness = 150 mm	184
6.28 Variation of pullout force with saturation, $\sigma_N = 200$ kPa, RC = 95%, soil thickness = 150 mm	185

LIST OF TABLES

TABLE		PAGE
2.1	Mineralogical composition of residual soils of Shasta Bally batholith	15
2.2	A classification scheme for decomposed granite (after Lee and de Freitas, 1989)	22
2.3	Some physical properties of decomposed granite	24
3.1	Oedometer test program	41
3.2	Triaxial test program	47
3.3	Direct shear/pullout test program	68
5.1	Volumetric strain and breakage of dense (RC = 95%) triaxial specimens consolidated at 900 kPa confinement under different K_c values	135
6.1	Mechanical properties of some decomposed granite samples ..	154
6.2	Construction details and design parameters used in some decomposed granite embankments	187

CHAPTER 1

INTRODUCTION

The suitability of decomposed granite as a construction material for use in a high compacted embankment fill has been investigated. The investigation consisted of a review of the physical characteristics of decomposed granite and a laboratory testing program to evaluate the behavior of relevant mechanical properties under a range of field conditions. The broader objective of this investigation is to provide enough information to modify the practice of design and construction of earthworks to accommodate the special character of this material. The specific objective is to investigate the mechanical properties of compacted decomposed granite from the Shasta Bally batholith near Redding, CA. The Department of Transportation of the State of California (CALTRANS) plans to incorporate this material in a few 100+ m high embankments in the realignment of the highway SH299, which crosses the batholith at the Buckhorn summit. This investigation aims at providing recommendations for material placement conditions and economical embankment designs.

In Chapter 2 physical characteristics of decomposed granite are reviewed and the application of current classification techniques are discussed. Chapter 3 describes the laboratory testing program, which used oedometer and triaxial tests to investigate the influence of particle breakage on two of the most important mechanical properties in a granular embankment fill: volume change and shear strength characteristics.

In addition, a series of direct shear interface strength and pullout tests was performed to investigate the feasibility of using geosynthetic reinforcements to enable steepening of side slopes of decomposed granite embankments.

In Chapter 4, particle breakage is defined, and the factors that control particle breakage of decomposed granite, both inherent and external (i.e., mechanical and environmental) are examined. Chapter 5 compares the volume change characteristics of decomposed granite to those of other granular materials under conditions of high breakage, and analyzes the results from both oedometer

and triaxial test programs. Chapter 6 is divided into two parts: part I contains an analysis of laboratory triaxial shearing tests and the influence of breakage on shear strength of decomposed granite; part II focuses on the performance of decomposed granite in direct shear interface strength tests and pullout tests under high normal pressures and discusses the variability of geosynthetic-soil strength parameters under probable fill placement and environmental conditions.

Finally, in Chapter 7, the important findings of the study are summarized, followed by recommendations on fill placement conditions and suggestions for a preliminary design of the proposed embankments. Directions for further research work that may be needed to finalize the design parameters are also given.

CHAPTER 2

A REVIEW OF PHYSICAL CHARACTERISTICS OF DECOMPOSED GRANITE

In this chapter, the nature of decomposed granite is described. First the products of granitic weathering, identified collectively as decomposed granite, are described, and the major factors that control the formation of decomposed granite are discussed. Examples are cited from around the world, to illustrate the influence of these factors. Then the factors that may have dominated the weathering process in producing decomposed granite at Shasta Bally batholith, the material under investigation in this study, are examined. Test procedures for physical properties that are commonly used to describe embankment fill materials face some unique problems when applied to decomposed granite, and they are discussed next. Lastly, a generalized classification system for decomposed granite is presented, which can be used to supplement the existing soil classification procedures.

2.1 Stages of weathering of granitic rocks

Decomposed granite is formed by in situ (or residual) weathering of granitic rocks. Both physical disintegration and chemical decomposition play important roles in this process. A typical highly weathered granitic rock profile from Hong Kong is shown in Figure 2.1. Weathering of intact granitic rocks typically proceeds inward from joint surfaces which separate the rock mass into individual blocks, as shown in the figure. This process, when sufficiently advanced, is known as spheroidal weathering, and leads to the formation of rounded boulders called **corestones**. Some deposits contain corestones several meters in diameter as a result of widely spaced joint sets in the parent rock. At a more advanced stage of weathering, the rock loses most of its compressive strength, and yet retains its rock texture and structure intact, with traces of fissures, joints and other discontinuities still visible. A weathered rock in this stage is called a **saprolite**. Further decomposition, combined with load related strains, destroys the

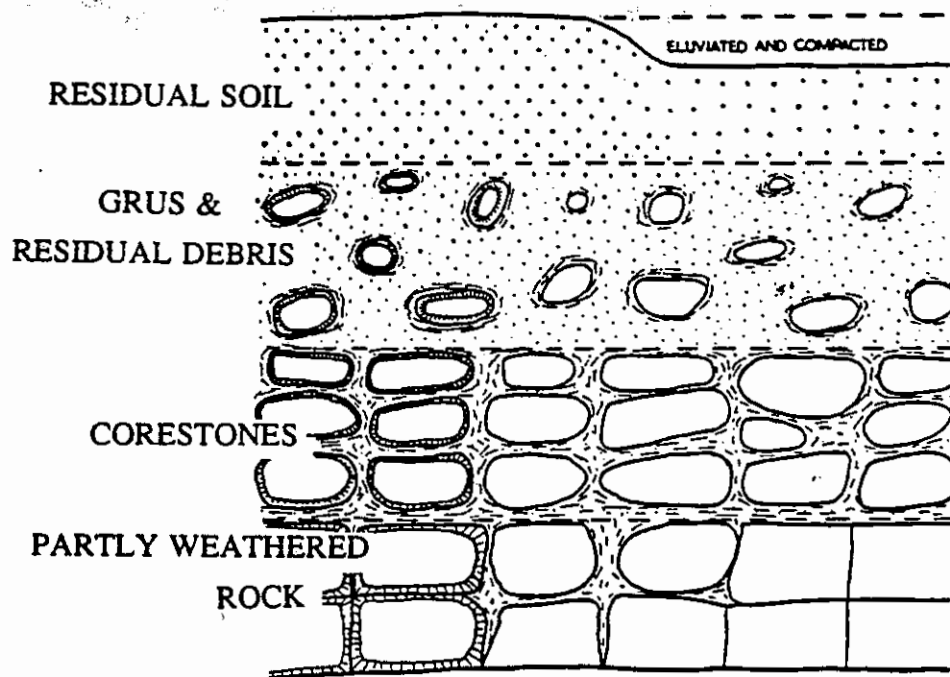


Figure 2.1 A highly weathered granitic rock profile (after Ruxton and Berry, 1957)

parent rock texture and structure, and transforms the rock to a **residual soil**. If weathering occurs mainly through physical disintegration, the weathered product becomes an accumulation of mineral grain fragments, commonly known as **grus**.

Thus the term "decomposed granite" can describe many different materials: residual soils or grus that can be excavated by hand; saprolite which usually requires a shovel for excavation; boulder-size corestones; jointed, but slightly weathered rock that may not even be rippable; and other materials at intermediate stages of decomposition. The depth to unweathered rock in a decomposed granite deposit varies from location to location, and weathered deposits of depths up to 65 m have been recorded (Eggler and others, 1969).

2.2 Factors controlling granitic weathering

In general, parent rock characteristics and the weathering environment are likely to control the characteristics of a residually weathered material like decomposed granite. The process of rock weathering is well documented (see for example, Ollier, 1969; Yatsu, 1988; Mitchell, 1993). Granitic rock weathering has also been described, in general by Lee (1987) and Goodman (1992), and with regard to rocks in particular locations by a number of authors (e.g., Ruxton and Berry, 1957; Wahrhaftig, 1965; Newbery, 1971; Isherwood and Street, 1976; Moore, 1979; Krank and Watters, 1983).

Of the parent rock characteristics, the mineralogy, the texture and the joint structure heavily influence the final form of the weathered product.

- 1) **Mineralogy** - the term decomposed granite typically refers to a material formed not only from granite, but also from other closely associated plutonic igneous rocks such as granodiorite and quartz-diorite. The main minerals in granitic rocks are quartz and the two types of feldspar, orthoclase and plagioclase. Hornblende and biotite are also present in smaller, but significant quantities. The different minerals have varying levels of resistance to weathering, and they may decompose into different weathering products.

- 2) Texture - coarse grained granite rocks, tested in the laboratory by Goswami (1984), were found to be less durable than fine grained rocks. However, field observations, in Korea for example (Lee, 1987), indicate that fine grained parent rocks produce greater depths of weathered deposits. Thus no correlation seems to exist directly linking the texture of parent rock to the weathered product.
- 3) Joint structure - in a granitic rock, the joint structure and other discontinuities control the rock surface area that is easily accessible to water and other weathering agents. The closer the joint or fracture spacing, the greater the exposed surface area and the quicker the weathering. Shearing of rock along fault zones further increases the susceptibility to weathering.
- 4) Other factors - In some cases, hydrothermal activities that occurred either during the crystallization of the rock, or at some later time, would alter the feldspars and micas, and hence influence the composition of the final weathered product.

The weathering environment, i.e., local climate and ground water drainage pattern, is also a major controlling factor in the weathering process because water is the main agent of weathering and the chemical reactions of weathering are heavily environment-dependent.

Generally, the conditions favorable to physical weathering, quartz-rich rocks, a temperate climate, good drainage, etc., may produce gravelly or sandy soil, low in plasticity: quartz usually remains unaltered and forms the bulk of the sandy particles when the rock breaks down; freeze-thaw activity and the temperature changes in temperate climates accelerate the physical breakdown of the rock; good drainage may remove ions that tend to flocculate silica and may prevent formation of highly plastic clay minerals. On the other hand, the conditions favorable to chemical weathering, rocks low in quartz but rich in feldspar and biotite, warm humid climate, poor drainage, etc., may produce silty/clayey soil with medium plasticity: both feldspar and biotite react with water and CO_2 to produce clay minerals like kaolinite, and under poorly drained

conditions even highly plastic minerals like vermiculite may be formed. The influence of various weathering factors on the extent of weathering and the final weathering product is best illustrated using a few selected examples:

Sierra Nevada Batholith, California

In California, the rocks at higher elevations in the Sierra Nevada mountain range seem to have weathered differently from the rocks of the western foothills, though the rock composition is generally the same. The parent rock varies from quartz-monzonite to granodiorite, with biotite and hornblende occurring in significant quantities. Physical disintegration is said to be the primary mode of weathering at higher elevations (Krank and Watters, 1983), as evident from the high level of microfracturing due to expansion of biotite minerals, observable in thin sections, and the low clay mineral content in the residual soil. In contrast, in the western foothills, significant quantities of highly plastic clays are present (Huntington, 1954; Wahrhaftig, 1965), produced by chemically altered biotite, indicating a stronger chemical weathering process. The regional differences in the weathered products, though not discussed by the previous writers, may be caused by a combination of factors including more active and extensive glaciation in the higher elevations and the warmer climate in the foothills.

Rocky Mountain Range, Colorado

Trail Creek granite and Cap Rock quartz monzonite, Precambrian rocks that form a part of Laramie range in Wyoming (an extension of the Rocky Mountain range), have produced contrasting topographic features upon weathering, though their mineral compositions are not very different: Trail Creek granite has weathered completely to form a smooth rolling topography, known as the Sherman erosion surface, whereas Cap Rock quartz monzonite forms a less weathered, rugged topography (Eggler and others, 1969). Oxidation of biotite, which occurred during late stages of crystallization, is thought to have accelerated the weathering of Trail Creek granite.

Isherwood and Street (1976) suggested that the percentage of biotite present in Precambrian Boulder Creek granodiorite in the Rocky Mountain range in Colorado has controlled the level of decomposition of the rock. Deep grus profiles are found in hilltops and along valley sides as pockets of weathered material between masses of unaltered bed rock. Average modal analyses using thin section studies showed that the grus has a substantially higher level of biotite compared to corestones, surface boulders and fresh bedrock. The physical disintegration of granodiorite, caused by expansion of biotite among other reasons, dominates in the cooler mountainous area, decomposing only the biotite-rich portions of the rock.

Snowy Mountain Range, Australia

The Snowy Mountain Range in New South Wales, Australia, is composed mostly of intrusive granites and granitic gneisses (Moye, 1955). Much of the area is covered with a mantle of residual soils, sometimes as deep as 20 to 30 m. Weathering is not uniformly developed, and it is more intense and penetrates deeper in fault zones and in closely jointed rock. In places, highly or completely weathered rock profile changes abruptly to fresh rock. Chemical weathering is thought to be the dominating mode, and a medium to coarse grained, grey granite with abundant biotite is the rock type most susceptible to weathering.

Spain

The development of structural microcracks, not induced by weathering but possibly by past cataclastic activity, has caused Caldas de Reyes granite of Spain to disintegrate physically rather than decompose chemically (Bisdorn, 1967). Corestones show microcracks decreasing in density and width with increasing depth from the surface. The crack system controls the final weathering products, the flaky mineral and rock fragments.

Hong Kong and Malaysia

The humid tropical climate in Hong Kong makes chemical decomposition dominant in the granitic rock weathering process. Much of the rock is weathered to depths in excess of 30 m. Corestones are abundant in weathered rock profiles, and the ratio of corestones to residual soil, in a given volume, gradually increases with depth (Ruxton and Berry, 1957). The residual soil is rich in halloysite (Yatsu, 1988).

In the Main Range of West Malaysia, microfractures, possibly produced by past cataclastic processes, cut indiscriminately across the rock fabric in coarse grained biotite granite (Newbery, 1971). Chemical weathering, aided by wet tropical climate, is the dominant weathering process. Corestones are almost non-existent in the weathered deposits here because the microfractures facilitate groundwater penetrations beyond the major joints. Furthermore, along a vertical profile in the Main Range, the condition of the rock changes from decomposed to fresh abruptly, in contrast to the gradual variation seen in Hong Kong granites.

South Korea

Differences in two granitic landforms in the Korean peninsula are said to be due to the differences in mineralogy, texture and joint structure of the parent rock types (Lee, 1987). The areas of high relief have dome shaped mountains and a shallow average depth of weathering (about 20 m), whereas the areas of low topography have no dome shaped mountains and the average depth of weathering is about 30 m. The primary rock type in the areas of high relief is Jurassic granite, while the low level areas have mainly Cretaceous granite. The Jurassic granite has coarse grain texture and relatively wide joint spacing, and its K-feldspar is mainly microcline (a mineral stable at low temperatures). The K-feldspar in the Cretaceous granite is mainly perthitic orthoclase (a mineral generally stable at high temperatures), and the rock has fine to medium grained texture and more intense joint spacing. In both types of weathered deposits, weathering decreases with depth, corestones are rare, formed only where the joint spacing changes locally, and the soil/rock interface is sharp.

Japan

Large deposits of decomposed granite (Masa) in western Japan, especially near Hiroshima and Kobe, are derived from orthoclase-rich granite rocks, whereas the deposits in the Abukuma mountains in northeast Japan are derived from plagioclase-rich granodiorite with a high percentage of colored minerals, mainly mica. Masa soil in northeast Japan is commonly low in gravel content but high in sand content. The high colored mineral content of the parent rock causes its specific gravity to be generally greater than that of Masa in west Japan (Mori, 1985). Many Masa deposits are deeper than 30 m, and the main clay minerals present are variations of vermiculite and halloysite (Yatsu, 1988).

2.3 Decomposed granite at Shasta Bally batholith

2.3.1 Characteristics of parent rock

Albers (1964) presents a detailed geologic record of the Shasta Bally batholith, roughly centered around the Shasta Bally, a mountain located about 25 km west of Redding, CA (see, Figure 2.2). The batholith is markedly elongate, with an exposed length of about 50 km, trending about N 45° W, and a width of about 15 km. Rocks that form the bulk of the batholith range from light colored quartz-diorite to granodiorite, with an age of approximately 130 million years, i.e., late Jurassic to early Cretaceous (Lanphere and Irwin, 1965). To the northeast, the batholith is bordered by amphibolite and banded gneiss, derived by contact metamorphism from Devonian metavolcanic rocks and Mississippian marine sediments, and to the southwest by mainly Mesozoic basic and ultrabasic intrusive rocks. At least six satellite outcrops of sizes varying from about 100 m² to about 3 km² exist within a few kilometers from the eastern border of the batholith.

The batholith is inferred to have been emplaced mainly by forcible injection and to some extent by piecemeal stoping. A finer grained portion of the batholith, which has sharp contacts against coarser grained portions, is presumed to be of a later phase of the intrusion. The stratum overlying the batholith at the time of intrusion is estimated to have been not more than 12000 m thick.

The average mineral composition of the batholith, according to Albers (1964), is plagioclase (50 - 70%), quartz (25 - 40%), orthoclase (1 - 10%), and biotite and hornblende in minor quantities. Albers (1964) divides the batholith into three zones, depending on the mafic mineral content and grain size; namely, coarse biotite zone, biotite-hornblende zone and fine biotite zone.

- 1) Coarse biotite zone - the minerals in this zone have an average grain size of 2 mm, and the zone forms a belt 1 to 6 km wide in the northeastern part of the batholith. The area which is most biotite-rich and darkest in color is near the northeast border, and the percentage of biotite decreases from 20 percent to 5 percent within a thousand meters inward from the border. Hornblende is visible only in thin sections and present only in minor amounts. Thin sections show a planar structure defined by preferred orientation of biotite plates parallel to the contact of the intrusive mass. The following relict cataclastic structures are also revealed by thin sections: plagioclase crystals are bent; biotite books are locally bent and some have rugged ends as if they have been pulled apart; quartz crystals are more or less segregated in discrete layers.
- 2) Biotite-hornblende zone - the coarse biotite zone grades into the biotite-hornblende zone which forms the western two-thirds of the intrusive mass. This zone, which also has an average grain size of about 2 mm, contains up to about 10 to 15 percent mafic minerals. Hornblende is generally more abundant than biotite, and planar structure is absent or only weakly defined.
- 3) Fine biotite zone - the light colored, fine grained biotite zone, which has an average grain size slightly less than 1 mm, is formed of rather small discrete masses. The contacts between the fine grained zone and the surrounding coarse grained types are either sharp, or gradational over a short distance.

A petrographic examination of excavated rock fragments from the Clear Creek tunnel, driven for 13 km through the northern part of the batholith, showed that the rock there is medium to fine grained quartz-diorite (USBR, 1988). Thin

sections indicated the composition of these rock samples to be; 35 to 40 percent hornblende, 25 to 30 percent feldspar (with minor amounts of orthoclase), 15 to 20 percent biotite and 5 to 10 percent quartz. These quantities deviate somewhat from the quantities previously reported by Albers (1964), and attest to the possible variations between different zones.

The individual mineral grains are in general medium to coarse. A petrographic examination of a slightly weathered core sample at Buckhorn dam site revealed grain sizes up to 6.5 mm in diameter with a mode of 3.5 mm (Eubank, 1990). According to Albers (1964), orthoclase, existing in the form of irregular crystals, could be as large as 5 mm in diameter.

The Clear Creek tunnel is also an excellent source of information on the joint structure of the rock (USBR, 1965). The batholith is generally fault free and impervious in the interior. However, near the contacts with metamorphosed rock, there are several major faults, the most important being the Hoadley fault along the northeastern contact. Several drill holes, driven from canyon bottoms along the tunnel centerline, revealed variable levels of jointing, fracturing and hydraulic conductivity in the rock. Some holes recorded artesian water conditions. During tunnelling, large inflows of water were encountered, sometimes up to 10 m³/min. It was thought that large open joints may have created an aquifer system in the rock. There were fairly wide heavily faulted zones across the tunnel centerline. In these zones quartz-diorite was intensely crushed and softened, and had taken a whitish appearance.

2.3.2 Climatic setting

Precipitation in the area is primarily from frontal storms that originate over the Pacific Ocean. The storms occur predominantly during winter months, mainly in the form of rain, except at higher elevations where snow falls occasionally. Average annual precipitation is about 100 cm at Lewiston, CA, and may reach up to 200 cm at some higher elevations (USBR, 1965). The climate in the area is mild. Average annual temperature (at Weaverville, CA) is about 12°C.

2.3.3 Characteristics of the weathered product

Currently, the batholith is covered with a thick mantle of residual soil everywhere except at the bottoms of canyons and at the tops of high ridges (Albers, 1964; USBR, 1965). Cores obtained from eastern and western slopes of the batholith reveal very intensely weathered deposits up to depths of about 13 m (Eubank, 1990; Duffy, 1990), while a core sample at a depth of 33 m showed the rock to be slightly to moderately weathered (Eubank, 1990). A borehole made for Clear Creek tunnel indicated weathered granite as deep as 130 m (USBR, 1965).

The mineralogy of an intensely weathered granite core sample, taken from the foundation of Buckhorn dam on the western slope of the batholith at a depth of 13 m, is as follows (Eubank, 1990):

- 1) (55 - 60%) feldspar, mainly plagioclase, moderately altered to clay minerals, with grain size ranging from 0.1 to 7.5 mm,
- 2) (about 20%) quartz, with grains ranging from 0.05 to 4.0 mm, randomly oriented and exhibiting numerous fractures,
- 3) (5 - 10%) mica, mainly vermiculite with biotite highly altered, and particle diameter ranging from 0.01 to 3.0 mm with many grains bent and contorted,
- 4) (5 - 10%) hornblende, fresh to incipiently altered, grain lengths ranging from 0.05 to 4.5 mm,
- 5) (2 - 3%) kaolinite, occurring as aggregated masses in altered feldspar grains, and
- 6) minor amounts of magnetite, hematite, illite and sericitized mica.

The rock core recovered from a depth of 33 m at the Buckhorn dam site had a slightly higher feldspar content and a slightly lower hornblende content than the sample above (Eubank, 1990).

Average mineralogical compositions of two sets of bag samples of residual soil, one collected from the eastern slope of the batholith along State Highway 299 (Duffy, 1990), and the other from the western slope near the Buckhorn dam site (USBR, 1987), are given in Table 2.1. As can be seen, the feldspar content is

Table 2.1 Mineralogical composition of residual soils of Shasta Bally batholith

Mineral	Eastern Slope Duffy (1990)	Western Slope USBR (1987)
Quartz	20 - 30%	20 - 30%
Feldspar	(plagioclase) 30 - 45%	30 - 55%
	(orthoclase) 5 - 15%	
Vermiculite	5 - 15%	5 - 15%
Biotite	(degraded) 5 - 15%	-
Kaolinite	trace	5 - 10%
Hornblende	0 - 10%	5 - 10%

slightly lower and the quartz content is slightly higher in the bag samples than in the weathered rock core from the Buckhorn Dam foundation. Overall, however, these mineral quantities appear to be well within the range expected from deep weathering of the parent rock.

A few samples of residual soil collected from the eastern slope of the batholith contained 5 to 10 percent metahalloysite (nonhydrated halloysite), two contained about 30 percent vermiculite, and one sample each contained about 20 percent montmorillonite and kaolinite (Duffy, 1990). These observations suggest that chemical weathering is dominant. However, Atterberg Limits tests performed on both sets of bag samples indicate that the soil is generally non-plastic, and the soil is classified as silty sand. Therefore, Duffy (1990) postulated that the residual soil is in an early stage of chemical decomposition, and that both physical and chemical weathering processes are active near the surface. Weathered, but relatively hard rocks in newly exposed rock surfaces in the slopes of the access road to the Buckhorn dam and at its spillway foundation excavation seem to disintegrate within a few weeks to a level that they can be excavated by hand (verbally communicated by officials at the dam site).

The groundwater levels encountered in boreholes made near the Buckhorn summit in Highway 299 were about 20 m below the surface (Duffy, 1990), whereas the groundwater level at the Buckhorn dam site was much shallower.

2.4 Use of common physical properties to describe decomposed granite

The particle size distribution, specific gravity, and Atterberg Limits are some of the most important physical properties that are conventionally used to describe an embankment fill material. Unique problems associated with measuring these physical properties in decomposed granite are discussed below.

2.4.1 Particle size distribution

The easily breakable nature of decomposed granite makes it difficult to establish a unique gradation curve. During the sieving process, aggregated particles may separate depending on the sieving load, the sieving time and the shaking level. Some researchers have recommended that strong forces be applied to separate the aggregated particles before performing sieve analyses (e.g., Sandroni, 1985). Others disagree, noting that such a procedure leads to disintegration of softer feldspar grains (see, e.g., Phillipson and Brand, 1985).

Separation of aggregated particles also increases with increasing sieving time; however, a shorter time may not be sufficient for the finer particles to fall through to the bottom sieves. The changes in the gradation curve of Masa soil due to varying sieving time were investigated by Miura and O-Hara (1979). After comparing D_{30} and D_{60} values from mechanical sieving and those obtained by careful manual sieving, they decided that five minutes of mechanical sieving time is the best compromise between ineffective sieving and excessive breakage. To establish proper sieving protocols, a similar procedure must be followed for each type of decomposed granite material, as the level of particle breakage in each may be different.

2.4.2 Specific Gravity

The specific gravity of soil grains is sometimes used as an indicator of the average strength of the grains; in general, the higher the specific gravity, the stronger the grains. To obtain the specific gravity of soil grains in a specimen the weight and the volume of the solids portion (soil) must be determined.

Determination of the volume of soil grains is difficult, however. The volume of a soil specimen consists of two major portions; the volume of solids and the volume of voids. The volume of voids can be separated into two parts again; the volume of intergranular voids, which occurs between the grains and depends on the type and the level of packing, and the volume of intragranular voids, which is the cumulative volume of voids that may exist within individual grains. Intragranular voids may be divided again into two parts; the portion which is accessible to water and the portion which is inaccessible.

Conventionally, in the determination of the soil volume for specific gravity, the volume of intergranular voids does not come into play, as all the grains are separated before conducting the test. The soil grains are then immersed in water to measure the equivalent volume of water displaced, V_s . In this process, the water accessible portion of the intragranular voids (V_i), which does not displace any water, will not be included in V_s . The current standard procedure, ASTM C127-88, recommends two types of weight measurements; the weight in air of oven-dry material (W_s) and the weight in air of saturated-surface-dry material (W). Note that W includes the weight of the water that fills the volume V_i in addition to the weight of the solids (see Figure 2.3). Bulk specific gravity can now be expressed in two ways: bulk specific gravity (dry), G_d , is defined using W_s ;

$$G_d = \frac{W_s}{V_s \gamma_w} \quad (2.1)$$

and bulk specific gravity (saturated-surface-dry), G_s , is defined using W ;

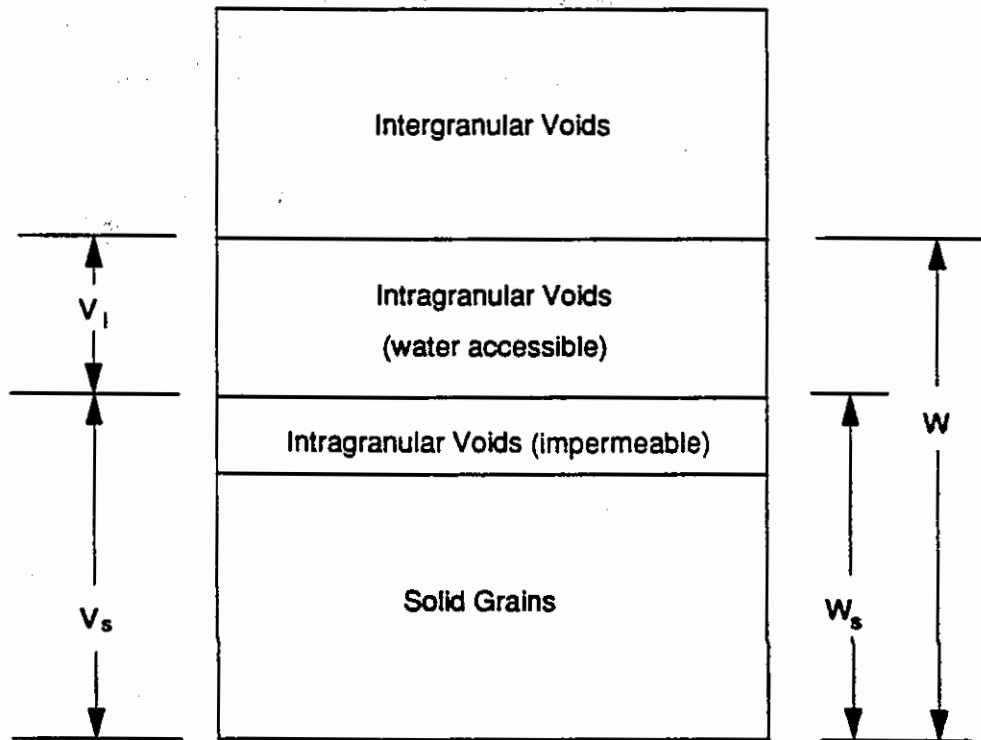


Figure 2.3 Schematic model of compacted soil mass

$$G_s = \frac{W}{V_s \gamma_w} \quad (2.2)$$

The strength of decomposed granite particles decreases significantly as weathering progresses because altering crystal structures open up grain boundaries and also create microfractures across the grains. However, with weathering the change in G_s , for example, is very minimal (Matsuo and Nishida, 1970), because the volume of intragranular voids which increases gradually with weathering is not represented properly in the definition of G_s . Matsuo and Nishida pointed out that, the omission of the water accessible portion of intragranular voids, V_i , from the denominator of equation 2.2 and the use of W (which includes the weight of water filling V_i) in the numerator essentially preclude the effect of weathering being reflected in G_s . The use of W_s in G_d , on the other hand, may decrease its value somewhat with increased weathering, but that decrease may not be significant as V_i is still not included in the denominator.

Apparent specific gravity

Apparent specific gravity (G_a), defined by Matsuo and Nishida (1970), increases the impact of intragranular voids, as V_i is now added to V_s in the denominator:

$$G_a = \frac{W_s}{(V_i + V_s) \gamma_w} \quad V_i = \frac{W - W_s}{\gamma_w} \quad (2.3)$$

ASTM C127-88 (Standard Test Method for Specific Gravity and Absorption of Coarse Aggregate) also attempts to recognize the importance of V_i by defining an apparent specific gravity, but unfortunately, subtracts V_i from V_s in the denominator, and in doing so essentially masks the anticipated reduction in G_a in a sample with a higher V_i . Therefore, in this study, G_a is used as defined in equation 2.3 by Matsuo and Nishida (1970).

In an experiment using a series of Masa soil samples at different stages of weathering, G_s values varied between 2.73 and 2.60, whereas G_a values exhibited a greater range, varying between 2.46 and 1.94 (Matsuo and Nishida, 1970). The lower end of the range comprised mainly of highly weathered samples.

2.4.3 Atterberg Limits

The standard test specifications require that the soil particles used for the Atterberg Limits tests must be small enough to pass through a #40 sieve (0.42 mm opening) (ASTM D4318-84), and the use of much finer soil is encouraged (Lambe, 1951). In decomposed granite, the portion finer than the #40 sieve is usually very small, and this requirement poses a problem because the behavior of this fine portion may not be representative of the total soil sample. If the amount of fines present is not sufficient to fill the voids among coarse particles or to form a thick enough coating around them, the total soil sample may not exhibit plastic behavior even if the finer portion is plastic (Mitchell, 1993).

Furthermore, in some decomposed granite deposits, Atterberg Limits test results may not be repeatable, because the finer portion of the soil sample may contain a high proportion of mica. In the Liquid Limit test, the repetitive blows applied to the cup initiate sliding of soil from either side of the standard groove. The presence of mica flakes in decomposed granite may aid in the sliding of soil, and therefore, different specimens, even at the same water content, may exhibit the closure of the groove at different number of blows. In the Plastic Limit test, the rolled soil thread length is dependent on the water content. Again, the mica flakes in soil may influence the stable thread length and hence the Plastic Limit. Consequently, researchers have raised questions regarding the applicability of Atterberg Limits test to soils with high mica content (Sowers and Richardson, 1983; Gidigas, 1985). Moreover, some clay minerals in decomposed granite, like halloysite, may undergo structural changes upon drying significantly changing plasticity characteristics of the soil (Mitchell and Sitar, 1982).

In spite of the difficulties, the use of Atterberg Limits tests for decomposed granite is desirable, given the strong ties of these tests to geotechnical engineering

since its inception. However, any difficulties associated with performing Atterberg Limits tests on a particular soil type should be clearly identified.

2.5 A generalized classification system for decomposed granite

As already indicated, the term "decomposed granite", as commonly used, encompasses granitic rocks at all stages of weathering. It includes a wide range of materials that exhibit widely varied characteristics. To understand the engineering behavior, a material needs to be classified with other materials that exhibit similar behavior. For the purpose of using decomposed granite as an embankment fill material, the emphasis of the classification shall be on material properties, not on mass properties.

Following the pioneering work by Moye in 1955, a number of classification systems for decomposed granite have been developed by researchers, but most were either site-specific or application-specific. Presented below is a generalized classification system proposed by Lee and de Freitas (1989), who either clarified or discarded some of the ambiguous terms previously used to describe weathering of rocks. In this system a clear distinction between classifying rock material and rock masses was also drawn. Granitic rock materials are classified into six grades, each defined by detailed visual descriptions of the levels of both chemical decomposition and physical disintegration of the material and a range of values of mechanical properties determined by simple field and laboratory tests. Rock mass is also classified into six grades, using the same terms as for rock material. However, a particular grade of rock mass may contain one or more grade(s) of the relevant rock material.

In Table 2.2, the six grades of material classification are given with descriptive definitions and approximate values of relevant geological and engineering properties. The ranges of moisture content and Uniaxial Compression Strength values are for Korean granite samples only, while other values may be typical for granites elsewhere. The Simple Permeability test, though so named, is actually a water adsorption/infiltration test and the index values should be treated as such. Lee and de Freitas (1989) caution that this classification scheme should

Table 2.2 A Classification scheme for decomposed granite (after Lee and de Freitas, 1989)

Grade	Material Description	PLS (MPa)	SHV (MPa)	MC (%)	UCS (MPa)	Perm. Cl	Slake Cl
I. Fresh (rock)	All mineral constituents are sound. No evident microfracturing. Feldspars cannot be scratched with a knife. Sample requires many blows of geological hammer to fracture it.	9-18	59-62	0.06-0.30	125-260 (80-240)	1	-
II. Slightly Weathered (rock)	Plagioclases are occasionally slightly decomposed (gritty). Biotites are slightly decomposed and beginning to stain some of the surrounding minerals. Moderately microfractured (over 10 mm spacing). All microfractures and grain boundaries are tight. Feldspars cannot be easily scratched with a knife. Sample requires more than one blow of geological hammer to fracture it. Slightly weaker than fresh rock.	5-12.5	51-56	0.15-0.29	100-175 (55-135)	1	-
III. Moderately Weathered (rock)	Most plagioclases and some potash feldspars are moderately decomposed (gritty). Biotites are moderately decomposed staining many of the surrounding minerals. Moderately microfractured (5-10 mm spacing). Most microfractures and grain boundaries are tight, but some of them may be slightly open. Feldspars can be noticeably scratched with a knife, cannot be peeled by a knife. Sample can be fractured with single firm blow of geological hammer. NX core cannot be broken by hand. Cannot be excavated with a spade.	2-6	37-48	0.25-0.45	60-120 (35-65)	2	-
IV. Highly Weathered (rock/soil)	All plagioclases and some potash feldspars are highly decomposed (gritty to clayey) and most potash feldspars are moderately decomposed (gritty). Biotites are highly decomposed staining most rock minerals. Highly microfractured (2-5 mm spacing). Microfractures which are mainly grain boundaries tend to be slightly open. Feldspars can be peeled by a knife with difficulty. Sample cannot be indented by a geological pick or knife, but can be crumbled under firm blows with geological hammer. NX cores may be broken by hand with difficulty. Material can be excavated with a spade with great effort and cannot be disintegrated by agitating in water.	0.3-0.9	12-21	0.37-3.80	35-55 (10-15)	3-4	1
V. Completely Weathered (soil)	All plagioclases and most potash feldspars and biotites are completely decomposed (clayey), some potash feldspars are highly decomposed (gritty to clayey). Original texture is present. All microfractures and grain boundaries tend to be open. Feldspars can be readily peeled by a knife. Sample cannot be indented by thumb, but can be readily indented by a geological pick or knife, can be excavated by hand with difficulty, and can be disintegrated by agitating in water.	-	-	7.84-21.00	-	4	2-3
VI. Residual Soil	All feldspars, biotites are completely decomposed (clayey). Original texture is absent. The existence of microfractures and grain boundaries are hardly distinguishable due to the absence of original texture. Feldspars can be readily peeled by a knife. Sample can be indented by thumb with moderate effort, can be easily excavated by hand, and can be disintegrated by agitating in water.	-	-	12.24-22.1	-	2-3	4

- PLS - Point Load Strength (Goodman, 1980)
- SHV - Schmidt Hammer Value (Zamba and Mendl, 1976)
- MC - Moisture Content (for Korean granites only)
- UCS - Uniaxial Compressive Strength (values within brackets are for saturated samples - for Korean granites only)
- Perm. Cl - Permeability Class (from the Simple Permeability test)
- Slake Cl - Slaking Class (from the Simple Slaking test)

Procedure for Simple Permeability Test:

Hydraulic Conductivity is qualitatively assessed by observing the penetration of a few drops of water from a dropper on a hand specimen, over a period of about one minute (Lee and de Freitas, 1989).

- Class 1 - The specimen is almost impermeable--most of the water remains on the surface (K= 1E-7 cm/s or less)
- Class 2 - The specimen is slightly permeable--some water is absorbed but more than half of the water remains (K= 1E-5 to 1E-7 cm/s)
- Class 3 - The specimen is moderately permeable--more than half of the water is absorbed (K= 1E-3 to 1E-5 cm/s)
- Class 4 - The specimen is highly permeable--most of the water is absorbed (K= 1E-3 cm/s or greater)

Procedure for Simple Slaking Test:

Samples weighing 40 to 50 g are immersed in water for 5 minutes, and if the samples have not disintegrated completely, then they are slightly agitated a few times (Lee and de Freitas, 1989).

- Class 1 - Most of the specimen has not disintegrated even after it has been agitated a few times.
- Class 2 - Less than 50% of the specimen has disintegrated into soil after soaking for 5 minutes; after it has been agitated a few times the specimen breaks into debris.
- Class 3 - Over 50% of the specimen has disintegrated into soil after soaking for 5 minutes; after it has been agitated a few times the specimen almost entirely disintegrates into soil and debris.
- Class 4 - Completely disintegrates into soil within 5 minutes of soaking.

not be applied using exclusively the geological test values or the engineering index values; instead, both types of test values should be used.

For the purpose of describing mechanical properties of the "soil" portion of the profile (mainly the grades HW, CW and RS), it is useful to divide those grades into smaller definable subgroups, using the Unified Soil Classification system. For example, the material in weathering grade Completely Weathered rock may be subdivided into well graded gravel (GW), poorly graded sand (SP), silty sand (SM), etc. Nevertheless, the conventional index tests that are used for such divisions may be inappropriate for decomposed granite, as discussed in section 2.3. In questionable situations, it is recommended that a detailed description of the material be provided to clarify the differences between subgroups.

2.6 Range of variation of some physical properties of decomposed granite

Some physical properties of decomposed granite deposits from a number of locations are listed in Table 2.3 along with their classifications, either as provided by the investigators, or as estimated from the information available. This table exemplifies the wide variation in character in the types of materials identified collectively as decomposed granite.

A great number of the investigations listed in Table 2.3 are on decomposed granite of Japan (Masa soil) because of the heavy use of the material there. Even within Japan, samples from different locations vary greatly in character, ranging from silty to gravelly sand. Samples from Shasta Bally batholith generally are non-plastic, though some have a high proportion of fines. The gravel content is noticeably low in these samples. Samples from Hong Kong and Colombia have fairly high amounts of fines and also have relatively high plasticity, which is not surprising given that both countries have humid, tropical climates.

Table 2.3 Some physical properties of decomposed granite

Ref	Location	Soil Type	Gradation (%)			Gs	Ga	LL	PI	Wii (%)	Wfl (%)	Classifi- cation
			Gravel	Sand	Silt/Clay							
1a	Colombia	Silty Sand	0-25	50-75	0-25	2.70-2.73		30-50	0-15			IV-V - SM
b		Sandy Silt		25-75	25-75	2.70-2.75		30-50	0-15			V - ML
2	Czechoslovakia	Landstejn Sand	25	68	7			NP	NP			SW
3a	Hong Kong	Granite-Clayey	25	25	50	2.67		92	52			VI - CH
b		Granite-Sandy	25	45	30	2.66		46	10			V - SM
c		Granite-Dam	15	55	30			29	10			V - SC
d		Granodiorite-Lab	15	35	50			42	11			V - ML
e		Granodiorite-Dam	15	35	50			35	14			V - CL
4a	Japan	Kawakubo	37	45	18	2.64	2.22	49	20			VI - SM
b	(Saga,	Yabuta	40	56	4	2.61	2.20	45	21			V - SM
c	Kyushu)	Kanzaki	36	51	13	2.64	-	48	17			V - SM
d		kawakami	24	63	13	2.60	2.34	NP	NP			IV - SM
5a	Japan	Kanakuma	8	58	34	2.65		39	10			SM
b	(Kyushu)	Kanayama	8	63	29	2.63		36	5			SM
6a	Japan	Granite		20-35	65-80						20.6-21.4	
b		Granodiorite		10-20	80-90						22.5-27.9	
c		Diorite		10-30	70-90						26.4-35.8	
7a	Japan	Clayey		40-65	35-60	2.65-2.68						VI
b		Sandy	0-5	65-85	10-35	2.66-2.70						V
c		Gravelly	0-50	50-90	0-10	2.69-2.73						IV-V
8	Japan	Granodiorite	5-30	60-80	0-20	2.70-2.82		NP	NP	1.7-4.0	20-30	SM
9a	Japan	Kanakuma	9	58	34	2.65		39	10			SM
b	(Fukuoka	Kawakubo (Saga)	24	66	10	2.71		35	10			SM
c	& Saga,	Saga	36	53	11	2.64		NP	NP			SM
d	Kyushu)	Washed Saga	26	73	1	2.63		NP	NP			SP
10a	Japan	Slightly weathered		100		2.64	2.379					
b	(Rokko Mtn)	Highly weathered		100		2.62	2.050					
11a	Japan	Clayey			15-23	2.63-2.65				5.8-8.3		
b		Silty			5-21	2.61-2.69				3.3-5.4		
c		Sandy			2-3	2.62-2.67				1.3-2.3		
12a	Shasta	33R-1		40	60	2.72		26	6			CL-ML
b	Bally (Spring	33R-2		50	50	2.71		NP	NP			SM-ML
c	(Creek dam)	33R-3		48	52	2.73		NP	NP			ML
13a	Shasta	B2R-1	8	70	22	2.69		NP	NP			
b	Bally	B2R-4	15	73	12	-		NP	NP			
c	(Hwy 299)	B2R-5	7	74	19	2.72		NP	NP			
d		B2Ra	1	78	21	2.70		NP	NP			
14a	Shasta Bally	X89		47	53	2.65		28	3			ML-SM
b	(Buckhorn dam)	X90	5	64	31	2.70		NP	NP			SM
15a	Shasta Bally	BS-1	5	35	60	2.70		35	12			ML-CL
b	(Hwy 299)	BS-2	16	79	5	2.74		NP	NP			SW
16a	N. Sierra	Stockpile	5	75	20			NP	NP			
b	Nevada, CA	Bag Sample	18	64	18			-	-			

- Gs - Specific Gravity of soil (conventionally measured)
 Ga - Apparent Specific Gravity (Matsuo and Nishida, 1970)
 Wii - Loss on Ignition (Onodera and others, 1976)
 Wfl - Flow Limit (Matsuo and others, 1970)

References:

- | | | |
|-------------------------------|----------------------------------|-----------------------|
| 1. Li and Mejia (1967) | 7. Ito and Others (1990) | 13. Duffy (1990) |
| 2. Feda (1977) | 8. Furukawa and Fujita (1990) | 14. Solbos (1990) |
| 3. Guilford and Chan (1969) | 9. Onitsuka and Yoshitake (1990) | 15. Prysock (1979) |
| 4. Onitsuka and Others (1985) | 10. Nishida and Kagawa (1972) | 16. Macfarland (1990) |
| 5. Uchida and Others (1968) | 11. Onodera and Others (1976) | |
| 6. Matsuo and Others (1970) | 12. USBR (1960) | |

CHAPTER 3

EXPERIMENTAL PROGRAM

The experimental program carried out in this study was aimed at investigating the mechanical behavior of compacted decomposed granite with a specific emphasis on: a) the impact of mechanical and environmental processes on particle breakage; b) the influence of particle breakage on important mechanical properties; and c) the feasibility of enhancing mechanical properties of an embankment using geosynthetic reinforcements. In a granular embankment fill, the most important mechanical properties are the volume change and shear strength characteristics. The volume change characteristics of importance are, the settlement during consolidation, the rapid settlement upon wetting under load (hydrocompression), and the time rate of settlement. Oedometer tests were used to study each of these three components of volume change. The friction angle, or the angle of shear resistance, is the most important shear strength parameter, and its variation within the possible range of stresses was investigated using a series of triaxial tests.

Another important parameter from embankment design perspective is the steepness of the embankment side slopes. With recent advances in product development and research on the use of geosynthetics, economically advantageous geosynthetic-reinforced steep slopes have been constructed, albeit for embankments of much smaller height than 100 m. Commonly, direct shear interface strength tests and pullout tests are used to evaluate mechanical properties of a reinforced soil mass. Therefore, a direct shear/pullout test series, under fairly high normal pressures, was designed to investigate the feasibility of reinforcing the currently proposed 100+ m high decomposed granite embankments as well.

In this chapter, the physical characteristics —mineral composition and classification properties— of the material under investigation, decomposed granite from the Shasta Bally batholith, are presented first. Then, material preparation techniques, the compaction characteristics, general placement conditions and the

appropriate test loads or pressures are discussed. Details of individual test programs, oedometer, triaxial and direct shear/pullout, are given next. Under each test type, equipment design, specimen preparation, installation of measuring devices, test schedule, possible experimental errors, and preliminary tests conducted are described. Finally, a set of typical results is presented for each test type. The actual experimental results are presented with analysis in the chapters to follow, and a summary of results for each test program is given in Appendix A.

3.1 Preliminary analyses and tests

3.1.1 Physical characteristics of the material

Because of the difficulty in procuring a large quantity of material at one time, the decomposed granite used for the entire test program was procured in three different batches. All the samples were obtained from the same location, at the side hill excavation near post mile 0.6 (Shasta County) along the highway SH299. However, there were some differences in gradation because the first two batches of material were obtained from near-surface manual excavations, whereas the third was obtained from a deep excavation using heavy machinery. Therefore, the batches of material were kept separate, and each test type used materials from only one batch. Possible differences in breakage between specimens due to gradation differences were thus avoided.

The average mineral composition of the material was estimated from several x-ray diffraction tests. About 70 to 80 percent of the material is composed of quartz and feldspar minerals, in roughly equal quantities. The portion of plagioclase feldspar is about as twice as that of orthoclase. Small quantities of the minerals smectite, vermiculite, kaolinite, biotite, mica and amphibole (mainly hornblende) constitute the rest. The sample obtained last, excavated from a greater depth, showed a slightly higher quantities of clay minerals. These results are generally comparable to the data presented in Table 2.1.

The material excavated is somewhat moist (natural water content is between 3 to 5 percent), and the fine particles seem to coat the larger particles. In determining particle gradation, drying the material before sieving makes it

difficult to separate the finer particles that coat the larger ones. This precludes estimating breakage accurately through dry sieving, because an increase in fines content due to breakage will not be properly reflected in the gradation curve. Thus, the practice of "wet sieving" has been adopted in determining the gradation curve throughout this test program. In wet sieving, a known weight of material is washed over a #200 sieve (with a coarser sieve on top to protect the finer mesh), being careful to minimize the break up of any particle aggregations. The material retained is then oven-dried, weighed and sieved. This method, as expected, increased the amount of separable finer particles (see Figure 3.1).

The sieving time is also important in establishing proper gradation curves, especially in fragile materials like decomposed granite, as discussed in Chapter 2. A preliminary study was conducted, following the procedure outlined in section 2.3.1, to examine the effect of sieving time on gradation. A sieving time between seven to ten minutes for a sieving load of about one kilogram of material was sufficient to sieve the material effectively.

Average initial gradation curves established for the three batches of materials used in triaxial, oedometer and direct shear/pullout test programs are shown in Figure 3.2. To determine the initial curve, at least four specimens from each batch of material were sieved and the quantities averaged. The batch used for oedometer tests, obtained from the deeper excavation, seems to have the highest fines content, about 10 percent passing the #200 sieve. The largest sieve used had a 0.5 in (12.5 mm) mesh, and all particles passed through this sieve. Some occasional large, hard pieces of rock (about 100 to 250 mm in diameter) that were present in the last batch of material were removed before sieving. The particles retained on the #4 sieve were generally less than about 8 mm in diameter, much smaller than the maximum sieve size (12.5 mm). Moreover, the amount retained on the #4 sieve was less than 5 percent except for the batch used in triaxial tests.

The average bulk specific gravity (dry) of the material, G_d , defined by Equation 2.1, was 2.684. The bulk specific gravity (saturated surface dry), G_s (Equation 2.2), determined on the portion retained on the #8 sieve, was 2.737.

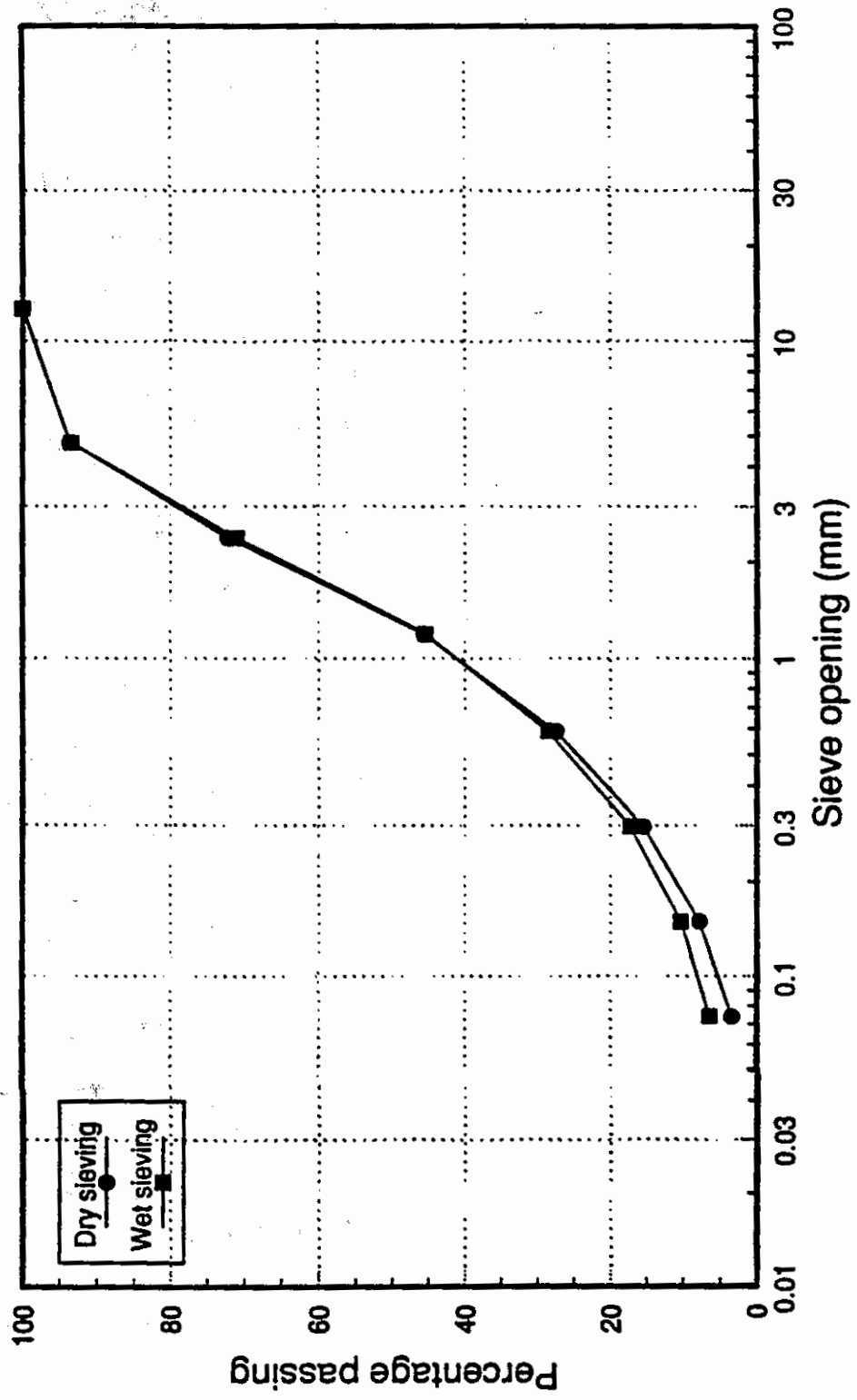


Figure 3.1 Effect of wet sieving on gradation curve

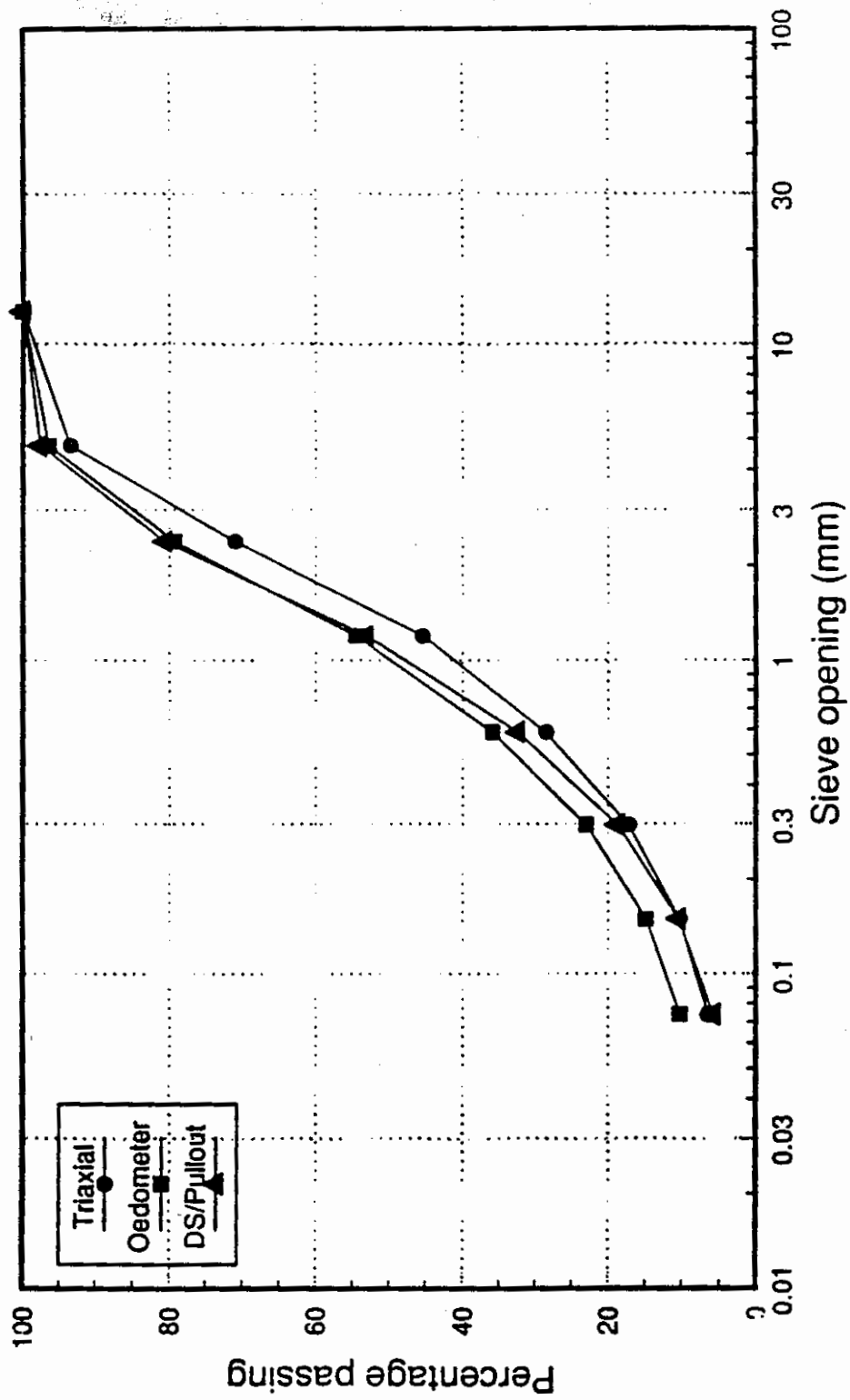


Figure 3.2 Initial gradation curves of decomposed granite samples used in laboratory testing

The apparent specific gravity, G_a (Equation 2.3), was 2.577. The Atterberg Limits were determined on the portion passing the #40 sieve (0.425 mm opening), which represented less than 25 percent in weight of material (see Figure 3.2). Both Liquid Limit and the Plastic Limit were not determinable, and hence the material is considered non-plastic. In the Liquid Limit test, the material slid in the cup, probably because the content of mica was high.

Based on the classification system proposed by Lee and de Freitas (1989), this decomposed granite can be classified as Grade VI (residual soil). It can be further classified, based on Unified Soil Classification, as SW-SM.

3.1.2 Material preparation

Particle breakage includes both separation of aggregated particles and particle crushing. Quantifying particle breakage generally involves comparing the particle size distributions (gradation curves) prior to and after a test. As mentioned in Chapter 1, comparison of breakage between test specimens is an integral part of this experimental program. Therefore, ideally, every test specimen in a test program should have the same initial gradation. Conventionally, this is achieved by separating the original batch of material into a series of sieve fractions and then re-mixing them according to a given proportionality.

However, this technique of sieving and re-mixing cannot be used for decomposed granite from Shasta Bally batholith, for the following reasons: a) this somewhat moist material cannot be sieved without drying; b) drying, in turn, makes the finer particles that coat the coarser ones inseparable essentially invalidating the sieve analyses; and c) sieving process itself may cause additional breakage (as discussed in Chapter 2). Hence, a significant effort was spent on making the test specimens as "uniform" as possible, while using the material in its original state. First, the entire amount of soil needed for a particular test series was thoroughly mixed at its natural moisture content. Then a sufficiently large batch of material was divided, using a material separator, into smaller portions as required for individual tests. This random division of particles may still cause some scatter in gradation, especially in large particle sizes.

3.1.3 Compaction test

A compaction test series, following the ASTM D1557-78 procedure (Modified Proctor method), was conducted to determine the moisture-density relationship for decomposed granite. The tests were conducted using the same material that was later used in the triaxial test program. The 4 inch (101.6 mm) diameter mold was used, although the particles larger than the #4 sieve opening were not discarded. This was deemed justified because: a) about 94 percent of the material passes through the #4 sieve; and b) removing larger particles would have hindered the secondary goal of studying compaction-induced particle breakage. The material was not dried prior to testing, and no specimen was reused. The compaction curve, shown in Figure 3.3, indicates that the maximum dry density is 20.3 kN/m^3 (129 pcf) and the optimum moisture content is 8.5 percent.

During the compaction test, specimens are prepared at different moisture contents and they are compacted using the same compactive effort. Thus, the compaction test series provides an excellent opportunity to study the effect of remolding moisture content on compaction-induced particle breakage. To estimate breakage, compacted specimens were carefully broken apart, washed and sieved. The breakage results are discussed in section 4.3.

3.1.4 Material placement conditions

Commonly decomposed granite is compacted in the field with equipment that uses kneading type compaction, such as the sheep-foot roller. Kneading compaction technique was used for this laboratory test program also, for the following reasons: a) the specific objective of this program is to obtain design parameters for embankment construction which will most likely use the same technique; and b) kneading compaction is the best technique to obtain the high densities required for this material, both in the field and in the laboratory. To simulate the conditions generally used in field compaction by sheep-foot rollers, the pressure under the kneading foot was kept at a level not greater than about 860 kPa (125 psi) (Hilf, 1975).

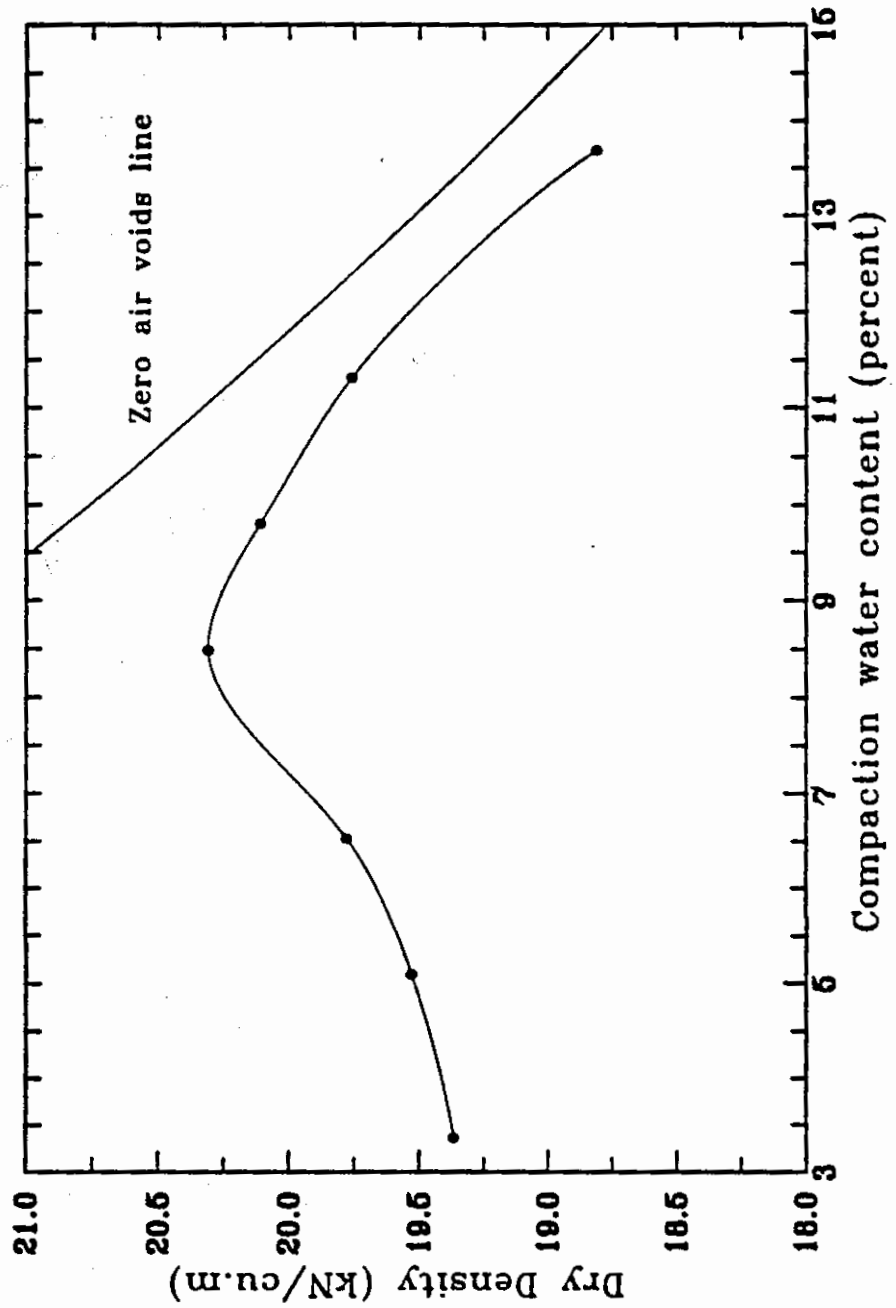


Figure 3.3 Compaction curve for decomposed granite from SH299 PM 0.6, Shasta County, CA (Modified AASHTO method)

The other possible laboratory compaction techniques are vibratory, static and impact compaction. Compaction-induced breakage is expected to vary with the type of compaction used. To assess the effect of the compaction technique on particle breakage, a series of specimens were remolded under all four compaction techniques; kneading, static, vibratory and impact compaction. These specimens were prepared at 90 percent relative compaction only, because of the difficulty in achieving higher densities under some of the compaction techniques. The specimens were then dismantled to estimate breakage, and the results are discussed in section 4.3.

Generally the test specimens were compacted at a water content slightly on the dry side of optimum, about 8 percent ($\pm 0.5\%$), following the common field practice for compacting this type of materials. A few specimens compacted at lower water contents required a significantly higher effort to achieve the same relative compaction.

Test specimens were prepared at two densities, corresponding to 90 and 95 percent relative compaction (18.3 kN/m^3 and 19.3 kN/m^3 respectively), based on the compaction curve by Modified Proctor method (Figure 3.3). Two levels of compaction were chosen mainly to study the change in mechanical properties with void ratio. The lower level of relative compaction, 90 percent, is the density usually stipulated for highway embankments constructed of similar material. The technical and economic viability of compacting the material at a greater level of compaction also needed to be explored for the following reasons: a) given the large height of the proposed embankment, substantial savings can be achieved by having steeper slopes, i.e., by having greater material shear strength; b) given the fragility of the material, the breakage related settlement may be reduced by applying more compactive effort causing more breakage initially; and c) the expected breakage related reduction in shear strength may be partly compensated by having higher shear strength in the first place. The 95 percent relative compaction was chosen so that: a) the increase in mechanical property values with increased compaction is substantially greater than the expected experimental

error; and b) the compactive effort required is still within the practically feasible range.

3.1.5 Test parameters - general

Since the overburden pressure at the bottom of a 100 m high embankment may be about 1500 kPa, all mechanical properties should ideally be investigated in the laboratory at least up to these levels of normal stress or corresponding confining stress. However, the geosynthetic reinforcements in the embankment may not be subjected to such high stress levels, as they are located at the side slopes. Preliminary analyses indicated the maximum normal pressure on earth reinforcements in a 100 m high embankment may be about 800 kPa. The test equipment was designed taking these stress levels into account.

The worst case scenario for mechanical properties of a granular embankment is the completely soaked situation. The stakes may be greater in a decomposed granite embankment because of the water sensitive nature of the material. Therefore, most of the tests were conducted under saturated or soaked condition. Some specimens were soaked at a later stage of loading in hydrocompression tests. The effect of soaking on mechanical properties was also examined in some tests. Since the material used in testing is fairly well-graded and has only a small fines content, it drains fairly rapidly. Thus all the tests could be conducted under drained conditions using a slow loading rate.

3.2 Oedometer test program

3.2.1 Specimen dimensions

According to ASTM D2435-90 (the Standard Test Method for One-Dimensional Consolidation Properties of Soils) the minimum specimen height should be the greater of $10 \times D_{\max}$ and 12 mm. The D_{\max} for this decomposed granite batch is 12.5 mm (0.5 in), and thus the specimen height should at least be about 125 mm. However, about 96 percent of the material passes through the #4 sieve (4.76 mm opening), and the particles that are retained are not much larger than about 6 mm. Therefore, a specimen only 50 mm (2 in) high was judged to

be sufficient. The minimum diameter to height ratio stipulated by ASTM D2435-90 is 2.5, and thus the diameter of the specimen should be greater than 125 mm. The top portion of a CBR mold, a stainless steel ring with an inside diameter of 150 mm and a height of 50 mm fits well with these requirements. It also meets the stipulated criteria on ring rigidity under the maximum applied pressure. Therefore, specimens were fabricated using the CBR ring as the mold with a diameter of 150 mm and a height of about 50 mm. When material was placed in the mold, occasional large particles were positioned in the middle of the mold to reduce possible adverse effects.

3.2.2 Specimen preparation

The specimens were brought to the required water content at least a day prior to compaction. The material was placed inside the mold and compacted by kneading technique using a modified hand press with a 63 mm diameter kneading foot. The foot is spring-loaded, and when the soil pressure under the foot reaches the set value, a micro-switch lights up an indicator bulb. The mold is placed on an eccentrically rotating base which allows the compactive effort be applied at a given overlap (about 40 to 60 percent in this case) all around the specimen. The full specimen height was reached in two 25 mm layers. The height of a layer was first controlled roughly by monitoring a marker on the kneading foot. Precise height control was achieved using a height-adjustable tamper which was also used to apply the final round of compaction forces. Since the diameter was the same for all specimens, the height of a specimen was controlled so that the specimen density fell within ± 1 percent of the required level. The weight of each layer was carefully controlled maintaining about 0.5 percent (of relative compaction) undercompaction per layer. After compaction, the height and the weight of the specimen were determined. To facilitate drainage, the specimen was sandwiched between two 148 mm diameter porous brass plates, each lined on either side with a filter paper. The outer filter papers help in drainage while the inner filter papers prevent large pores in brass plates from getting clogged by soil particles.

The specimen was then placed in a large water bath kept under the loading piston.

3.2.3 Testing and measuring equipment

The oedometer test set up is shown schematically in Figure 3.4. A recess to fit the bottom brass plate was made in the base of the water bath, so that the mold ring can rest on the base at the edge of the recess. A Karol-Warner Conbel 354 hydraulic loading machine was used to apply the normal load. It can apply the load "instantaneously" and can maintain the load constant regardless of sample compression. The piston has about 60 mm of travel. The load is transferred through a load cell to an aluminum loading plate, which rests on the top brass porous plate. The highest normal pressure the Conbel 354 machine can apply on a 150 mm diameter specimen is about 1600 kPa, which is higher than the maximum pressure requirement stated in section 3.1.5. Therefore, most of the tests were carried out using this testing equipment. Another compression machine with a larger loading capacity was used for two additional tests under higher pressures. The normal pressures used in the regular test program, doubled at each step, as usually done in consolidation testing, were approximately 50, 100, 200, 400, 800 and 1500 kPa. The two high pressure tests had a maximum normal pressure of approximately 6000 kPa.

The normal load was measured by a 40000 lbf (175 kN) diaphragm type load cell placed between the loading piston and the specimen. The compression of the specimen was measured by two LVDTs fixed to the base of the bath and placed at opposite ends of the specimen diameter. The use of two LVDTs would average out the errors if loading causes the top of the specimen to tilt. The data was recorded, usually at logarithmic time intervals, by a computerized data acquisition program.

3.2.4 Preliminary tests

Several preliminary tests were conducted to study the effect the duration of load at each load increment has on the final settlement. Nobari (1971) conducted a similar investigation on a rockfill material. He concluded that, since the primary

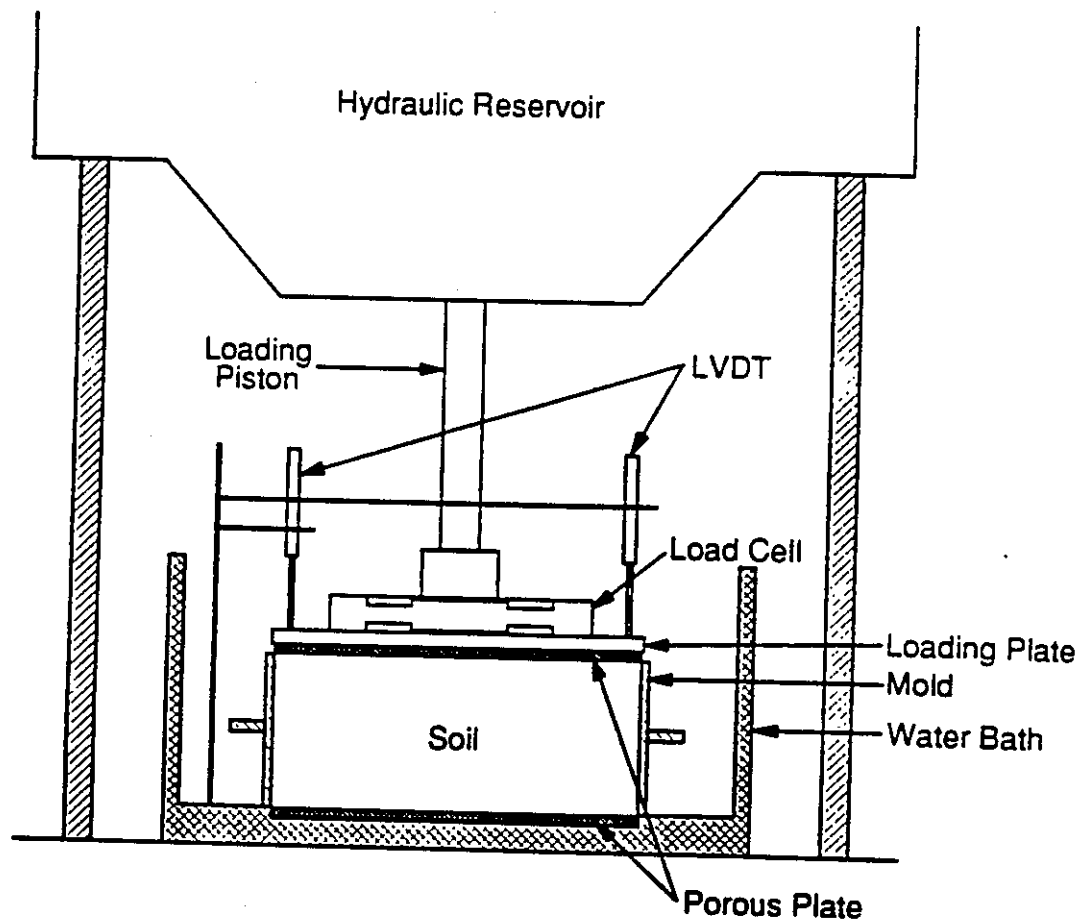


Figure 3.4 Schematic diagram of oedometer test apparatus

settlement is almost instantaneous, 8 minutes at each load increment provides sufficient time to correctly estimate the subsequent time delayed settlement. Figure 3.5 shows the results of a test in the current study, where three load increments were maintained for 5000 minutes each, while others were maintained for only 10 minutes each. The value alongside each curve is the corresponding total normal pressure at the particular load increment. The settlement-log time curves become straight lines almost immediately from the start (first measurement is taken 6 seconds after the loading), indicating that primary consolidation is very rapid. The curves for the first two long term loading increments are practically parallel to each other. However, the curve for the last load increment dips at a rate about 3 times greater. The results for a denser specimen, shown in Figure 3.6, indicate almost identical behavior, except that the strain levels are smaller and the slopes are flatter. The significance of such behavior is discussed later in section 5.3. Overall, the results confirm the rapid completion of primary consolidation and the log-linear nature of the time rate of settlement. Therefore, in subsequent tests, each load increment was maintained only for 10 minutes, except the last increment which was maintained for 100 minutes to better define the slope of the time-settlement curve.

3.2.5 Test program

Table 3.1 summarizes the oedometer test program. The C100 test series is designed to estimate the settlement of decomposed granite under varying normal loads. (Note: Test specimens are identified with the test number plus a letter identifying the order of replication; e.g., C101a represents the first specimen subjected to test C101). In C100 test series, the specimens were inundated under a 5 to 10 kPa seating pressure before the load increments were applied. In some tests, the loading was terminated at intermediate loading stages, 100 and 400 kPa, mainly to analyze the relationship between particle breakage and settlement under varying loads. At the end of a test, water content and breakage were determined from every specimen. C104 and C154 are the two high pressure tests. C105 and C155 tests were conducted to study the long term settlement. Two other tests,

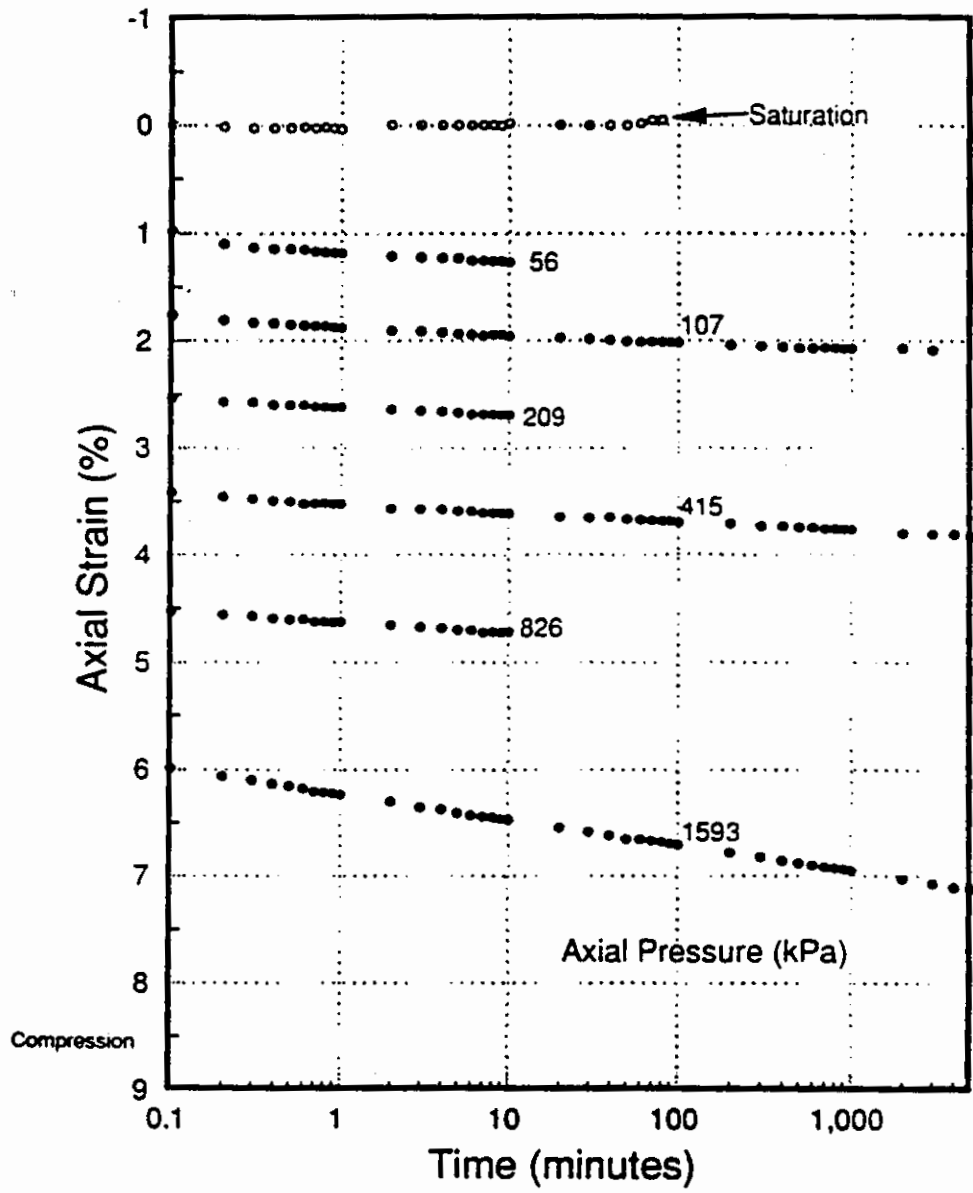


Figure 3.5 Axial strain versus log time in oedometer specimen C105a, RC = 90%,
 $w_c = 8\%$

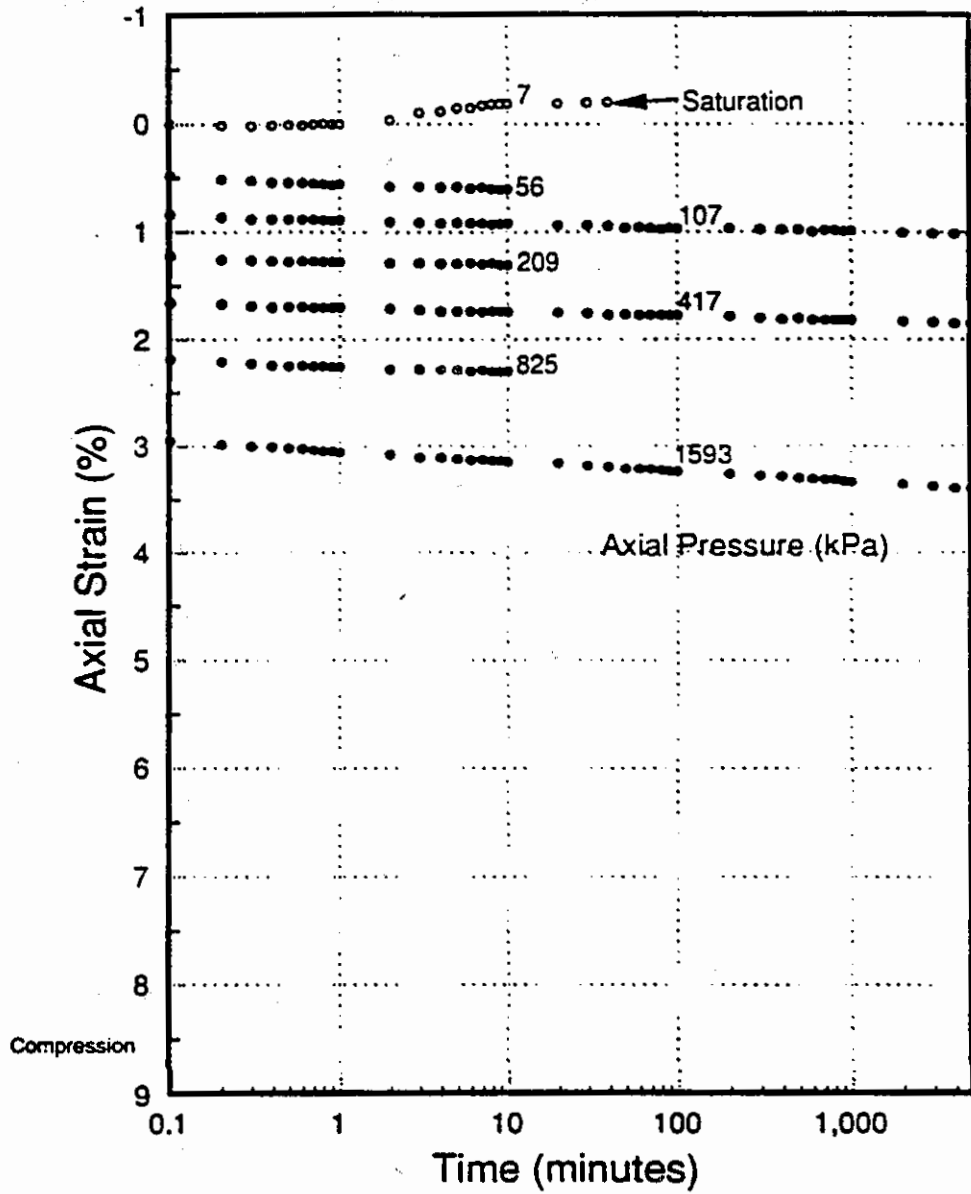


Figure 3.6 Axial strain versus log time in oedometer specimen C155a, RC = 95%, $w_c = 8\%$

Table 3.1 Oedometer test program

Test #	RC (%)	Last Loading Stage		Wetting Stage		Remarks
		Pressure (kPa)	Duration (min)	Pressure (kPa)	Duration (min)	
C101	90	100	100	10	total	
C102	90	400	100	10	total	
C103	90	1500	100	10	total	
C104	90	6000	100	10	total	Tested in a different set-up
C105	90	1500	5000	10	total	5000 min. at 100 & 400 kPa as well, Unloaded at 400 kPa to 100 kPa & reloaded
C106	90	1500	100	10	total	Water content = 6.5%
C107	90	1500	100	10	total	Water content = 5.0%
C151	95	100	100	10	total	
C152	95	400	100	10	total	
C153	95	1500	100	10	total	
C154	95	6000	100	10	total	Tested in a different set-up
C155	95	1500	5000	10	total	5000 min. at 100 & 400 kPa as well, Unloaded at 400 kPa to 100 kPa & reloaded
C201	90	100	100	100	100	Wetted after 100 min. under maximum load
C202	90	400	100	400	100	Wetted after 100 min. under maximum load
C203	90	1500	100	1500	100	Wetted after 100 min. under maximum load
C206	90	1500	100	1500	100	Wetted after 100 min. under maximum load, Water content = 6.5%
C207	90	1500	100	1500	100	Wetted after 100 min. under maximum load, Water content = 5.0%
C251	95	100	100	100	100	Wetted after 100 min. under maximum load
C252	95	400	100	400	100	Wetted after 100 min. under maximum load
C253	95	1500	100	1500	100	Wetted after 100 min. under maximum load
C301	90	0	0	-	-	Compaction only
C302	90	0	0	10	100	Soaking only
C351	95	0	0	-	-	Compaction only
C352	95	0	0	10	100	Soaking only

- Note:
1. Specimens are labeled in the order of replication, C101a, C101b, etc...
 2. Normal load is maintained for 10 min. only, unless otherwise specified.
 3. RC - Relative compaction (Maximum dry density = 20.3 kN/cu.m.)
 4. Remolding water content is 7.5 - 8.5%, unless otherwise specified.

C106 and C107, were conducted on specimens compacted at water contents lower than the usual 8.0 percent.

The C200 test series was performed to investigate the extent of hydrocompression in decomposed granite. First, one specimen each was loaded in increments as-compacted, up to the stages 100, 400 and 1500 kPa. The specimen were wetted after 100 min. under the particular maximum load, and further settlement was recorded for another 100 min. By then, generally, the settlement-log time curve had become straight again. Two drier specimens, C206a and C207a, were also subjected to hydrocompression to study the effect of compaction water content. No denser specimens were prepared at reduced water contents, mainly because it is difficult to achieve 95 percent relative compaction under these conditions.

Breakage levels prior to loading were obtained by conducting the C300 series tests. Two specimens were used as-compacted and the other two were inundated under the seating load for 100 minutes.

Typical results from a specimen at 90 percent relative compaction (C103a) are shown in Figure 3.7. The compression curve shows a gradually increasing slope up to the maximum pressure used, about 1500 kPa.

3.3 Triaxial test program

3.3.1 Specimen dimensions

ASTM D4767-88, the Standard Test Method for Triaxial Compression Tests, recommends the diameter of triaxial specimens be at least 6 times the D_{\max} . The specimen diameter of 2.81 inches (71 mm), for which there are standard equipment, was judged to be sufficient for this material, since D_{\max} is 12.5 mm and 94 percent of the material passes through the #4 sieve (4.76 mm opening). Specimen height was chosen as 150 mm (6 in) to be within the 2 to 2.5 height/diameter ratio stipulated by ASTM D4767-88.

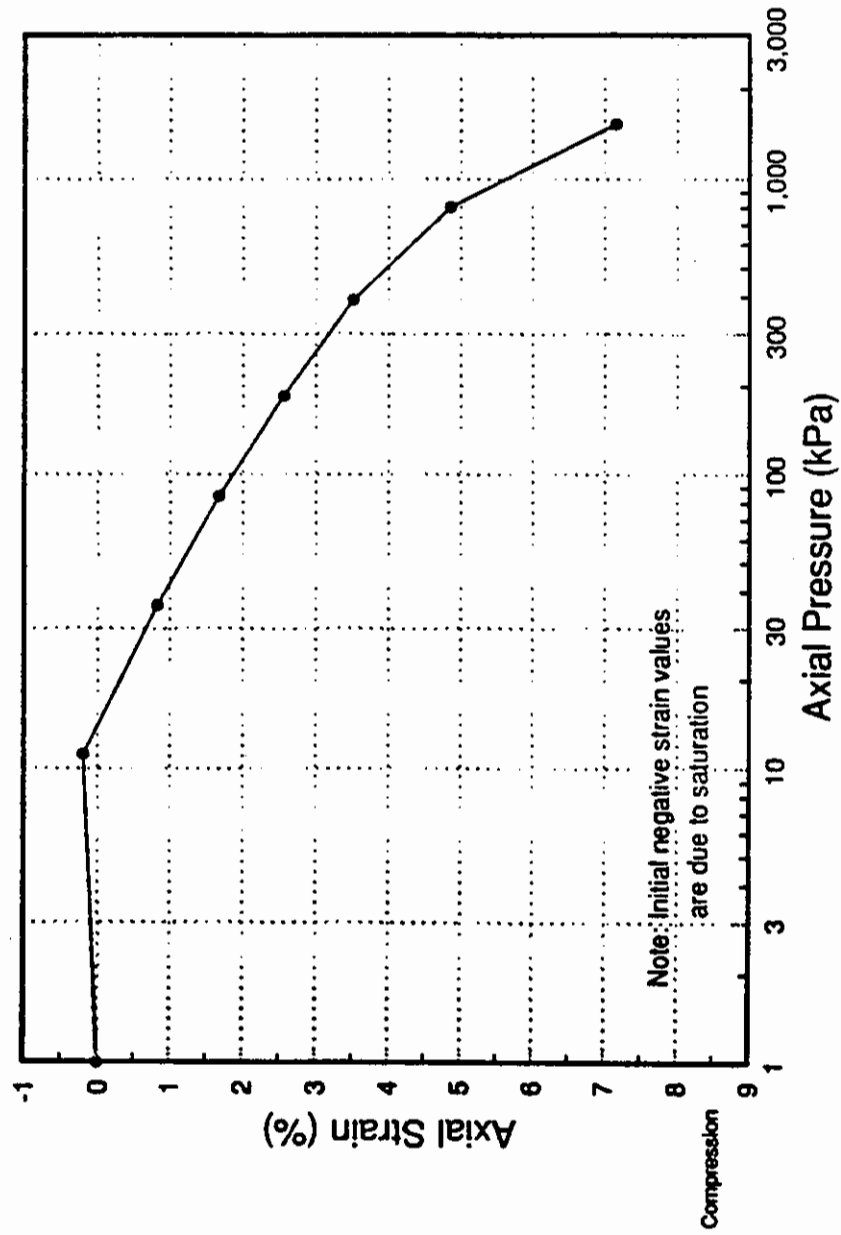


Figure 3.7 Axial strain versus log axial pressure in oedometer specimen C103a, RC = 90%, $w_c = 8\%$

3.3.2 Specimen preparation

Specimens were compacted in a split mold with an inside diameter of 71 mm. The modified hand press, used for oedometer testing, was used to compact the material here as well. The kneading foot was changed to a diameter of 38 mm. The spring, mounted inside the press, was adjusted to set off the signal at the same maximum compaction pressure, about 860 kPa. The full specimen height was reached in six layers of 25 mm each. Each layer height was first roughly controlled using a marker in the compacting foot. More precise control was maintained using a height-adjustable tamper, which was also used to apply the final compactive forces. Weight of soil per each layer was controlled maintaining about 0.5 percent (of relative compaction) undercompaction per layer.

After compaction, the specimen was weighed and transferred to the triaxial base, and then two membranes were stretched over it. Two membranes were used as a single membrane may be punctured during the test by angular decomposed granite particles. At confining pressures above 900 kPa, three membranes had to be used, as two were not sufficient. Porous stones, or at high pressure porous brass discs, were provided at the top and the bottom of the specimen to facilitate drainage. The height and the diameter of the specimen were measured after applying a low vacuum. Next, the triaxial chamber was assembled and a vacuum of about 95 kPa was applied. For specimens consolidated under low pressures, the chamber was also supplied with enough vacuum to keep the effective stress below about 70 kPa. The specimen was then slowly flooded with de-aired water through the bottom while a high vacuum was applied to the top. After thoroughly flushing the specimen with water, vacuum was reduced while introducing back pressure. Back pressure was increased until a B-value of 0.96 or greater was achieved.

3.3.3 Testing and measuring equipment

Two test facilities were used for the triaxial test program. The first test facility has the capacity to conduct triaxial tests under confining pressures up to about 600 kPa. The series of tests conducted at this facility, identified as the low

pressure phase hereafter, consisted of 9 specimens. Back pressure, confining pressure, and the axial load were provided by pressurized air. For axial load, pressurized air input is fed into a 140 mm (5.5 in.) diameter hydraulic Bellowfram piston through a servo valve. The piston, mounted on the cross bar of a loading frame, is also connected in parallel to a hydraulic reservoir. Pressurized oil drives the 20 mm diameter piston rod which transmits the axial load to the specimen. The servo valve, controlled by a computer, provides a closed-loop system, with feedback either from the load or the displacement transducer. The consolidation phase of all triaxial tests was carried out under load control and the shearing phase under displacement control, at a rate of about 0.25 mm/min, which corresponds to a strain rate of 0.2 percent/min.

Axial load is measured by an external 3000 lbf (13 kN) S-type load cell, attached to the loading piston through a swivel coupling. A 2.0 inch (50 mm) full range LVDT, attached to a small cross bar immediately below the load cell, is used to measure the axial displacement. Confining pressure, effective pressure (difference between the confining pressure and the back pressure) and the volume change are measured by three pressure transducers. All measuring devices are connected to the computer that controls the servo valve. A software package, named Automated Testing Systems (Sousa and Chan, 1991), along with the relevant hardware, facilitated instrument calibration, servo valve control, data acquisition and real-time data display for this test program.

The high pressure test facility has the capacity to test specimens under confining pressures up to 1000 psi (7 MPa). All triaxial tests at confining pressures above 600 kPa were conducted at this facility. Here, back pressure is supplied by compressed air. Confining pressure is supplied by dry Nitrogen, stored under about 2500 psi (17 MPa) pressure in 255 cu. ft. (7 m³) tanks. The axial load, during the consolidation phase, is supplied by a 3000 lbf (13 kN) hydraulic actuator. The actuator is controlled by a hydraulic servo valve. However, the force supplied by the piston is not sufficient to shear the triaxial specimens under confining pressures used in the test program, pressures as high as 1500 kPa. Therefore, a gear driven 10,000 lbf (44 kN) loading machine, capable

of a wide range of constant displacement rates, was employed to provide the deviator load.

The same set of measuring devices as in the low pressure phase were used in the high pressure phase of testing, except for the measurement of deviator load, where a 10,000 lbf (44 kN) diaphragm type load cell was used. The equipment calibration, servo valve control and data acquisition were conducted with the same computer program as before.

3.3.4 Test program

Table 3.2 summarizes the triaxial test program. The T100 test series was designed to study the variation in shear strength and volume change with increasing confinement. It also allowed the investigation of the effects of stress level on particle breakage. Specimens for tests T101, T102, T104 and T105 and the corresponding denser specimens were tested during the low pressure phase. A few more T105 and T155 tests were conducted at the high pressure facility to check whether there were any differences in results due to changes in equipment. In addition, two tests at 300 kPa confining pressure, T103 and T153, were also conducted at the high pressure facility to ensure the trends of the mechanical behavior of the material were consistent between the two apparatuses. The highest confining pressure used was 1500 kPa, which is sufficient to meet the maximum stress requirements stated in section 3.1.5. The test T159 was performed to estimate the breakage only due to consolidation.

All tests in T100 series were terminated at about 20 percent axial strain level. Therefore, the effect of applied strain level on particle breakage results of T100 series specimens will be the same. There is strong evidence that the applied strain level has a great impact on particle breakage, especially under triaxial conditions (Fedaa, 1971). The three tests in T200 series were conducted to investigate this effect. Two were performed at 900 kPa confinement, the same as test T156, and were terminated at axial strain levels of 10 and 15 percent. At these strain levels, the specimens had already passed the shear failure, the maximum obliquity, and hence all of them are subjected to (approximately) the

Table 3.2 Triaxial test program

Test #	RC (%)	Type	Conf. Pres. (kPa)	T.A.Strain (%)	CSR (Kc)	Remarks
T101	90	ICD	100	20	1.0	
T102	90	ICD	200	20	1.0	
T103	90	ICD	300	20	1.0	
T104	90	ICD	400	20	1.0	
T105	90	ICD	600	20	1.0	
T106	90	ICD	900	20	1.0	
T107	90	ICD	1200	20	1.0	
T108	90	ICD	1500	20	1.0	
T151	95	ICD	100	20	1.0	
T152	95	ICD	200	20	1.0	
T153	95	ICD	300	20	1.0	
T154	95	ICD	400	20	1.0	
T155	95	ICD	600	20	1.0	
T156	95	ICD	900	20	1.0	
T157	95	ICD	1200	20	1.0	
T158	95	ICD	1500	20	1.0	
T159	95	-	900	20	1.0	Consolidation only
T251	95	ICD	1000	5	1.0	
T252	95	ICD	900	10	1.0	
T253	95	ICD	900	15	1.0	
T351	95	ACD	900	20	1.8	
T352	95	ACD	900	20	2.5	
T353	95	-	900	-	1.8	Consolidation only
T354	95	-	900	-	2.5	Consolidation only
T401	90	-	-	-	-	Compaction only
T451	95	-	-	-	-	Compaction only

- Note:
1. Specimens are labeled in the order of replication, T101a, T101b, etc...
 2. RC - Relative compaction (Maximum dry density = 20.3 kN/cu.m.)
 3. T.A.Strain - Axial strain at which a test is terminated
 4. CSR - Consolidation Stress Ratio (Kc)
 5. Remolding water content is 7.5 - 8.5%.

same maximum stress level. The third, test T251, was conducted under about 1000 kPa confinement so that at about 5 percent axial strain (i.e., prior to failure), the specimen would be subjected to a similar maximum stress level.

The test series T300 was designed to study the effect of stress path on particle breakage, and hence on volume change and shear strength characteristics. Two specimens were anisotropically consolidated at two K_c levels, 1.8 and 2.5, and then dismantled to estimate breakage. Two others were continued on the same path and then sheared. All tests in the series T200 (except T251) were performed at a confining pressure of 900 kPa and a relative compaction of 95 percent. The same conditions were chosen for the test series T300 so that portions of the test results could be used interchangeably to strengthen the final conclusions. Furthermore, dense specimens were expected to provide larger differences than loose specimens in volume change and shear strength characteristics, when subjected to different K_c values. The T400 test series is an attempt to estimate particle breakage due to compaction alone.

Typical results from the shearing phase of a triaxial test are shown in Figure 3.8, in terms of the deviator stress, the principal stress ratio and the volumetric strain, against the axial strain. The specimen was compacted at 95 percent relative compaction and sheared under a confining pressure of 400 kPa. It exhibits a clear peak in principal stress ratio, and with additional strain reaches a residual value. Volume change behaves accordingly, contracting initially but then dilating rapidly as the specimen reaches the failure.

3.3.5 Correction for membrane penetration

During a triaxial test, whenever the confining pressure is increased, the membrane surrounding the specimen may penetrate deeper into the valleys between granular particles on the surface. During consolidation, this membrane penetration adds to the volume change caused by contraction of the soil skeleton. In conventional drained triaxial tests where the confining stress is kept constant in the shearing stage, such as the tests conducted in this test program, this error occurs only in the consolidation phase. Anwar (1989) provides an excellent

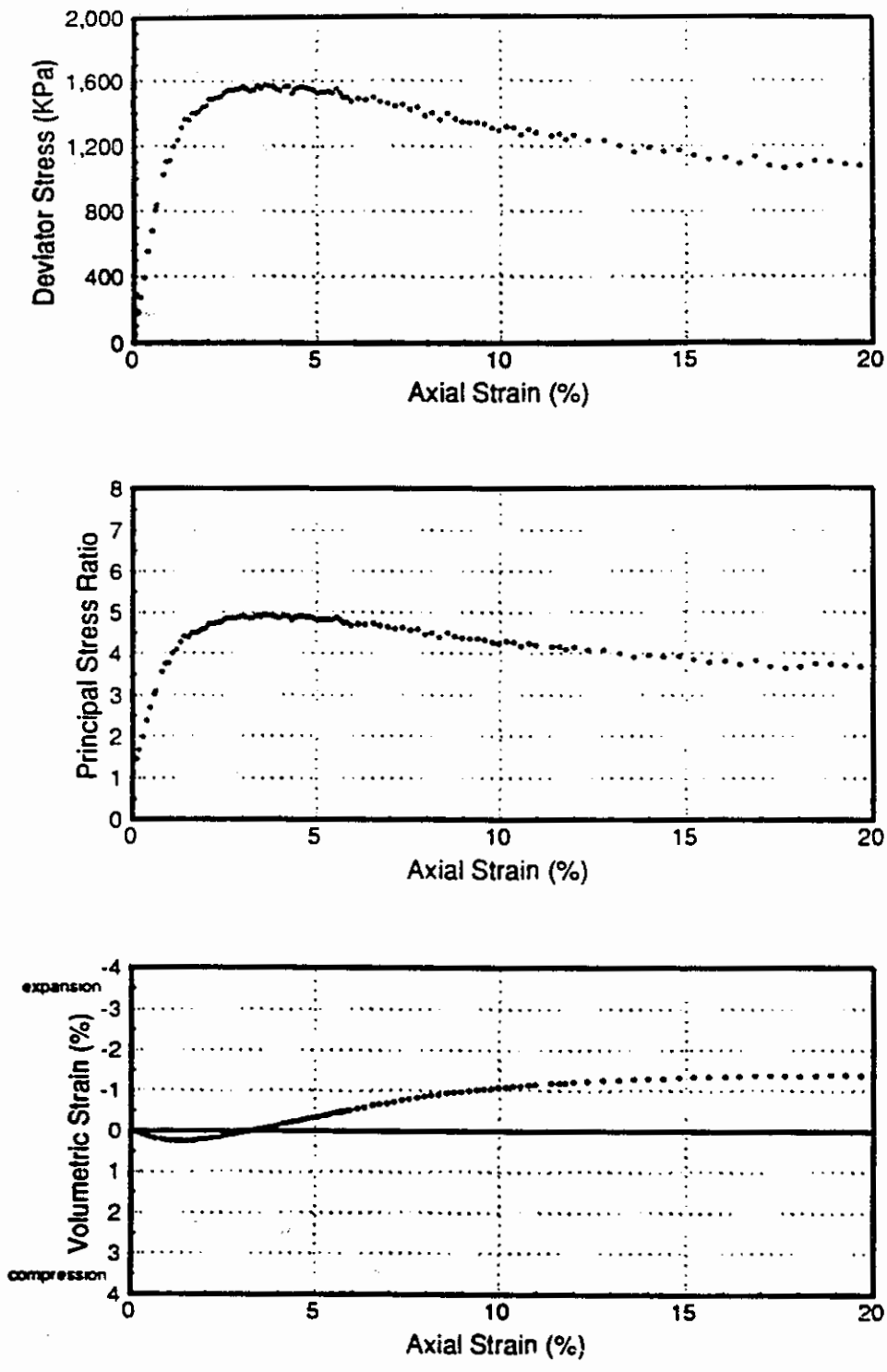


Figure 3.8 Test results of triaxial specimen T145a, RC = 95%, $\sigma_c = 400$ kPa

discussion of the effect of membrane penetration on volume change measurements in triaxial tests of granular materials. His main findings are that particle gradation is the single most important factor affecting membrane penetration, and that the other factors, density, particle angularity, membrane thickness, etc., are insignificant compared to the influence of particle gradation. These findings are said to be valid not only for Monterey sand that he used, but also for a range of granular materials, from gravel to fine sand. The membrane penetration is expressed in terms of Unit Membrane Penetration, S (cm^3/cm^2), which is defined as the amount of volume change per unit of membrane surface area per log cycle of change in confining pressure. This parameter is linked to D_{20} (in mm) by the following equation:

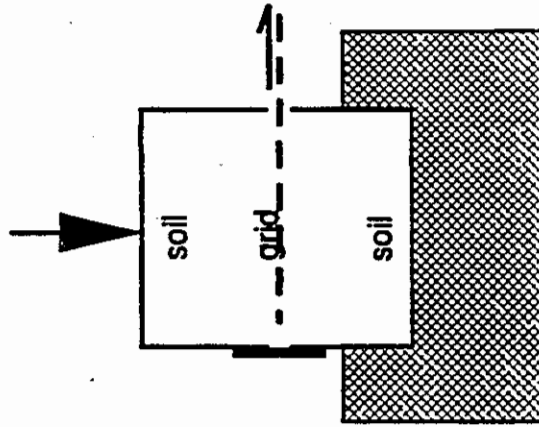
$$S = 0.0009 [\log_{10} D_{20} + 2.1]^{3.57} \quad (3.1)$$

Lee (1991) established a value for S for the type of decomposed granite material he was testing. He used an experimental technique which is questioned by Anwar (1989) on the grounds of greater experimental error. However, the value of S obtained by Lee corresponds fairly well with the value calculated from equation 3.1 using the D_{20} value for the material Lee used.

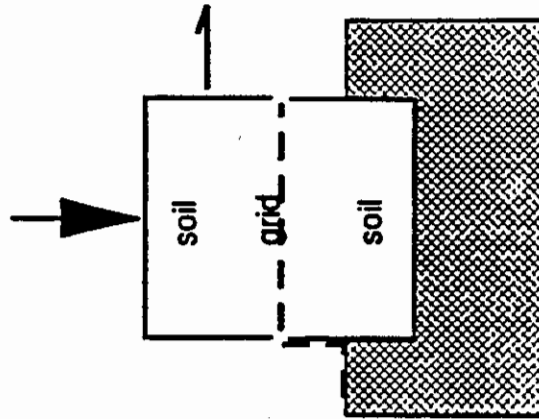
Therefore, for the use of this test program the S value was calculated using Equation 3.1. The D_{20} value for the batch of material used for the triaxial test program is 0.3 mm and the corresponding S value is $0.0046 \text{ cm}^3/\text{cm}^2$. The results given in later chapters have been corrected for membrane penetration using this S value.

3.4 Direct shear and pullout test program

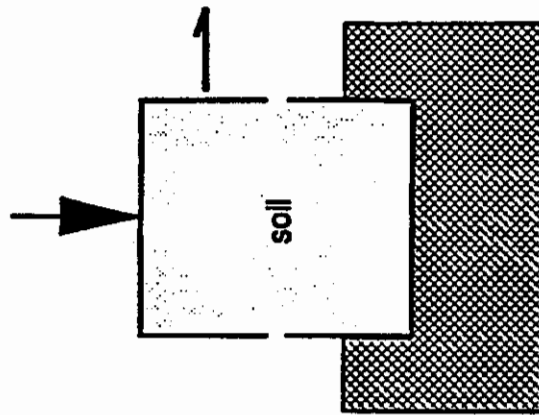
The direct shear and pullout tests were conducted to evaluate the feasibility of employing geosynthetic reinforcements to steepen the side slopes of a decomposed granite embankment. There are three relevant test configurations: a) direct shear tests of soil alone; b) direct shear tests of soil over the geosynthetic reinforcement; and c) pullout tests. They are illustrated in Figure 3.9. The interface friction between soil and the reinforcement is determined by test type



c) Pullout Test



b) Direct Shear Test
(soil over grid)



a) Direct Shear Test
(soil over soil)

Figure 3.9 Typical direct shear and pullout test configurations

(b). The anchoring of the reinforcement by soil under normal pressure, the pullout capacity, is determined by the test type (c). The test type (a), the conventional direct shear test, is used to obtain the normalizing shear strength properties of decomposed granite. Conventional triaxial test results from the previous test program are not used for this purpose because the failure mechanism and the size of triaxial specimens are very different from those of pullout tests.

3.4.1 Specimen dimensions

The type of reinforcement most useful for this gravelly sand material is a geogrid. The interaction between a geogrid and soil particles is discussed in detail in Chapter 6. A geogrid with large apertures will trap the soil particles and may move the shearing plane away from the interface, thus increasing the shear resistance. Also, the bearing members of a geogrid will develop some passive resistance. Thus, to conduct pullout tests of geogrids, a relatively large scale equipment is needed. Farrag and others (1993) discuss in detail the various factors such as, equipment configuration, specimen placement conditions, testing conditions, etc., that could affect the results of a laboratory geogrid pullout test. The ASTM standard test method for pullout testing (1992 draft) recommends a pullout box with minimum dimensions of 1.5 m x 0.6 m and a minimum soil thickness of 150 mm each above and below the grid. But, considering that decomposed granite cannot be reused after a laboratory test, using such a large box would require a large amount of valuable material, which was available only in limited quantity.

The University of California at Berkeley geotechnical laboratory has a large direct shear box with a plan area of 435 mm x 283 mm (17.1 in x 11.1 in) and a total depth of 300 mm (12 in). This box could also be modified for pullout testing. For direct shear tests, the minimum width stipulated by ASTM D3080-90 (the Standard Test Method for Direct Shear Test of Soils under Consolidated Drained Conditions) is ten times the D_{max} . The D_{max} being 12.5 mm for the decomposed granite used in the test series, the said shear box easily satisfies this

requirement. The minimum soil thickness stipulated by ASTM D3080-90 is six times the D_{max} , and the minimum width/thickness ratio is 2:1. A soil thickness of 100 mm thus seemed sufficient for direct shear tests. No standard guidelines have yet been set for geogrid interface shear strength tests. The shear box discussed above, therefore, was used for interface strength tests as well, with a slight modification to facilitate clamping the grid at one end. The same total soil thickness with 50 mm of soil above and below the grid was deemed sufficient because, in this case, dilatancy of soil has been found to lower than in shearing of soil alone (see Chapter 6 for details).

Because of the general similarity in the mode of soil failure in pullout and direct shear tests, it was decided that the above shear box, which satisfies the direct shear test criteria, is suitable for pullout tests as well, at least for research purposes. The total soil thickness, as described later, was set at 150 mm after conducting several preliminary tests to investigate its effect on pullout test results.

The high pullout loads, expected under high normal pressures, dictated that a high strength geogrid be used. Moreover, a limitation on the maximum pulling distance in the apparatus (about 50 mm) allowed the use of only relatively inextensible grids. To reduce end effects, the grid should preferably have a minimum of 4 or 5 bearing members within the confined length and a sufficient number of apertures cross-wise. The geogrid that met most of the set criteria was Matrex 240, a woven grid whose aperture size is about 90 mm x 8 mm and the tensile strength at 5 percent strain is about 146 kN/m. Tensar geogrid UX1700 (SR-4) also met many of the criteria but its relatively low tensile strength could have resulted in tensile failures at high normal pressures.

3.4.2 Design and fabrication of testing equipment

The unusually large normal pressures required for the test series, up to 800 kPa as stated in section 3.1.5, posed several difficulties that again prevented close adherence to the ASTM (draft) guidelines on pullout test equipment. The provision of an air bag to evenly distribute the normal load, as ASTM recommends, was found to be impractical under these high pressures.

Furthermore, the ASTM draft recommends the clamp that holds the grid be placed between a metal sleeve which is to be fixed inside the shear box adjoining the gap through which the pull is applied (see, Figure 3.10). This technique, it is expected, would reduce the additional restraining effects on the grid caused by soil pressure against the front wall. It would also keep the grid confined by soil throughout the pullout process. However, providing such a sleeve that can withstand the high normal pressures, and designing such a pulling mechanism for the high pullout loads expected in this case were impractical. To reduce friction from side walls of the box, as suggested by ASTM guidelines, 3 mm thick Teflon sheets were glued to the walls.

The final design of the shear/pullout box is schematically shown in Figure 3.11. The top half of the shear box is movable during direct shear tests, and the two halves were clamped during pullout tests leaving an opening of about 8 mm. The box halves are made up of 12.5 mm thick steel plates bolted together at the corners. The normal load is applied by a 20 ton (200 kN) hydraulic piston and the reaction is provided by a iron box girder attached to the fixed bottom box by two steel cables. The normal load is transferred by the steel platform containing the piston housing, through a 37 mm thick aluminum plate, to the 12.5 mm thick steel loading plate that closely fits the top box. A set of plywood planks, each 25 mm thick, attached to the bottom of the steel loading plate, finally transfers the normal load to the soil. A similar set of plywood planks is placed at the bottom of the bottom box. These easily removable planks allow the thickness of the soil layer to be varied without any major modification to the apparatus. Hydraulic pressure to the vertical piston is supplied by a hydraulic jack, operated manually. Minor adjustments to the hydraulic pressure can be made using a screw pressure intensifier connected in parallel (not shown in the figure).

The horizontal shear load, or pull, is applied using another 20 ton (200 kN) hydraulic piston which pushes against a sturdy box girder linked by steel cables to the movable box (in direct shear tests), or to the clamp (in pullout tests). Figure 3.12 shows the apparatus as set up for a pullout test. During a direct shear test, the cables are connected to a rectangular steel frame that is loosely attached to

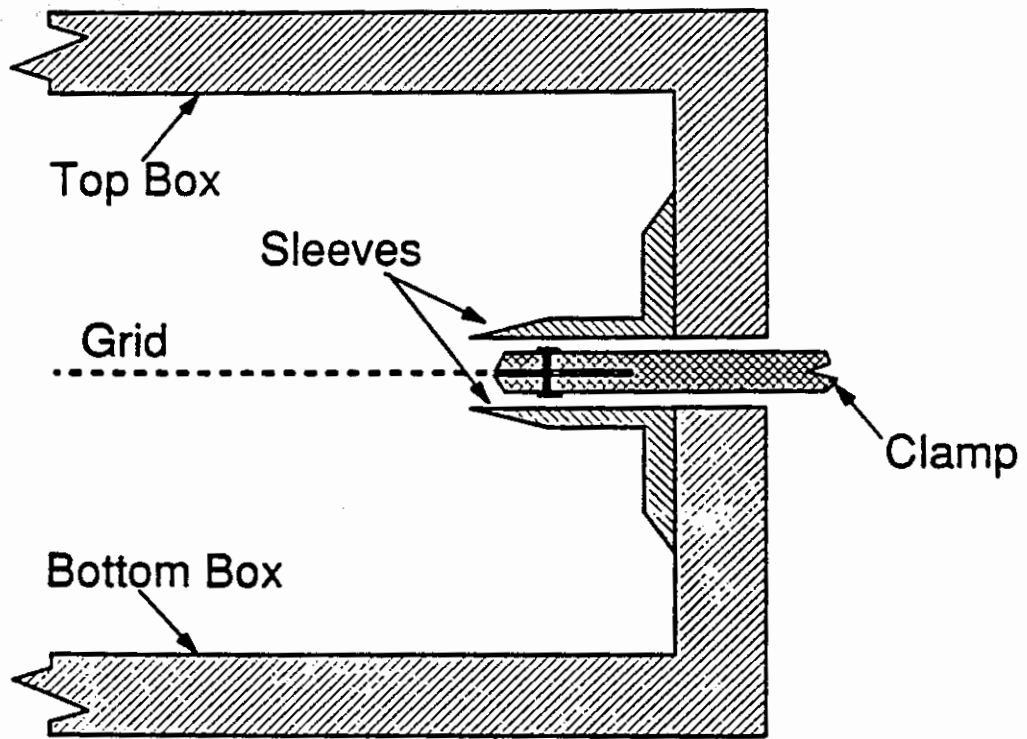


Figure 3.10 Pullout test clamping arrangement recommended by ASTM (1992 draft)

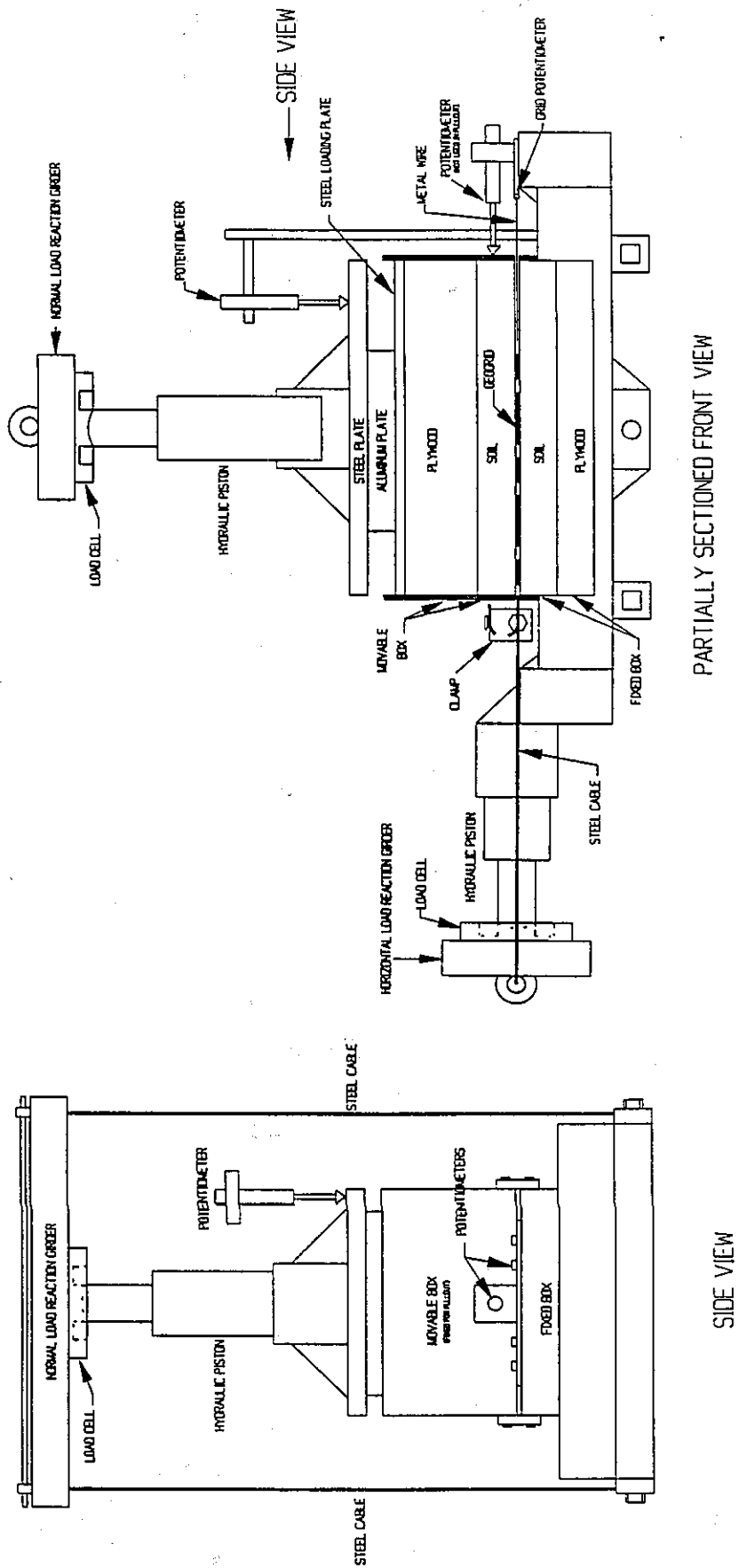


Figure 3.11 Schematic diagram of direct shear and pullout apparatus

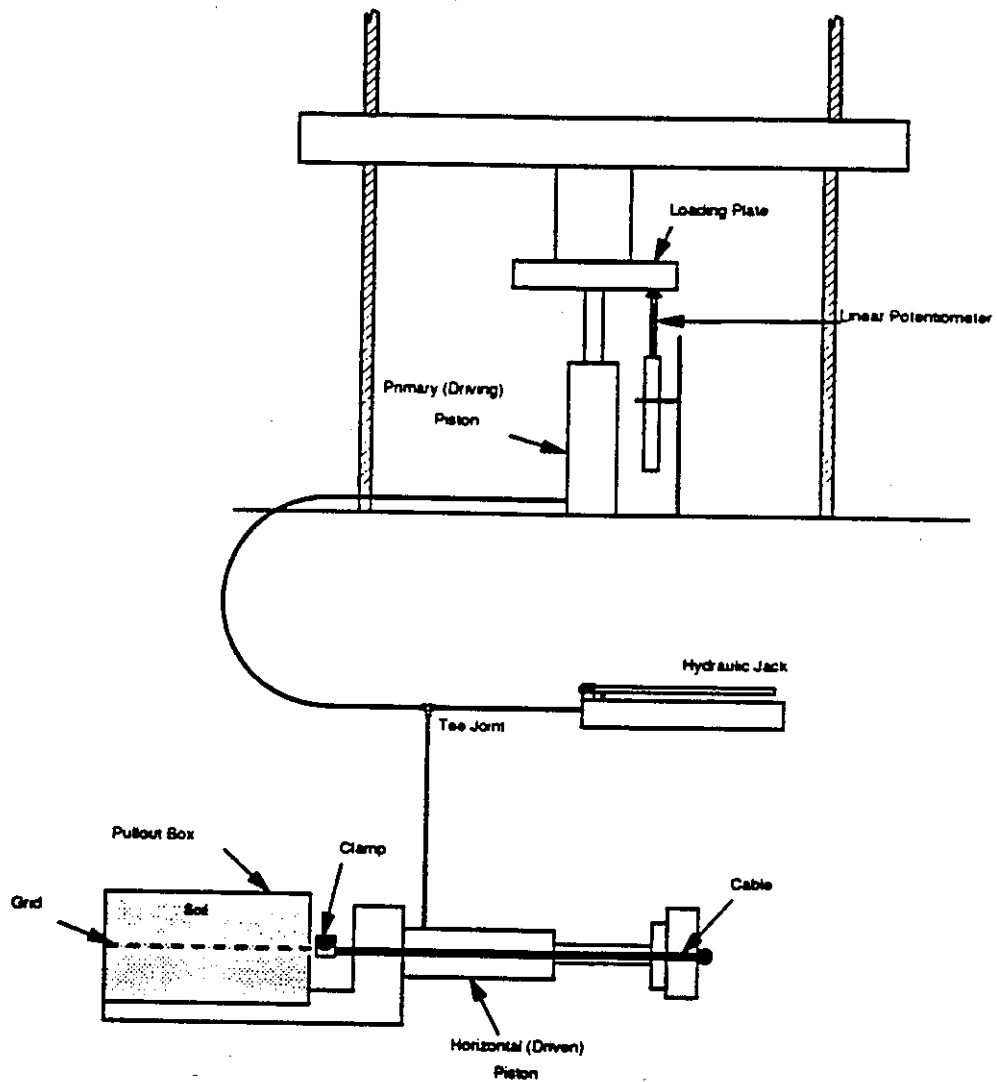


Figure 3.12 Schematic diagram of the horizontal loading mechanism for pullout tests

the movable top box just above its bottom edge. The piston housing fixed to the bottom box provides the reaction in either case. Since it is imperative that the grid or the top box should be pulled at a constant rate of displacement, a screw driven compression loading machine is also employed during the tests. It drives-in another piston, similar and hydraulically connected to the horizontal piston. A hydraulic jack, connected in parallel, is used initially to push the pistons out—the horizontal piston until the cables become slightly taut, and the driving piston (placed vertically under the compression machine) until it touches the loading plate of the machine (see, Figure 3.12). As the compression machine pushes-in the driving piston at a constant rate of displacement, the displaced hydraulic oil pushes-out the horizontal piston at the same rate. The rate of horizontal displacement used was about 0.5 mm/min.

The clamp that holds the geogrid had to be designed to withstand loads up to about 65 kN (15,000 lbf). A 275 mm (11 in) long, 38 mm (1.5 in) in diameter, tempered 4140 steel rod was used as the clamp. The grid is wrapped around the rod about 270°. A steel strip, whose underside is knurled for a better grip, is then placed over the grid and attached to the rod with six evenly spaced bolts (see, Figure 3.13). This arrangement reduces concentrated loads in the grid near the bolts and distributes the pull fairly well. The steel cables that pull the clamp are attached to the clamp with bolts, which are located at the same plane as the geogrid to reduce twisting.

3.4.3 Specimen preparation

Because of the large amount of material and effort required to perform a single test in this apparatus, only one level of soil density was chosen for the test series. The denser level, 95 percent relative compaction, was chosen since it is expected that the differences in shear strength at different normal pressures will be greater in dense samples. The compaction water content was maintained at about 8 percent as before.

Kneading compaction technique was used again to compact the soil to the required density. To achieve uniform soil density, both the pressure under the

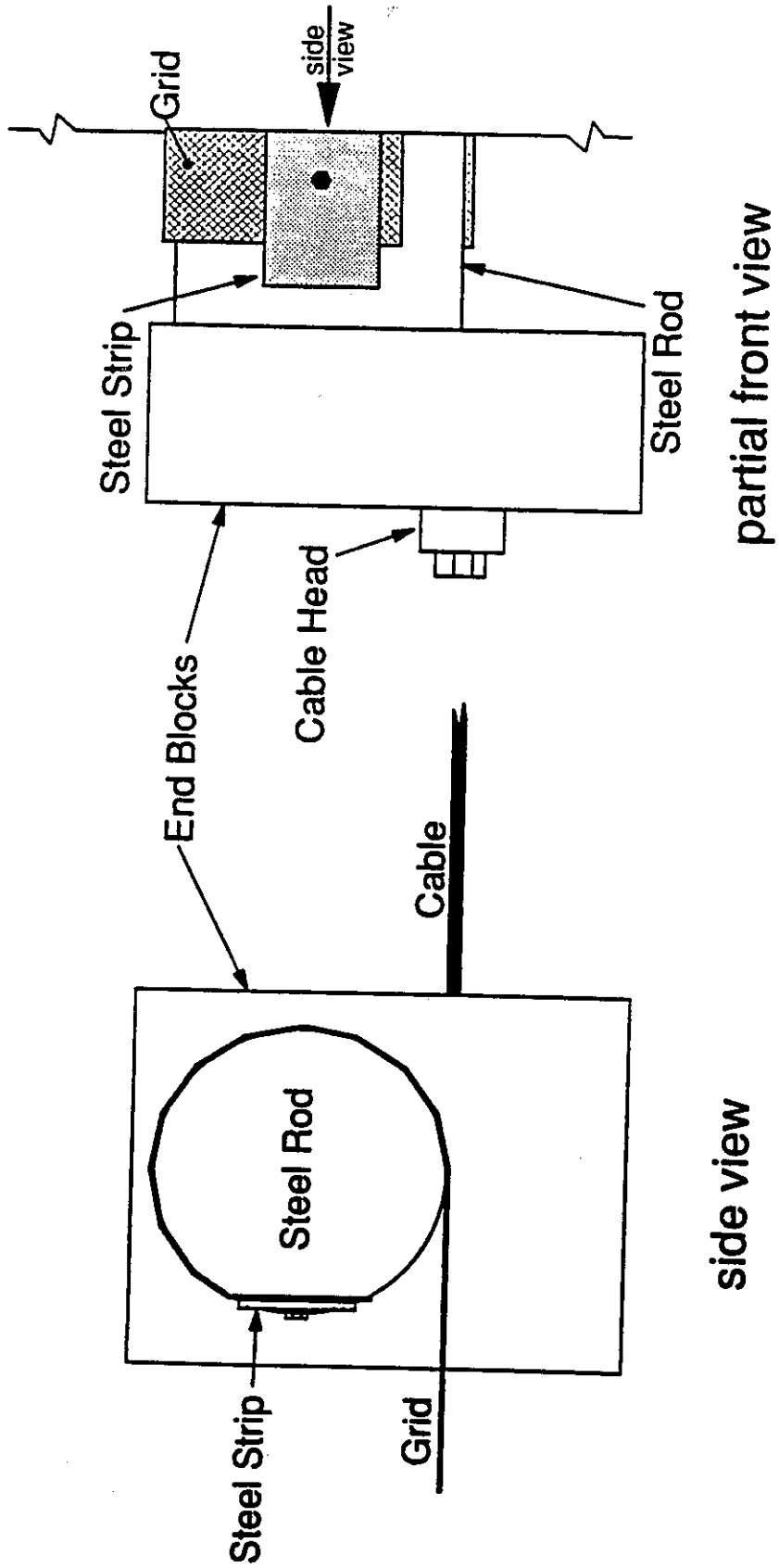


Figure 3.13 Schematic diagram of the clamp used in the pullout tests

compaction foot and its depth of travel must be controlled. Figure 3.14 shows a sketch of the kneading foot designed. Two 150 mm x 150 mm x 12.5 mm steel plates are welded to a 38 mm diameter steel pipe. A 3 mm thick steel plate is welded about a third way from the top to serve as a platform for the dial gage that monitors the depth of travel. Soil was usually compacted in 25 mm thick layers. The shear box was placed under the loading plate of a compression machine, and about 860 kPa (125 psi) pressure was applied on the kneading foot, kept vertically on top of soil. Prior to that, the dial gage reading for the final height for that layer was set. Compression was continued until either the loading ram registers a load equivalent to 860 kPa, or the dial gage registers the set height upon rebound. At 95 percent relative compaction, 4 or 5 compression passes of the foot were required, including an initial low pressure pass. Compaction was carried out with a 40 to 60 percent overlap of the kneading foot.

The ASTM D3080-90 recommends that, in conventional direct shear tests of soil, a compaction interface near the shear plane (the gap between the box halves) must be avoided. Therefore, the 100 mm soil thickness in soil-soil direct shear tests was reached in three layers avoiding an interface near the gap, located halfway. During both soil-grid direct shear tests and pullout tests, the compaction interface where the geogrid is laid had to be kept about 5 to 10 mm above the lip of the bottom box, so that the grid would not touch the lip when the soil consolidates under the normal pressure. Therefore, the thickness of the soil layer corresponding to the interface was adjusted to suit. The gap between the box halves in direct shear tests was kept at 6 mm (0.25 in) and in pullout tests at 8 mm.

3.4.4 Measuring devices

Two 40,000 lbf (175 kN) diaphragm type load cells were used to measure the vertical load and the horizontal pull (see Figure 3.11). The spherical seat between the load cell and the piston would prevent eccentric loads if a misalignment were to occur. A spring loaded 75 mm linear potentiometer, mounted on the bottom box, was used to measure the vertical displacement. A

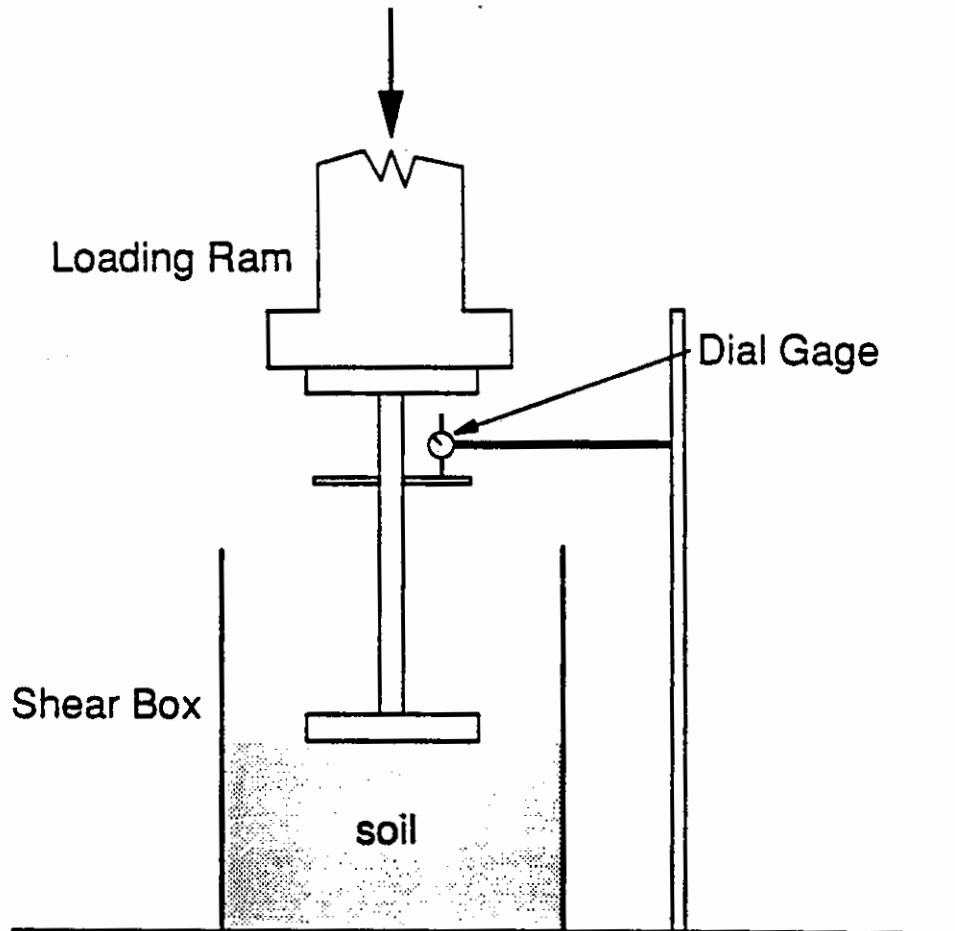


Figure 3.14 *Schematic diagram of the kneading compaction apparatus for direct shear and pullout tests*

similar potentiometer was used to measure the movement of the top box during direct shear tests (set up as shown in Figure 3.11). In pullout tests, the same potentiometer was used to measure the displacement of the driving piston (as shown in Figure 3.12), thus measuring the clamp displacement indirectly.

The extension of the geogrid in soil-grid direct shear tests was measured using four 50 mm spring loaded linear potentiometers fixed to the back of the bottom box. These potentiometers were connected to geogrid bearing members by metal wires, which were run inside 3 mm diameter plastic tubing to avoid soil friction on wires. The same technique was used to measure the geogrid extension in pullout tests. First, the potentiometer wires were laid at a spacing of about 50 mm, resulting in two of the potentiometers connected to the grid near the side edges. After a few tests, it was found that the potentiometer extensions were higher when attached to the middle of the grid (cross-wise) than when attached near the edges of the grid. This difference occurs because the boundary effects cause the grid to deform non-uniformly (cross-wise). This problem was avoided in some pullout tests by removing the two potentiometers at the edges and mounting them on the now fixed top box, just on top of the other two. Mechanical difficulties prevented this corrective measure from being applied to direct shear interface strength tests.

3.4.5 Testing problems and preliminary tests

In both direct shear soil-soil and soil-grid tests, the initial normal pressure increased when shear displacement is increased because of dilation. The normal pressure increase was low in soil-grid tests compared to soil-soil tests. The apparatus has no automatic normal pressure adjustment procedure, and therefore, six initial tests (three each) were conducted without adjusting this increase in normal pressure. Later, to check the impact of varying normal pressure, two other soil-soil direct shear tests (D101b and D103b) were carried out keeping the normal pressure constant manually at about 70 and 400 kPa respectively. In the previous direct shear tests, the reported normal pressure is the value averaged over the full range of shear displacement. It will be shown later that the shear

strength was not affected greatly by the use of average normal pressure. All pullout tests were conducted under almost constant normal pressure, and they did not require any pressure adjustment except in the test under the lowest normal pressure.

It was necessary to determine the effect of soil thickness on pullout strength before proceeding with the full test program. Figure 3.15 shows the results of the P100 pullout test series, where the total soil thicknesses used in the three tests were 100, 150 and 200 mm. Pullout force is shown against the displacement at the back end of the geogrid (gage #1) for each case. The results indicate that a change in the thickness of the soil layer from 100 to 200 mm had some effect on the development of the pullout force. In specimen P101a, where the soil thickness is only 100 mm, the grid seems to have lost the anchoring effect earlier than the others, although the pullout force slowly increased even when the grid is being pulled out. The difference between pullout curves of the 150 mm thick specimen and the 200 mm thick specimen is not significant, and as will be seen in the next paragraph, this difference can be considered within the experimental error. All three tests were terminated at the same amount of pull as measured at the clamp (about 25 mm). Figure 3.15 shows that each test developed almost the same pullout force at termination, regardless of the differences in soil thickness. One reason for this behavior could be that the grid in the 100 mm thick specimen had greater restraining forces acting on it at the front wall, even though it lost anchoring at a lower pull. More discussion on this will follow in Chapter 6. For the rest of the pullout test program, a soil thickness of 150 mm, rather than 200 mm, was used because that allowed significant savings on additional material and effort without jeopardizing the results.

Since this test apparatus does not strictly follow any standard test guidelines, and also since this is the first use of the apparatus for pullout testing, a repeatability check was deemed necessary. The tests P102 and P202 are almost identical except that P202 was pulled out longer. Figure 3.16 shows the pullout force in each test against the displacement at the back end of the geogrid (gage #1). The difference between the pullout forces at the maximum pull of P102 is

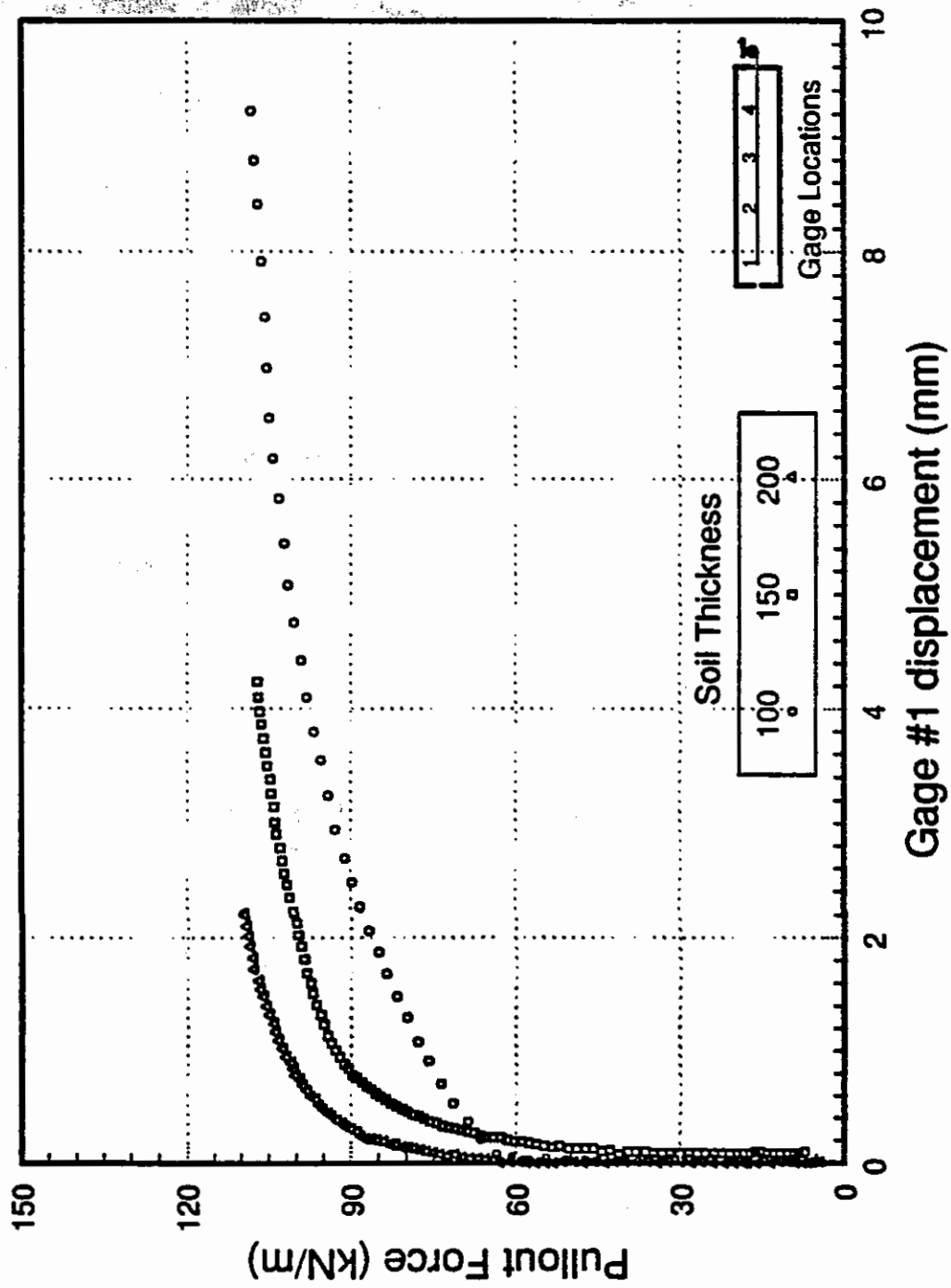


Figure 3.15 Effect of soil thickness on pullout force, $RC = 95\%$, $\sigma_N = 200 \text{ kPa}$

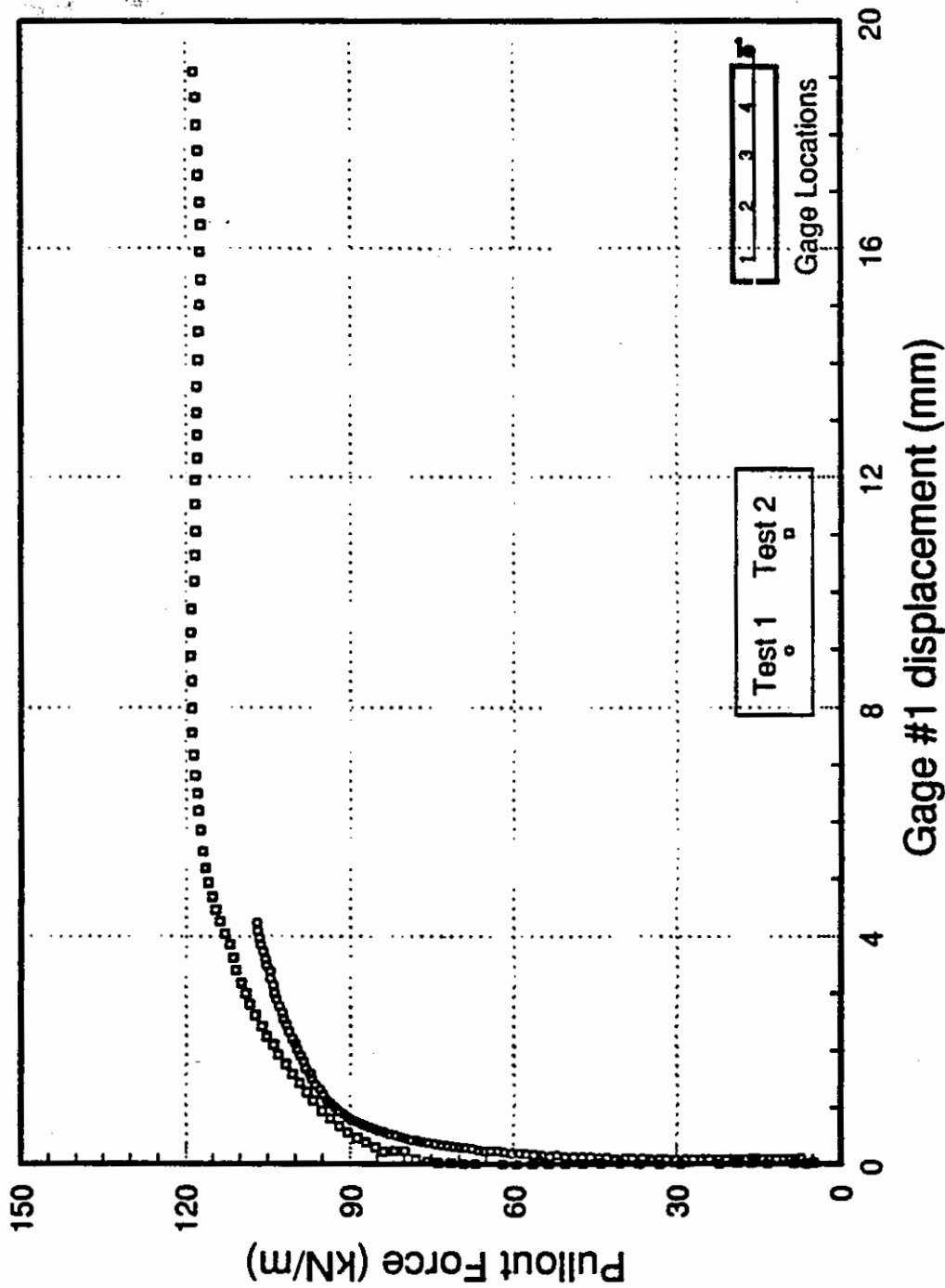


Figure 3.16 Comparison of two similar pullout tests, $RC = 95\%$, $\sigma_N = 200 \text{ KPa}$, soil thickness = 150 mm

less than 10 percent. This difference is accepted as possible experimental error given the possible variations in materials—both the soil and the grid, in compacted density, in setting up measuring devices and in applied forces, both within a single specimen and between specimens.

The intended maximum normal pressure in the direct shear and pullout test series is about 800 kPa, as stated in section 3.1.3. The normal load piston is capable of carrying the corresponding load. However, there were safety concerns about the capacity of the hydraulic lines and the integrity of the cables that provide the reaction to the normal load. In pullout tests, an additional worry was the integrity of the clamping system. Therefore, the direct shear tests were limited to a maximum of 400 kPa normal pressure. One pullout test was performed at a pressure of about 700 kPa at the end of the test program. This pressure is a little less than planned, but still is many times greater than the normal pressures used commonly in pullout tests of this scale.

The vertical displacement in direct shear tests was measured using a potentiometer set up on top of the steel platform that contains the vertical piston housing (see Figure 3.11). This measurement should be considered accurate only up to about 25 mm of shear displacement, because beyond that the steel platform may tilt. Even the prior readings may be somewhat in error because the vertical movement of the platform may not be uniform throughout the specimen cross section.

All pullout and direct shear tests were conducted under soaked conditions, except one pullout test which was conducted as-compacted purposely to check the difference in results. However, keeping the direct shear tests soaked throughout the full range of shearing proved to be a very difficult task. A flexible paraffin film (Parafilm) was mounted covering the gap between the top and bottom box halves. As the top half of the box moves, the film would stretch keeping the box sealed while adding minimum restraint on the pulling mechanism. However, beyond about 25 mm of shearing, the film began to tear apart, letting the water to leak out. Since the soil could still be kept fairly wet by frequently pouring water over it, no other alternative measures were taken to keep the box sealed. The

soil-grid direct shear tests posed a greater problem as the grid had to be fixed outside the back end of the bottom box. The gap in this side was covered first with relatively rigid pipe insulation material, mounted on top and bottom lips, sandwiching the grid. The piece mounted on the top lip brushed the grid keeping the soil inside as the top box moved forward. Both this flexible gate and the clamped part of the grid were later enclosed completely with a polyethylene cover. The polyethylene cover acted as a semi-mobile water bag hanging behind the slowly moving top box. In pullout tests, the only window was at the front where the grid is pulled out, and it was "sealed" with a similar flexible gate made up of pipe insulation material. Another polyethylene bag covering the gap and the moving clamp prevented any leaks.

3.4.6 Test program

The D100 test series, listed in Table 3.3, was designed to investigate the variation of the peak friction angle of soil with normal pressure. The normal pressure given in the table is the initial value, which as mentioned before, tended to increase with shear displacement. The D200 test series was used to investigate the variation of soil-grid interface shear strength with normal pressure.

The purpose of the P100 test series, as discussed before, was to check the effect of soil thickness on the pullout strength. In this series of tests, the tests were terminated at a pull of about 25 mm, in order to compare breakage results from these tests with corresponding tests that were pulled longer. The P200 series tests used a soil thickness of 150 mm and they were terminated at a pull of about 50 mm, measured at the clamp. The P301 test is an attempt to check the effect of density on pullout capacity, and the specimen was compacted at 90 percent relative compaction as opposed to the 95 percent value used in the regular test program. The P401 test was conducted to check the effect of soaking on pullout capacity. It was conducted very early in the test program, and used a soil layer only 100 mm thick.

Post-test particle breakage estimates were made in all the tests. Because of the large volume of each specimen, only a representative portion, two 100 mm x

Table 3.3 Direct shear/pullout test program

Test #	Type	Norm. Pres. (kPa)	Soil Thick. (mm)	Pull Dist. (mm)	Remarks
D101	DS (s-s)	70	100	-	
D102	DS (s-s)	200	100	-	
D103	DS (s-s)	400	100	-	
D201	DS (s-g)	70	100	-	
D202	DS (s-g)	200	100	-	
D203	DS (s-g)	400	100	-	
P101	Pullout	200	100	25	
P102	Pullout	200	150	25	
P103	Pullout	200	200	25	
P201	Pullout	70	150	50	
P202	Pullout	200	150	50	
P203	Pullout	400	150	50	
P204	Pullout	700	150	50	
P301	Pullout	200	150	50	Relative compaction = 90%
P401	Pullout	200	100	25	Tested as-compacted

- Note:**
1. Specimens are labeled in the order of replication, D101a, D101b, etc...
 2. Relative compaction = 95%, unless specified otherwise. (σ_{DD} = 20.3 kN/cu.m.)
 3. Specimens tested inundated, unless specified otherwise.
 4. Pull distance is measured at the clamp.
 5. Remolding water content is 7.5 - 8.5%.

100 mm x 25 mm blocks—one above and the other below the shearing interface, was used for this purpose. During a few pullout tests, a detailed investigation on the thickness of the shear zone around the grid was made using flexible cords installed inside the box prior to pulling. These results will be discussed later along with the results of the rest of the test program.

Results from a typical direct shear (soil-soil) test is shown in Figure 3.17. In this test, the normal pressure was maintained constant manually at about 400 kPa during shearing. The dilatation pressures, that led to manual normal pressure control, are evident in the expansive vertical displacement and in the peak in horizontal force. Figure 3.18 shows the results from a typical pullout test. Pullout force is essentially constant after a pull of about 8 mm, measured by the gages at cross bearing members of the grid. However, at this point, the pull recorded at the clamp is much greater (about 35 mm). The difference is due to stretching of the unconfined portion of the grid (outside the box). The gage #1 was mobilized the last, as expected. However, as the pull continued, it recorded greater displacements than the gages ahead. This may be due to the previously discussed boundary effects that restrain the grid at the edges and thus the gages mounted near the edges, or to some installation problems.

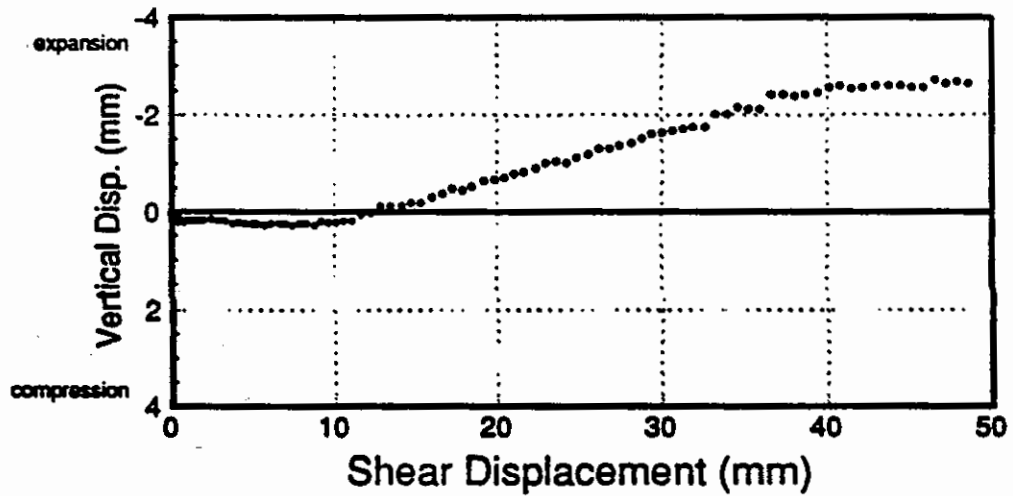
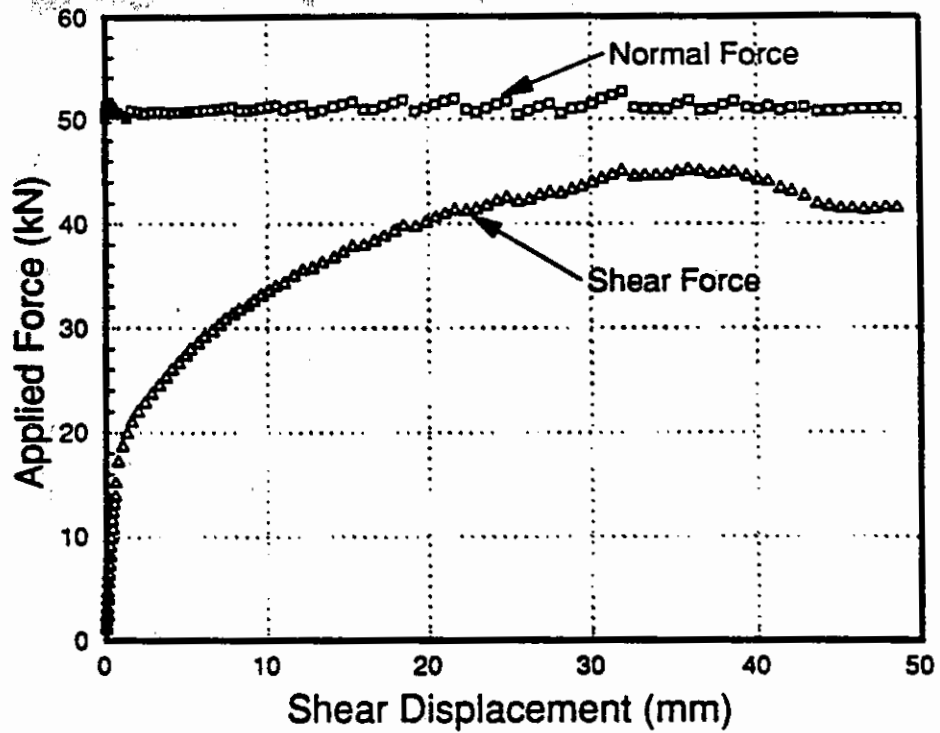


Figure 3.17 Test results of direct shear specimen D103b, RC = 95%, $\sigma_N = 400 \text{ kPa}$

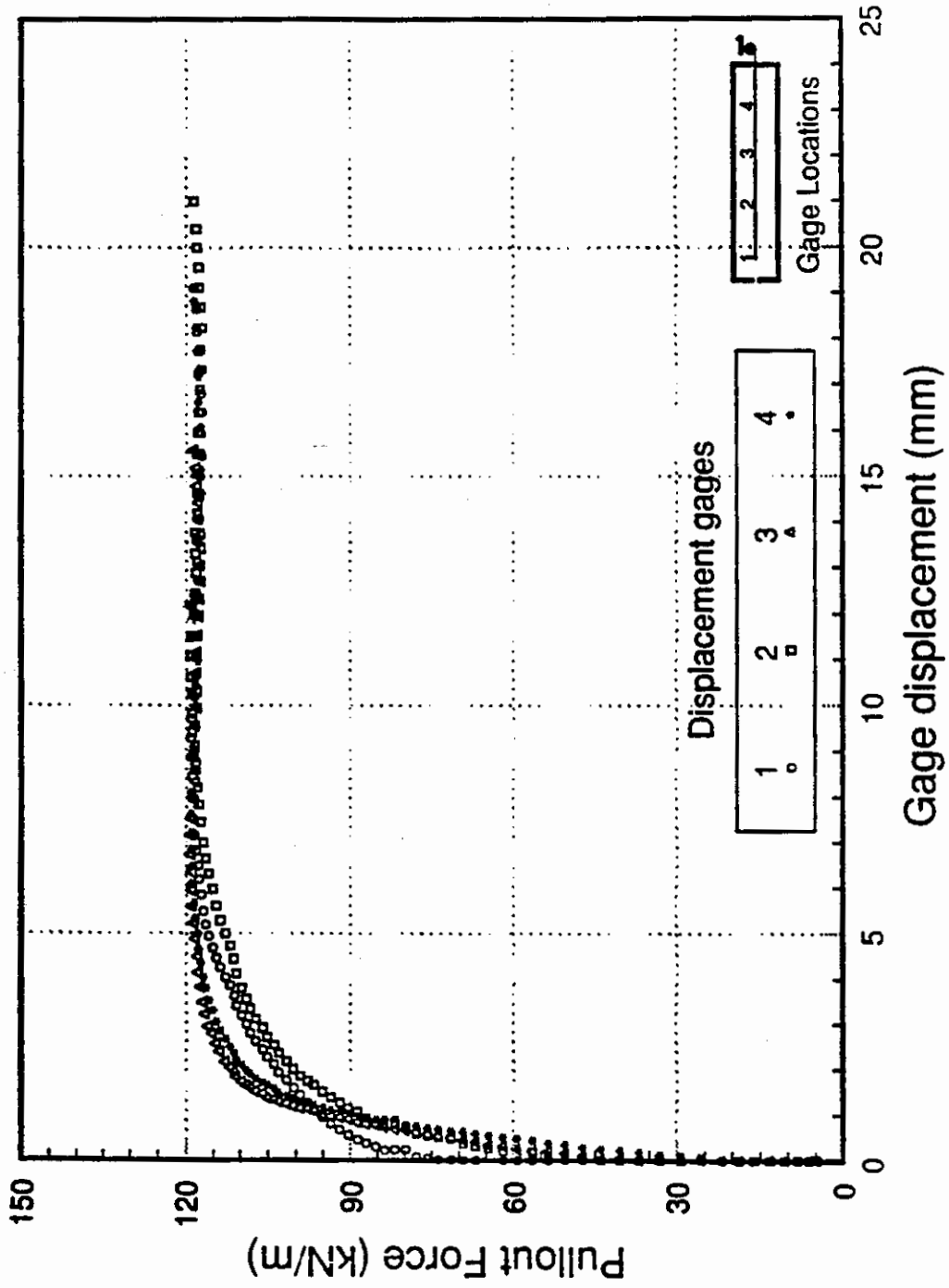


Figure 3.18 Pullout force versus gage displacement in specimen P202b, RC = 95%, $\sigma_N = 200 \text{ kPa}$

CHAPTER 4

FACTORS GOVERNING PARTICLE BREAKAGE

Particle breakage that occurs either in laboratory testing or under field loading conditions consists of two phenomena, namely, separation of aggregated particles and particle crushing. Separately quantifying the contribution of each is difficult. A residual soil like decomposed granite is composed, in large part, of aggregated particles. Some particles are aggregated loosely and some rather strongly, depending on the local effects of the weathering process. Many loosely aggregated particles are separated during excavation and the subsequent mechanical processes of transporting, spreading, and embankment construction. In laboratory sieve analysis, it is mainly the aggregated particle separation that forces adopting more stringent protocols for decomposed granite than for other soils (see Chapter 2). Particle crushing is directly associated with the application of load. In granular materials with little particle aggregation, particle crushing may be the primary mechanism of breakage. In this study, the term particle breakage refers to the total breakage produced by both of these mechanisms.

This chapter is dedicated to the phenomenon of particle breakage of granular materials in general, and of decomposed granite in particular. Decomposed granite's greater susceptibility to breakage, the motive behind this extensive study, is attributed to a number of factors that can be traced back to the origin of the material. A clear understanding of the impact of these inherent factors will help in choosing a fill material appropriate for the particular field application. The next step is estimating the level of breakage in different mechanical processes. A fill material is subjected to a number of mechanical processes in its transit from the borrow area to the embankment. The first, the material handling process, i.e., excavation, transportation and spreading at site, does not impose large compressive forces on particles. In decomposed granite, breakage during handling could still be significant, although very difficult to quantify. Breakage during compaction of decomposed granite is quite significant and also quantifiable. Once compacted, particles in an embankment undergo

breakage due to various combinations of stress and strain levels, imposed by live or dead loads. Finally, soaking also causes substantial breakage in decomposed granite.

4.1 Factors controlling the susceptibility to breakage

Decomposed granite is more susceptible to breakage than many other types of soils due to a number of factors including:

- 1) the angularity of the particles,
- 2) the presence of aggregated particles of weak and strong minerals,
- 3) the high intragranular void content, and
- 4) the coarse and uniform gradation of particles.

Angularity

The more angular the granular particles, the sharper the contact points and the smaller the contact area between grains. Therefore, the higher the contact stresses and the greater the possibility of breakage for a given stress increase. Decomposed granite, being residually weathered, has not been subjected to rounding by the transport processes. Spheroidal weathering may leave large boulders somewhat rounded. But on a smaller scale, the irregular shapes of quartz crystals and the elongated nature of feldspar minerals produce an evident angularity (Wu, 1977, Miura and O-Hara, 1979).

Aggregated Particles

Decomposed granite consists predominantly of polymineral grains, at least in coarse fractions, with the main constituents being quartz and feldspar. Quartz undergoes very little weathering and hence maintains its high compressive strength even in highly weathered decomposed granite. Feldspar, on the other hand, may become very weak due to weathering. Aggregations of stronger quartz and weaker feldspar minerals, which exist in decomposed granite because of the residual nature of weathering, are more susceptible to breakage than mono-mineral grains. Although most of the aggregate separation generally occurs in the

material handling process, it may remain dominant during the loading process as well, especially in less weathered materials. Triaxial tests on a decomposed granite from southern Bohemia showed that the soil fraction that experienced the highest breakage was composed predominantly of polyminerals (Fedá, 1977). Mineralogical analyses on that fraction indicated that the minerals that crushed were exclusively feldspar minerals. However, the grains in the fraction of high breakage were not only polyminerals but were also coarser than the other fractions.

Intragranular Voids

Voids and microcracks in decomposed granite particles create weaker planes along which the cracks may propagate under increased stress and cause particle breakage. The water accessible portion of the intragranular voids can be quantified using apparent specific gravity, G_a (see section 2.3.2). It has been observed that the higher the value of G_a the greater the breakage (Nishida and Kagawa, 1972).

Gradation

Some decomposed granite materials are fairly well-graded (Wu, 1977; Mori, 1985; Solbos, 1990; this study, see Figure 3.2), while others are poorly and coarsely graded (Shannon and Wilson, 1957; Adesunloye, 1985; Eubank, 1990). Poorly and coarsely graded materials may exhibit higher particle breakage than well-graded materials under the same conditions. A well-graded material can be compacted to a higher density than a poorly graded material under the same compaction energy. In a dense specimen, the average load per particle is low, and therefore, the contact stresses are smaller than in a loose specimen. Experiments on rockfill have shown that under triaxial conditions, the breakage in dense, well-graded samples is in fact smaller than in uniformly graded samples (Marsal, 1973).

4.2 Quantifying breakage

There is no consensus on the best parameter to quantify particle breakage. The particle size distribution (gradation) curves, estimated through sieving before and after a given testing process, have been the most popular means of graphically comparing breakage. The gradation curve, in fact, has become the basis of all the parameters developed to quantify breakage. The increase in the weight percentage passing the #200 sieve has been used by many investigators as a single parameter for quantification of particle breakage. Nevertheless, that alone will not represent the breakage that occurs throughout the full range of the gradation curve, because many coarser particles may break down to pieces larger than the #200 sieve size.

The "Relative Crushing Index" (D_{15b}/D_{15a}), the ratio of the D_{15} before and after a test, was proposed by Lee and Farhoomand (1967). The choice of D_{15} , however, may not be the most appropriate for all applications.

The "Grain Breakage Index" (B_g), suggested by Marsal (1967) seems to provide a measure of the overall fragmentation process. To obtain B_g , the percentage (in weight) retained in each sieve fraction after a test is subtracted from the percentage retained before the test, and only the positive differences are summed, as shown in Figure 4.1.

The "Index of Crushing" (IC), used by Feda (1977) and Hale and others (1981), and "Relative Breakage" (B_r) used by Lee (1991), also take into account the size of particles that contribute to breakage. However, each investigator defined the breakage parameter differently. Feda (1977) measured the area under the gradation curve, and defined the ratio between the areas from curves after and before a test as the index. Hale and others (1981) multiplied the percent retained in each sieve by the mean diameter of the sieve fraction and summed the product over the entire range of sieves used. They defined IC as the difference between the totals before and after a test, expressed as a percentage of

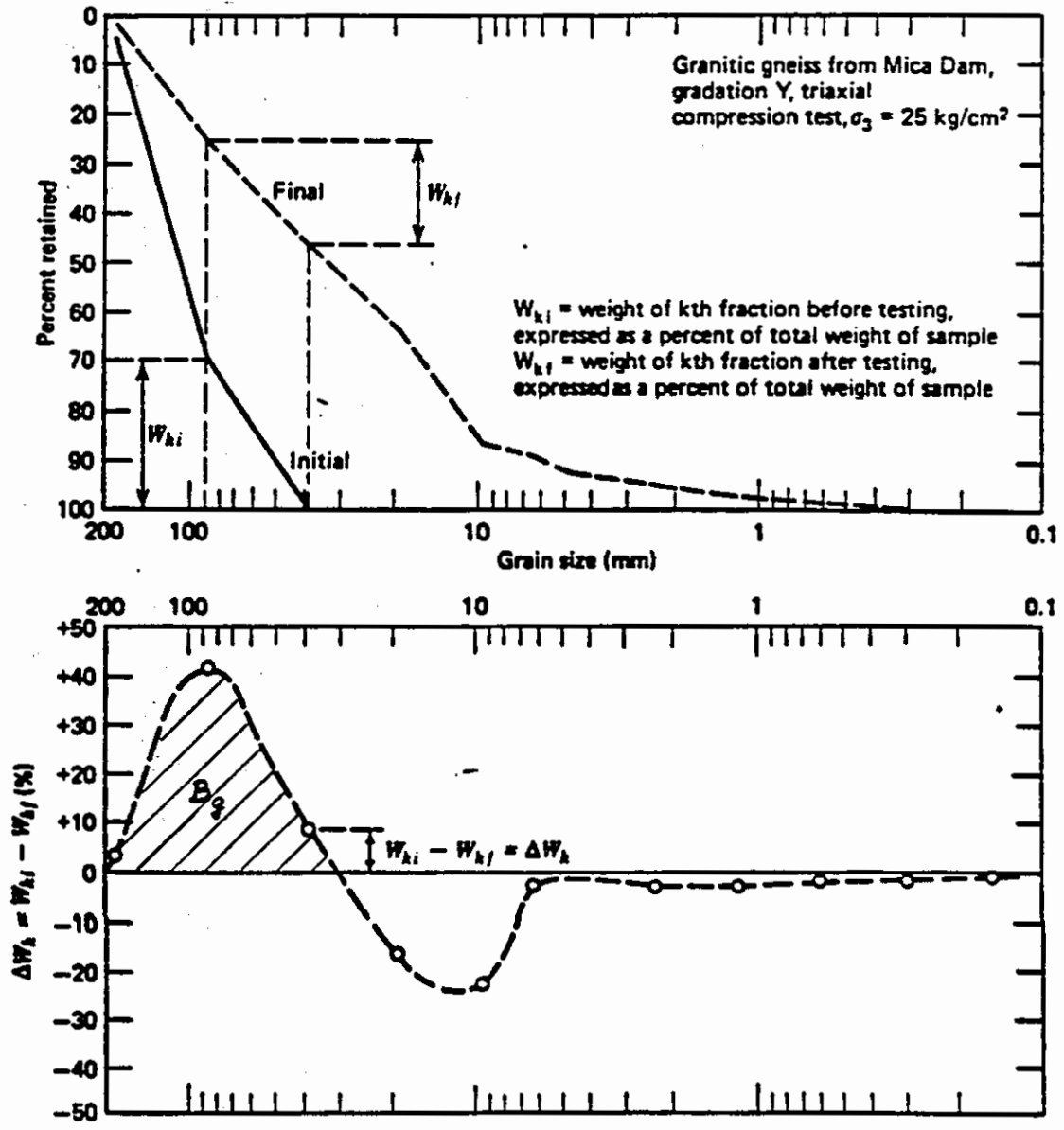


Figure 4.1 Calculation of Breakage Index - B_g (after Marsal, 1973)

the total before the test:

$$IC = \frac{(\sum w_i d_i)_{initial} - (\sum w_i d_i)_{final}}{(\sum w_i d_i)_{initial}} \times 100\% \quad (4.1)$$

where, w_i is the percent retained (in weight) in fraction i , and d_i is the mean diameter (average of sieve openings) of fraction i . Lee (1991) first calculated the area to the left of the gradation curve of the original material and bound by the vertical line at the #200 sieve opening size. He defined B_r as the area between the gradation curves before and after a test and bound by the vertical at the #200 size, expressed as a percentage of the previously calculated area. The methods used by Feda (1977) and by Lee (1991) implicitly interpolate the mean diameter from the semi-logarithmic gradation curve when calculating the area. In Equation 4.1, the diameter is calculated as the arithmetic mean between sieve sizes.

Another set of breakage parameters has been developed using the (breakage-induced) increase in the specific surface area of particles, S , expressed as the surface area per unit volume. To calculate S , a representative sample is divided into several fractions by sieving and the number of grains in each fraction is counted. Each grain is assumed to be spherical with a diameter equal to the geometric mean diameter of the particular sieve fraction. The value of S is then given by the sum of surface areas of particles divided by the total volume of the particles.

One such breakage parameter is the change in S (ΔS) during a given testing process (Miura and Yamanouchi, 1973, Miura and O-Hara, 1979). The rate of breakage is said to be indicated by dS/dW , the ratio of the change in specific surface area to the amount of plastic work done (W) (Miura and Yamanouchi, 1973). The value of W , in a conventional triaxial test, is calculated by summing the areas under the shear stress versus shear strain curve and the mean principal stress versus total volumetric strain curve.

Another variation of S , S_w , takes the particle shape into account in calculating the surface area (Fukumoto, 1979):

$$S_w = \frac{10 \xi D_s^2}{G_s D_v^3} \quad (4.2)$$

where, ξ - the particle shape factor (DallaValle, 1943),
 D_s - the mean surface diameter ($=[\sum n_i d_i^2 / \sum n_i]^{1/2}$),
 D_v - the mean volume diameter ($=[\sum n_i d_i^3 / \sum n_i]^{1/3}$),
 d_i - mean diameter in fraction i , and
 n_i - number of particles in fraction i .

The ratio of final and initial S_w values, S_{wa}/S_{wb} (Particle Surface Ratio) has been used as a breakage parameter. In a compaction study of decomposed granite from Japan, Fukumoto (1979) found that particle surface ratio is better than the percent passing the #200 sieve for comparing breakage.

The indices based directly on the gradation curve seem more appealing than those involving specific surface area, because the calculation of specific surface area is a tedious process. Among the former, the Index of Crushing, IC, seems to best represent the change in gradation. In this study, IC is calculated with Equation 4.1 because the underlying concepts are physically meaningful while the calculations are easy to perform.

4.3 Compaction-induced breakage

Precise determination of particle breakage under field compaction is very difficult because the post-compaction and pre-compaction gradation curves of the fill must be established through samples obtained from the fill mass. In a large fill, the variation in gradation between the samples may be greater than the difference due to compaction. Nevertheless, Wu (1977) compared the gradation curve of a field compacted decomposed granite sample with that of its borrow material. The difference was very small, and the increase due to field compaction in the percent passing the #200 sieve was only 2 percent. In comparison, an

attempt at reproducing the same compaction process in the laboratory yielded a 4 percent increase in the amount passing the #200 sieve.

Fukumoto (1979) conducted an extensive compaction study on decomposed granite (Masa soil) from the Kinki district in Japan. At optimum moisture content, the particle breakage, in terms of B_p , ranged from 25 percent for a coarse, uniformly graded specimen to 6 percent for fine, well-graded specimens. In samples that have about 10 percent passing the #200 sieve, particle breakage is about 50 percent greater when compacted at the optimum moisture content than at the oven-dried state. The compactive energy applied was 33 percent greater than the Standard Proctor method (Fukumoto used 100 blows instead of the standard 75 blows).

With increased compactive effort, breakage of decomposed granite increases, but at a decreasing rate. In Figure 4.2, results from a series of compaction tests on three samples of Masa soil compacted at optimum moisture content exhibit such a trend (Fukumoto, 1979). The compactive effort ranged from 10 to 400 blows and the resulting breakage is expressed in terms of the particle surface ratio. Figure 4.2 also shows that the highest breakage under compaction occurred in the medium-weathered sample. The less weathered sample has particles of greater compressive strength. The highly weathered sample, though its particles are much weaker, has more fines and hence a greater particle surface area prior to testing; the result is a low particle surface ratio, or low breakage.

Particle breakage was estimated from the Modified Proctor compaction test specimens of decomposed granite obtained from the Shasta Bally batholith. Figure 4.3 shows the breakage results in terms of IC against the compaction water content. The compaction curve is also shown for comparison. In contrast to the results reported by Fukumoto (1979), breakage does not seem to have a strong correlation with the compaction water content in this material. The differences in IC are more or less within the expected experimental error in breakage estimates. Due to the water sensitive nature of the material, greater breakage is expected under higher water contents. However, the increased density near the optimum

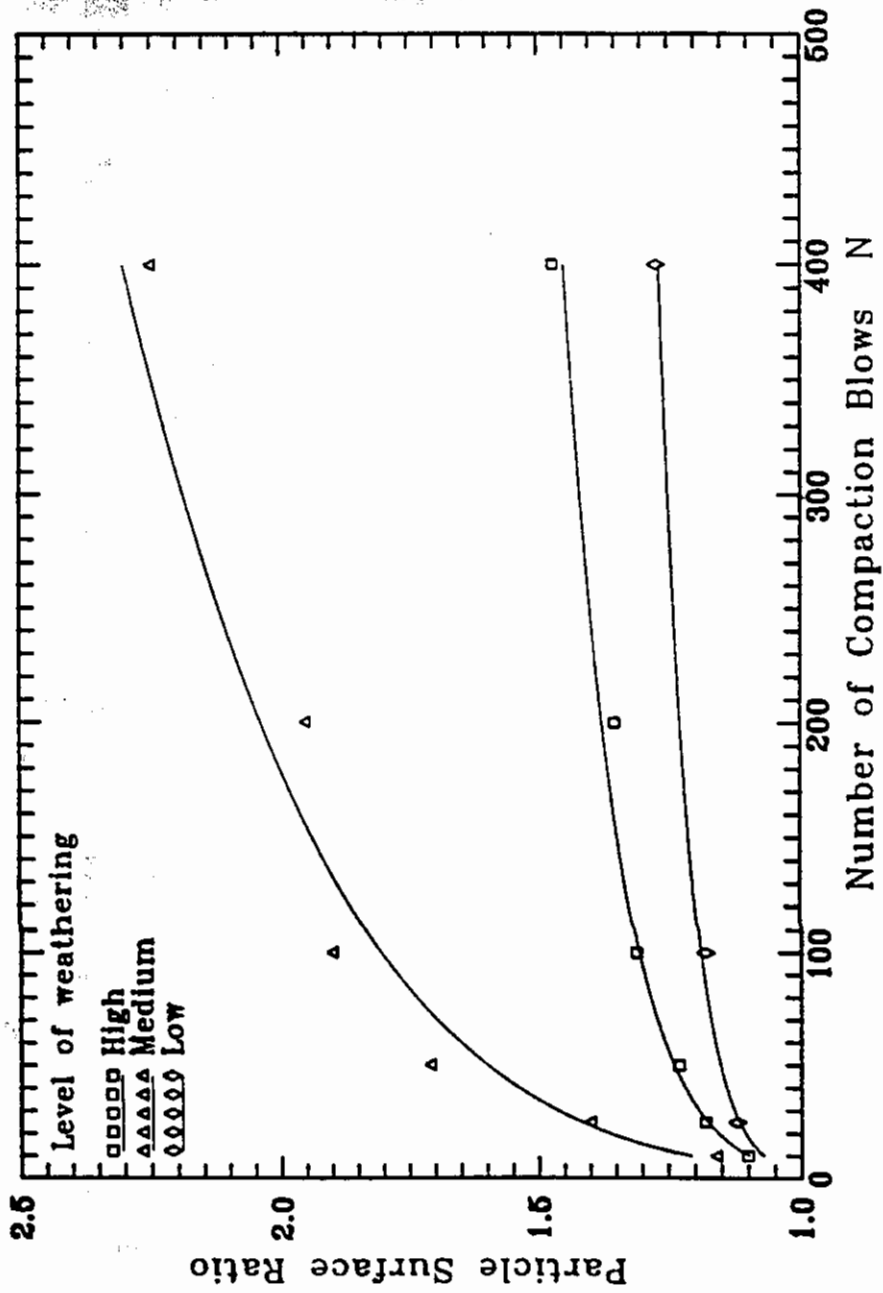


Figure 4.2 Variation in breakage with compactive effort and weathering (after Fukumoto, 1979)

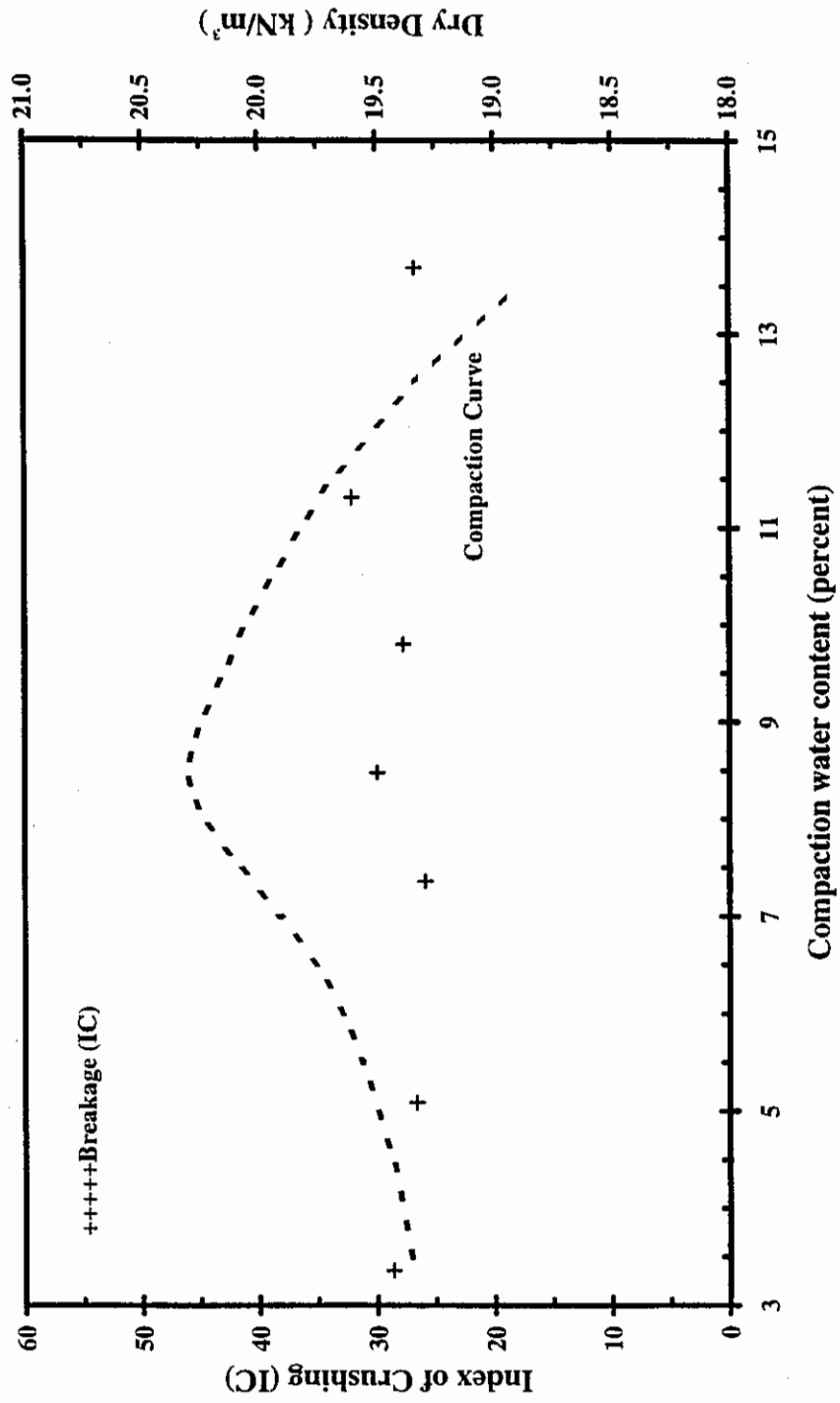


Figure 4.3 Variation in compaction-induced breakage with compactive water content under Modified Proctor compactive effort

water content may have reduced that possibility. Beyond the optimum though, the density is less and breakage should increase. This again may be counteracted by the lubricating effect of excess water, which was quite notable during compaction of the specimen at the highest water content. Although the samples used by Fukumoto have about the same gradation curve as the material from the Shasta Bally batholith, there is one major difference in the testing process that may explain the discrepancy in the results. In Fukumoto's study (1979), soil was first separated by sieving and then re-mixed to obtain controlled gradations, whereas in the current study, soil was not subjected to pre-drying or sieving (see Chapter 3). The additional drying and sieving processes involved in the preparation of Fukumoto's material may have changed its behavior. It is interesting to note that another sample, artificially created by Fukumoto to have the same D_{50} as the other samples, but with about 30 percent passing the #200 sieve, generated about the same amount of compaction-induced breakage at the optimum moisture content as at the oven-dried state.

As described in section 3.1.2, a series of tests was conducted to investigate the effect of compaction technique on breakage. Four specimens were compacted to 90 percent relative compaction in a 71 mm diameter triaxial mold under impact, vibratory, kneading and static compaction. The resulting breakage is shown in terms of IC, index of crushing, in Figure 4.4. The differences in IC are relatively small. However, as expected, impact compaction generated the highest breakage, followed by kneading. Breakage induced by static compaction may not quite represent what occurs in the field, because the restraining effects at the boundary forced us to apply more compactive effort than would be required in the field. That may be the reason that the statically compacted specimen has greater breakage than the vibrated specimen. Kneading compaction, the same technique used by sheep-foot rollers, has been adopted in this test program.

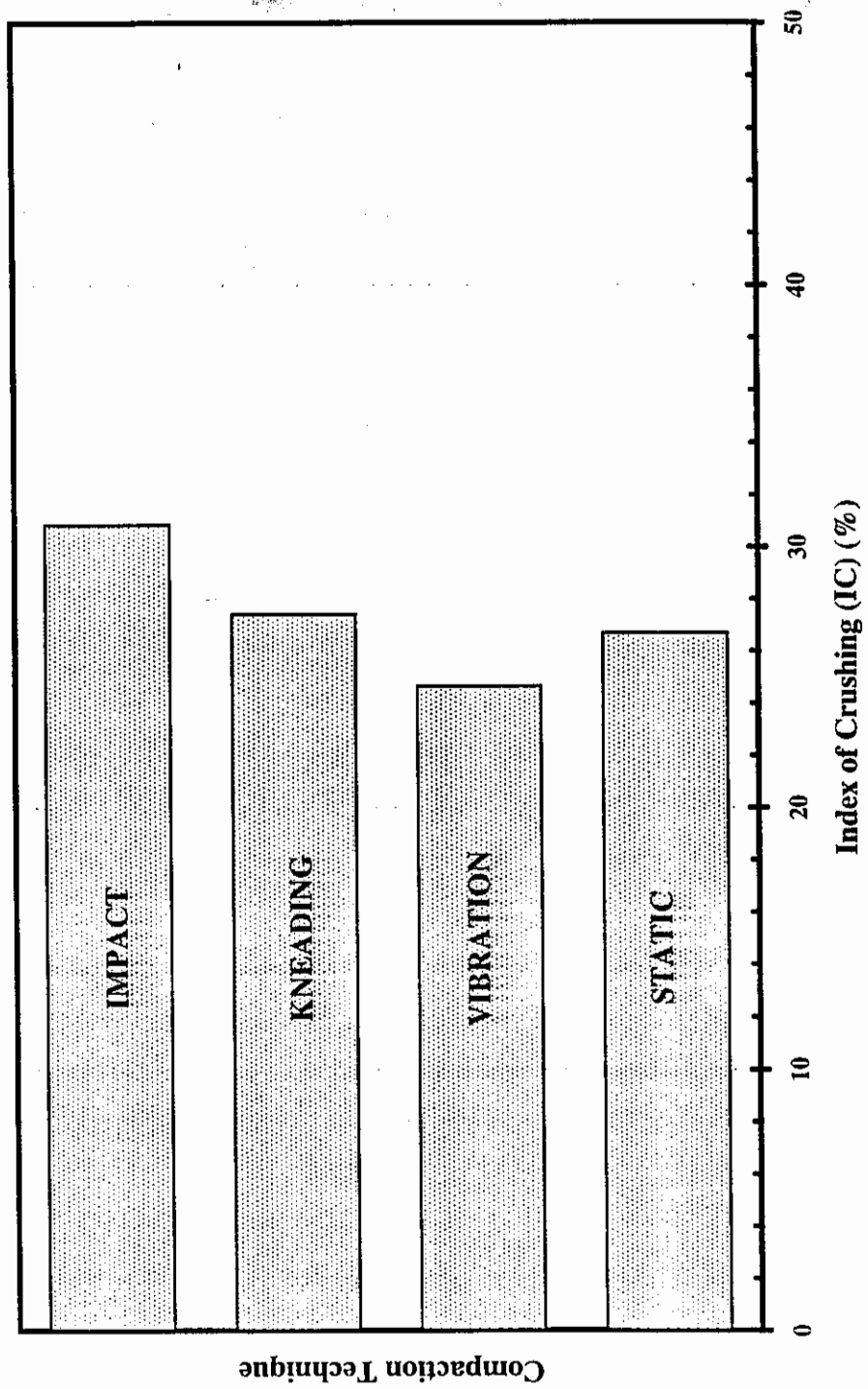


Figure 4.4 Effect of compaction technique on breakage, $RC = 90\%$, $w_c = 8\%$

4.4 Load-induced breakage

4.4.1 Effect of stress level

The applied stress level has been recognized as an important factor governing particle breakage in a granular mass. In the laboratory, the level of breakage differs under different loading conditions such as, unconfined uniaxial compression, isotropic compression, K_0 -compression and triaxial and direct shear. The particles in an embankment may be subjected to different combinations of stress conditions, and thus to different levels of breakage, depending on their location within the embankment. Instead of trying to simulate all possible combinations of field loading, researchers have investigated particle breakage behavior in the laboratory for possible worst case scenarios.

Using theories of crack propagation, Marsal (1973) showed that the uniaxial compressive force needed to split a particle, P_a , is a function of its diameter, d :

$$P_a = \eta d^\lambda \quad (4.3)$$

where, η and λ are statistical parameters. For a spherical grain, the value of λ should theoretically be equal to 1.5. A simple crushing test by Marsal (1973) on several types of rock particles indicated that λ indeed deviates only slightly from the theoretical value. Nevertheless, this type of study does not produce a quantitative measure of particle breakage of the granular mass.

Isotropic compression does produce significant breakage if the confinement is high compared to the compressive strength of the particles. Since embankment stress conditions invariably involve certain amount of shearing, which is known to increase breakage substantially, breakage studies on isotropic compression have not been pursued much further.

Marsal (1973) noted that particle breakage characteristics are similar in both triaxial and oedometer loading (K_0 -compression) conditions, except under low stress levels. As shown schematically in Figure 4.5, at low stresses the rate of breakage under oedometer conditions is comparatively small. In an oedometer test the principal stress ratio (σ_1/σ_3) is lower than in a conventional triaxial test, and

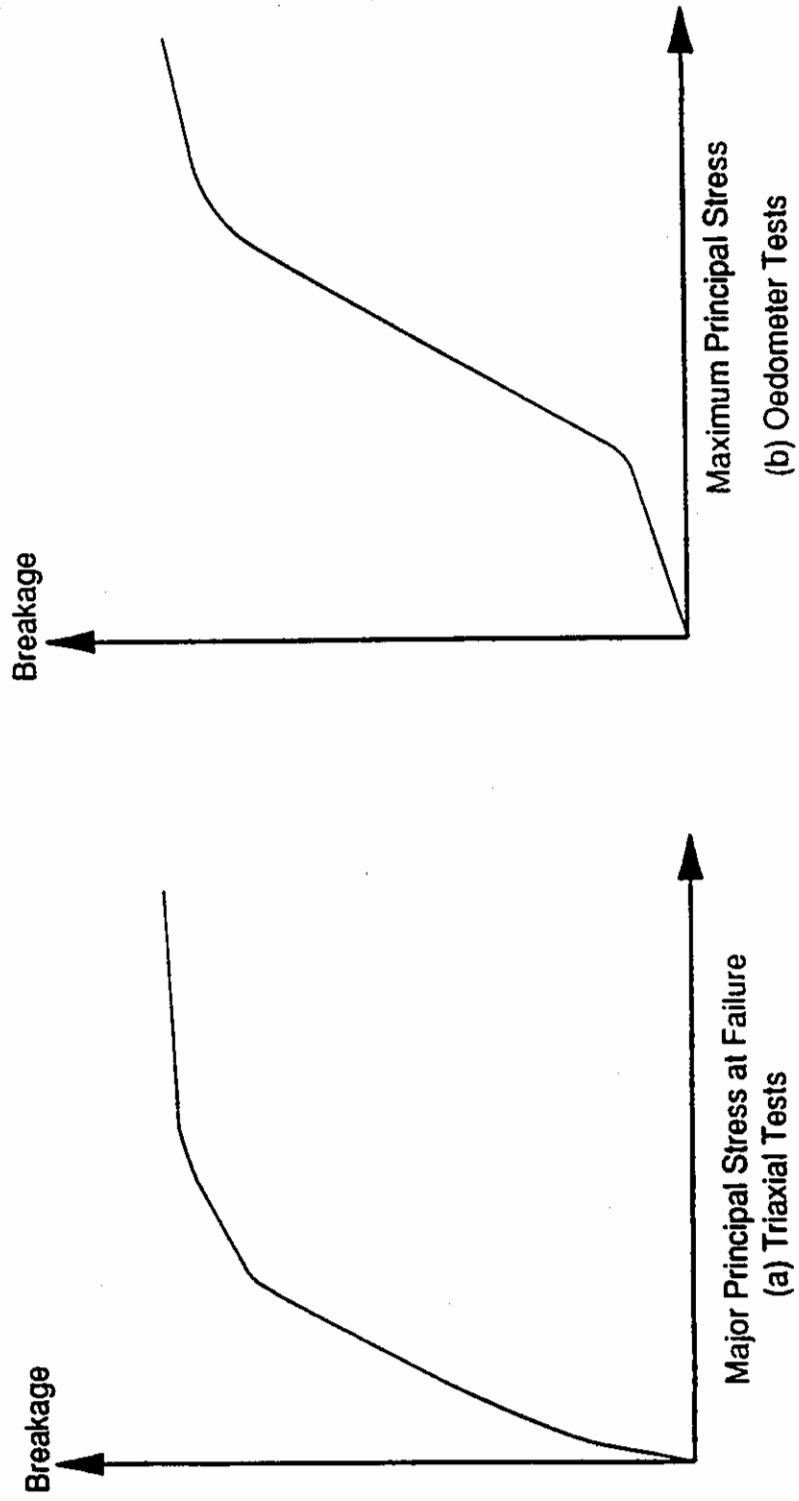


Figure 4.5 Variation of breakage with stress level (after Marsal, 1973)

especially so compared to a triaxial test under low confinement. For granular materials, σ_1/σ_3 is generally between 2 to 3 for the oedometer test and between 3 to 9 for the triaxial test. Thus, the greater shearing effect in a triaxial test causes a greater increase in breakage compared to an oedometer test.

Under both oedometer as well as triaxial conditions, as stress level increases particle breakage increases, but the rate of breakage decreases gradually (see Figure 4.5), producing little further breakage under high stresses. Two different explanations are given for the reduction in the rate of breakage.

- 1) As the stress level increases, previously "idle" particles and fragments also begin to carry a portion of the load because of structural rearrangement and densification. This greater participation of grains in carrying the load reduces the contact stresses, and therefore, the breakage (Marsal, 1973).
- 2) The energy required for breakage increases proportionally with the total surface area of the granular mass. Since particle breakage increases the total surface area, a given amount of energy will produce less breakage in a given specimen at higher stress levels (Hendron and others, 1963).

Marsal (1973) developed the schematic pattern of breakage shown in Figure 4.5 based on a large number of tests on rockfill materials. A number of different gradations were used in triaxial tests but only uniform gradations in oedometer tests. The initial steep rise in breakage with stress level (under triaxial conditions) is an extension of the experimental data. The results yielded a straight line trend in breakage with maximum principal stress at failure, σ_{1f} (failure being defined at the peak principal stress ratio), but the line could not be extrapolated through the origin, suggesting a steep drop near the origin. The flattened portion of the curve at high stress levels is also an extension of the triaxial test data, which under the stress levels used suggested only the beginning of such a trend. Hendron and others (1963) based their explanation for the reduction in the rate of breakage on K_o -compression test on different sands, but the breakage estimates were merely qualitative.

Particle breakage characteristics like those shown in Figure 4.5 can be established by using decomposed granite without resorting to the unconventionally large equipment such as Marsal (1973) used for rockfill materials, or the extremely high pressures used by Hendron and others (1963) for strong sand, because of the fragile and sandy nature of decomposed granite. Feda (1977) conducted conventional triaxial tests on dense Landstejn decomposed granite from southern Bohemia, a well-graded sandy gravel, at confining pressures up to 10 MPa. Lee (1991) conducted triaxial tests on Seoul decomposed granite from South Korea, a well-graded gravelly sand, at confining pressures mainly in the range of 50 to 500 kPa, and a few at 2 to 5 MPa. In these tests, compaction densities varied from about 95 to 85 percent relative compaction. Some tests were conducted keeping mean effective stress level (σ_m) constant, and others keeping confining pressure constant as conventionally done. The results of Feda's and Lee's test programs are shown in Figures 4.6 and 4.7, respectively. Feda (1977) uses a different "index of crushing" (identified here as I_c to differentiate from the IC used in this study) to quantify breakage, while Lee (1991) used "relative breakage", B_r .

The left half of each figure shows the variation of breakage with σ_{1f} . Feda's results (Figure 4.6), though consisting of only a few data points, show general agreement with the trend suggested by Marsal (1973) (Figure 4.5a). The large number of tests conducted by Lee (1991) at the low pressure range confirm Marsal's suggestion of a steep increase in breakage at low pressures (see Figure 4.7). As the stress level increases, the rate of breakage decreases but the data points are widely scattered. Lee suggested correlating breakage with the deviator stress at failure (σ_{df}), which led to a well-defined parabolic trend (the right half of Figure 4.7). Feda's results are also plotted against σ_{df} in the right half of Figure 4.6. The heavy influence of shearing stresses on particle breakage is the basis for Lee's suggestion. Lee (1991) then proposed a straight line correlation of B_r with $(\sigma_{df})^{0.5}$, irrespective of the stress path. However, such a conclusion may not be warranted because of the following reasons:

- 1) All the triaxial tests by Lee were terminated, and the breakage levels were estimated when the specimen reached the critical state (which is defined as

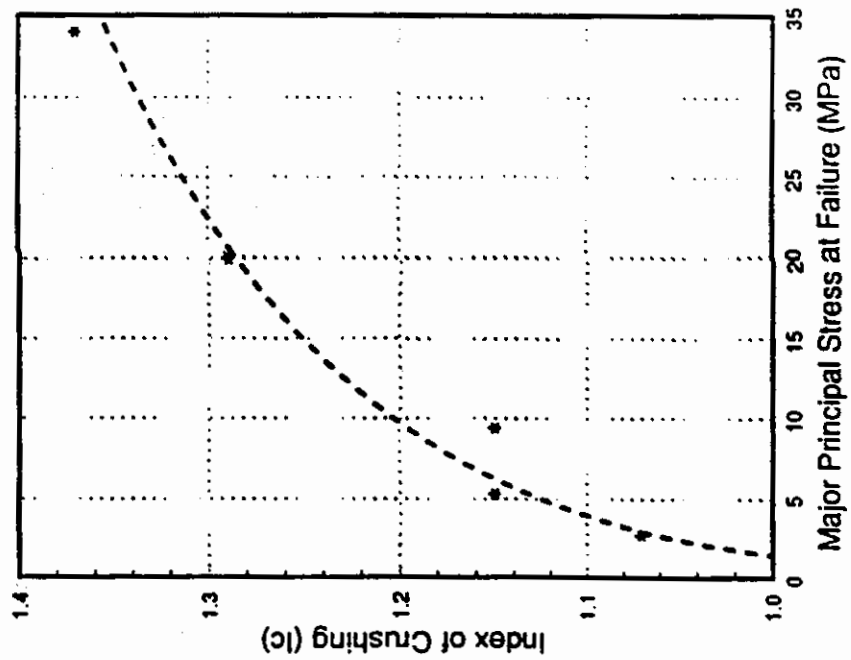
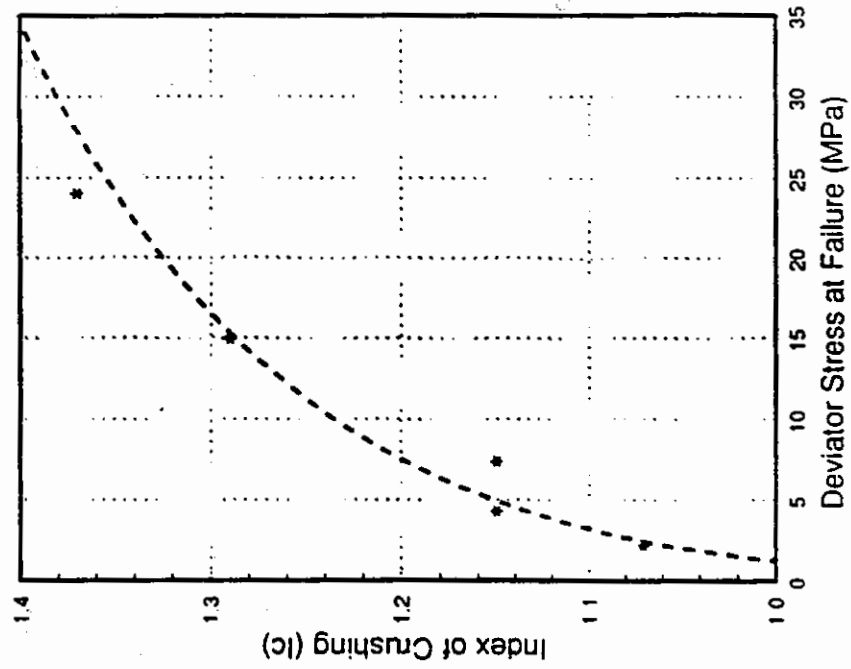


Figure 4.6 Variation in breakage with stress level in triaxial tests on decomposed granite (after Fedda, 1977)

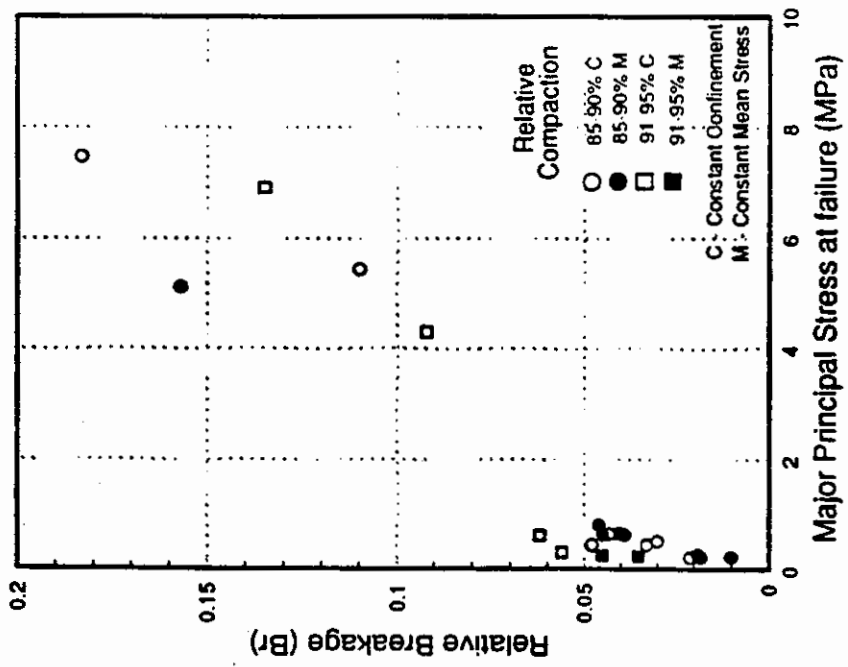
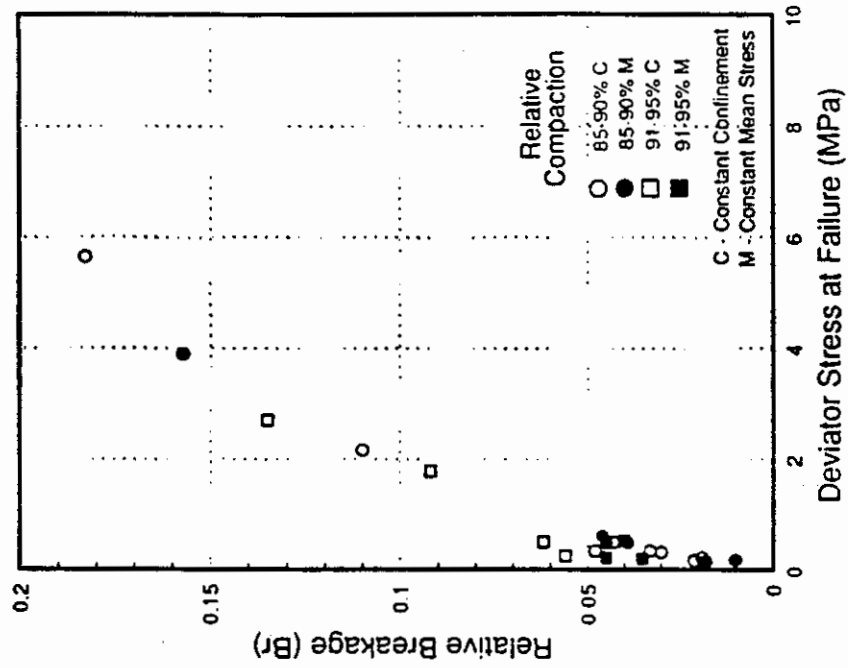


Figure 4.7 Variation of breakage with stress level in triaxial tests on decomposed granite (after Lee, 1991)

when the criteria $\Delta(\sigma_d/\sigma'_m) < 0.03$ and $\Delta\epsilon_v < 0.1$ are satisfied during the last 3 percent of the axial strain). Specimens at different stress levels and at different densities reached the critical state at different strain levels.

However, the applied strain level may have a controlling effect on breakage (as will be discussed in section 4.4.2), and hence should not be ignored.

- 2) Lee's test specimens were prepared at a wide range of densities. He states that very dense specimens required a greater compactive effort as compared to loose specimens. As discussed in section 4.3, the compactive effort has a great influence on the level of breakage. Apparently, breakage values at the end of the tests were not corrected for compaction-induced breakage.
- 3) Under triaxial conditions, dense specimens under low stress levels are known to dilate and fail along a well-defined slip plane. Greater amounts of breakage can be expected in the failure zone of the specimen compared to the end zones. On the other hand, loose specimens (including dense specimens under high stress levels) may bulge in failure, and breakage within a specimen may be more uniform. Usually the specimen as a whole is used to estimate breakage, and therefore, breakage values are averaged over the total mass. Thus it seems necessary to separately identify dilative and compressive specimens to better interpret breakage results.

In the current test program involving decomposed granite from the Shasta Bally batholith, the effect of stress level on breakage was investigated using several laboratory test configurations, namely, triaxial, oedometer, direct shear and pullout. Two different density levels (90 and 95 percent relative compaction with respect to Modified AASHTO) were used in triaxial and oedometer tests, while most direct shear and pullout tests were conducted at 95 percent relative compaction. In oedometer, direct shear and pullout test programs, the stress path remained the same throughout each program. Most triaxial tests were of the ICD type while a few ACD tests were also conducted. All triaxial test results presented in this section are from the tests which were terminated at almost the same axial strain level (about 20 percent). All direct shear and pullout tests considered here

also have been terminated at equal shear displacement levels. Oedometer tests by nature do not facilitate such control.

Figure 4.8 shows the total amount of breakage, in terms of IC, that occurred during triaxial tests, against both σ_{1f} and σ_{df} . The densely compacted specimens are indicated with darker symbols. The dilative and compressive behaviors in shearing are also identified separately. When all the data points are considered together, there exists a general trend indicating that breakage increases with increasing stress level, but at a gradually decreasing rate, which agrees with the results discussed so far. The plot against σ_{df} shows a narrower range. The scatter is produced because of a number of reasons, some of which were discussed before. A major reason for the scatter is the possible initial variation in specimen gradations, which is inevitable because the initial gradation was not controlled except for the random separation of particles from the original batch using a material separator. Another reason for scatter is the possible difference in average breakage estimates when the specimen dilates or contracts in shearing. As indicated in Figure 4.8, dilative behavior occurs at low stress levels and those data points tend to form a band near the upper end of the general trend. The high relative movement at the failure zone in a dilating specimen may cause greater breakage there, but that is averaged over the entire specimen in the calculation process. Thus, establishing separate trends for breakage depending on the shearing behavior is difficult, and all the data points will be treated together in future discussions.

The other major contributor to the scatter in the data is the compacted density. In Figure 4.8 though, breakage results from both loosely compacted and densely compacted specimens seem to follow the same trend. A closer inspection, however, reveals that the darker data points (corresponding to the specimens compacted at 95 percent relative compaction) do not show a significant correlation with the stress level. In fact, comparing the total amount of breakage in densely and loosely compacted specimens against the stress level is misleading. The total breakage may not reflect the true shearing-induced breakage, because there is a significant difference in the portion of breakage that was

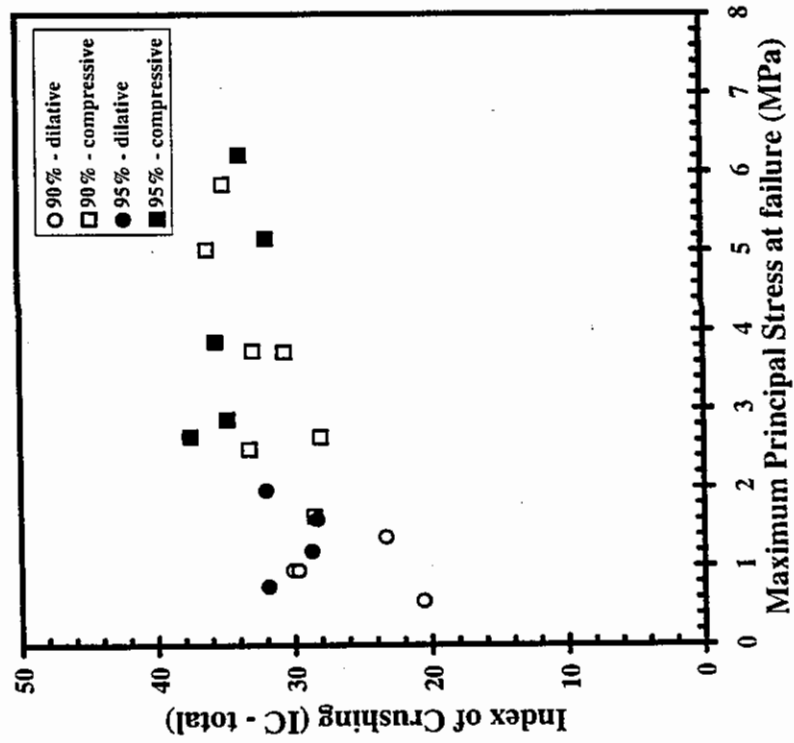
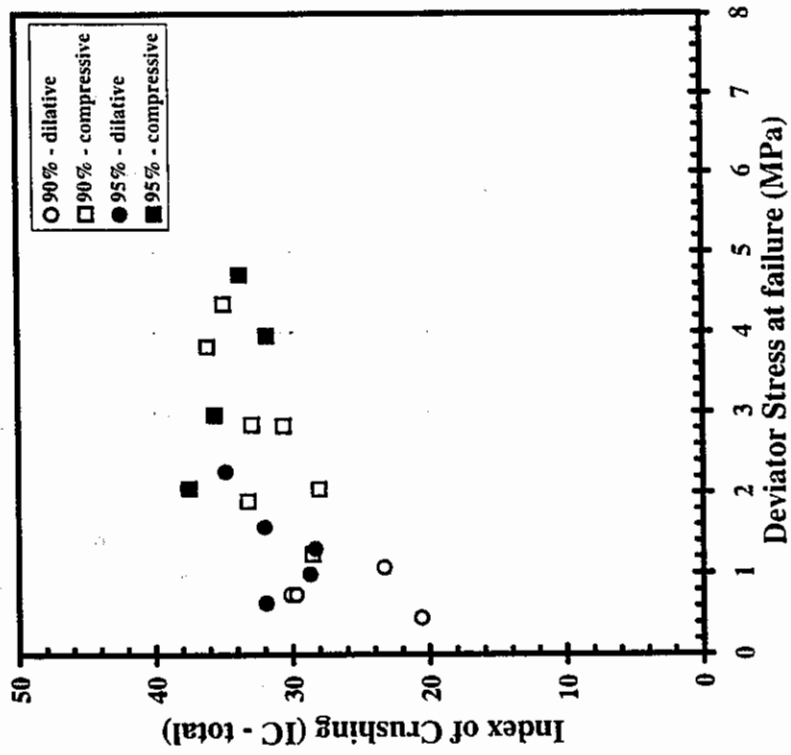


Figure 4.8 Variation of breakage (total) with stress level in triaxial tests on decomposed granite from SH299 PM 0.6, Shasta County, CA

compaction-induced. The average compaction-induced breakage, in terms of IC, in a triaxial specimen at 8 percent water content is 18 for 90 percent relative compaction and 28 for 95 percent. Therefore, in Figure 4.9, the same triaxial test results are plotted, now in terms of post-compaction IC value. The differences in shearing-induced breakage in loose and dense specimens are now clearly identifiable. The loosely compacted specimens still show an increasing trend (albeit widely scattered) in breakage with increasing stress level. The dense specimens show no such trend, and in fact, the shearing-induced increase in IC is no greater than 10 even at high stress levels. A major reason for the low breakage level may be the reduced contact stresses in a dense specimen, as suggested by Marsal (1973). Another is the possible reduction in weak, angular particles, that are more susceptible to breakage under the intense compaction process. Most densely compacted specimens dilated upon shearing, and the rate of dilatancy reached zero at about 1200 kPa confinement (see Chapter 5 for details). Breakage estimates obtained from specimens that were changing from dilative behavior to compressive behavior may not follow any trend because the zone of breakage would also be in transition from the narrow slip plane to the bulging total mass.

Total breakage under oedometer tests performed in the current study is plotted against σ_1 in Figure 4.10. The data points are widely scattered and show no significant trend with increasing stress level. For comparison, a wide band that incorporates most of the triaxial test results is also plotted in the figure. Clearly, oedometer conditions produce less breakage than triaxial test conditions. The darker data points in the figure correspond to denser specimens (95 percent relative compaction). They seem to fall slightly above the points representing looser specimens. Again, this is misleading, because higher compactive effort produces higher initial breakage in denser specimens. The average values of the compaction-induced IC, corresponding to the two levels of compaction are also shown for comparison. It is interesting to note that very little increase in breakage, if any, has occurred under the normal load. Some specimens show total breakage levels less than the compaction-induced level. That is mainly because

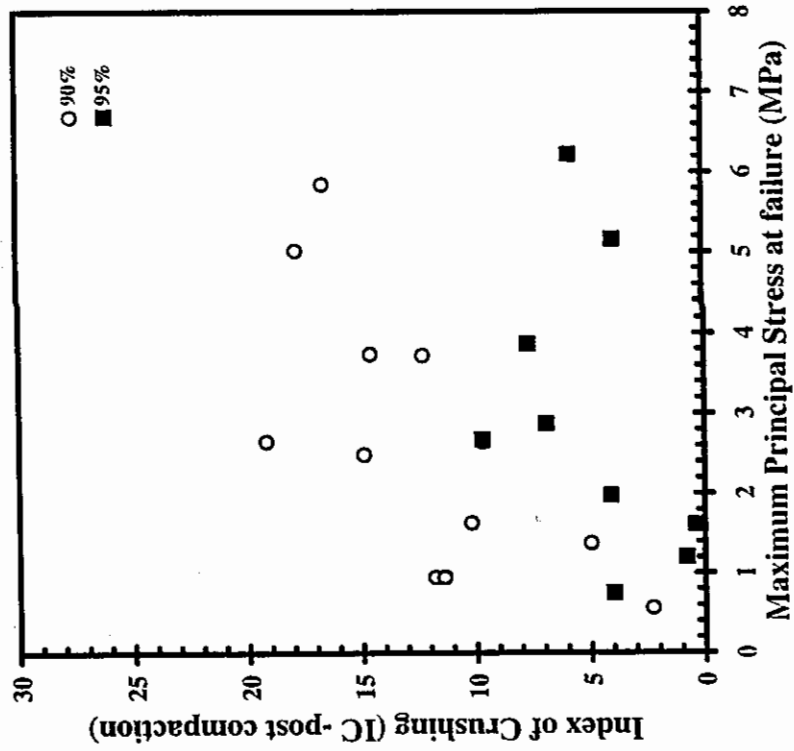
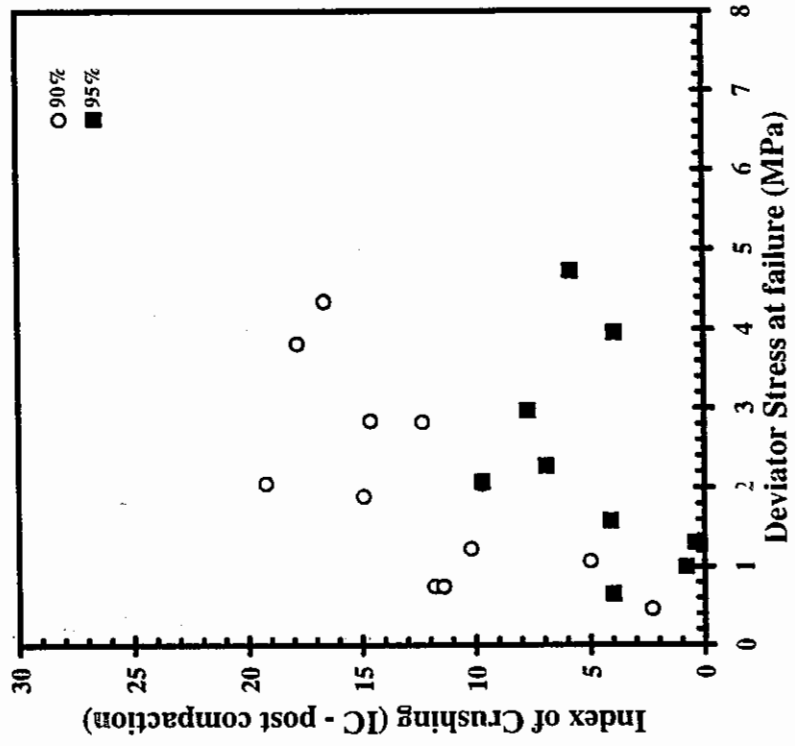


Figure 4.9 Variation of breakage (post-compaction) with stress level in triaxial tests on decomposed granite from SH299 PM 0.6, Shasta County, CA

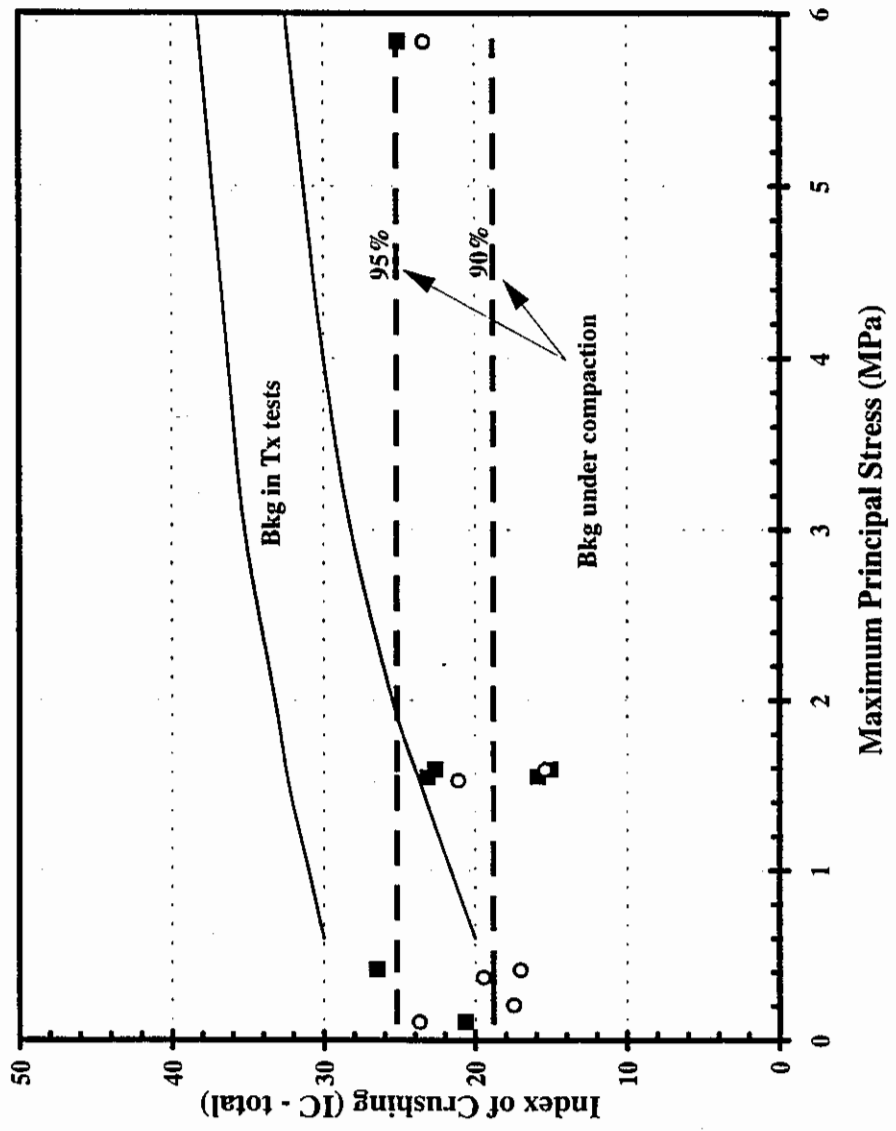


Figure 4.10 Variation of breakage (total) with stress level in oedometer tests on decomposed granite, $w_c = 8\%$

the scatter in compaction-induced breakage data is much higher than in the triaxial case.

Figure 4.11 shows the total breakage in direct shear test specimens. Both soil-soil direct shear tests and soil-grid direct shear tests produced comparatively low levels of breakage. However, it must be noted that, because of the very large soil volume involved, only a small portion (1000 cm^3) of it was sampled. Although this sample included the shearing plane, breakage in the sheared zone is averaged over the total sample mass. All the specimens indicated in the figure were compacted at 95 percent relative compaction. However, compaction-induced breakage in soil-grid shear configuration may be different from soil-soil configuration. In the former, the geogrid laid in the middle of the soil thickness evenly distributes the compactive forces applied on soil layers above. Estimating compaction-induced breakage in direct shear and pullout tests was not attempted because of a) the differences between configurations such as above, b) the large amount of material required per test, and c) the small post-test breakage that does not allow much room for possible scatter in compaction-induced breakage data.

Total breakage in pullout test specimens is shown in Figure 4.12. All the specimens used in this plot were subjected to about the same amount of pull, and all were compacted to the same density (95 percent relative compaction). As in direct shear tests, the breakage is very small and there does not seem to be a significant trend in breakage with stress level. This is not surprising, because a) the range of normal load used does not induce much breakage as seen in the oedometer results, and b) pullout seems to generate only a small shear zone on either side of the moving grid (see Chapter 6 for details).

4.4.2 Effect of strain level

Feda (1971) postulated that the amount of breakage is controlled by the amount of applied strain energy rather than the stress level. Of two identical decomposed granite triaxial specimens, one was subjected to shearing only up to the peak deviator stress level (at an axial strain of 7.5 percent) and the other up

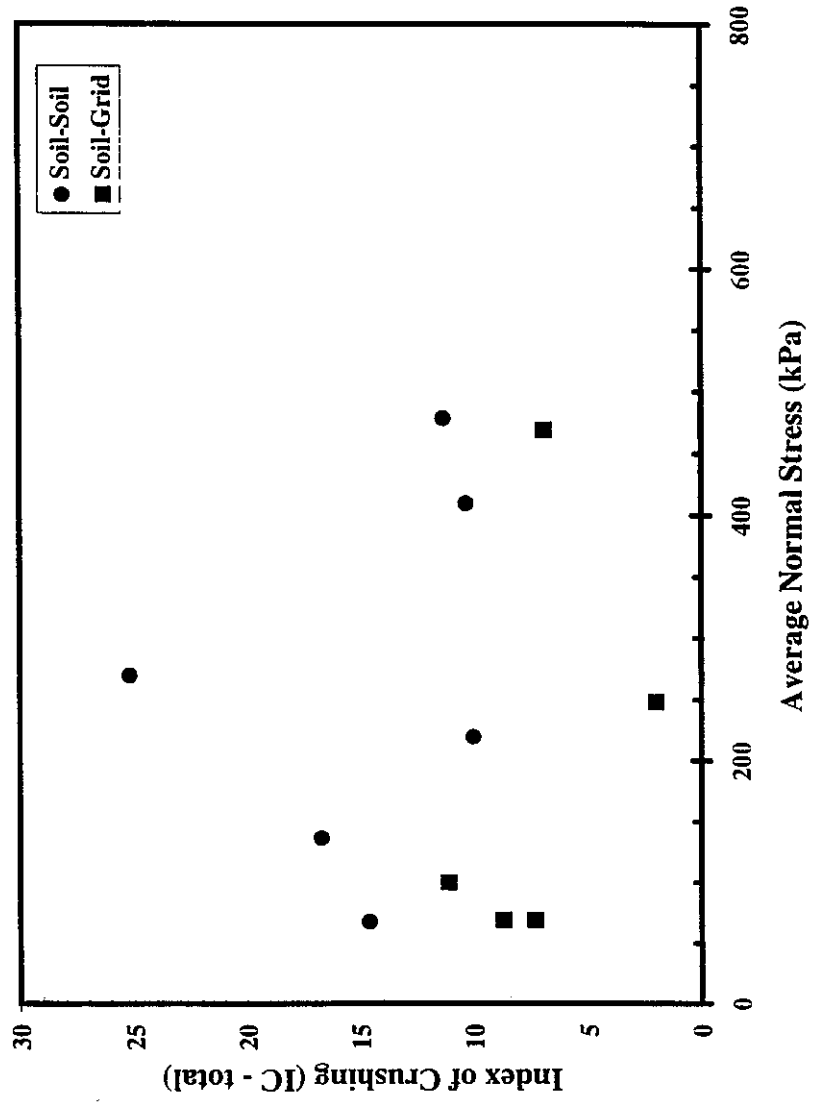


Figure 4.11 Variation of breckage (total) with stress level in direct shear tests on decomposed granite, RC = 95%

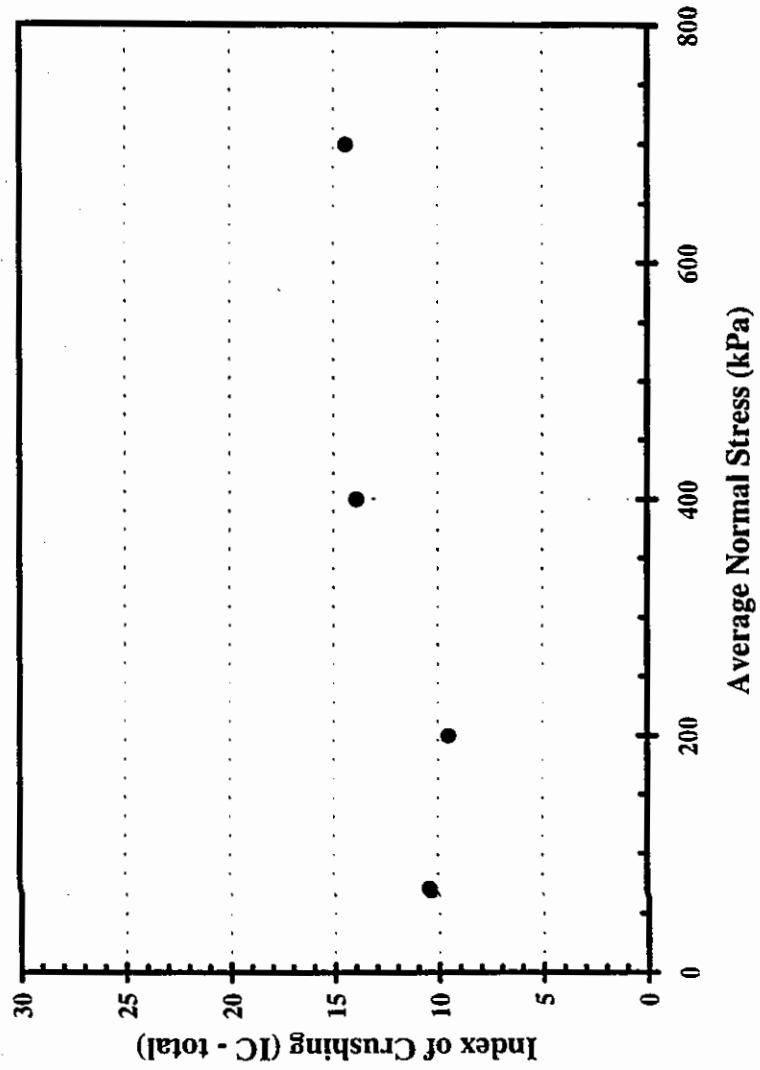


Figure 4.12 Variation of breakage (total) with stress level in pullout tests on decomposed granite, RC=95%, pull=50 mm

to a strain level of 24 percent. The latter produced a large amount of breakage. In terms of the IC, the breakage was 34 percent in the latter and 14 percent in the former. Thus, intense breakage seems to occur only after the peak strength has been reached.

This important postulate is studied in detail in the current test program. As discussed in the previous section, the investigations on the effect of stress level in triaxial, direct shear and pullout tests were limited to the tests which were subjected to the same strain level, axial or shear. An additional triaxial test series, the T200 series, was conducted to investigate this issue specifically. Three identical specimens (including T156b) were subjected to shearing under the same confinement (900 kPa) up to three different axial strain levels, 10, 15 and 20 percent. All specimens were sheared beyond the peak deviator stress level. The fourth specimen, T251a, was subjected to a confining pressure of 1000 kPa, so that at about 5 percent axial strain it would reach about the same deviator stress level as the peak level in others. At that point test T251 was terminated. The breakage level of each specimen, corrected for the compaction-induced breakage, is plotted in Figure 4.13. As a reference, the stress-strain curve for the tests under 900 kPa confinement is also plotted. It is interesting to note that in specimens at either 5 or 10 percent strain level, just before the peak (though subjected to the same stress level) and just after the peak respectively, shearing had induced almost no breakage. It should also be noted that these specimens were prepared at 95 percent relative compaction, and in these, even at the highest stress and the strain levels used, the shearing-induced breakage (in terms of IC) is no more than about 10. Both the specimens at 15 and 20 percent strain level under 900 kPa confinement also exhibited about that much breakage. These results provide strong evidence to support the postulate by Feda (1971) that applied strain levels are the controlling factor in breakage. It has strong implications, not only in planning future laboratory investigations, but most importantly in refuting arguments of those who discount the use of fragile materials like decomposed granite. The parallel investigation in the pullout test program, the P100 test series, where the pull, or the shear displacement, was only about half that of the P200 series, was

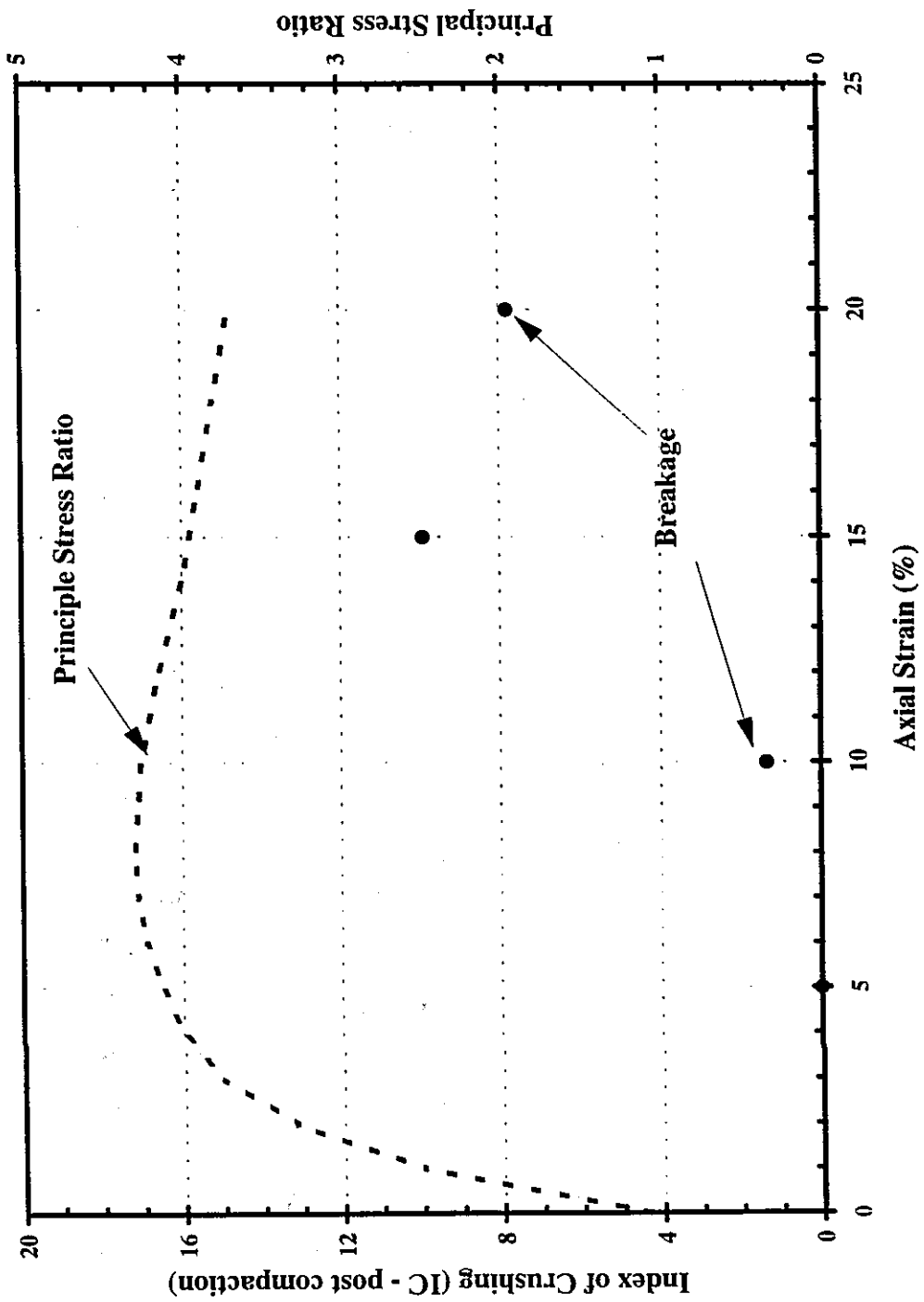


Figure 4.13 Variation of breakage (post-compaction) with axial strain in triaxial tests on decomposed granite, RC = 95%, specimens subjected to the same maximum principal stress

not fruitful. The breakage levels at full displacement were too small to make any meaningful comparisons with those at the reduced pull.

4.5 Effect of soaking

At very high stress levels, soaking activates or accelerates particle crushing in rocks as well as in sand, which causes settlements in rockfill and reductions in shear strength in sand (Terzaghi, 1960; Sowers and others, 1965; Lee and others, 1967; Nobari, 1971; Miura and Yamanouchi, 1975). Miura and Yamanouchi observed that breakage in saturated Toyoura sand is substantially higher than in dry sand under isotropic pressures of about 50 MPa. They theorized the following: at particle contact points, water may penetrate the cracks generated by high stresses; adsorption of water molecules may lower the surface energy at the crack tip, which accelerates further crack growth and subsequent crushing.

Although sand, when soaked at low stress levels, does not show significant changes in particle breakage characteristics, decomposed granite particles do, as demonstrated in Figure 4.14. In a series of triaxial tests on decomposed granite from Japan, conducted at 98 KPa confining pressure, water is introduced (step 2) at different deviator stress levels, indicated as a percentage of the deviator stress at failure, q/q_f . The breakage from steps 1 to 2 and steps 2 to 3 (with no change in stress) are indicated in terms of ΔS , the change in specific surface area. Soaking caused significant breakage at stress levels as low as $q/q_f = 20$ percent, and breakage increased substantially with increased soaking stress level (Miura and others, 1983).

In the current test program, investigating the effect of soaking in the triaxial tests was difficult because the equipment available was not suitable for such a study. In pullout testing, one specimen was tested without soaking. However, the breakage results in all pullout tests were too low to make meaningful comparisons between them. In Chapter 6, triaxial test results from previous investigators are used to illustrate the effects of soaking on shear strength characteristics of decomposed granite.

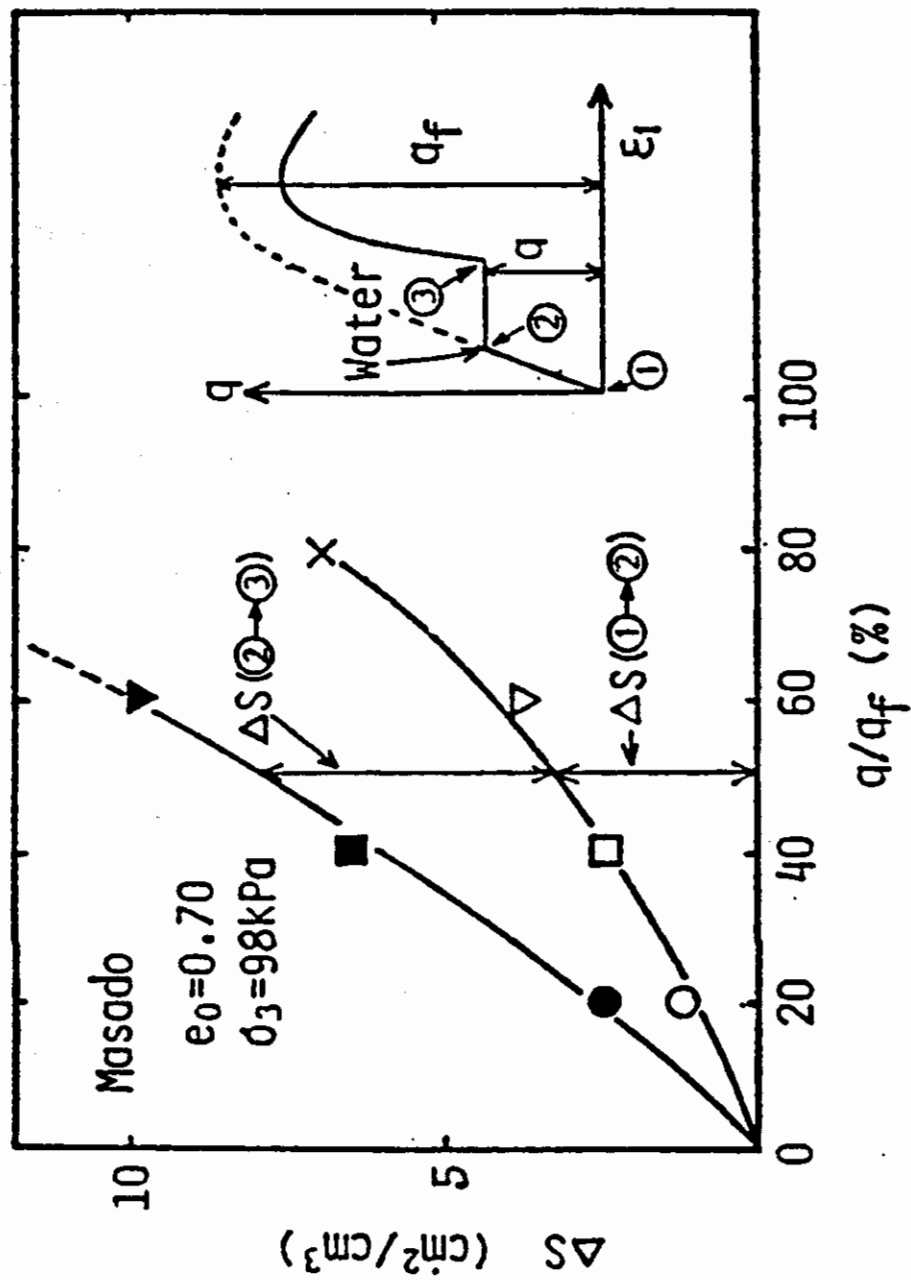


Figure 4.14 Effects of soaking on breakage (from Miura and others, 1983)

CHAPTER 5
VOLUME CHANGE CHARACTERISTICS
AND THE INFLUENCE OF PARTICLE BREAKAGE

In this chapter, volume change characteristics of compacted granular materials subjected to conditions of high particle breakage are examined. First, the settlement of compacted laboratory specimens under a wide range of axial pressures is discussed. Hydrocompression, another aspect of settlement that assumes significance in breakage-susceptible materials is discussed next. In addition, when the loading conditions promote breakage, the time rate of settlement in compacted granular materials may become significantly large. Therefore, the trends of time-dependent settlement among different types of materials are compared. These volume change characteristics, based primarily on oedometer test results, can be supplemented with breakage-induced volume change characteristics in strength tests which are discussed next. In each section, past investigations are reviewed first to establish the trends which the decomposed granite specimens would be expected to follow. The results of the current test program are then analyzed and the deviations from these trends are discussed.

5.1 One-dimensional settlement

Results of oedometer tests on compacted granular materials, when plotted in a conventional void ratio versus logarithm of axial pressure (e -log p) plot, resemble the behavior of an undisturbed cohesive soil sample: an almost horizontal line representing the "recompression" stage, followed by a steeply dipping "virgin compression" stage. If loading is continued to very high pressures e -log p curve may begin to flatten out again. In Figure 5.1, e -log p curves of several granular materials are illustrated; two types of sands and El Infiernillo conglomerate rockfill, along with soft Detroit clay. The Pennsylvania sand curve begins to dip steeply at about 1 MPa pressure, and then flattens out beginning from about 100 MPa. Both dense and loose Ottawa sand specimens also dip steeply, but under higher axial pressures, because Ottawa sand particles are

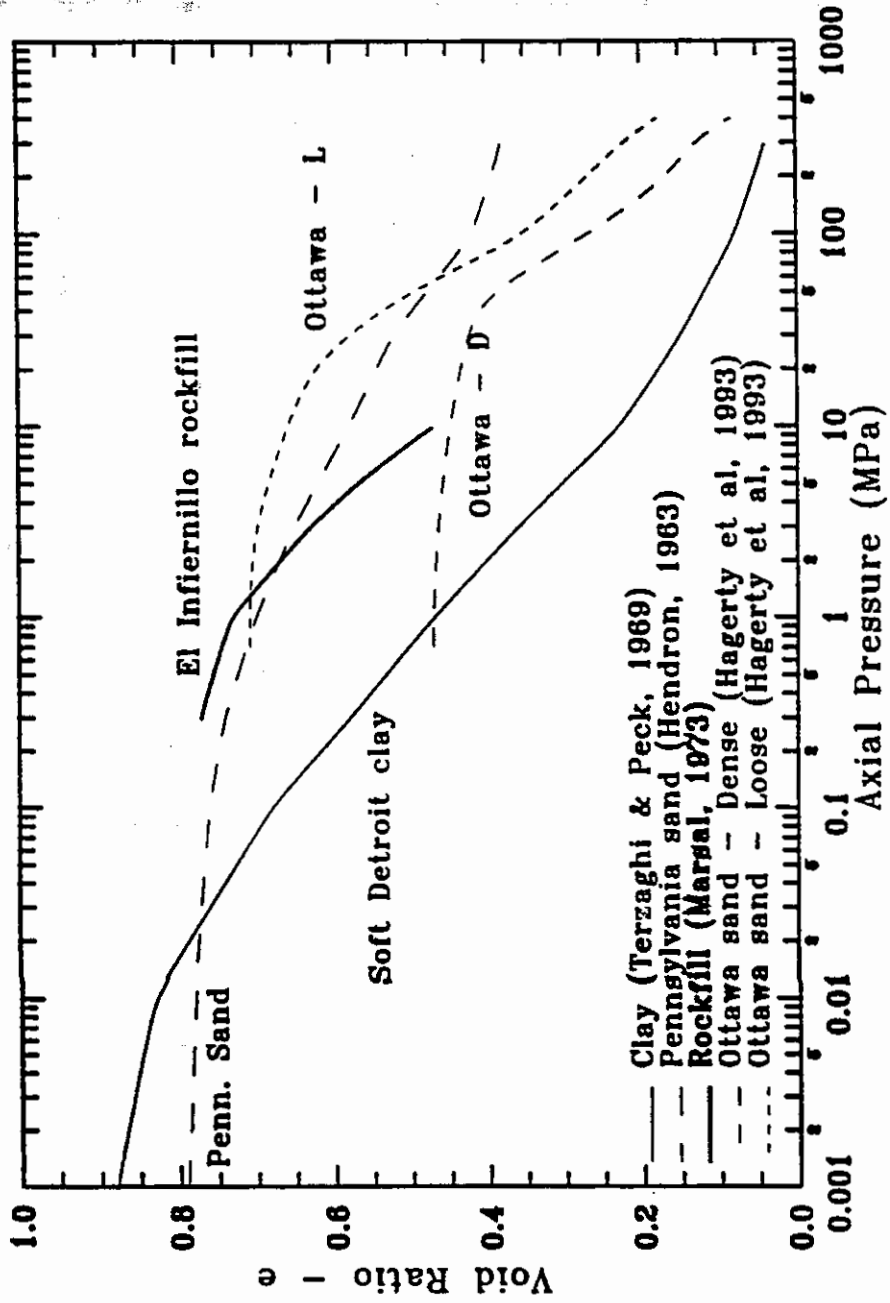


Figure 5.1 Compressibility of sand, rockfill and clay

stronger than Pennsylvania sand particles. Probably for the same reason, Ottawa sand compressibility curves exhibit no significant reduction in slope with increasing axial pressure. The rockfill sample also shows a steeply dipping curve but the maximum pressure applied, apparently, is not sufficient to produce any reduction in the slope. In contrast to granular materials, the curve for the Detroit clay sample dips steeply at a pressure of about 0.1 MPa.

Hendron (1963) explained the behavior of sand in the oedometer test as follows: during the recompression stage, compression occurs mainly due to particles rearranging to a more stable and closer packing, which causes only a minor settlement in an already densely packed sample; when the normal stress is increased, particle breakage increases gradually and the settlement depends on the rate of particle breakage (virgin compression). However, since the rate of particle breakage decreases under increasing pressure (as discussed in Chapter 4), the rate of settlement may also decrease.

This direct correlation between particle breakage and settlement is further substantiated by the results of Hagerty and others (1993), re-analyzed and shown in Figure 5.2. In this test series, oedometer tests were conducted to axial pressures as high as 700 MPa on dense specimens of Ottawa sand, glass beads and angular glass (created by crushing the beads), each having a maximum particle size equal to the #20 sieve opening. In Figure 5.2, the curves without any markers are associated with the left y-axis, and are the plots of axial strain versus axial pressure. The other set of curves are associated with the right y-axis, and are the plots of breakage, expressed in terms of the index of crushing (IC), versus axial pressure. As expected, the angular glass specimens show the highest breakage as well as the highest settlement. The steeper portion of the settlement curve roughly corresponds to the steeper portion of the breakage curve. When breakage rate decreases under increasing pressure, the settlement curve flattens. In Ottawa sand, the settlement curve steepens gradually as breakage becomes significant. The settlement curve of glass beads dips sharply because the breakage in beads increases quite abruptly at about 50 MPa.

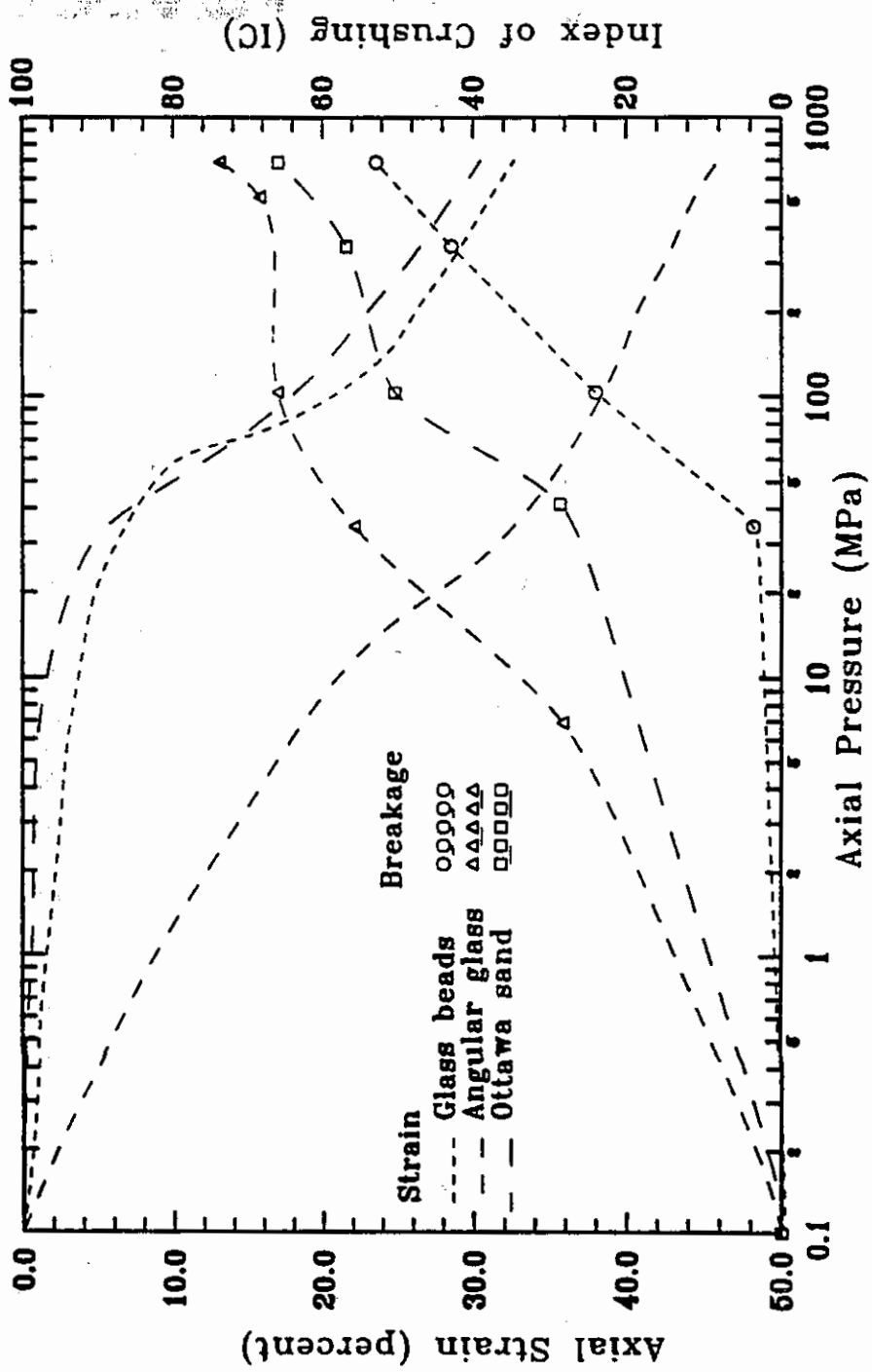


Figure 5.2 Relationship between compressibility and particle breakage of granular materials (after Hagerly and others, 1993)

The results of the oedometer tests on decomposed granite from the Shasta Bally batholith are presented in Figures 5.3 and 5.4. In Figure 5.3, the results of the T100 series tests, compacted at a water content of about 8 percent, are shown. The two curves drawn are not regression lines but merely represent the trends indicated by the data points. The loosely compacted (90 percent relative compaction) specimens apparently have reached the steeper portion of the settlement curve (virgin compression) under the maximum applied pressure of 1600 kPa. However, the denser specimens seem to require much higher pressures to reach virgin compression stage. (The settlement results of the high pressure tests C104 and C154 were not included here because the recorded axial strains were incompatible with those of the other tests, probably due to differences in the measuring devices used.) Since none of the two curves in Figure 5.3 shows significant virgin compression under the applied pressures, high breakage cannot be expected to have occurred in these specimens. Breakage estimates of oedometer specimens, shown in Figure 4.10, seem to agree with this observation: there is little post-compaction breakage in densely compacted specimens, and breakage is very small in loosely compacted specimens as well.

Figure 5.3 also shows the unload/reload portions of settlement. Unloading of the loosely compacted specimen occurred at a fairly steep portion of the settlement curve, and the recompression index is less than 25 percent of the compression index, which indicates that the settlement is mostly unrecoverable. For loose specimens, the compression index is about 0.25 (when settlement is expressed in terms of void ratio) and the precompression pressure is about 200 kPa. For denser specimens, compression index is about 0.10 in the 500 to 1600 kPa axial pressure range.

In Figure 5.4, the settlement curves are shown for the tests C106 and C107, compacted at water contents 6.5 and 5.0 percent respectively. Also shown is the average settlement curve for the specimens compacted at 8 percent water content and at the same density, 90 percent relative compaction. The curves show no significant change in settlement with the compaction water content because the deviations in axial strains are not much greater than the expected experimental

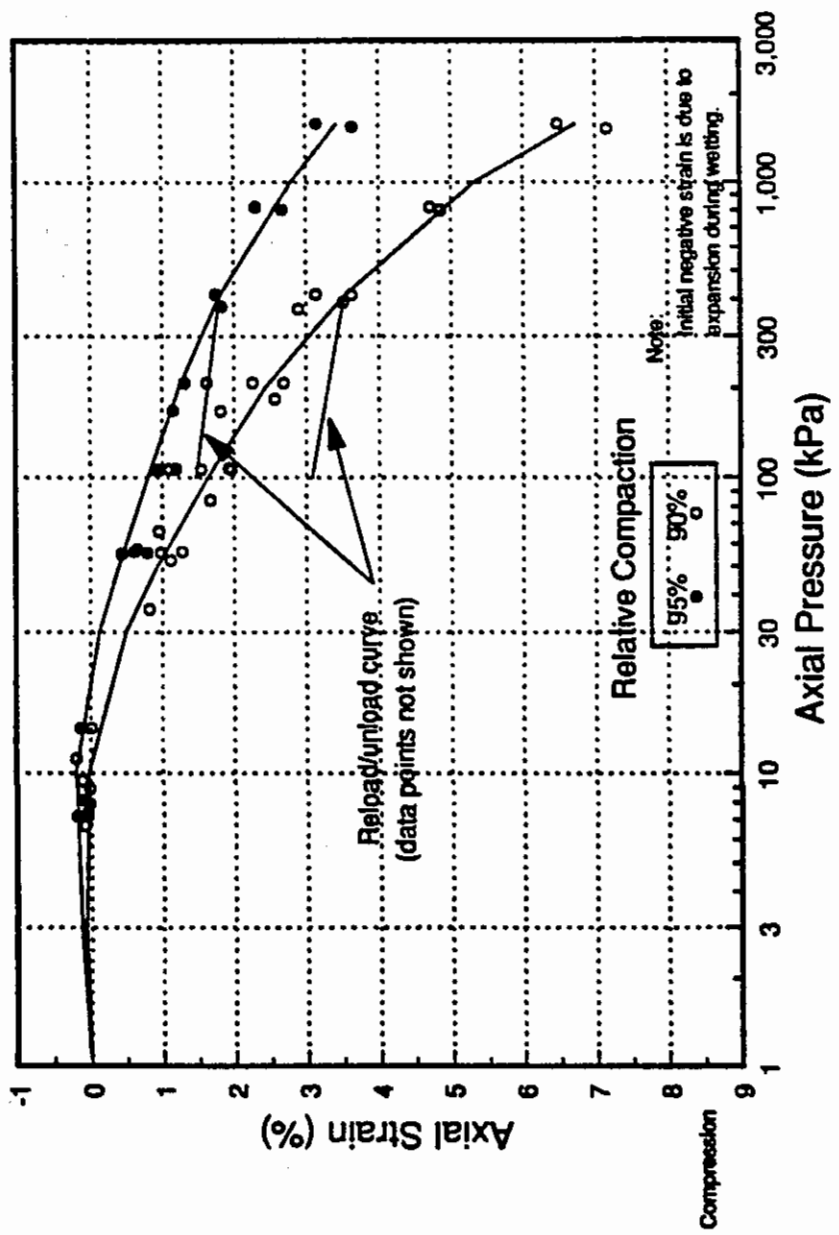


Figure 5.3 Settlement curves of decomposed granite from the Shasta Bally batholith, $w_c = 8\%$

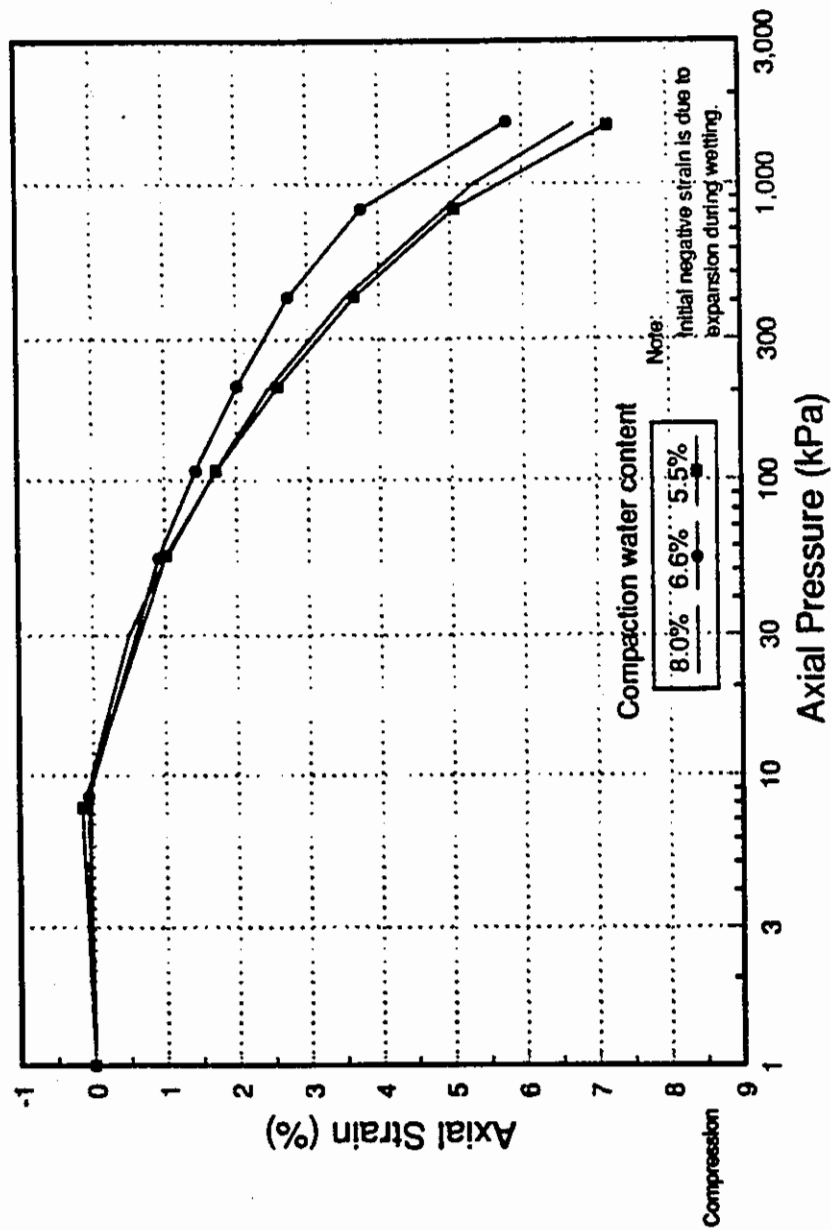


Figure 5.4 Effect of compaction water content on settlement of decomposed granite, RC = 90%

error. The compactive effort required to prepare the specimens, however, increased significantly with decreasing water content. Moreover, this test series could not be extended to the 95 percent relative compaction level because of the difficulty in compacting drier specimens. Therefore, it may not be economical to compact this material at water contents much drier than 8 percent, although the settlement is not dependent much on the compaction water content.

Decomposed granite samples from other locations, however, have shown greater dependency of compressibility on the compaction water content. In oedometer tests conducted on decomposed granite from borrow areas near Mammoth Pool dam in central California by the State Department of Water Resources (1958), specimens compacted at the optimum water content or wetter showed greater compression than the specimens compacted drier than the optimum. The compression index (C_c) of decomposed granite from Japan also depends on the compaction water content; the maximum C_c value was exhibited by a specimen compacted wet of the optimum water content (Onitsuka and Yoshitake, 1990). The compaction water content plays a more significant role in another aspect of settlement of granular materials, discussed next.

5.2 Hydrocompression

Hydrocompression, the relatively rapid settlement (the collapse) that occurs when a loaded, compacted granular soil mass is wetted, could be large enough in rockfill and earthfill embankments to cause serious concern (Sowers and others, 1965; Brandon and others, 1990). A thorough investigation on hydrocompression in rockfill was conducted by Nobari (1971) using oedometer specimens (on the portion passing the #4 sieve) of Pyramid argillite. The observations based on these tests are summarized below.

- 1) Compaction water content is the most influential variable in hydrocompression. After wetting, specimens compacted near the optimum water content exhibited no collapse, whereas those compacted at lower water contents, but at almost the same density, collapsed significantly.

- 2) When wetted under a given load, the total settlement (both due to loading and wetting) of an initially dry specimen was found to be essentially equal to the settlement of an initially saturated, similarly loaded specimen, compacted to the same density, as illustrated in Figure 5.5.
- 3) Hydrocompression decreases with increasing relative compaction.
- 4) Samples of uniform gradation exhibit greater hydrocompression than well-graded samples of equal relative density.
- 5) The hydrocompression exhibited by a specimen with maximum particle size equal to the #8 sieve opening is almost the same as the hydrocompression in a specimen with a parallel gradation and the #16 sieve opening as the maximum size.
- 6) A basalt sample exhibited less hydrocompression than an argillite sample of the same gradation and relative density, but of lower particle compressive strength.

Observation #2, above, paves the way for a more convenient means of estimating hydrocompression in a granular soil: saturate one of two identically compacted specimens and load both at the same rate; then the difference in settlements in the two specimens measured at a given load level will be the corresponding hydrocompression.

To verify this technique in estimating hydrocompression in decomposed granite, a series of oedometer tests (the C200 series, Table 3.1) was performed in the current study. In Figure 5.6 the settlement of each specimen that was loaded as-compacted (compacted at 8 percent water content) is shown, along with the average settlement curve for specimens which were loaded initially wetted. Figure 5.6a shows the results of the dense (95 percent relative compaction) specimens and Figure 5.6b shows the results of the loose specimens. The differences in settlement between the specimens loaded as-compacted and loaded initially wetted are very small, less than one percent in axial strain at every load level. In fact, in dense specimens, the settlement under initial wetting is slightly less than that under as-compacted loading. Although the initially wetted specimens were

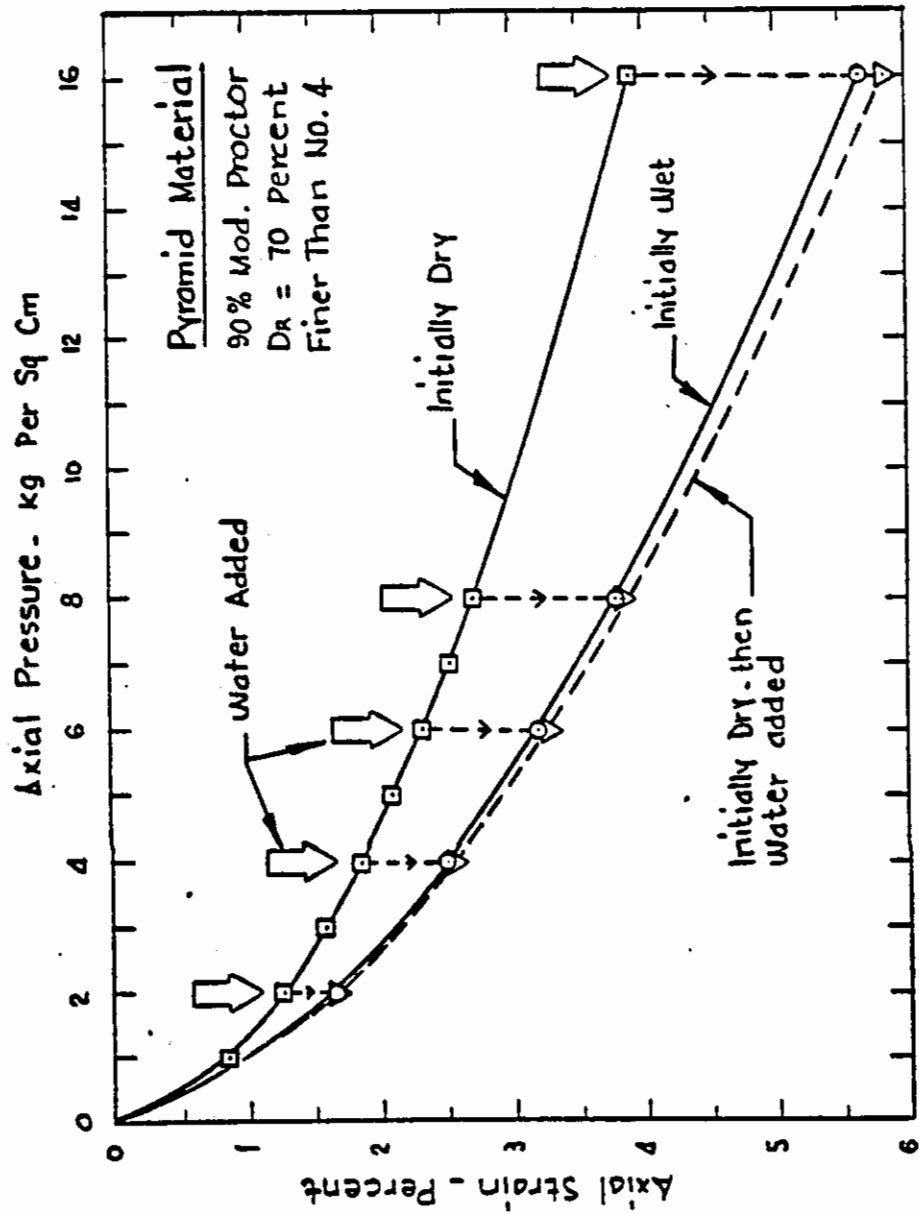
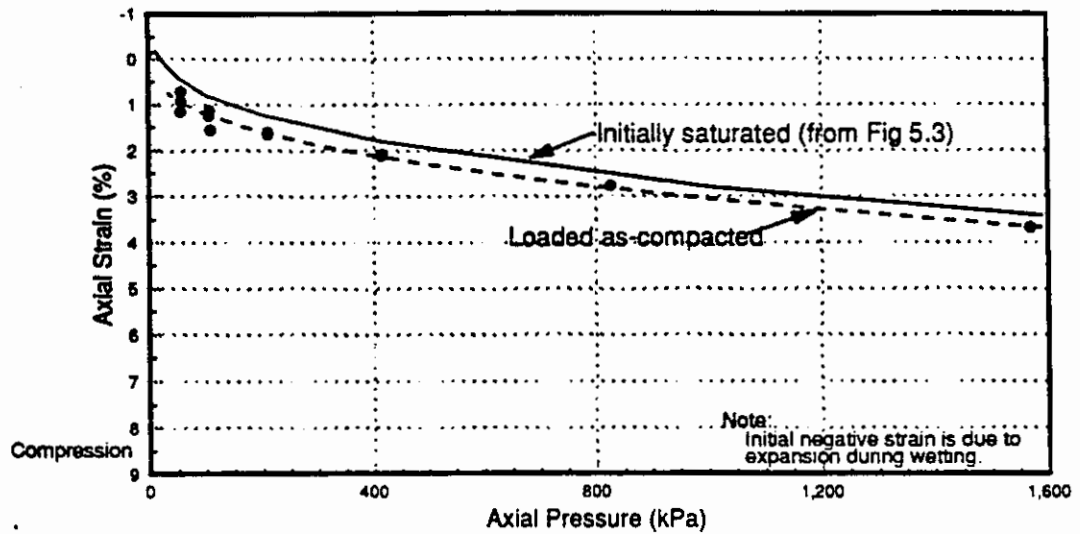
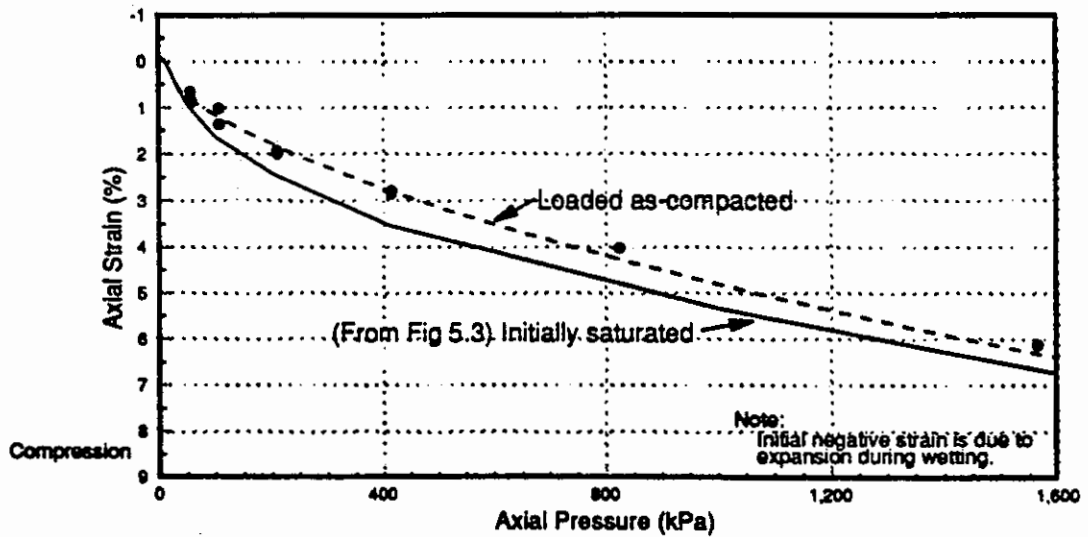


Figure 5.5 Effect of the stage of soaking on hydrocompression of Pyramid rockfill (from Nobari, 1971)



(a) 95% Relative compaction



(b) 90% Relative compaction

Figure 5.6 Settlement of initially saturated and as-compacted decomposed granite specimens, $w_c = 8\%$

allowed to soak for more than an hour under a small surcharge load, the tendency to expand upon soaking may have prevailed under subsequent loading and reduced the settlement levels. The specimens loaded as-compacted were also wetted, but at the end of loading. The axial stress levels at which the specimens were wetted are approximately 100, 400 and 1600 kPa. The resulting settlements, or hydrocompression levels, were very small; the highest was less than 0.2 percent in axial strain. These results are shown in Figure 5.7. Under 100 kPa axial pressure, the hydrocompression is negative because of the tendency to expand upon soaking. As the axial pressure increases, hydrocompression increases slightly. At the lower density, 90 percent relative compaction, hydrocompression is greater because there is greater capacity for particle reorientation. These results generally support observation #3 by Nobari (1971), that the settlement levels of initially wetted specimens constitute the upper limit on settlement of compacted granular materials. The data for dense specimens (Figure 5.6a), that show greater as-compacted settlements than the initially wetted (suggested upper limit), should not be construed as a contradiction, because in this case the applied loads were not large enough to overcome the tendency to expand upon soaking. The strongest conclusion to be derived from this test series is that hydrocompression will not be significant, if this decomposed granite material is compacted at about 8 percent water content and at a density greater than or equal to 90 percent relative compaction.

Observation #1 by Nobari (1971) argues clearly in favor of compacting granular fill materials near the optimum water content to reduce hydrocompression. A similar trend was observed in tests involving decomposed granite from Mammoth Pool dam borrow areas (Department of Water Resources, CA, 1958). In the current test program involving decomposed granite from the Shasta Bally batholith, most of the test specimens were compacted at 8 percent water content (slightly dry of the optimum) to simulate the field practice. Additionally, two other hydrocompression tests, C206 and C207, were performed at compaction water contents of 6.5 and 5.0 percent, respectively. The results, the amount of hydrocompression under 1600 kPa axial pressure at different

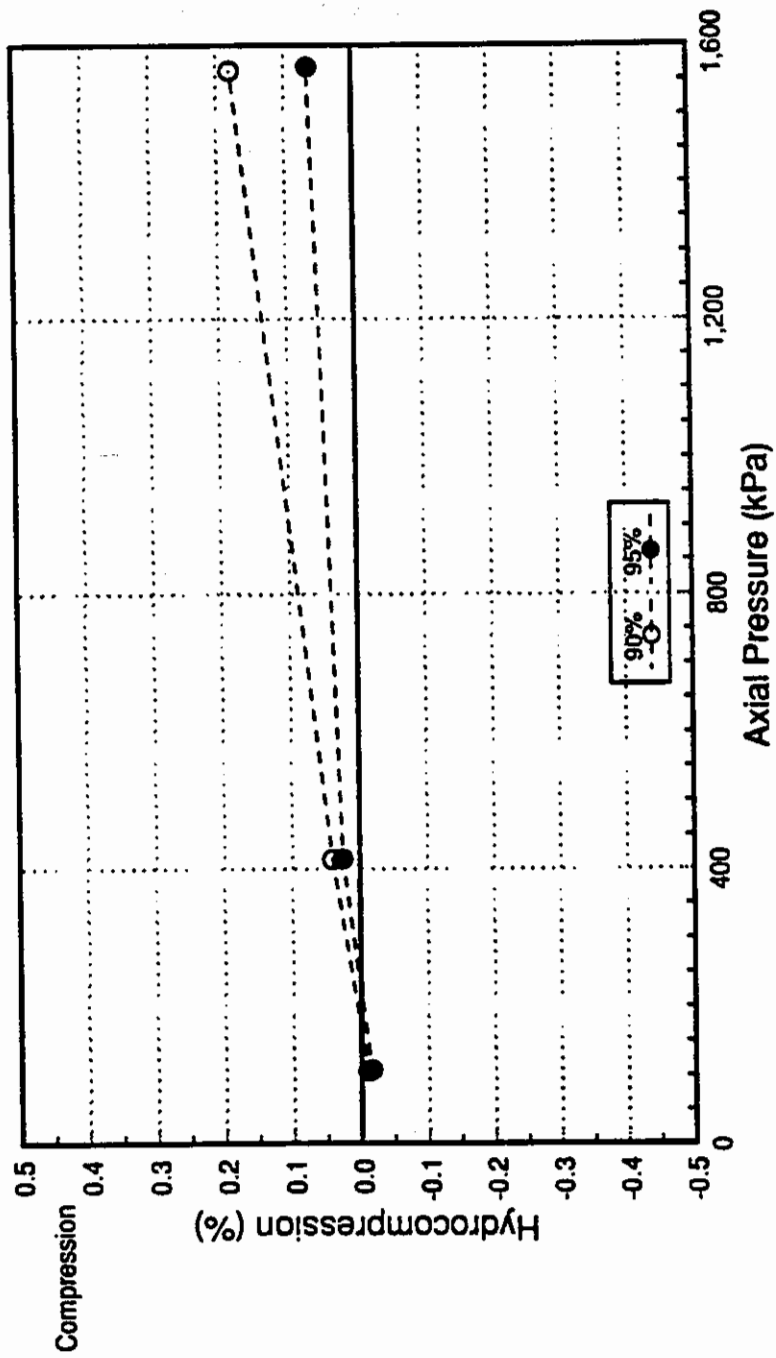


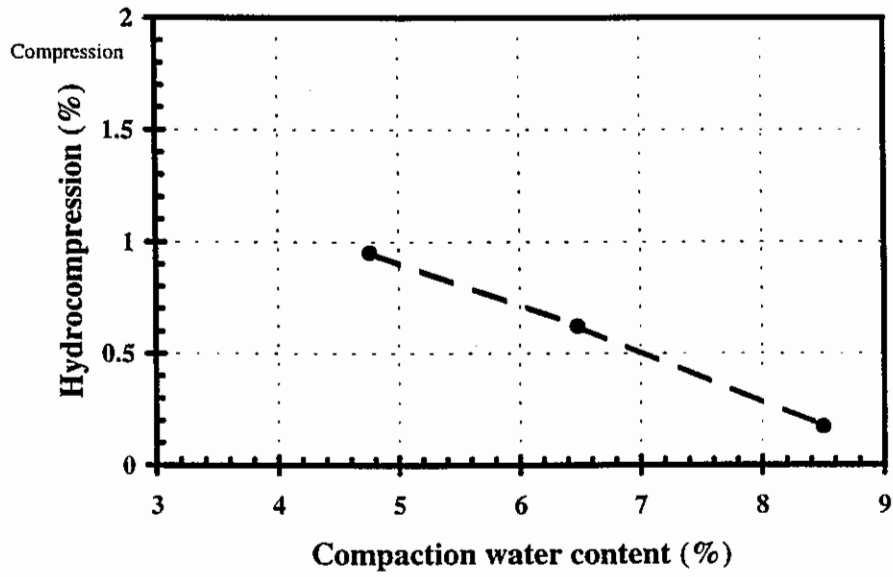
Figure 5.7 Effect of the soaking axial pressure on hydrocompression of decomposed granite, $w_c = 8\%$

compaction water contents, are shown in Figure 5.8a, and the resulting particle breakage levels are shown in Figure 5.8b. Hydrocompression increased from about 0.2 to 0.9 percent axial strain when the compaction water content was reduced from 8.0 to 5.0 percent. Note that all specimens were compacted at 90 percent relative compaction. The plot of particle breakage seems to provide the reason for the differences in hydrocompression. The breakage, in terms of IC (total value), in initially wetted specimens does not seem to vary with the remolding water content. However, the specimens that were loaded as-compacted and then wetted show a clear trend of increased breakage with decreasing compaction water content. This increased breakage may be largely responsible for the increased hydrocompression in drier specimens.

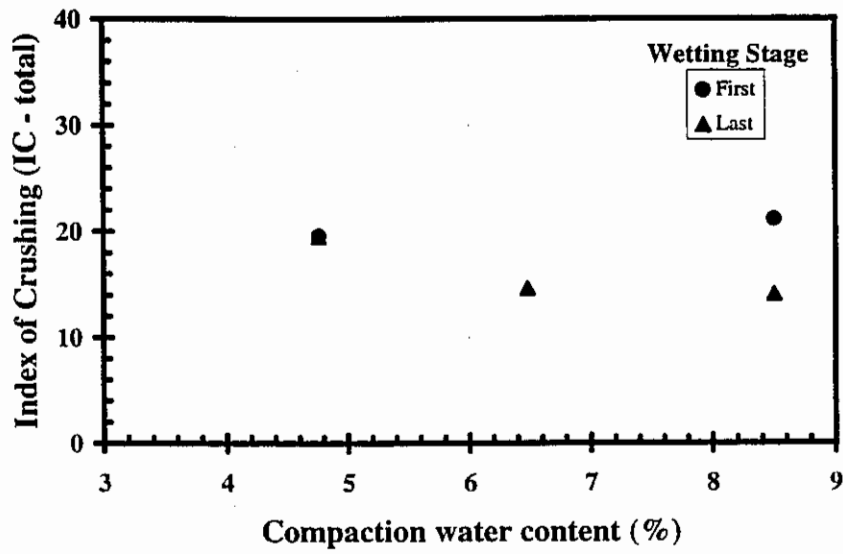
Observations #4, #5 and #6 by Nobari (1971) seem to be closely tied to the breakage characteristics of the material used. Uniformly graded specimens may exhibit greater breakage than well-graded specimens, and hence greater hydrocompression can be expected in the former, as observation #4 claims. Observation #5, that the particle size does not affect the amount of hydrocompression, seems contradictory to the evidence on breakage cited in Chapter 4. Coarse grains are known to undergo greater breakage than fine grains, especially upon wetting. Increased particle breakage may then cause an increase in settlement, contrary to Nobari's observation. In the tests that led to observation #6, Nobari states that the greater settlement of soaked argillite specimens correlated well with the greater breakage observed subsequently. However, the smaller amount of breakage in the basalt specimen could be a result not only of its greater particle compressive strength, but also of its smaller particle angularity compared to argillite.

5.3 Time effects on settlement

In general, the settlements in loaded granular masses are instantaneous compared to the settlements in clayey soils. However, under high pressures, settlements in granular specimens also increase gradually over time. A number of investigations point out that continual breakage of particles, even under a constant



(a) Hydrocompression



(b) Particle Breakage

Figure 5.8 Effect of compaction water content on hydrocompression and particle breakage in decomposed granite, RC = 90%

load, may be a major cause of this delayed settlement.

The settlement with time of a granitic gneiss rockfill sample, observed during several load increments in an oedometer test, is shown in Figure 5.9 (Marsal, 1973). Up to the third stage of loading (up to a normal stress of 800 kPa) the increase in settlement with time is fairly small. However, during the next load increment, about 20 to 25 percent of the total settlement occurred after the first minute. The settlement-time curve closely resembles that of a clayey soil, and therefore, can be divided into "primary" and "secondary" compression portions.

Vesic and Clough (1968) suggested that the theory of consolidation is inappropriate to explain the secondary compression in granular materials because it does not take the particle breakage phenomenon into account. A theoretical explanation, from a different perspective, for the primary compression portion of a granular material in one dimensional consolidation is presented by Marsal (1965). The movement of particles is assumed to be the result of; a) erratic impulses transferred to each grain by its neighbors, represented stochastically by a coefficient of diffusion, and b) constant forces which cause particles to drift at a constant speed. It is assumed that the particles move in a viscous medium, and the movements follow Markov's Random Walk process. The theoretical prediction closely matched the primary compression portion of the settlement-time curve for mica gneiss rockfill (Marsal, 1973). The secondary compression portion of the curve, Marsal (1973) speculates, is the result of a subsequent diffusion process, caused by sliding, breakage and rearrangement of particles, and is of a smaller order of magnitude than in primary compression.

In Figure 5.9, the slope of the secondary compression portion of the curve (C_{α}) seems to increase with increasing axial pressure. Colliat-Dangus and others (1988) reported a threshold pressure beyond which the secondary compression increases rapidly with confining pressure in triaxial isotropic compression tests of sand. For weak calcareous sand the threshold stress was about 0.8 MPa and for stronger siliceous sand about 6 MPa. Grain size analyses showed that increased compression with time correlated well with increases in particle breakage. Feda

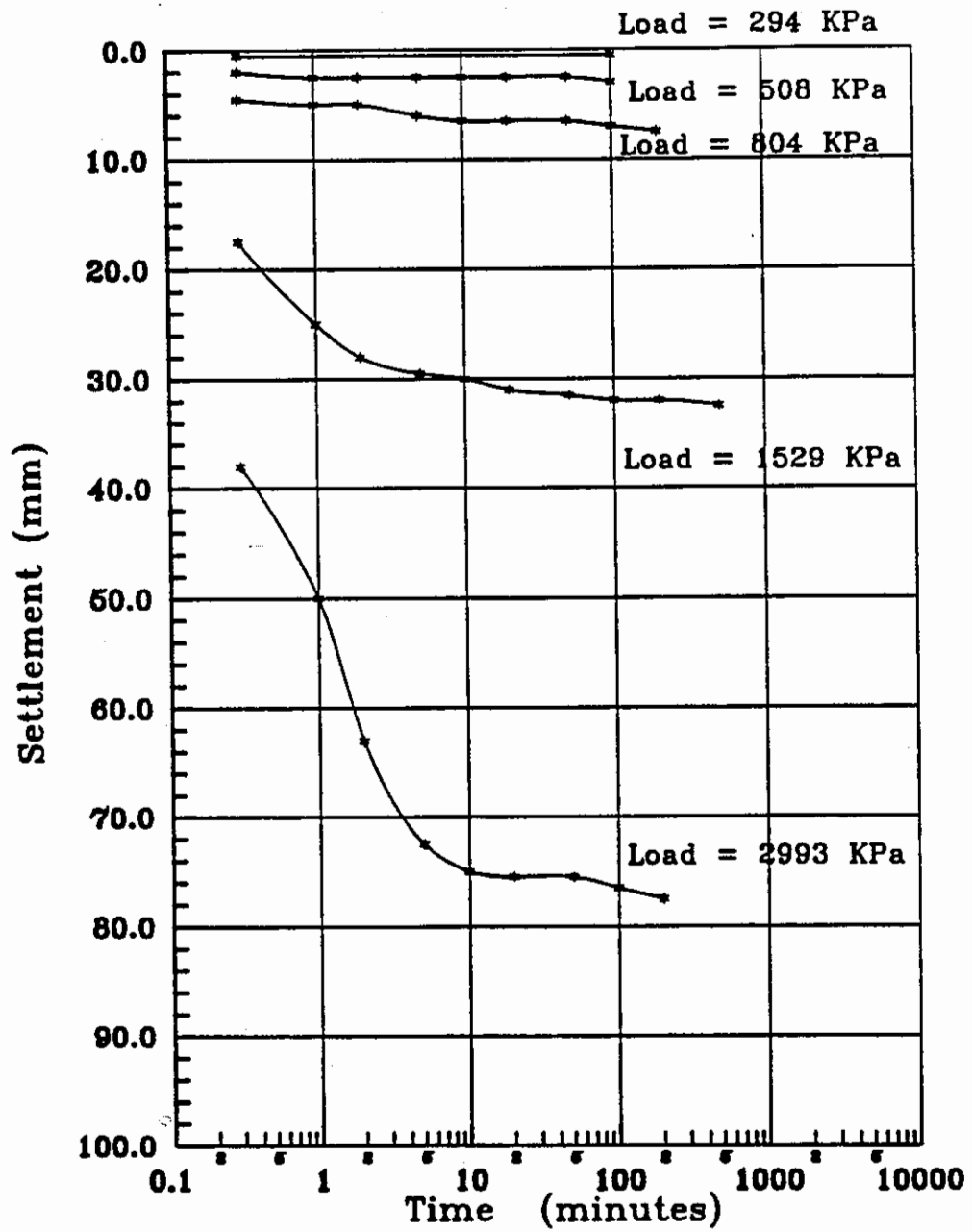


Figure 5.9 Time-settlement curves in rockfill (after Marsal, 1973)

(1992) also reported a substantial increase in C_α with axial pressure in oedometer tests of Goldisthal shale, a rockfill material that is highly susceptible to breakage. The increase is much higher in loose specimens (16.5 kN/m^3) than in dense specimens (20.0 kN/m^3), as shown in Figure 5.10. Moreover, in loose specimens the C_α value decreased under much higher pressures while it did not decrease in dense specimens. Fedá (1992) compares this behavior of rockfill to that of sensitive undisturbed clay.

Typical results of oedometer tests on decomposed granite from Shasta Bally batholith are shown in Figures 3.5 and 3.6. The load increments were applied "instantaneously", and the settlement values are log-linear with time from the beginning of the first test (first reading was taken 0.1 minutes after loading). Therefore, the primary compression in this material seems to be "instantaneous", contrary to the observations on rockfill by Marsal (1973). The C_α values for the loading stages 100 and 400 kPa are similar, and at the highest loading stage, 1600 kPa, C_α is about three times greater. These values for both dense and loose specimens are plotted in Figure 5.10 along with the results of Goldisthal shale. It is interesting to note that C_α values for decomposed granite are in the same range as those for shale, although the latter has a maximum particle size of 200 mm and was tested in 100 cm diameter x 33 cm high mold.

If C_α is independent of time, then the secondary compression in oedometer (or in uniaxial creep) is said to be logarithmic (Fedá, 1992). A common form of representing this behavior is the plot of the logarithm of the axial strain rate versus the logarithm of time. Then a material that follows logarithmic creep should generate a straight line (or a narrow band of points) that has a slope of -1.0. Fedá (1992) plotted test results of a number of granular and clayey materials in a similar plot, as shown in Figure 5.11. The softer, clayey materials usually lie above the stronger, granular materials. Most materials seem to follow the logarithmic creep law, except Sedlec loess (#7) and Goldisthal shale (#5) (in fact, the C_α values given for the shale in Figure 5.10 are only approximate values). Both these materials have structural instabilities. The loess tends to collapse upon saturation and the shale is very susceptible to breakage, as mentioned

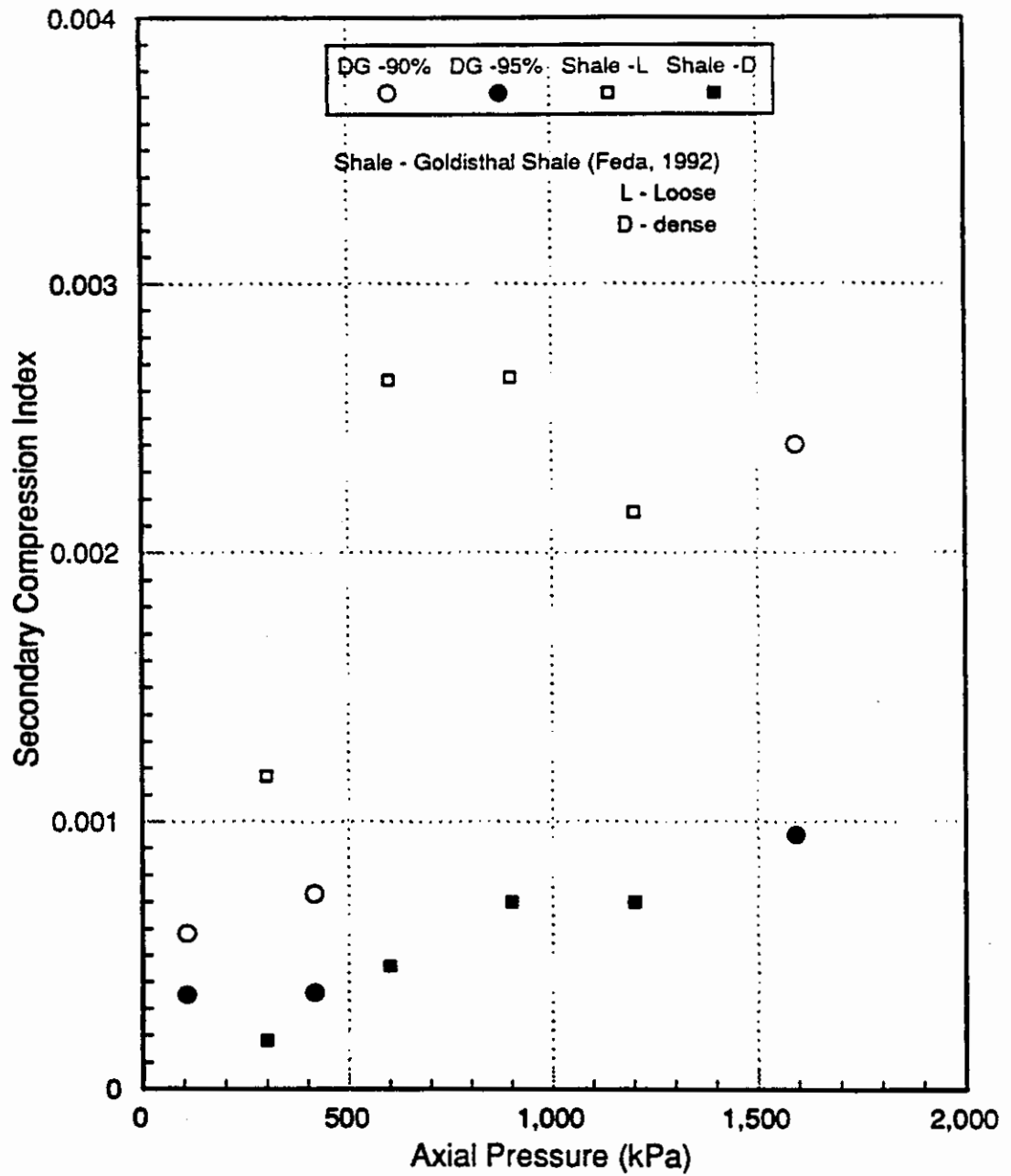


Figure 5.10 Effect of axial pressure on the secondary compression index in decomposed granite and in Goldisthal shale

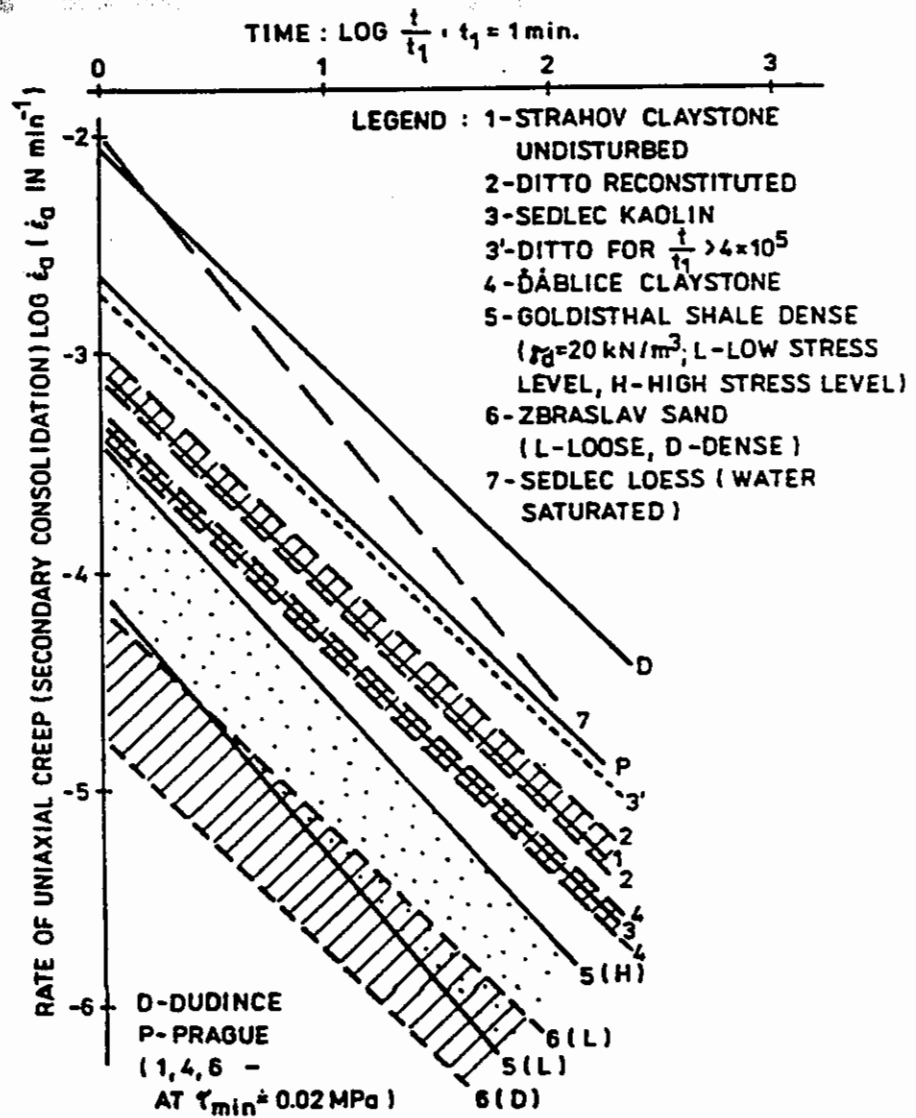


Figure 5.11 Relationship between creep rate and time of some clays and granular materials (from Feda, 1992)

before. Mejia and others (1988) also reported a deviation from logarithmic creep behavior in oedometer tests of an angular tailings sand, an initial steeper line later flattening out to a slope of -1.0.

In Figure 5.12, axial strain rates of decomposed granite from the current study are plotted against time. The data points form a relatively wide band, but they generally follow the logarithmic creep law (as the results in Figures 3.5 and 3.6 indicate). For comparison, the band corresponding to dense Goldisthal shale is also shown in the figure. The decomposed granite lies slightly above the shale. Although breakage is still the main reason for creep in decomposed granite, the relatively low breakage under the axial loads used (as seen in Figure 4.10) apparently prevented major structural instabilities, which otherwise would deviate the specimens from logarithmic creep.

5.4 Volume change in strength tests

The confining pressure controls the volume change behavior of a given specimen to a large extent. For example, although dense granular soils tend to dilate upon shearing, at greater confinement volumetric strain may change from dilation to contraction (from negative to positive, according to the sign convention adopted in this study). Seed and Lee (1967) showed that, in specimens compacted to the same relative density, the critical confining pressure (the pressure at which shearing-induced volumetric strain would be zero) is smaller for materials of lower particle compressive strength. In other words, at a given confinement, the dilation upon shearing is suppressed more if the particle breakage is higher.

The behavior of volumetric strain is discussed below in several stages: the behavior of volumetric strain in consolidation phase; shearing phase; and the combined total. Finally, another aspect of volumetric strain in strength tests, the rate of volume change, which links volume change to shear strength is also discussed. In the current test program volume change was measured in two types of strength tests, triaxial and direct shear. However, as mentioned in Chapter 3, the volume change measurements in direct shear tests were not so accurate as to

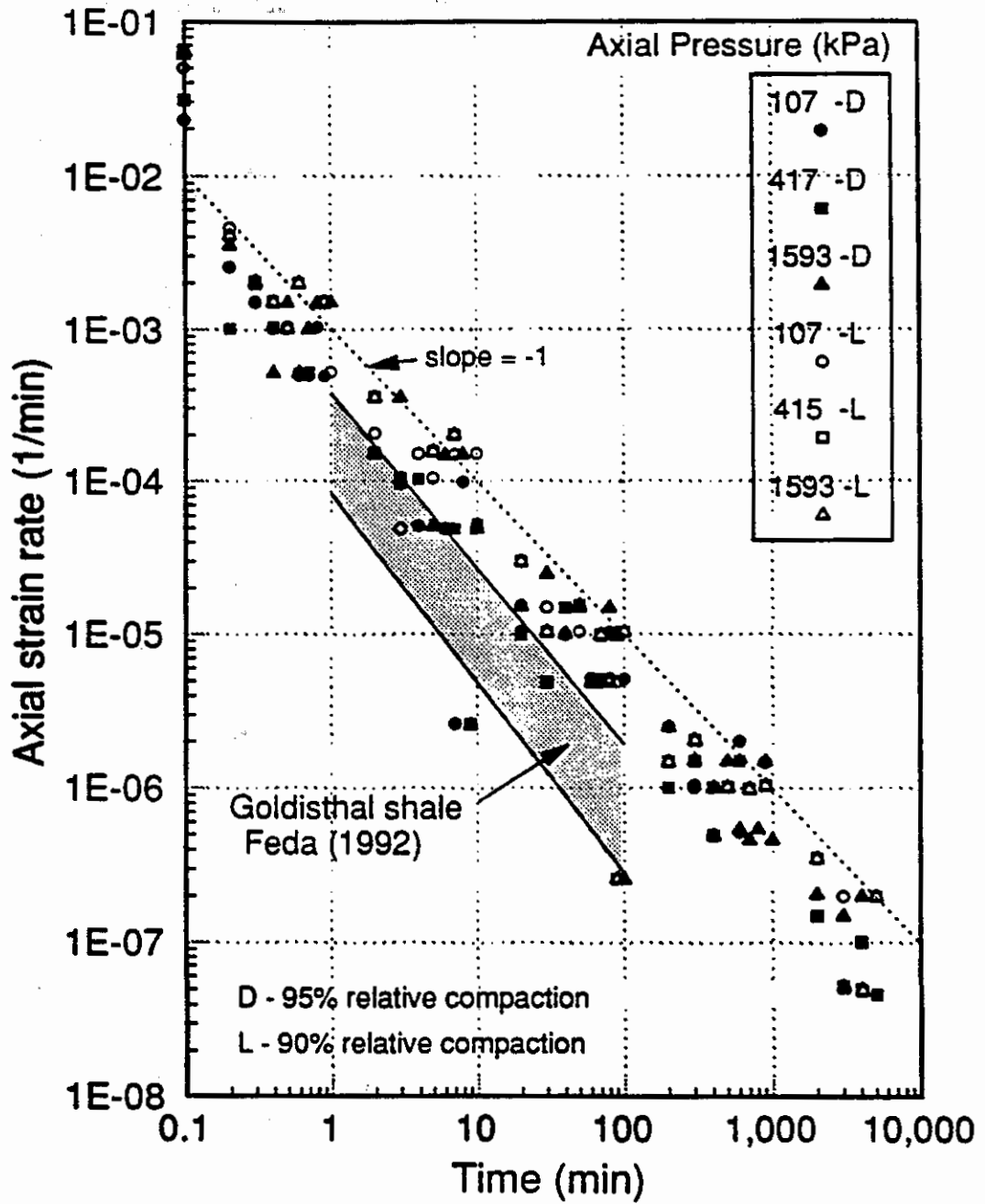


Figure 5.12 Relationship between creep rate and time for decomposed granite

allow detailed quantitative analyses. Therefore, only the results from triaxial tests are discussed below.

5.4.1 Volumetric strain in consolidation phase

Investigations of isotropic consolidation of gravelly sand by Lee and Farhoomand (1967) revealed a close relationship between particle breakage and compressibility of granular materials. Their observations can be summarized as follows: a) coarse cohesionless soils are more compressible than fine cohesionless soils; b) uniform soils are more compressible than well-graded soils of the same maximum particle size; and c) soils with angular particles are more compressible than those with sub-rounded particles. These inherent soil characteristics that increase compressibility are similar to those that increase particle breakage (see, Chapter 4). However, it must be noted that Lee and Farhoomand (1967) ignored membrane compliance in tests at confining pressures greater than 1 ksc (100 KPa). More recent work (e.g., Anwar, 1989) has shown that membrane compliance effects could be significant in triaxial tests of granular soils, especially when developing trends such as above.

The relationship between volumetric strain and maximum principal stress (σ_1) under anisotropic consolidation of granular materials has been discussed in detail by several investigators. After observing a unique relationship between volumetric strain and σ_1 in coarse sands consolidated under different K_c ($= \sigma_{1c}/\sigma_{3c}$) values (see Figure 5.13), Lee and Farhoomand (1967) suggested that the Rutledge hypothesis may be valid for granular soils also. The Rutledge hypothesis, which states that compressibility is uniquely dependent on σ_1 and is independent of either σ_3 or the shearing stress, was proposed originally for clayey soils only (Rutledge, 1947). Ladanyi (1967), among others, contested the generality of the proposition by Lee and Farhoomand (1967). At $K_c = 1$, Ladanyi argued, a particular σ_1 (which, at $K_c = 1$ is equal to the mean normal stress, σ_m) would produce primarily compression with little crushing, whereas the same σ_1 at $K_c > 1$ would produce less compression (because now $\sigma_m < \sigma_1$) but more crushing. Accordingly, though it is possible that tests at different K_c values could

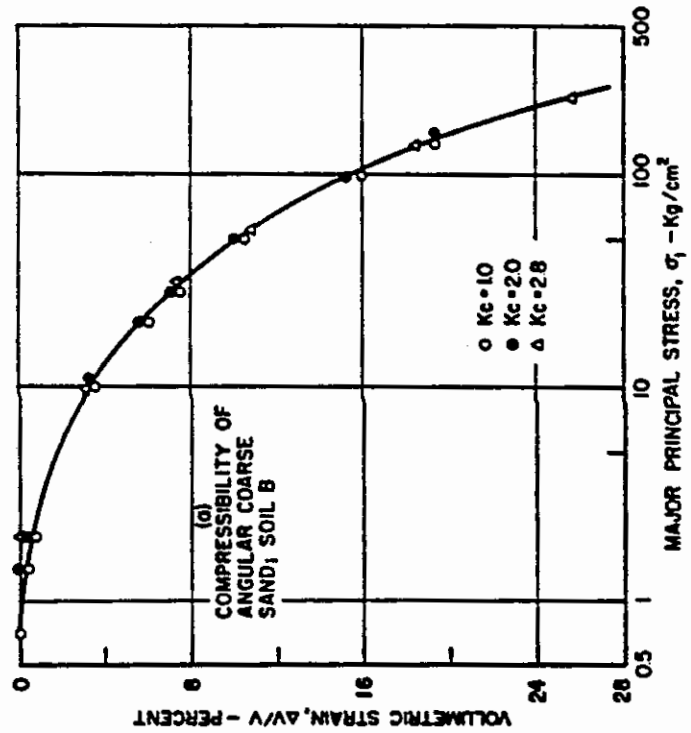
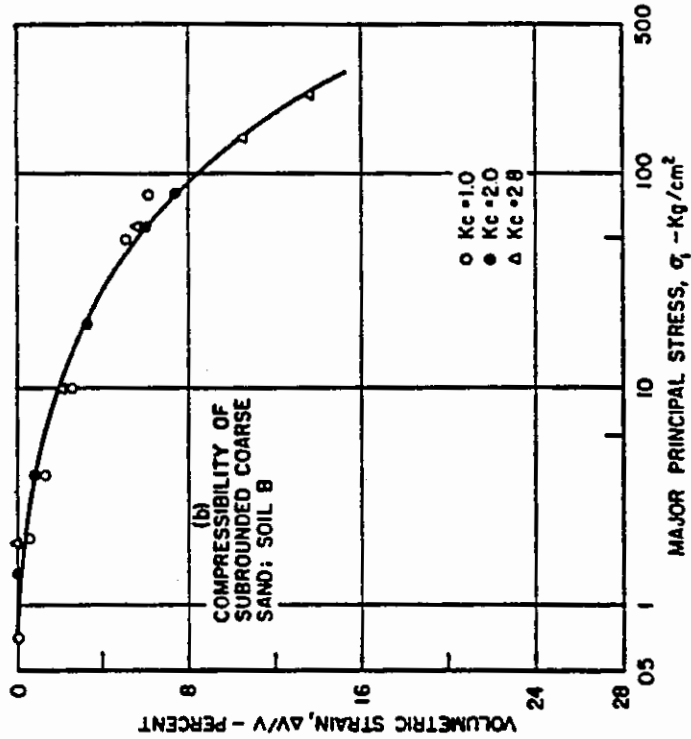


Figure 5.13 Effect of K_c value on compressibility of sands (from Lee and Farhoomand, 1967)

produce a unique compression curve, Ladanyi suggests that there is no basis to expect the same behavior from all stress paths.

Most triaxial specimens in the current test program were consolidated isotropically (the T100 and T200 series, Table 3.2). A few additional specimens, the T300 series, were consolidated anisotropically (at $K_c = 1.8$ and 2.5) to examine the validity of the above claim by Lee and Farhoomand. The consolidation phase volumetric strains of all the specimens, corrected for membrane penetration (see section 3.3.5), are plotted in Figure 5.14 against the maximum principal consolidation pressure (σ_{1c}). The data points for specimens at 90 percent relative compaction lie below those for denser specimens, as expected. Anisotropic consolidation tests were performed only on dense specimens, and the corresponding data points lie above the general trend for the isotropically consolidated specimens, contrary to the Rutledge hypothesis. All anisotropic consolidation tests were carried out at a confinement of 900 kPa, and the resulting volumetric strain values are not very different from the average volumetric strain of a corresponding isotropic test specimen. The reason why volumetric strain did not increase with the increase in σ_1 in anisotropic consolidation can be explained using the breakage results estimated at the end of consolidation. Post-compaction particle breakage values at the end of anisotropic consolidation, estimated from tests T353 and T354, were nearly equal to zero. Following Ladanyi's (1967) argument, volumetric strain in anisotropic consolidation will increase only if more crushing occurs, because the compression, controlled by σ_m , will not be much different from an isotropic test specimen at the same confinement. Since the breakage was insignificant, so was the breakage-induced volumetric strain, and hence the strain values in anisotropic tests were only slightly different from those of isotropic tests.

5.4.2 Volumetric strain in shearing phase

Volumetric strains that occur in the shearing phase of drained strength tests seem to depend heavily on the stress path. Conventional triaxial tests at very high confining pressures, performed by Vesic and Clough (1968) on

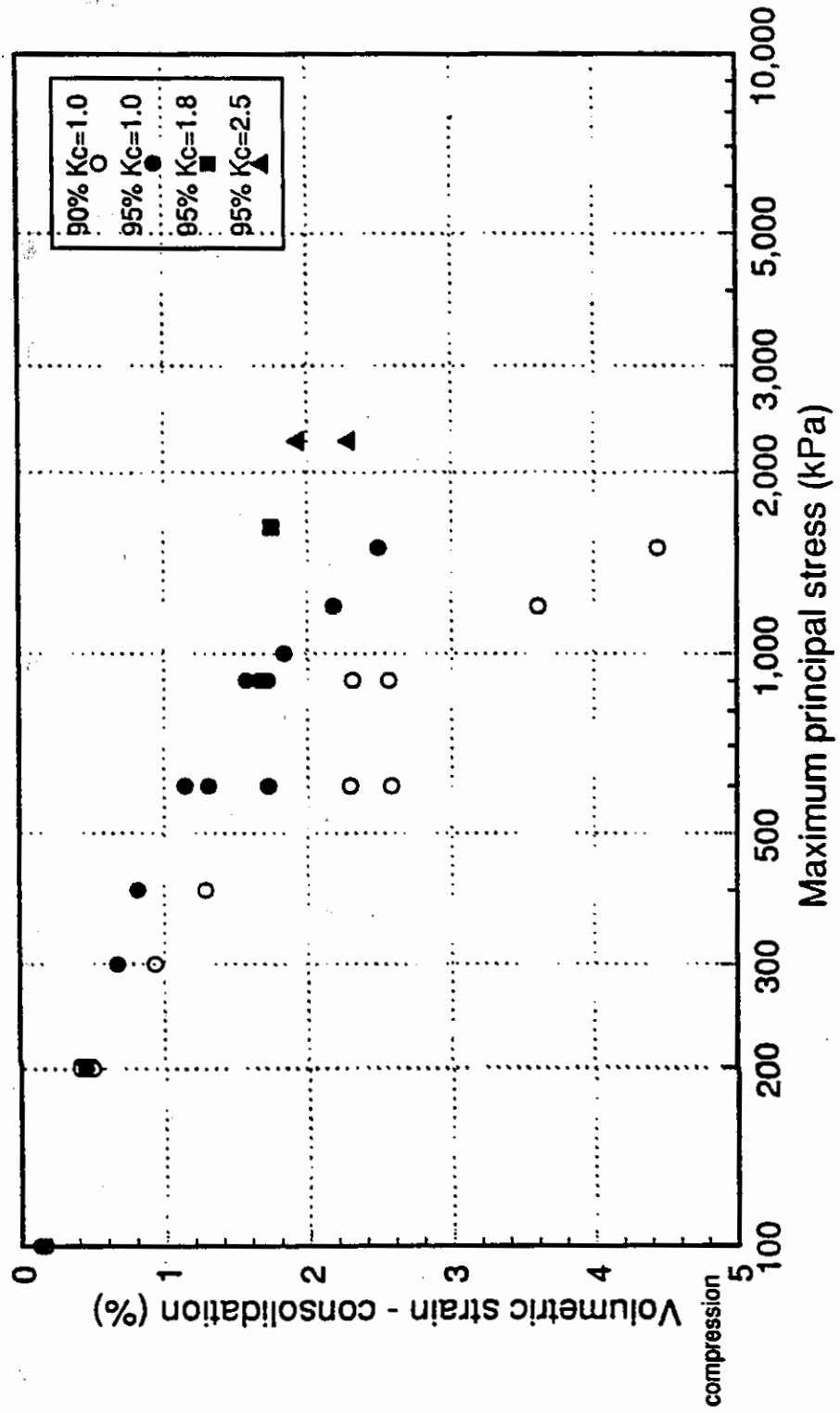


Figure 5.14 Variation of consolidation phase volumetric strain with σ_{1c} in decomposed granite triaxial specimens

Chattahoochee River sand, show that the (shearing phase) volumetric strain at failure does not increase monotonically with confinement; volumetric strain at failure at $\sigma_3 = 21$ MPa was about 13 percent and at $\sigma_3 = 63$ MPa only about 9 percent. When plotted against σ_m at failure, the results showed a peak in volumetric strain at failure at about 25 MPa, as shown in Figure 5.15. In comparison, in a series of "octahedral shear" tests, the volumetric strain at failure increased rapidly with increasing σ_m and reached more or less a constant value. In an octahedral shear test, σ_m is maintained constant while the specimen is subjected to increasing octahedral shear stress ($\tau_{oct} = 1/3[\Sigma(\sigma_i - \sigma_j)^2]^{1/2}$), whereas in conventional triaxial tests σ_3 is maintained constant while the specimen is subjected to increasing τ_{oct} and σ_m . This observation led Vesic and Clough (1968) to claim that τ_{oct} , rather than σ_3 , controls the (shearing phase) volumetric strain at failure in granular materials.

The (shearing phase) volumetric strains at failure of decomposed granite specimens of the current triaxial test program (conventional type) are plotted in Figure 5.16 against σ_m at failure. The volumetric strain values of loose (90 percent relative compaction) specimens lie above (more compressive than) those of dense specimens. This is expected because, up to failure, the main contribution to volumetric strain comes from compression, and compressive strains are higher in loose specimens. In Chapter 4, it was shown that particle breakage in a triaxial specimen becomes significant only after the point of failure (see Figure 4.13), at least within the range of pressures used in this test program. The trend shown in Figure 5.15, a peak in volumetric strain under conventional triaxial testing, was not exhibited in decomposed granite results, probably because the range of pressures used is not sufficiently large.

In weak granular soils, high confining pressures can produce very high compressive volumetric strains. In a triaxial test of fragile limestone sand, compressive volumetric strain at failure peaked at about 17 percent under a confining pressure of 2.6 MPa (Lo and Roy, 1973). Similarly high strains were exhibited by soft Venato sandstone (Becker, 1972), by a weak calcareous sand (Colliat-Dangus and others, 1988) and by weak Shirasu pumice-tuff (Kitamura and

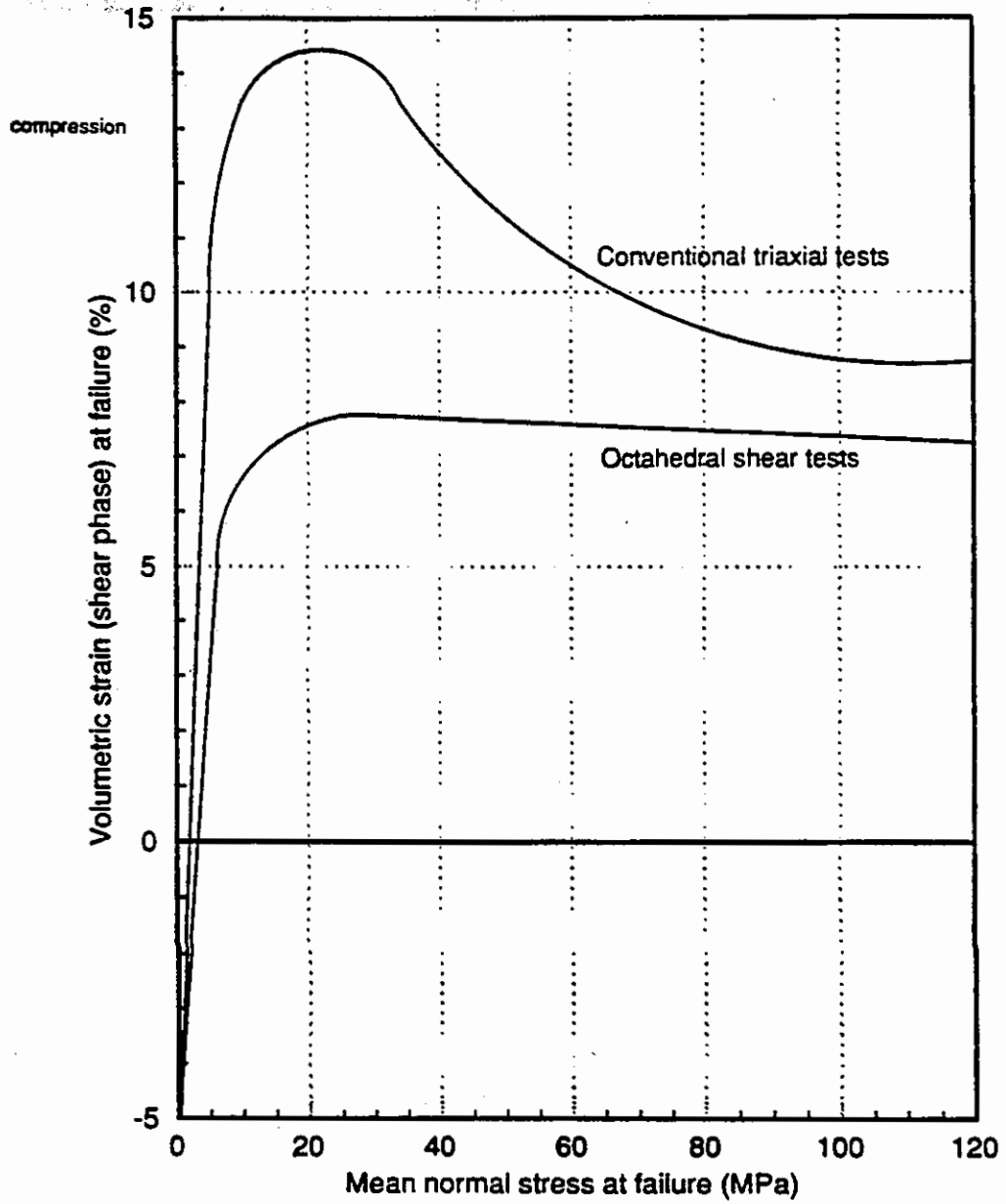


Figure 5.15 Variation of shearing phase volumetric strain with $(\sigma_m)_f$ in Chattahoochee River sand triaxial specimens (after Vesic and Clough, 1968)

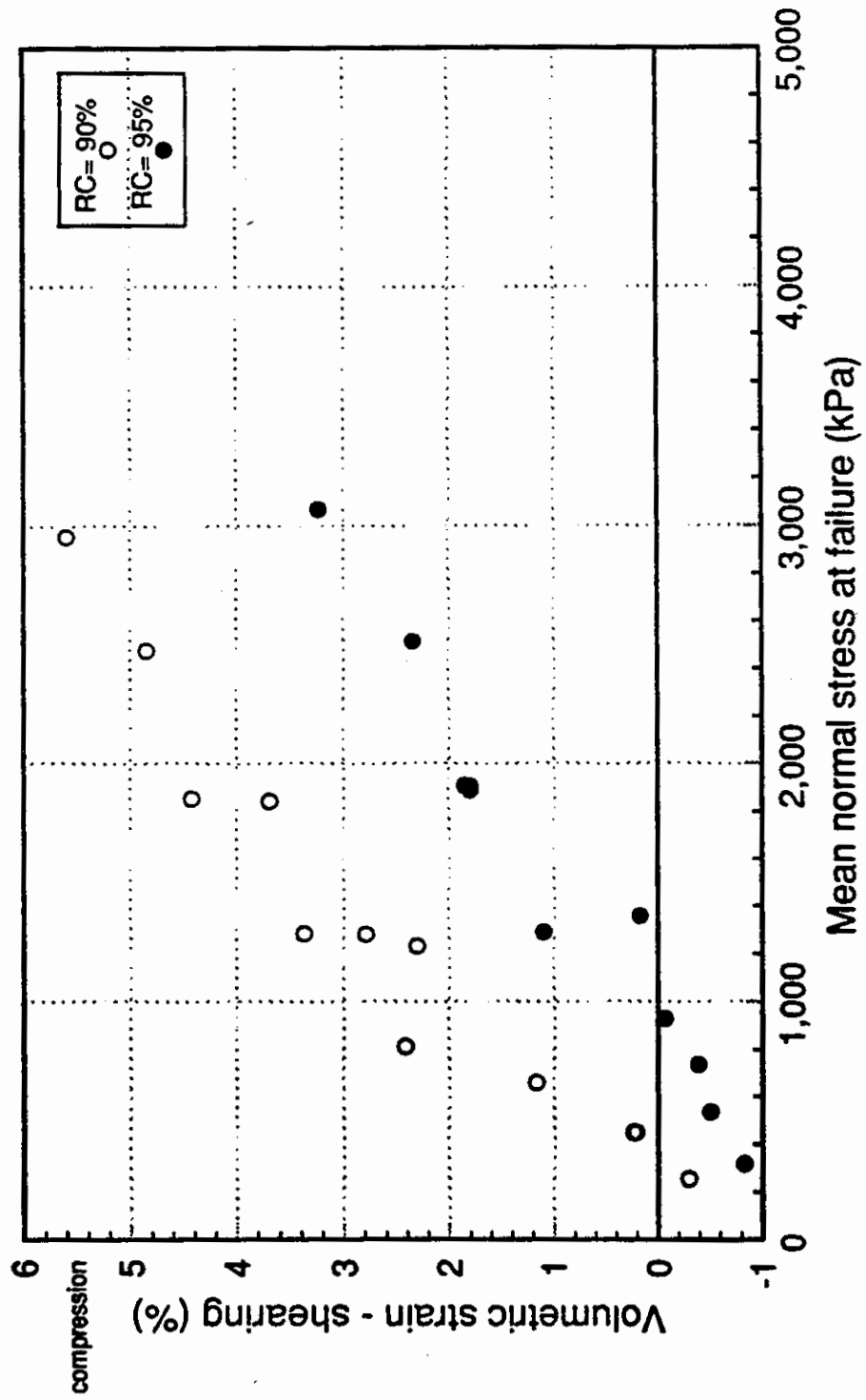


Figure 5.16 Variation of shearing phase volumetric strain with $(\sigma_m)_f$ in decomposed granite

Haruyama, 1988). In comparison, shearing phase volumetric strains in decomposed granite are somewhat lower. As shown in Figure 5.16, volumetric strains at failure under the maximum stress levels used (i.e., in specimens at 1.5 MPa confinement) are about 5.5 and 3.0 percent for the loose and the dense specimens, respectively. Lee (1991) reported about 10 percent volumetric strain at failure for a specimen of Seoul decomposed granite, compacted at about 85 percent relative compaction and tested at 1.8 MPa confinement.

5.4.3 Total volumetric strain

Experiments have shown that the total volumetric strain at failure (i.e., the sum of volumetric strains under both consolidation and shearing stages) of granular materials is independent of the stress path, at least in the context of triaxial compression testing. Both Billam (1971) and Colliat-Dangus and others (1988) speculated about the impact the breakage-related consolidation phase volumetric strains would have on subsequent shearing phase volumetric strains in triaxial testing of soft materials. Becker's (1972) results on Venato sandstone, shown in Figure 5.17, clearly display the impact: identical triaxial specimens, consolidated at different K_c values and at different confining pressures, indicate that the total volumetric strain at failure is uniquely related to σ_3 irrespective of the stress path. Much of the volumetric strain is attributed to particle breakage, which in this soft sandstone, is accelerated by the saturated and drained test condition. Post-failure gradation tests also confirmed that large amounts of breakage had taken place. Becker (1972), however, did not attempt to explain the unique relationship between total volumetric strain at failure and the confining pressure.

A total volumetric strain based hypothesis was put forth by Murphy (1987) primarily to explain breakage-related shear strength differences in materials of different hardness. It also explains the effects of different stress paths on breakage-related volumetric strain as follows:

- 1) "A given granular assembly has a fixed capacity for total volumetric strain. This capacity depends on initial density, assembly structure and the

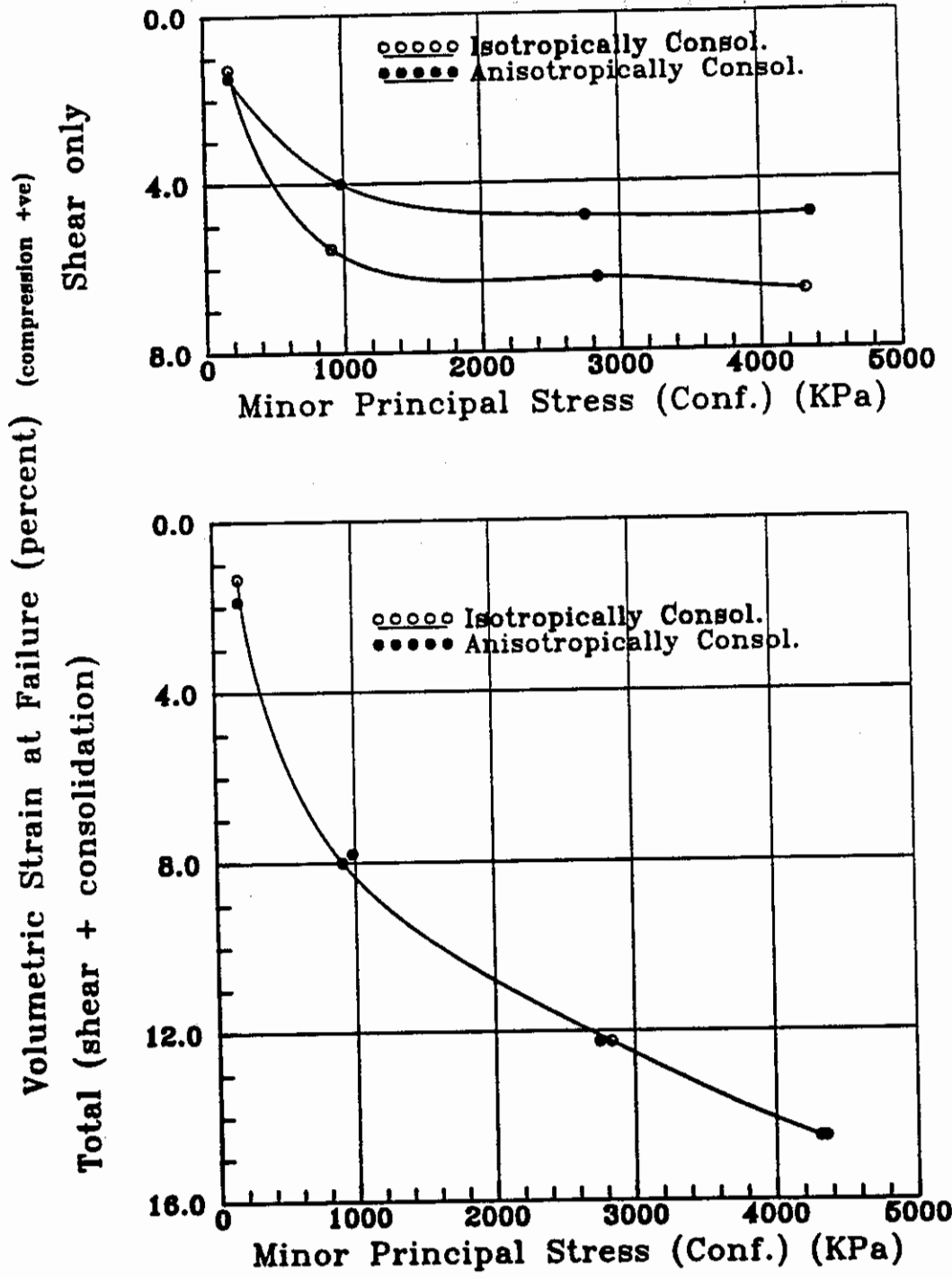


Figure 5.17 Variation of volumetric strain (in shearing phase and total) at failure with confinement in Venato sandstone (after Becker, 1972)

- crushing strength or mineralogical hardness of the material concerned.
- 2) Beyond some stress level (the magnitude of which varies with mineralogical composition) volumetric strain occurs primarily as a result of particle crushing. . . .
 - 3) . . . the crushing that can occur during shear depends on how much of the total volumetric strain (or crushing) capacity is spent during consolidation. . . ."

As seen in top half of Figure 5.17, the shearing phase volumetric strain at failure under a given confinement is lower if the specimen is consolidated anisotropically. This is commonly attributed to the smaller additional shearing needed to fail such specimens, compared to isotropically consolidated specimens. In materials where breakage-induced volumetric strains dominate, another reason could be the greater breakage under anisotropic consolidation (see, Chapter 4) which leaves less volumetric strain capacity available for the shearing phase.

The triaxial test series T300, conducted in the current study on decomposed granite from the Shasta Bally batholith, provides an opportunity to investigate the above hypothesis further. The volumetric strains and breakage levels of all T300 series tests and relevant T100 series tests are given in Table 5.1. Some specimens were subjected only to consolidation and then were dismantled to estimate breakage. Note that the shearing phase volumetric strain levels given are at failure, whereas the final breakage values were estimated at a point beyond failure, at about 20 percent axial strain. The results indicate that, with increasing K_c value, volumetric strain in shearing phase decreases rapidly while the strain in consolidation phase does not change as much. Therefore, the total volumetric strain values under different consolidation processes do not coincide as observed by Becker. The reason is obvious from the results of breakage. The IC values after consolidation indicate that no significant breakage has taken place during anisotropic consolidation. Therefore, the hypothesis by Murphy (1987), which applies primarily to breakage-related strains, seems inappropriate for this situation.

Table 5.1 Volumetric strain and breakage of dense ($RC = 95\%$) triaxial specimens consolidated at 900 kPa confinement under different K_c values

Specimen #	K_c	Volumetric strain (%)			IC (post-comp)	
		consol	shear	total	consol	final
T156b	1.0	1.70	1.80	3.50		8.0
T159a	1.0	1.67			n/a	
T351a	1.8	1.75	1.28	3.03		2.5
T353a	1.8	n/a			0.0	
T352a	2.5	1.94	0.98	2.92		3.0
T354a	2.5	2.29			0.0	
T354b	2.5	n/a			0.0	

5.4.4 The rate of volume change

The slope of the volumetric strain versus axial strain curve ($d\epsilon_v/d\epsilon_1$), or the rate of volume change (the rate of dilatancy, according to some investigators), in a drained triaxial test is also useful as a volume change indicator. The $d\epsilon_v/d\epsilon_1$ at failure, $(d\epsilon_v/d\epsilon_1)_f$, is usually negative if the specimen dilates upon shearing. At higher confining pressures, however, $(d\epsilon_v/d\epsilon_1)_f$ tend to increase towards zero. For a given placement condition, the confining pressure at which $(d\epsilon_v/d\epsilon_1)_f$ becomes zero seems to depend on the particle compressive strength (Lo and Roy, 1973). For example, in triaxial tests of aluminum oxide sand, quartz and limestone sand, the confining pressure at which $(d\epsilon_v/d\epsilon_1)_f$ became zero was about 750 psi (5 MPa) for aluminum oxide sand (the strongest of the three materials), about 300 psi (2 MPa) for quartz, and about 50 psi (0.3 MPa) for the weakest, limestone sand. In Figure 5.18, the behavior of $(d\epsilon_v/d\epsilon_1)_f$ with confining pressure for a number of sands, including the three types tested by Lo and Roy (1973), is summarized. Dense Ottawa sand seems to require the highest confining pressure, about 1500 psi (10 MPa), for $(d\epsilon_v/d\epsilon_1)_f$ to reach zero.

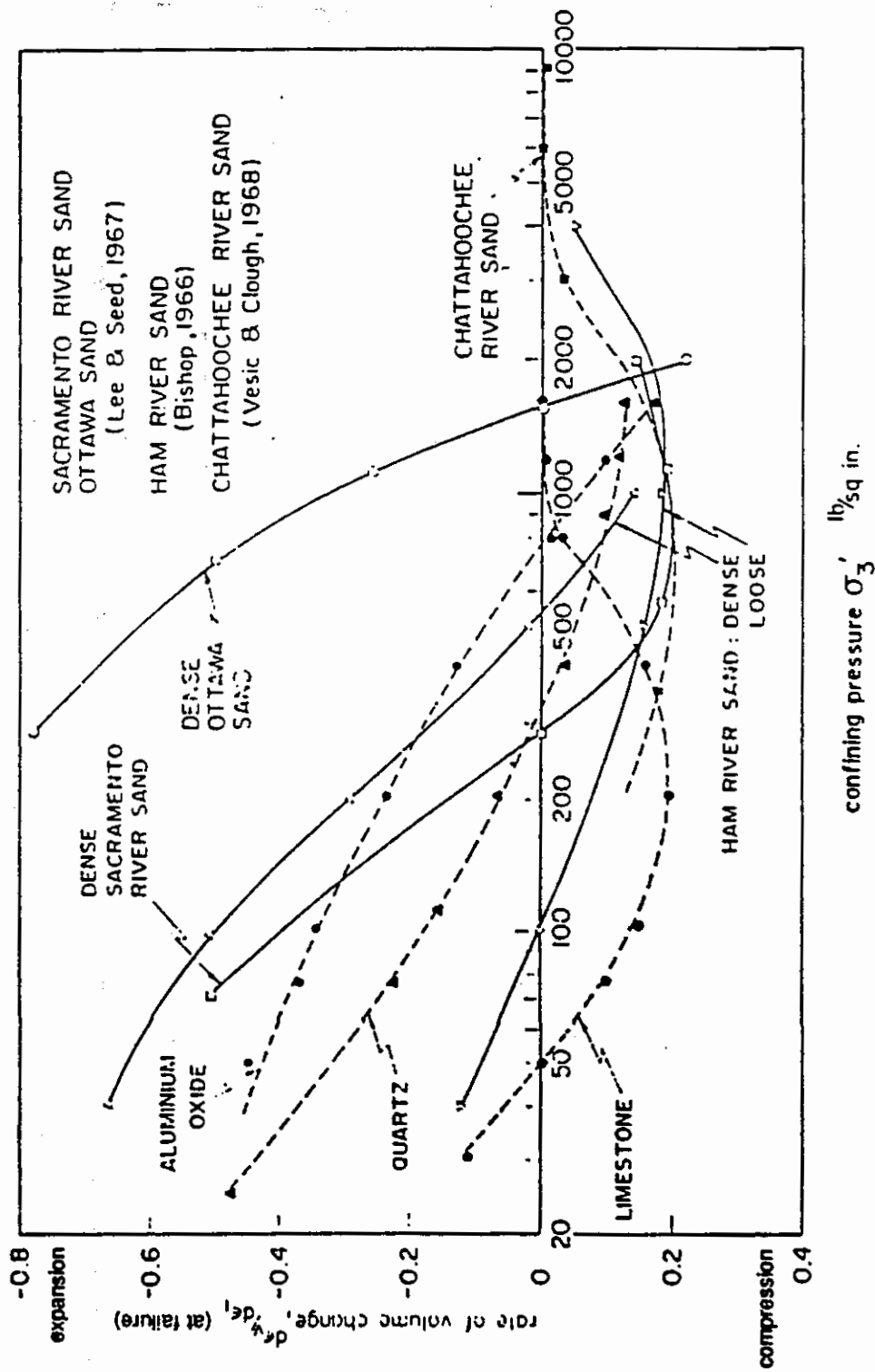


Figure 5.18 Behavior of $(d\varepsilon_v/d\varepsilon_1)_f$ with confining pressure in sands (from Lo and Roy, 1973)

The close link between volume change characteristics and particle breakage was demonstrated by an interesting observation by Lo and Roy (1973) in the three soil types they tested. In each specimen that exhibited $(d\epsilon_V/d\epsilon_1)_f = 0$, irrespective of the confining pressure at which it was achieved, the D_{50} value decreased (due to breakage) by a similar amount, about 15 to 20 percent.

At higher confining pressures the curve for Ottawa sand shows $(d\epsilon_V/d\epsilon_1)_f$ monotonically increasing, whereas the other sands indicate a tendency to reach a positive peak (see, Figure 5.18). In fact, the curves for limestone sand, Chattahoochee river sand and loose Ham river sand show $(d\epsilon_V/d\epsilon_1)_f$ decreasing towards zero again under further increases in confinement. This positive peak in $(d\epsilon_V/d\epsilon_1)_f$ is discussed further in Chapter 6 in relation to the shear strength characteristics.

The trends of decomposed granite specimens in the current test program, shown in Figure 5.19, are somewhat similar to those displayed in Figure 5.18. The loose (90 percent compaction) specimens show $(d\epsilon_V/d\epsilon_1)_f$ reaching zero at about 400 kPa while the dense specimens did the same at about 1000 kPa. However, none showed positive values of $(d\epsilon_V/d\epsilon_1)_f$ under any confinement, contrary to the trends exhibited by other fragile materials discussed above. This behavior will be discussed further in Chapter 6 with respect to the development of shear strength in triaxial tests of decomposed granite.

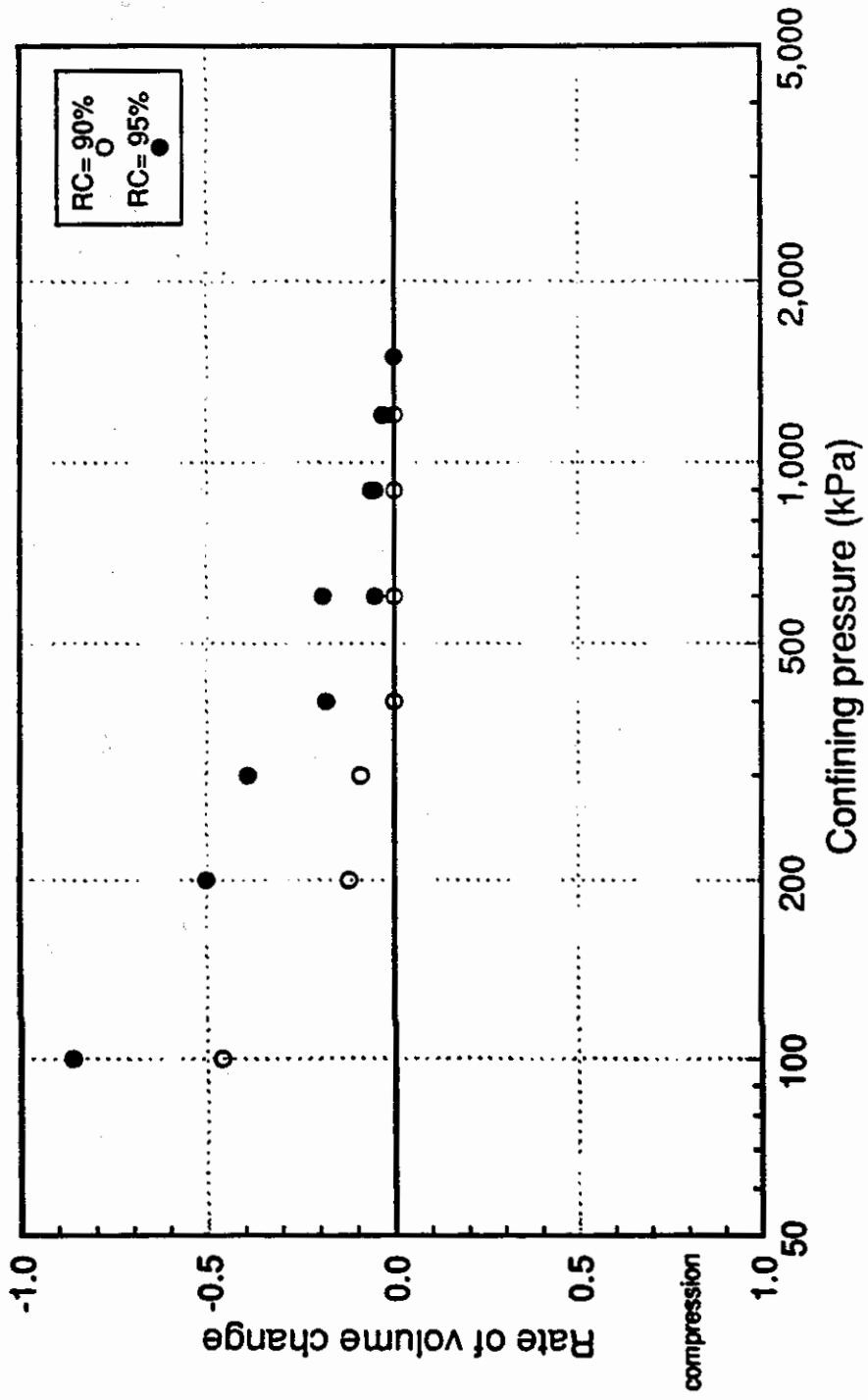


Figure 5.19 Variation of $(d\epsilon_v/d\epsilon_1)_f$ with σ_3 in decomposed granite triaxial specimens

CHAPTER 6

SHEAR STRENGTH CHARACTERISTICS AND THE INFLUENCE OF PARTICLE BREAKAGE

The discussion in this chapter focuses on shear strength characteristics of compacted granular materials under conditions where particle breakage is significant. The chapter is divided into two parts: in Part I, the discussion is focused on laboratory triaxial shear strength test results; in Part II, the use of earth reinforcements to enhance the shear strength of compacted granular fills is investigated. Part I first examines the commonly used parameters that describe shear strength under triaxial conditions, and reviews laboratory test results of various granular materials from previous investigations to identify the factors that govern shear strength, especially under high breakage. Triaxial test results from the current study are then analyzed to identify whether decomposed granite exhibits any peculiar variations from the trends. The first section of Part II investigates the variation of soil-reinforcement interface shear strength in decomposed granite as the normal pressure varies. Interface shear strength is then compared to the shear strength of compacted decomposed granite using direct shear tests. The last section analyzes the pullout strength of earth reinforcements in decomposed granite under relatively high normal pressures that correspond to the height of the proposed embankment. At the end of the chapter, a summary of construction practices and mechanical properties used in some decomposed granite embankments is presented.

Part I - Triaxial Test Results

6.1 Shear strength parameters of granular materials

In granular materials, shear strength is usually expressed using only the angle of shear resistance (ϕ) because cohesion is negligible, unless stress levels are low, and the material has a large amount of plastic fines. The angle of shear resistance was first considered to be composed of three components: the interparticle sliding friction component (ϕ_{μ}), the dilational component (ϕ_d) and the

reorientational component (ϕ_r) (Rowe, 1962). The portion of shear strength mobilized by the energy required to overcome interparticle sliding friction, ϕ_μ , is generally considered as approximately constant for a given material. The portion of the strength mobilized to overcome dilation upon shearing, ϕ_d , and the portion of the strength spent on particle reorientation, ϕ_r , depend heavily on the compositional, environmental and stress conditions of the granular mass. Lee and Seed (1967) pointed out the significance of particle breakage in granular materials and proposed that the shear strength mobilized by the energy spent on particle breakage be also included as a part of ϕ . However, recognizing the difficulty in separately accounting for the amounts of energy spent on particle breakage and particle reorientation, they recommended that both of these processes be considered together in ϕ_r .

The angle of shear resistance (ϕ) is calculated from the principal stresses σ_1 and σ_3 in a triaxial test using the equation;

$$\tan^2 \left(45 + \frac{\phi}{2} \right) = \left(\frac{\sigma_1}{\sigma_3} \right) \quad (6.1)$$

According to this equation ϕ is at its greatest, or the shear strength of the material is fully mobilized, when σ_1/σ_3 reaches the maximum value. Hence, a granular mass is said to have failed when it attains the maximum value of σ_1/σ_3 .

The interparticle sliding friction component of ϕ , ϕ_μ (values of which for a number of non-clay minerals are tabulated by Mitchell, 1993), seems to be heavily dependent on particle surface properties. The dilational component ϕ_d can be estimated from the equation (Rowe, 1962):

$$\tan^2 \left(45 + \frac{(\phi - \phi_d)}{2} \right) = \frac{\sigma_1}{\sigma_3} \times \frac{1}{1 - \frac{d\epsilon_V}{d\epsilon_1}} \quad (6.2)$$

To obtain the value of ϕ_d mobilized at failure of the soil mass, the terms ϕ , σ_1/σ_3 and $d\epsilon_V/d\epsilon_1$ in Equation 6.2 are substituted with the corresponding values at failure. The contribution of ϕ_r can now be obtained by subtracting ϕ_μ and ϕ_d from the value of ϕ .

The principal stress ratio at failure, $(\sigma_1/\sigma_3)_f$ is commonly used as an alternative shear strength parameter because of its direct involvement in determining ϕ as in Equation 6.1. The rate of volume change at failure, $(d\epsilon_V/d\epsilon_1)_f$ is also used as a shear strength parameter, especially to identify the behavior of the dilatancy component ϕ_d because $d\epsilon_V/d\epsilon_1$ appears in Equation 6.2. All the strength parameters used in this study are effective, or drained strength parameters, although for convenience the modifier ' (prime) is not used to identify them as such.

6.2 Factors governing shear strength parameters

The shear strength of a compacted granular material depends on a number of compositional and environmental factors; the most important of these are stress level, particle compressive strength, initial void ratio, maximum grain size, gradation, saturation level, and fabric of the soil matrix. Their importance to shear strength of granular materials has been known for a long time, and many publications discuss the effects of these factors on shear strength. For example, the effects of void ratio and stress level by Lee and Seed (1967), Vesic and Clough (1968) and Lambe and Whitman (1969); the effects of particle compressive strength and stress level by Billam (1971), Lo and Roy (1973), Murphy (1987), Colliat-Dangus and others (1988) and Lee (1991); the effects of maximum grain size and gradation by Marachi (1969), Becker (1972) and Marsal (1973); the importance of saturation level by Miura and others (1983), Murphy (1987) and Lee (1991); and the importance of fabric by Oda (1972). Since the emphasis in this study is on situations where particle breakage is significant, the impact of stress level and particle compressive strength on shear strength is discussed below in greater detail.

6.2.1 Effects of stress level

To understand the behavior of ϕ_f with stress level, it is useful to look at the influence of stress level on its components. The sliding friction, ϕ_μ , is generally treated as a constant for a given material within a reasonably large stress range.

This is shown schematically as a straight line in a τ - σ plot (Figure 6.1). The dilatancy component ϕ_d at a given void ratio varies greatly with the stress level; ϕ_d at failure decreases when confinement increases and may even become negative under higher confining pressure. Both particle reorientation and particle breakage that contribute to ϕ_r tend to absorb greater amounts of energy at higher stress levels, increasing ϕ_r . However, the total ϕ_f usually decreases under increasing stress levels because the increase in ϕ_r may not entirely compensate for the decrease in ϕ_d at all stress levels. The resulting failure envelope (ϕ_f) is curved, as indicated in Figure 6.1. This is treated in further detail by Kulhawy and Mayne (1990).

Under some circumstances, the decreasing trend of ϕ_f with increasing stress seems to reverse beyond a certain stress level. Drained triaxial tests on dense Sacramento River sand, conducted by Lee and Seed (1967) under confining pressures up to 140 ksc (13.7 MPa), showed that ϕ_f decreased by about 8° to reach a minimum at about 40 ksc (3.9 MPa) confinement and then slowly increased by about 1° at 140 ksc, as shown in Figure 6.2c. In Figure 6.2a, dV/V_e ($= d\epsilon_v/d\epsilon_1$ in current notation) at failure reaches a peak contractive value at about 40 ksc (3.9 MPa), the same confining pressure at which ϕ_f reaches a minimum. A behavior similar to that of Sacramento River sand was observed in dry, dense Toyoura sand by Miura and Yamanouchi (1977): $(\sigma_1/\sigma_3)_f$, which is directly related to ϕ_f , decreased with increasing confining pressure to reach a minimum at a confining pressure of 80 ksc (7.8 MPa) and then increased slowly (see Figure 6.3); the ratio $(d\epsilon_v/d\epsilon_1)_f$ of the same specimens increased with increasing stress and reached a peak positive (contractive) value at the same confining pressure.

Such trends in ϕ_f cannot be explained through Equation 6.2. Therefore, Lo and Roy (1973) suggested Equation 6.2 may not be valid for tests conducted under confining stresses greater than that corresponding to the peak $(d\epsilon_v/d\epsilon_1)_f$ for a particular material. Moreover, not all the samples that exhibited a contractive peak in $(d\epsilon_v/d\epsilon_1)_f$ in Figure 5.18 concurrently exhibited a minimum in ϕ_f . Using a line of thinking similar to Lo and Roy's, Vesic and Clough (1968) argued that

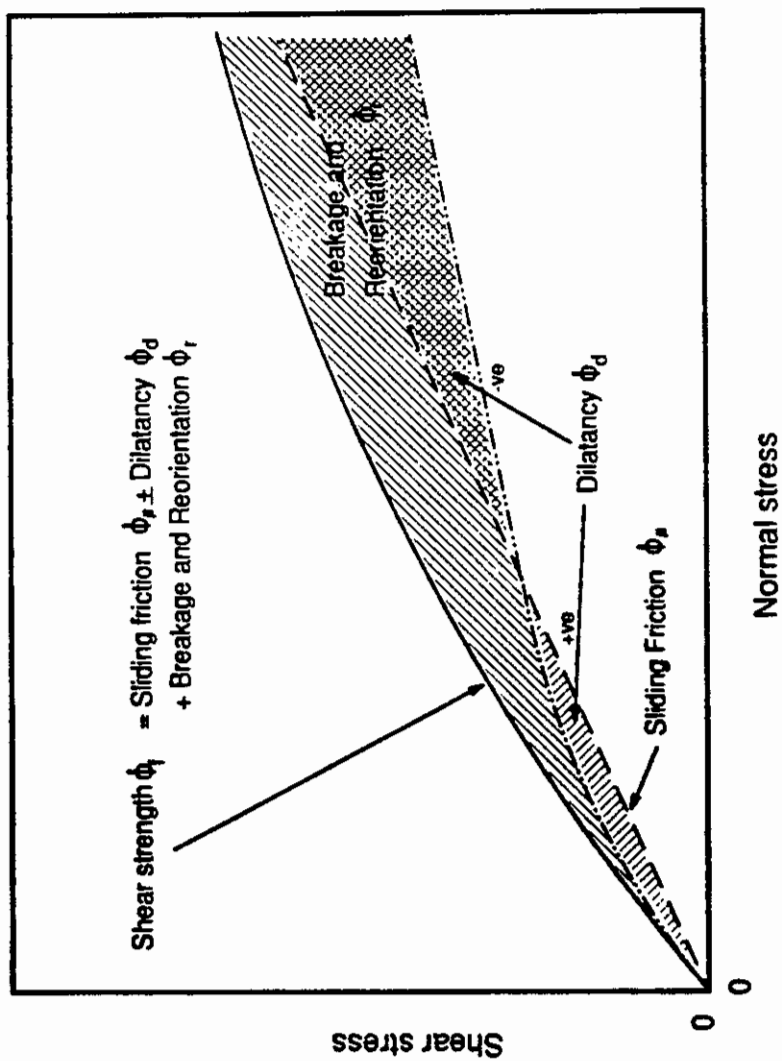


Figure 6.1 Variation of components of ϕ_f with normal stress in sand (after Lee and Seed, 1967)

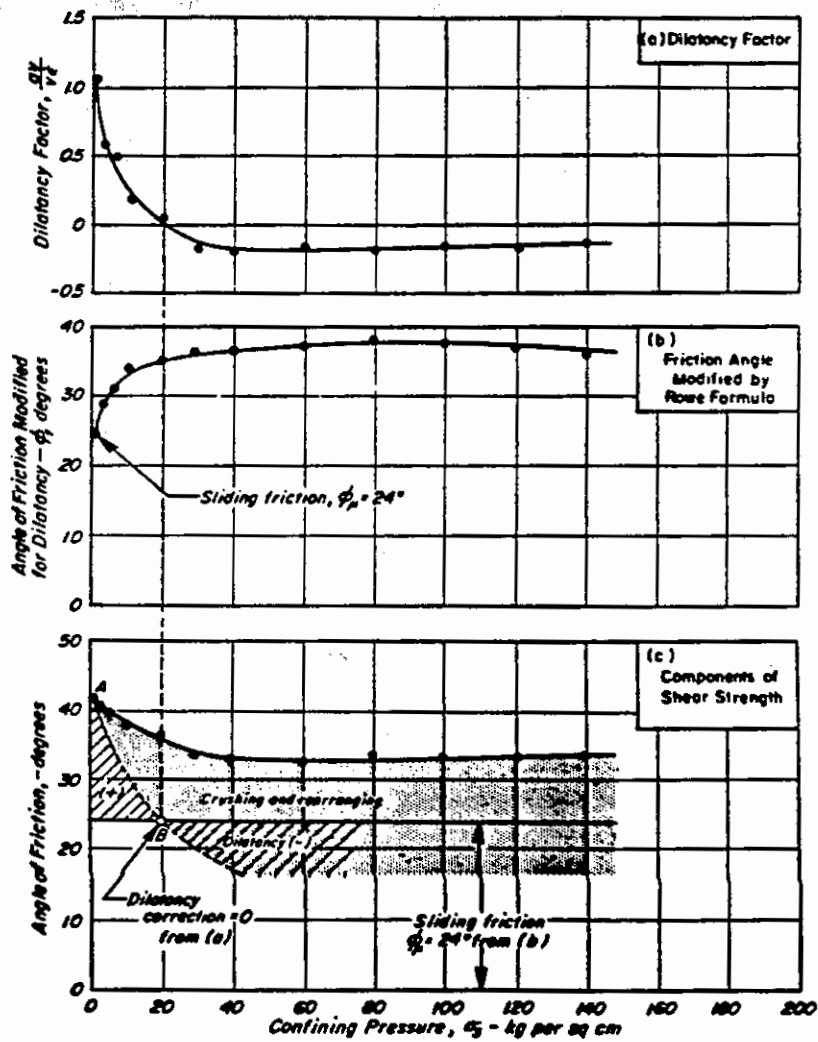


Figure 6.2 Effect of confining pressure on volume change and shear strength of Sacramento River sand (from Lee and Seed, 1967)

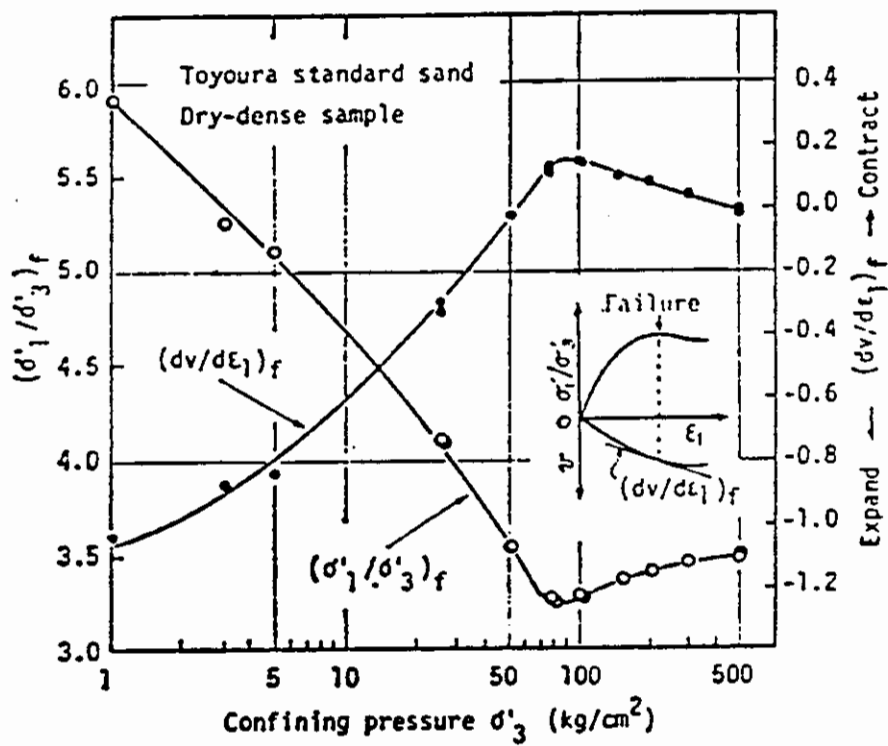


Figure 6.3 Effect of confining pressure on volume change and shear strength of Toyoura sand (from Miura and Yamanouchi, 1977)

the curvature of the Mohr-Coulomb envelope of a granular material vanishes, i.e. ϕ_f approaches a constant value, beyond a certain "breakdown stress". They suggested this breakdown stress depends on mineral composition, gradation and angularity of the material, and is lower in weaker, angular, or poorly graded materials. To check the applicability of this type of reasoning, the variation of ϕ_f with stress level is examined below for materials of different particle compressive strength.

6.2.2 Effects of particle compressive strength

The trends of ϕ_f with mean normal stress (σ_m) obtained from past investigations on different types of material are presented in Figure 6.4. Three granular materials of different particle compressive strengths, tested by Lo and Roy (1973), exhibited an approximately linear decrease in ϕ_f with increasing $\log \sigma_m$ (Figure 6.4a). In a linear plot, this behavior will be depicted as ϕ_f initially decreasing rapidly and then becoming gradually stable at high σ_m values because:

$$\frac{d\phi}{d\sigma_m} = \frac{1}{\sigma_m} \frac{d\phi}{d(\ln \sigma_m)} \quad (6.3)$$

It is interesting to note that the weakest of the three sands used by Lo and Roy (1973), limestone sand, exhibited the smallest drop in ϕ_f and the flattest slope. Substantially high stress-induced breakage and the resulting rapid densification of limestone specimens were suggested as the reason for this behavior (Lo and Roy, 1973). Colliat-Dangus and others (1988), however, obtained somewhat different results from a similar test program (Figure 6.4a): in their tests, calcareous sand exhibited a monotonically decreasing ϕ_f , while the ϕ_f of siliceous sand, the stronger of the two, reached a minimum value and then increased slightly with increased stress. Moreover, the calcareous sand curve showed a significant reduction in slope at a mean normal stress of about 0.5 MPa, while the ϕ_f of siliceous sand continually decreased at a fairly steep slope until it reached the minimum at about 6.7 MPa. In Chattahoochee River sand, ϕ_f reached an approximately constant value at a mean normal stress of about 33 MPa.

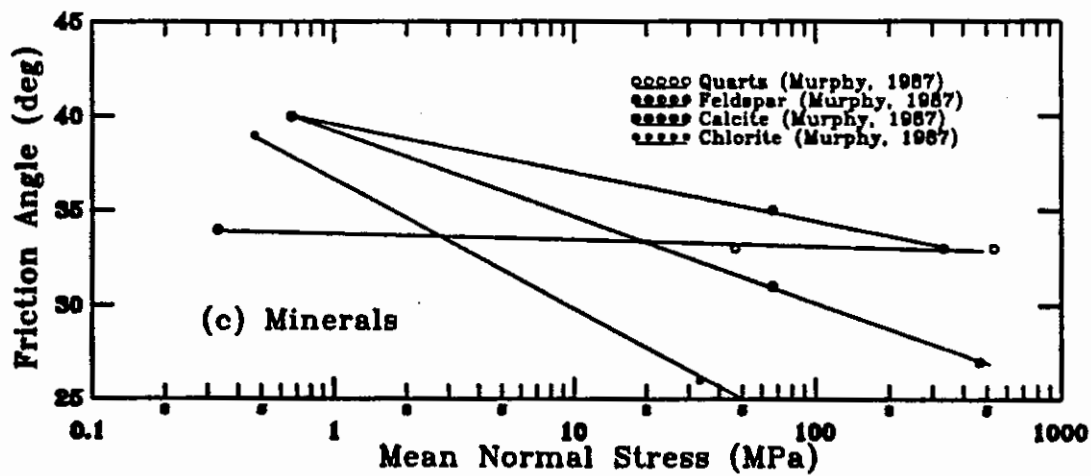
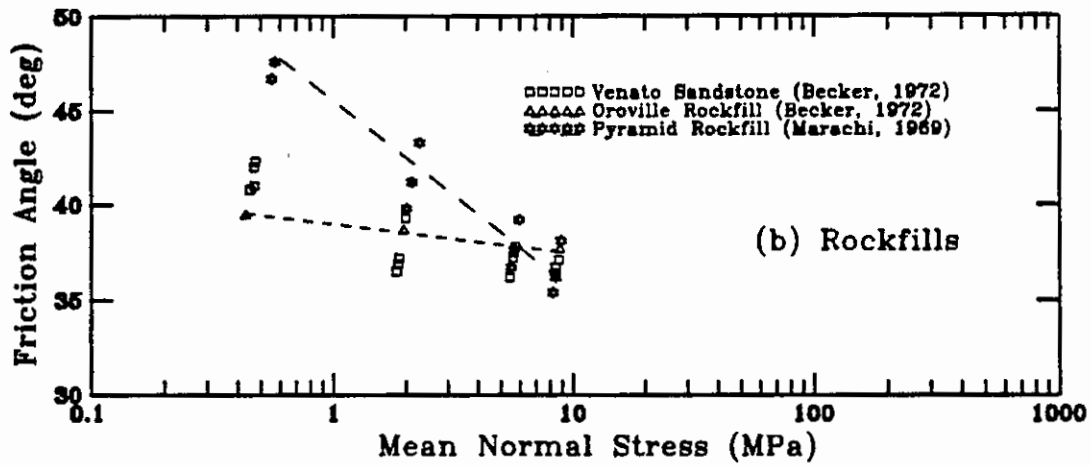
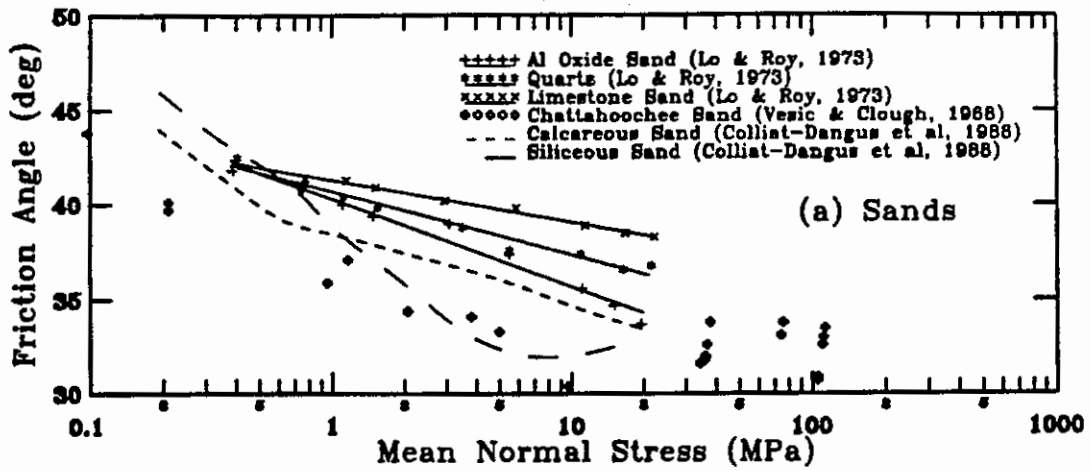


Figure 6.4 Variation of ϕ_f with σ_m at failure in sand, rockfill, and minerals

In Figure 6.4b, the behavior of ϕ_f is shown for three rockfill materials, Oroville dam material, Pyramid argillite and Venato sandstone, whose particle compressive strengths decrease in that order. In Oroville rockfill, ϕ_f decreases with stress at a fairly shallow slope, while the weakest of the three, Venato sandstone, exhibits a rapid drop in ϕ_f which then stabilizes with further increase in stress. The curve for the Pyramid material exhibits the steepest slope, which seems to be approximately constant within the range of stresses used.

Figure 6.4c is the result of an investigation on the variation of ϕ_f over a very large stress range. Four pure minerals, quartz, feldspar, calcite and chlorite, with Moh's hardness 7, 6, 3 and 1 respectively, were subjected to triaxial shearing under confinements of 0.2, 30 and 300 MPa (Murphy, 1987). Although the three data points obtained for each material (for chlorite, the third point is below 25°) seem to indicate straight line relationships between ϕ_f and $\log \sigma_m$, such interpretations may be misleading given the complicated nature of ϕ_f seen in Figures 6.4a and 6.4b. Nevertheless, the data indicate that in weaker minerals the decrease in ϕ_f with stress level is more rapid than in stronger minerals.

6.2.3 General trends of ϕ_f

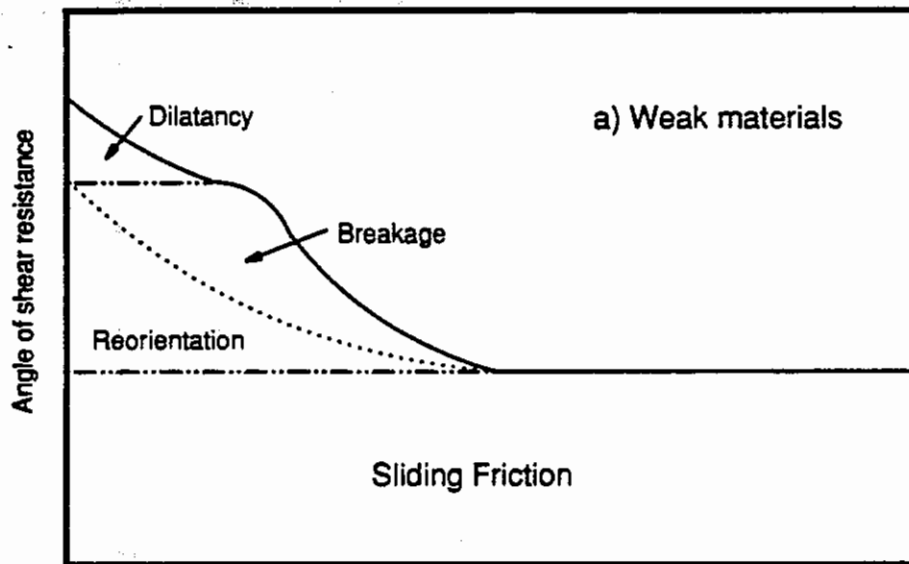
The concept that ϕ_f becomes a constant beyond a certain breakdown stress (Vesic and Clough, 1968) is not sufficient to explain the complex behavior of ϕ_f exhibited in Figure 6.4 for different materials. The ϕ_f of some materials may ultimately reach a constant value, but in some weak materials it continues to decrease with increased stress, and in some strong materials ϕ_f decreases at a higher rate.

The hypothesis proposed by Murphy (1987), part of which was quoted in section 5.4.3, combines all the above variable factors in terms of breakage, and also offers a more detailed explanation than the one by Vesic and Clough (1968). Murphy (1987) links the behavior of ϕ_f to shearing phase volumetric strain, which as stated before, depends on consolidation phase volumetric strain when breakage is the dominant cause of strain. Particle breakage is said to dominate volume change characteristics beyond a particular stress level, as in the "breakdown stress

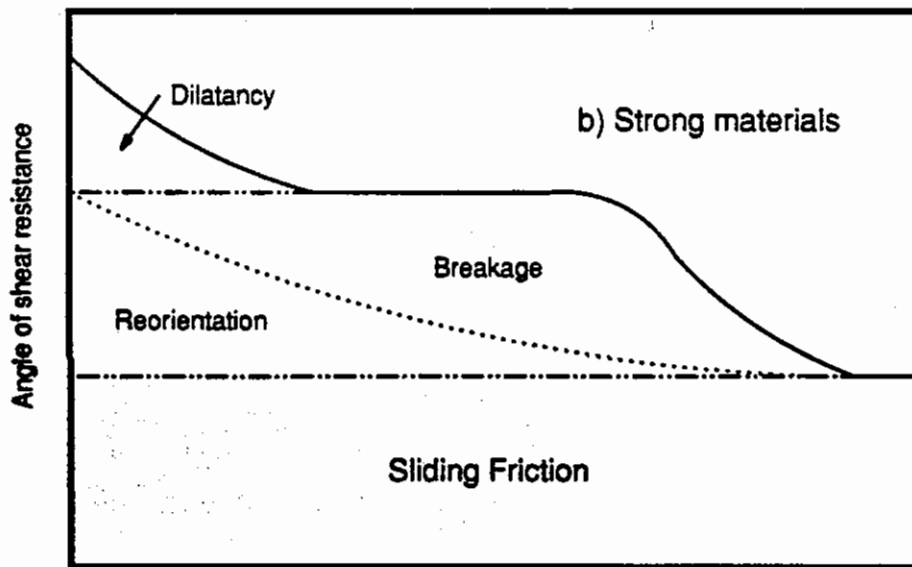
concept" put forth by Vesic and Clough (1968). The variation of ϕ_f in a given granular assembly will then be controlled by the particle breakage component of ϕ (say ϕ_{brk}).

Since a weak material undergoes substantial breakage during the consolidation stage, the remaining volumetric strain attributed to its shearing stage will be small, and hence ϕ_{brk} will be small. At a higher stress level, ϕ_{brk} will be much smaller. The ϕ_f of a weak material will therefore decrease rapidly with increasing stress, until at some stress level ϕ_μ is the only remaining component of ϕ_f . The behavior of ϕ_f with σ_m in a weak material is sketched in Figure 6.5a. Note that only the positive portion of ϕ_d (the contribution to ϕ_f by dilatancy) is shown here. Also, for convenience, ϕ_f is divided into ϕ_{brk} and ϕ_{reor} (the contribution due to particle reorientation). Figure 6.5b shows the behavior of ϕ_f expected in a strong material: the greater volumetric strain capacity remaining after consolidation represents a greater ϕ_{brk} component during the shearing stage; this large ϕ_{brk} and the low rate of breakage cause ϕ_f to decrease over a large stress range, and at a smaller rate than in a weak material.

This hypothesis provides a plausible explanation for a) the large decreases in ϕ_f over a large stress range in stronger materials as shown in Figures 6.4a (aluminum oxide sand and siliceous sand) and 6.4b (Pyramid rockfill compared to Venato sandstone); and b) the flatter slopes of the curves of stronger materials shown in Figures 6.4b (Oroville rockfill compared to others) and 6.4c. However, the relatively small slope of the curve for weak limestone sand in Figure 6.4a, and the slight increase in ϕ_f at high stresses in some materials in Figures 6.4a, 6.4b, 6.2 and 6.3, require further explanation. Under higher stresses, the diminishing ϕ_{brk} (due to decreasing breakage rate) and the slowly increasing ϕ_{reor} (due to increasing density) may gradually reduce the rate of decrease in ϕ_f and sometimes even increase ϕ_f slightly. Moreover, precise comparisons between materials are difficult, since not only the particle hardness, but also the gradation, the angularity, and all the other factors that contribute to breakage may affect the behavior of ϕ_f with stress level.



Mean normal stress at failure



Mean normal stress at failure

Figure 6.5 A schematic of variation of components of ϕ_f with $(\sigma_m)_f$ (after Murphy, 1987)

6.2.4 Behavior of decomposed granite

Shear strength of compacted decomposed granite is fairly high under low stresses, compared to that of conventional fill materials, but with increasing stress the strength decreases rapidly. The ϕ_f value of a decomposed granite from southern Bohemia (which is well-graded and relatively strong) decreased from 48° under 0.1 MPa triaxial confining pressure to about 34° under 10 MPa (Figure 6.6) (Feda, 1971, 1977). Breakage-induced volumetric strains are not so dominant in this material as indicated by breakage estimates: in a test that was terminated soon after the specimen reached failure under 5 MPa confinement, IC (total) value was only about 14. Feda postulated two hypotheses to explain this large decrease in ϕ_f . According to one hypothesis, the feldspar grains, which are angular and have a high ϕ_μ , dominate the shear characteristics at low pressures. As the pressure is increased, greater breakage of feldspar grains permits the stronger quartz grains to assume control of the shear strength of the material. At this stage, the already reduced ϕ_f (due to the stress increase) can decrease further, because ϕ_μ of quartz is lower than that of feldspar. The other hypothesis is illustrated in Figure 6.7. The stress-strain curve of specimen #5 (in Figure 6.7) shows a series of sudden increments of axial strain with no simultaneous increase in stress. These temporary loses of the specimen's ability to carry the load (structural metastability) could be due to a sudden breakdown of load carrying grains in the particulate assembly (as shown in the sketch). Trollope and Chan (1960) suggested that similar behavior could result from gradual mobilization of grains into the shear plane. In laboratory specimens of normal dimensions, even such localized movements may significantly reduce the shear strength. Feda (1977) suggested that both these processes may act together under high pressures to drastically reduce the shear strength of decomposed granite.

Lee (1991) conducted triaxial tests on decomposed granite from Seoul (Grade V) under different compaction densities and water contents. Some specimens were compacted dry and the others were compacted at a water content of 10 percent (2% less than the optimum). The specimen densities ranged from about 86 percent to 95 percent relative compaction (of Modified AASHTO). The

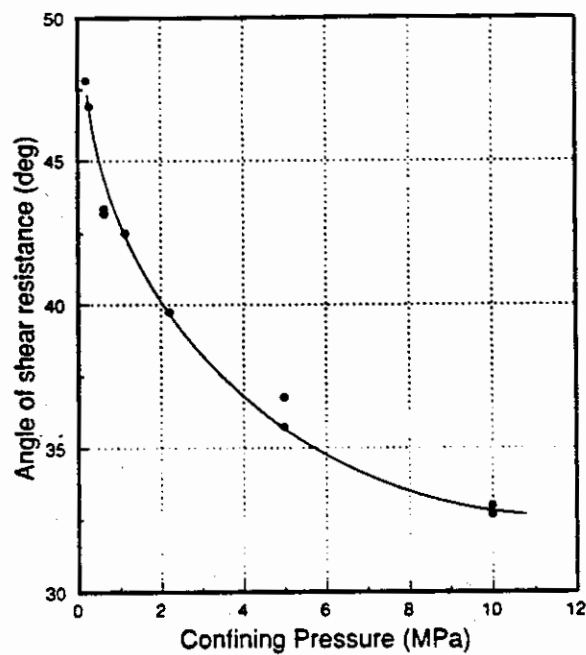


Figure 6.6 Variation of ϕ_f with σ_3 in decomposed granite from southern Bohemia (from Feda, 1977)

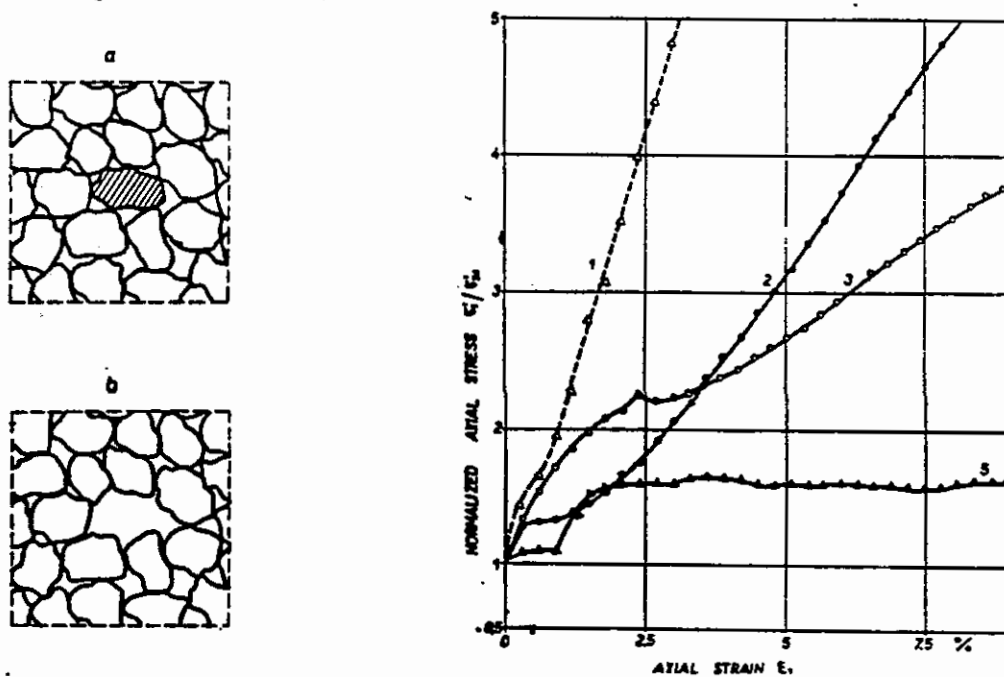


Figure 6.7 Effect of particle structure stability on stress-strain behavior in decomposed granite (from Feda, 1971)

confining pressures used for one series of tests ranged from 50 to 500 kPa, and for the other series from 1800 to 8100 kPa. Some triaxial tests were of conventional type (constant σ_3), both drained and undrained, and some were of octahedral shear type (constant σ_m). The main emphasis of the test program was to investigate the compatibility of the behavior of compacted decomposed granite with critical state soil models. Therefore, the bulk of the analysis centered around the ultimate (residual) state of the specimens rather than the peak state. Nevertheless, Lee reported that peak angle of shear resistance ranged from 51° to 39° for the full test program, and 39° was also the residual friction angle, irrespective of the initial state of specimens. The decomposed granite test specimens exhibit the basic features of the critical state soil model (Lee, 1991), i.e., the results show a unique isotropic normal compression line, a critical state line parallel to the normal compression line, and a state boundary surface, etc...

A few other investigators have also reported on the shear strength of decomposed granite from different parts of the world, a summary of which is presented in Table 6.1. Drained triaxial tests on decomposed granite from Honshu (Japan) gave ϕ_f values between 37.7° and 41.7° with zero cohesion (Nishida and Kagawa, 1972; Miura and others, 1983). Direct shear tests on similar material from Kyushu produced ϕ_f values between 32° and 36° and cohesion values between 6 and 27 KPa; the lower values were obtained from saturated specimens (Onitsuka, 1983). Two compacted decomposed granite samples from the northern Sierra Nevada mountains, California, were subjected to undrained triaxial tests under confining pressures ranging from 50 to 200 kPa; the effective ϕ_f values were 37.5° and 35° , and the effective cohesion values were 27 and 20 kPa, respectively (Macfarland, 1990). Drained triaxial tests on two Buckhorn dam borrow material samples (decomposed granite from the western slope of the Shasta Bally batholith) produced ϕ_f values of 37.3° and 28° , and cohesion values of 42 KPa and 53 KPa respectively, under confining pressures up to 1330 KPa (Solbos, 1990). However, none of the above samples from California has significant plasticity (see Table 2.3), and the cohesion values could not be as high as the results indicate. This discrepancy may have been caused by using

Table 6.1 Mechanical properties of some decomposed granite samples

Ref	Location	Soil type	Classification	Max. DD (1/1000m)	W _{opt} (%)	Cohesion (kPa)	Friction (deg)	C _c	C _v (mgm/sec)	K (1E-7) (cm/s)	Remarks
1a	Colombia	Silty sand	IV-V-SM	16*	19-22	0-7	32-38			100	*Sid Proctor
b		Sandy silt	V-ML	15*	23-25	0-7	32-38				Tx CD tests, conf. = 0.1-10 MPa
2	Carach.	sand	SW			0	34-48				Tx CD tests, conf. = 0.1-10 MPa
3a	Hong Kong	Granite-Clayey	VI-CH	15*	30.7	0	32	0.15**	200	0.6-7	Tx CD tests
b		Granite-Sandy	V-SM	14*	32.3	13	36.5	0.14**	10000	60-216	*Only specimen density & w.c. are given
c		Granite-Dune	V-SC	19*	12.3	20	37		11-66		**Loosely compacted
d		Granodiorite-Lab	V-ML	16*	20.2	-	-				
e		Granodiorite-Dune	V-CL	17*	18.6	17	31.3		9-22		Direct shear CD tests, conf. = 200 KPa
4a	Japan	Kawakubo	VI-SM	17*	17.0	20-40	33-34				*Compaction mtd n/a.
b	(Saga,	Yabuta	V-SM			7-20	30-34				
c	(Kyushu)	Kanzaki	V-SM								
d		Kawakuni	IV-SM			0-33	33-34				
5a	Japan	Kanayama	SM	17*	16.0	40-60**	27.5-29				Tx tests, conf. = 100-250 KPa, *Sid Proc.
b	(Iyosha)		SM	18*	15.0	26**	39				**at MDD & 80-90% sat.
6a	Japan	Granite	ML(7)	18*	11.5-15.0					100-7000**	*Sid Proc., ** at e = 0.7
b		Granodiorite	ML(7)	18*	14-16.5					100-7000**	
c		Diorite	ML(7)	16*	17-21					100-7000**	
7	Japan	Granodiorite	SM	21	8-10						CBR = 30 at Wopt
8a	Japan	Kanayama	SM	17*	16.0	13-52	30-36				Direct shear tests (part. saturated)
b	(Fukuoka &	Kawakubo	SM			20-33	30-35				conf = 13-150 KPa, *Sid Proc.
c	(Saga,	Saga	SM	19*	12.0			0.32**			** Loosely compacted
d	(Kyushu)	Washed Sage	SP			7-40	36-46				* energy corrected from Tx CD tests, conf. = 26-150 KPa
9a	Japan	Slightly weathered	Sand				37.7-41.7*				*Sat. Tx on RC=86-95%, Conf= 05-8.0 MPa
b	(Tokio Mus)	Highly weathered	Sand				37.7-41.7*				Tx CD tests, *Sid Proc.
10	S. Korea	Scoll	V-SW	17	12.0		39-51*				
11a	Shasta	33R-1	CL-ML	19*	13.3	73	29				
b	Bally Spring	33R-2	SM-ML	20*	10.9					21-3924	Tx CD tests, conf. = 50-200 KPa
c	Creek dam)	33R-3	ML	20*	10.6						Tx CD tests, conf = 200-800 KPa
12a	Shasta	BZR-1	SM								* comp. energy unknown
b	Bully	BZR-4	SM								12" dia., Tx UU (part sat.) tests
c	(SH 299)	BZR-5	SM								conf. = 0.7-2.8 MPa, 90-93% MDD
d		BZR-a	SM	20	8.5	27	42.6				Tx CD tests, conf. = 50-200 KPa
13a	Shasta Bully	X69	ML-SM	18*	16.2	53	28				
b	(Duckhorn)	X90	SM	18*	13.3	42	37.3				
14a	Shasta Bully	BS-1	ML-CL	19	15.0	250-340	15-22				
b	(SH 299)	BS-2	SW	21	8.7	247-340	27-29				
15a	N. Sierra	Stockpile	SM			27	37.5				Tx CD tests, conf. = 50-200 KPa
b	Nevada, CA	Bag Sample	SM			20	35				

References:

- 1 Li & Mejia (1967)
- 2 Feda (1977)
- 3 Guilford & Chen (1969)
- 4 Onisaka & Ohari (1985)
- 5 Uchida & Ohari (1968)
- 6 Matsuo & Ohari (1970)
- 7 Furukawa & Fujita (1990)
- 8 Onisaka & Yoshizaki (1990)
- 9 Nishida & Kagawa (1972)
- 10 Lee (1991)
- 11 USBR (1960)
- 12 Duffy (1990)
- 13 Solbow (1990)
- 14 Pryssock (1979)
- 15 Macfarland (1990)

MDD - Maximum dry density (Modified AASHTO, unless otherwise stated)
Wopt - Optimum moisture content
Cohesion - Effective cohesion (unless otherwise stated)
Friction - Effective angle of shear resistance (unless otherwise stated)
Cc - Compression index
Cv - Coefficient of consolidation
K - Hydraulic conductivity

linear approximations to curved failure envelopes.

In the current study, compacted decomposed granite samples from the Shasta Bally batholith (at SH299 PM 0.6, on the eastern slope) were subjected to a series of triaxial ICD tests (series T100 in Table 3.2). The results are shown in Figures 6.8 (specimens at 90 percent relative compaction) and 6.9 (95 percent compaction). The top half of each figure shows the variation of σ_1/σ_3 with axial strain under confining pressures ranging from 100 to 1500 kPa. The bottom half indicates the variation of the corresponding (shearing phase) volumetric strain. Increased confining pressure clearly reduces the peak shear strength, suppresses the dilatant tendencies of the compacted specimens, and increases the axial strain level at which the peak shear strength is attained. At the lowest confining pressure, 100 kPa, the peak strength is reached in dense specimens at about 1.5 percent axial strain, and at 1500 kPa peak strength is reached at 15 percent axial strain. At such large strain levels, the strength should actually be referred to as the residual strength. Although the strength, or σ_1/σ_3 , at this stage is expected to remain constant with increasing axial strain, some specimens exhibit stress ratio continually decreasing at a small rate. Most specimens that began to bulge under shearing at high confinement also exhibited a broad slip plane at the end of the test, at about 20 percent axial strain level. Such behavior would have led to the continual reduction in σ_1/σ_3 . However, between 15 and 20 percent axial strain, all the data points in either figure converge to a relatively wide band which can be interpreted as the residual strength. For specimens compacted to 95 percent density, the average residual angle of shear resistance is about 37° and for the loose specimens about 36.5° .

The peak angle of shear resistance of each of the above specimens is plotted in Figure 6.10 against the corresponding confining pressure. The reduction in ϕ_f with confining pressure is rather drastic: for dense specimens ϕ_f decreased from 50° to 38° , by about 25 percent; for loose specimens ϕ_f decreased from 44° to 36.5° , by about 15 percent. Moreover, for dense specimens ϕ_f nearly reached the lowest value, 38° , at a confinement of about 900 kPa, while for loose specimens this occurred at about 600 kPa. Such rapid reductions in shear strength

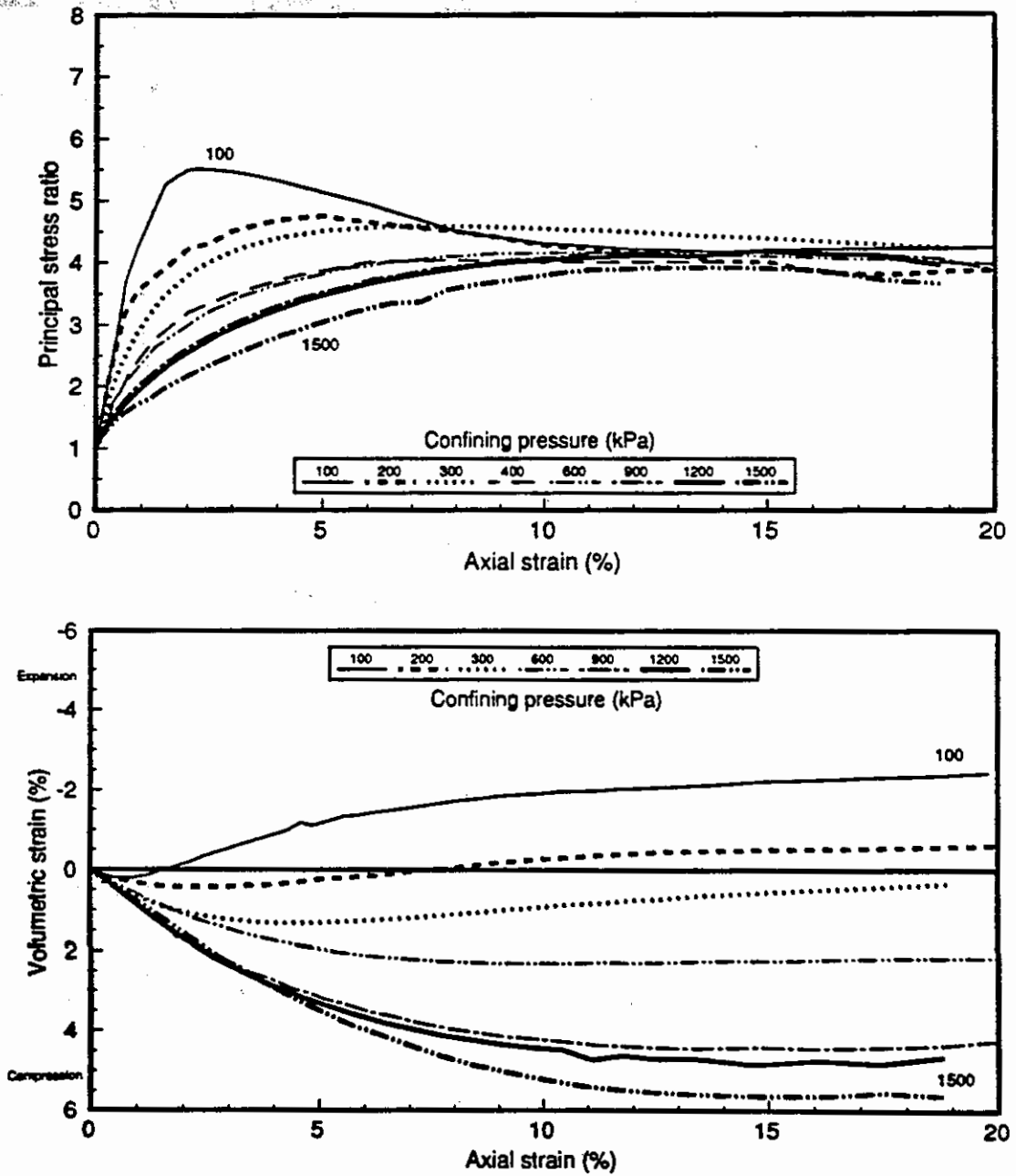


Figure 6.8 Effect of confinement on σ_1/σ_3 and ϵ_v of triaxial specimens of decomposed granite from the Shasta Bally Batholith, RC = 90%

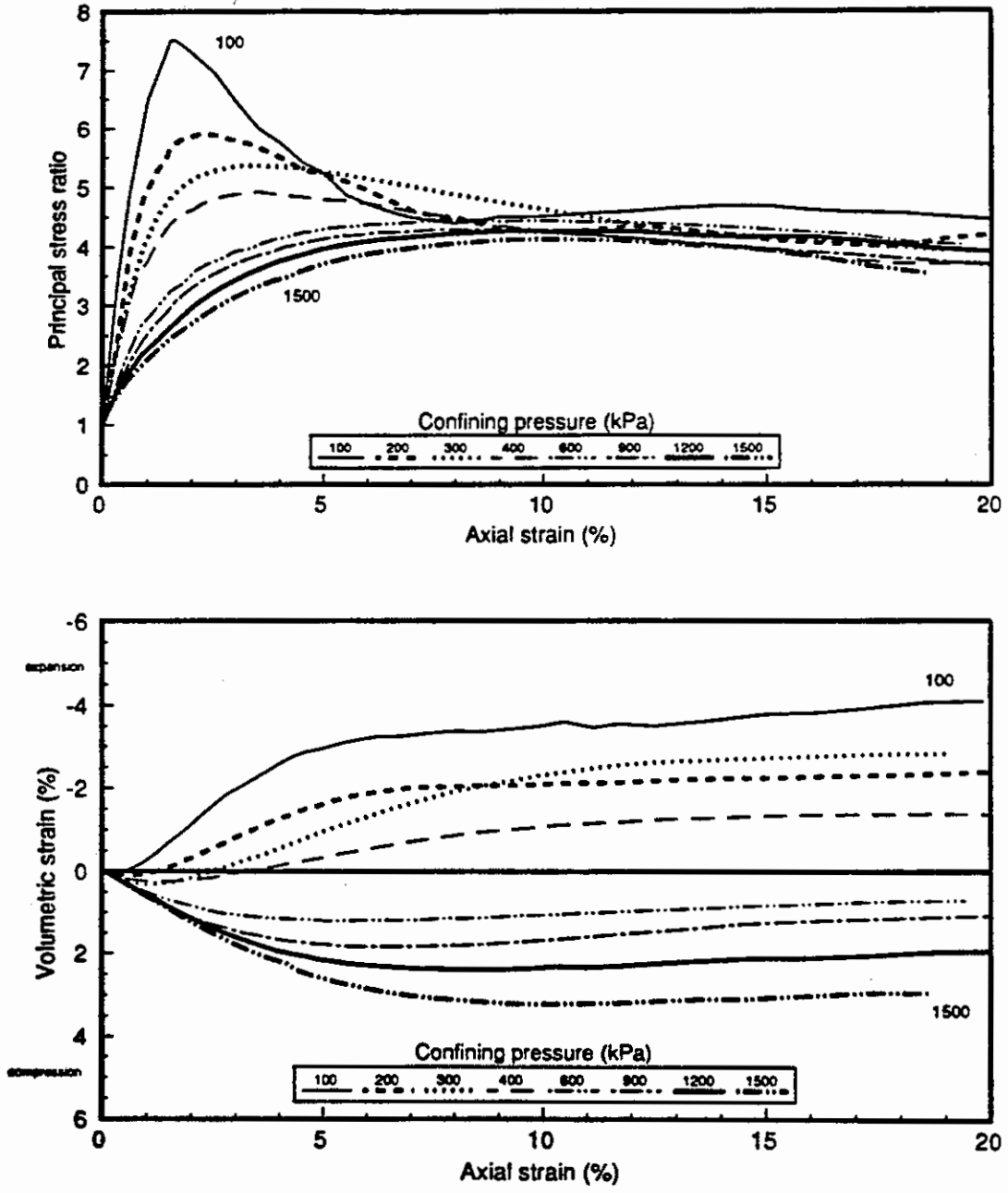


Figure 6.9 Effect of confinement on σ_1/σ_3 and ϵ_v of triaxial specimens of decomposed granite from the Shasta Bally Batholith, RC = 95%

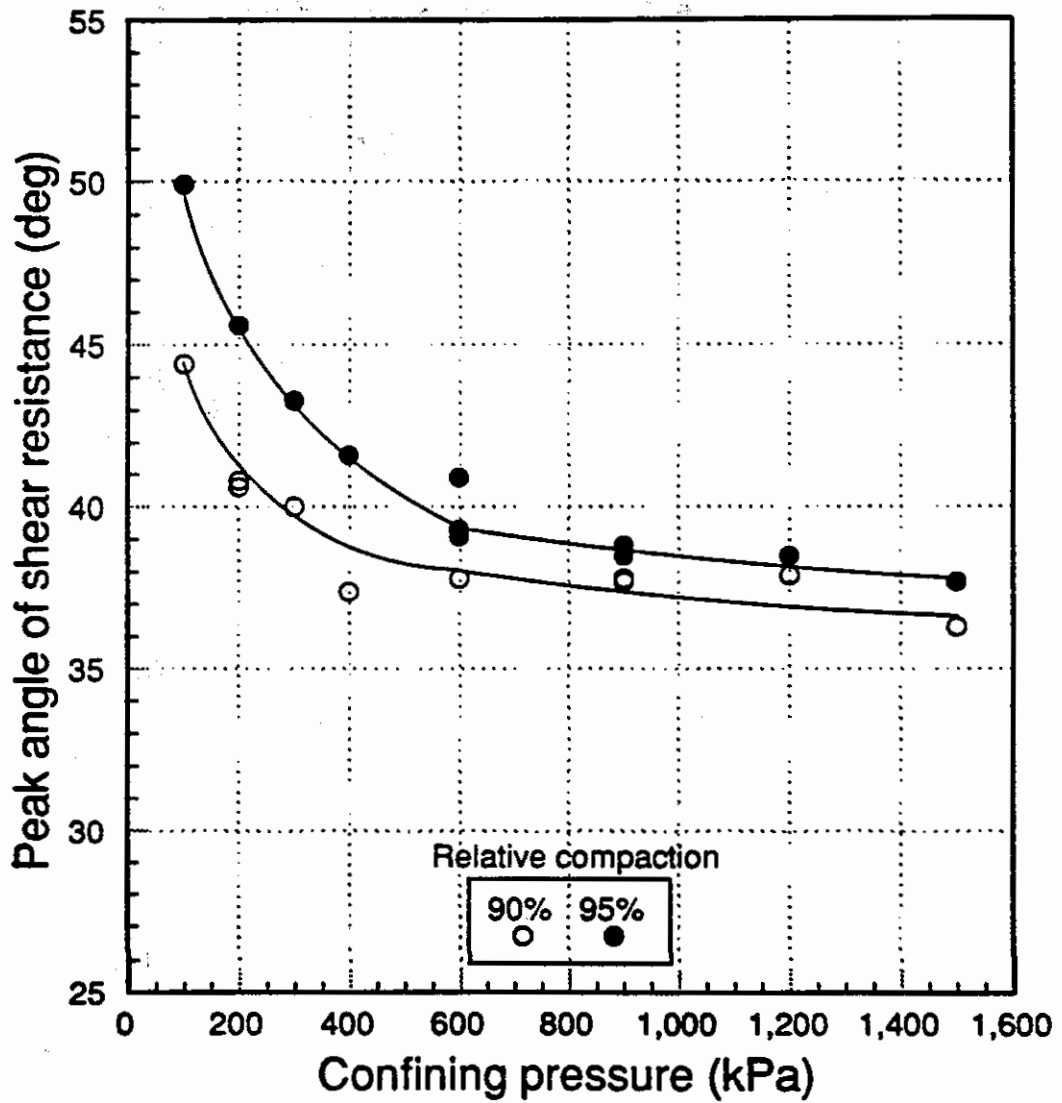


Figure 6.10 Variation of ϕ_p with confining pressure in decomposed granite from the Shasta Bally batholith

seem to agree with Feda's (1977) observations on decomposed granite from southern Bohemia, but are not common to other sands (compare with Figure 6.4a). Figures 6.11 and 6.12 show the variation of ϕ_f against the logarithm of $(\sigma_m)_f$. The variation in the rate of volume change at failure is also plotted in each graph. In Figure 6.12, the results from the test series T300 (anisotropically consolidated specimens) are also included and the data points seem to follow the same trend. In each graph, both ϕ_f and $(d\epsilon_V/d\epsilon_1)_f$ show bi-linear trends. In dense specimens the slope changes at about 1300 kPa and in loose specimens at about 450 kPa. Such trends are not common in other sands: in Figure 6.4a, only calcareous sand and Chattahoochee River sand (under very high pressures) exhibit similar behavior, while others exhibit generally linear trends.

It seems that the shear strength variations of this decomposed granite can be explained using previously presented hypotheses based on particle breakage by Feda (1971, 1977). However, breakage in this material prior to shear failure seems to be minimal, as discussed in Chapter 4. This apparent contradiction can be resolved by revisiting laboratory breakage estimates. A dilative triaxial specimen develops a rather narrow shear zone before it fails (Figure 6.13). At least up to failure, the bulk of the particle breakage that occurs in such a specimen will occur in this zone, notwithstanding its thickness. The behavior of the particles in this zone more or less determines the shear strength of the total specimen. However, breakage in a triaxial specimen is commonly estimated using the total mass of the specimen to preserve equity in comparison, because the shear zone width varies among specimens. These estimates, therefore, will not properly reflect the status of the particles in the shear zone which may comprise less than 20 percent of the total volume. The conclusion reached in section 4.4.2, that no significant breakage occurs until the specimen fails in shear, then, should be considered as correct only in the context where breakage is averaged over the total mass of the specimen. Within the specimen, however, widely varying levels of breakage may exist, but are difficult to quantify. An improvement in breakage estimates can be made by limiting the volume examined for breakage to the middle third of the specimen (see Figure 6.13). This eliminates the top and

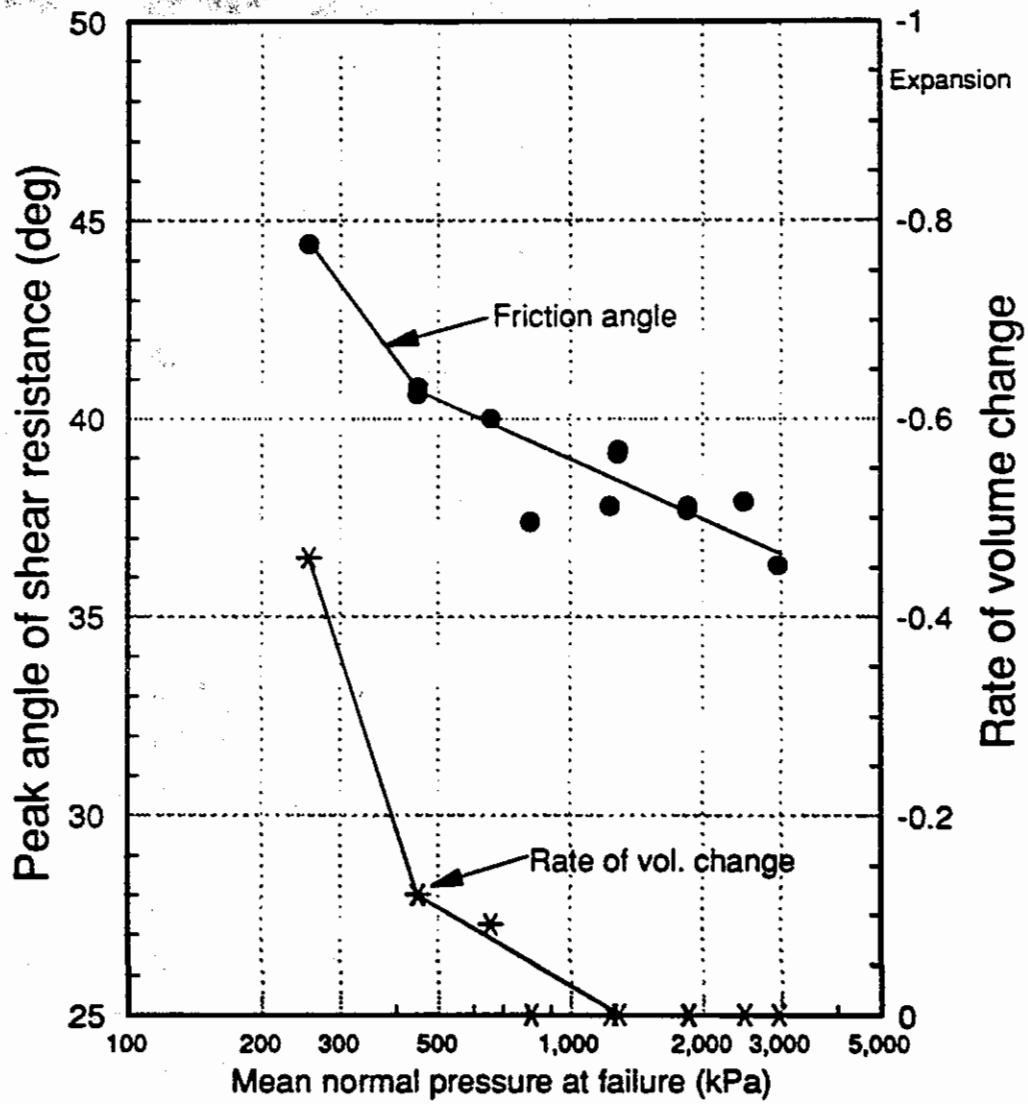


Figure 6.11 Variation of ϕ_f and $(d\epsilon_v/d\epsilon_1)_f$ with $(\sigma_m)_f$, RC = 90%

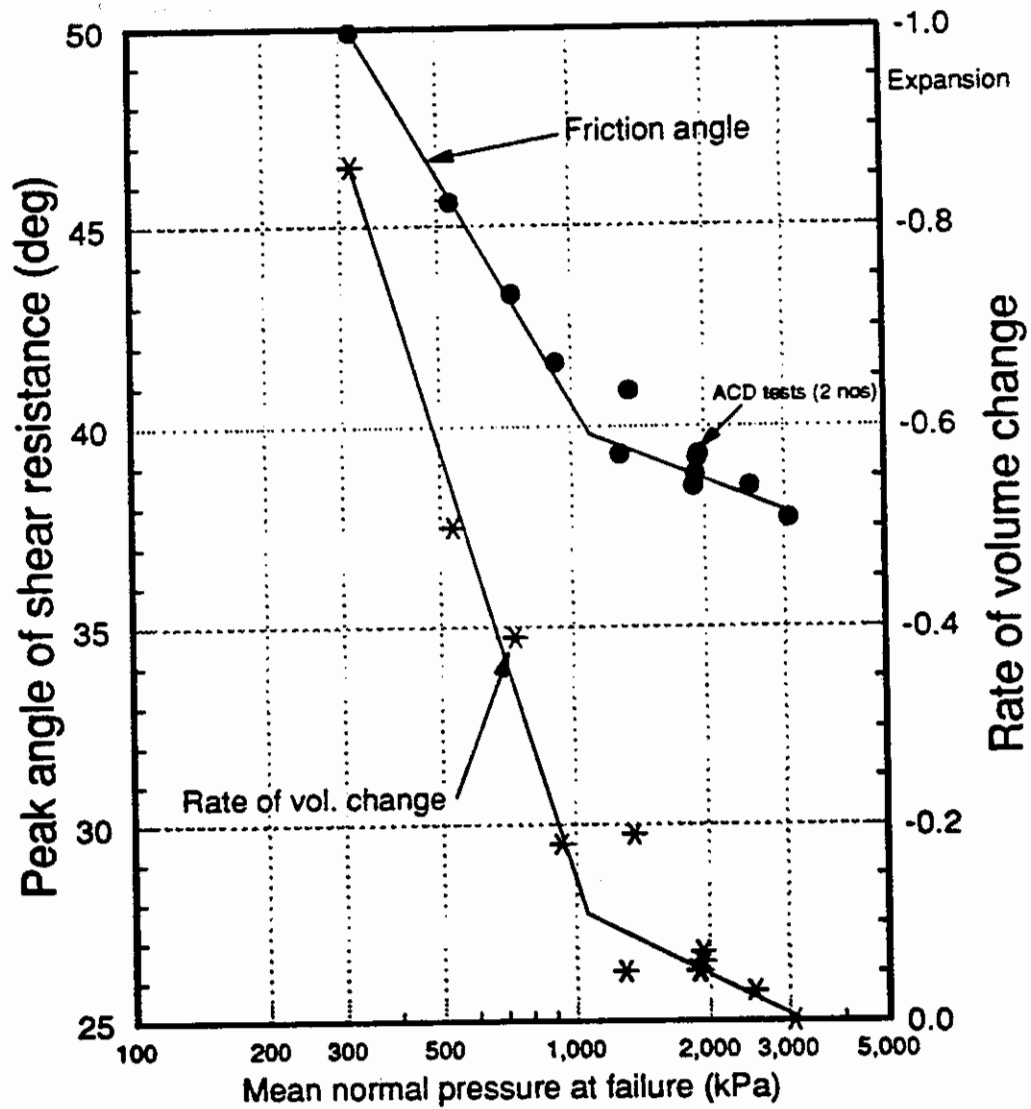


Figure 6.12 Variation of ϕ_f and $(d\epsilon_v/d\epsilon_1)_f$ with $(\sigma_m)_f$ RC = 95%

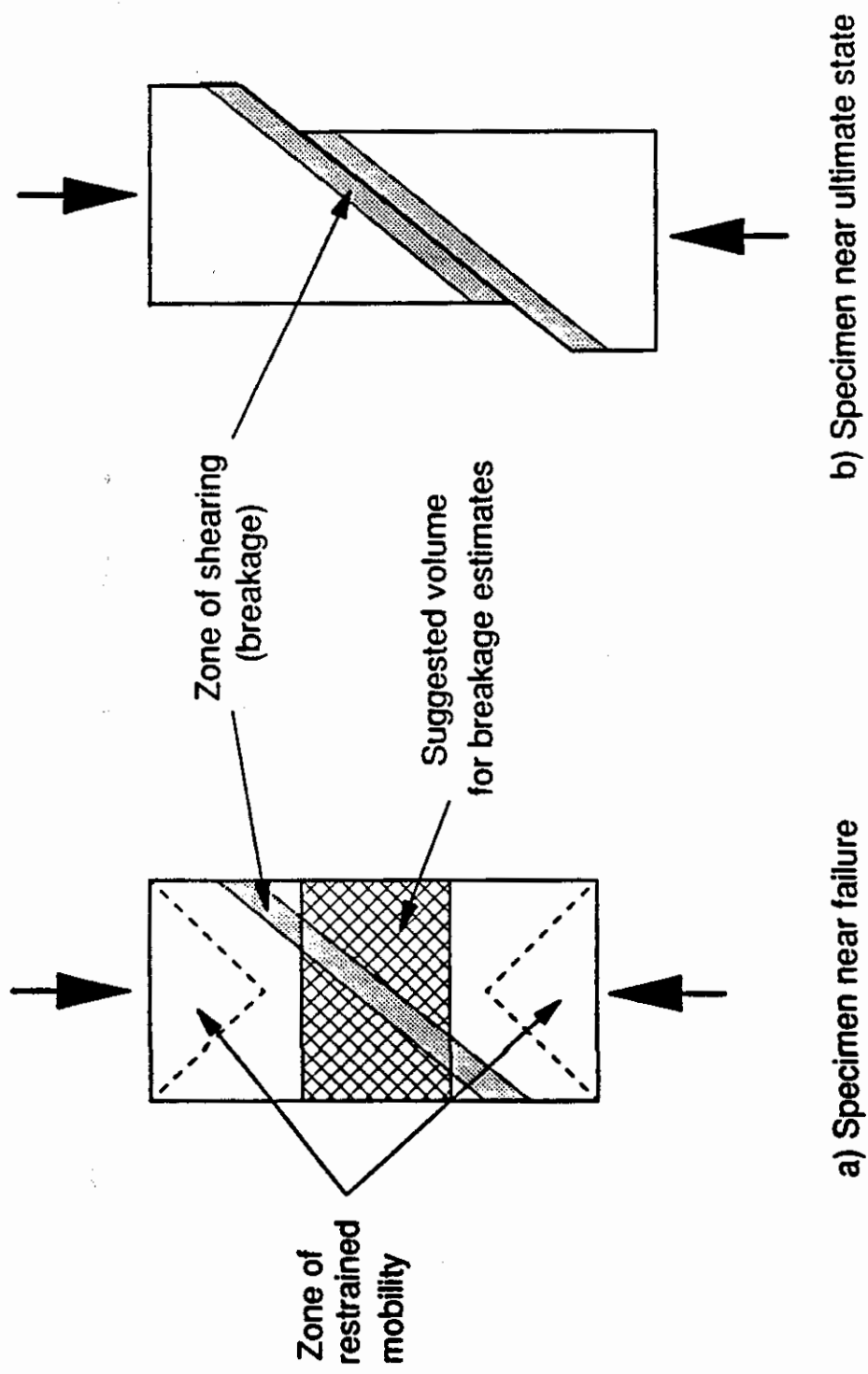


Figure 6.13 A schematic diagram of a dilatative triaxial specimen

bottom thirds where mobility is mostly restrained in specimens tested without lubricated ends.

The hypothesis that particle breakage occurring in the shear zone may turn feldspar particles' initial control on shear strength over to quartz seems to be the best explanation for the shear strength variations of decomposed granite depicted in Figures 6.8 to 6.12. The large quantity of feldspar in this material (about 40 percent) may dominate in shear under low pressures as Feda (1977) suggested. The other possibility suggested by Feda (1971), structural metastability, could also contribute to the reduction in ϕ_f , but no evidence, e.g., sudden significant changes in stress (under strain controlled loading), was visible in the data (see Figures 6.8 and 6.9). The behavior of ϕ_f of this material agrees generally with Murphy's (1987) depiction of a weak material (6.5a), but the volumetric strains at failure are not primarily breakage-induced as he hypothesized.

6.2.5 Effects of other factors on shear strength of decomposed granite

Void ratio, or the compacted density of a specimen, has a significant impact on its shear strength, at least in the low pressure levels as shown in Figure 6.10. Under a confining pressure of 100 kPa, the ϕ_f of a dense specimen (95 percent relative compaction) was about 50° and that of a loose specimen was about 44° . This difference however decreased rapidly, and beyond 600 kPa it was less than 2° . This means that the specimen density becomes less important in determining shear strength at higher pressures. Vesic and Clough (1968) observed the same phenomenon in triaxial tests of Chattahoochee River sand, but under much higher pressures. They refer to this level of stress as the breakdown stress, where the breakage rather than the density controls the shear strength.

Wetting of decomposed granite particles seems to cause a significant reduction in shear strength. In compacted triaxial specimens of decomposed granite from Japan, the deviator stress at failure, $(\sigma_1 - \sigma_3)_f$, was found to be about 20 percent lower in a saturated state than that in a dry state, under about 300 kPa confinement (Miura and others, 1983). The changes in capillary action or in interparticle friction due to wetting may decrease the shear strength, but probably

not by such a large amount. A major portion of the decrease was thus attributed to increased particle breakage due to wetting. In another test, a triaxial specimen under a deviator stress of 40 percent of the failure stress was wetted for 5 days and then allowed to dry slowly for another 4 days. This specimen, upon subsequent loading to failure, exhibited a shear strength 30 percent higher than an identical specimen that was never wetted. Significant particle breakage and densification in the wetted and redried specimen seems to have made it stronger (Miura and others, 1983).

Lee (1991) conducted an extensive series of triaxial tests on decomposed granite from South Korea to determine the effect of the saturation level on shear strength. Figure 6.14 shows the plots of $\sigma_1 - \sigma_3$ (indicated as q') versus axial strain for three specimens compacted at the same density; one compacted and tested dry, another compacted and tested wet (40 to 60% saturation), and the last compacted wet and tested saturated. The dry specimen shows a higher shear strength, whereas there seems to be no difference between the behaviors of wet and saturated specimens. The last two specimens show similar volumetric strains as well. Lee concluded that suction does not have a significant impact at 40 to 60 percent level of saturation. Under such conditions saturation did not significantly increase breakage also. However, in other tests Lee (1991) found that flooding of dry samples causes significant drops in shear strength, mainly due to increased breakage.

In the current test series on decomposed granite from the Shasta Bally batholith, all triaxial tests were conducted under saturated conditions. Unsaturated triaxial tests were not conducted because of the unavailability of proper equipment.

Part II - Direct Shear and Pullout Tests

The impetus behind the direct shear and pullout test series is the possibility of achieving substantial economies in embankment construction through geosynthetic-reinforced steeper side slopes. To reinforce an embankment of coarse sand/gravel material like decomposed granite, a geogrid is the best type of

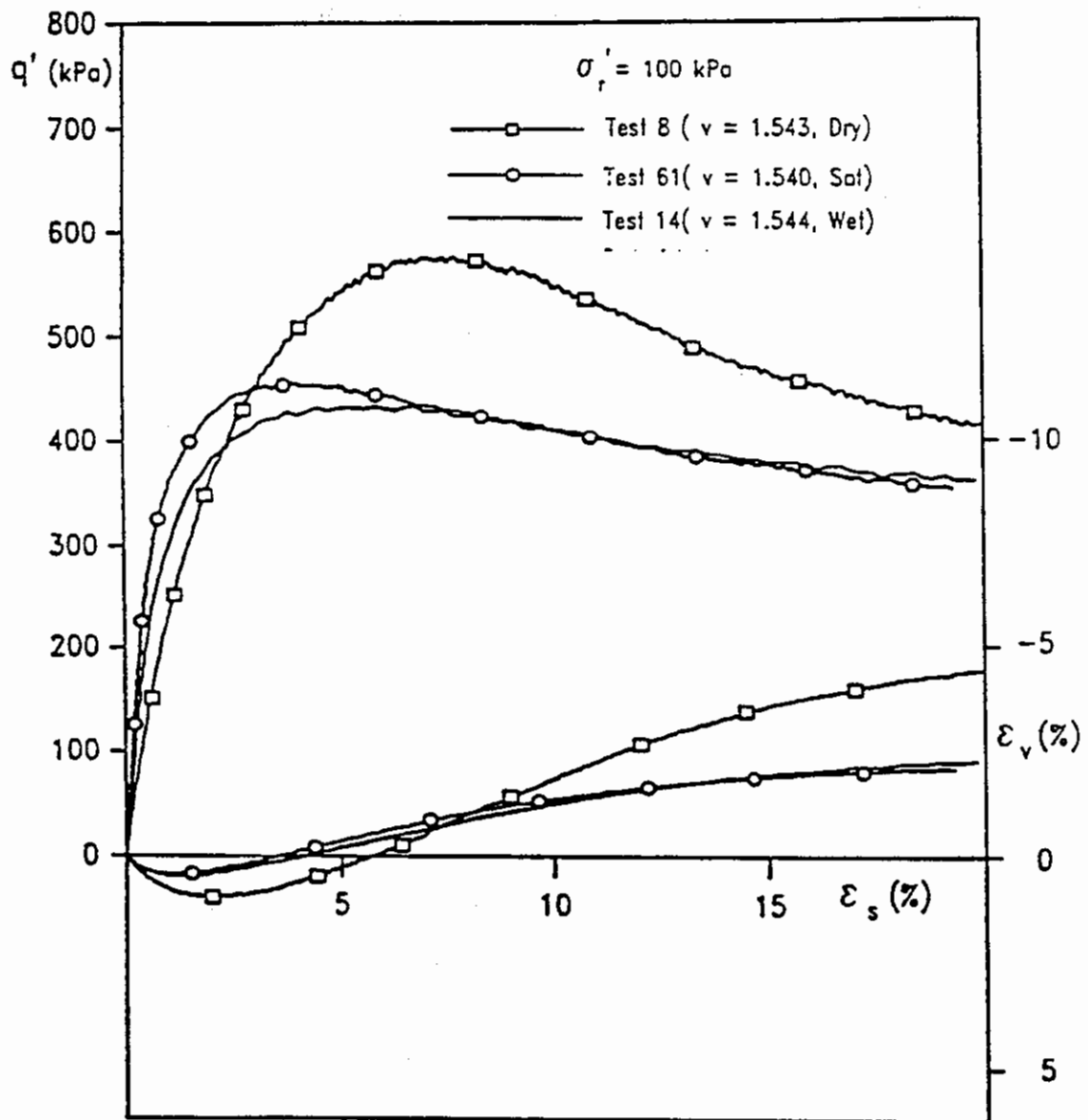


Figure 6.14 Comparison of stress-strain behavior for dry, wet, and saturated samples of decomposed granite from South Korea (from Lee, 1991)

geosynthetic, because its large apertures can trap soil particles and can provide more shear resistance than sheet reinforcement. Commonly, direct shear tests are used to measure the strength at the soil-grid interface, and pullout tests are used to measure the anchoring strength.

6.3 Direct shear tests

When a geogrid is placed in a compacted reinforced embankment, shear strength at the soil-grid interface will become a major concern in stability analysis. Jewell and others (1984) discussed the possible mechanisms that resist direct sliding at the interface, which are schematically illustrated in Figure 6.15. The first mechanism, shearing between soil and plane reinforcement surfaces (6.15a), is termed skin friction. This component of the angle of shear resistance will be the same as that measured in a test where the soil is sheared over a geosynthetic sheet made up of the same material. The second, the resistance offered by particles bearing on cross members of the grid (6.15b), requires that soil particles within the grid apertures move relative to the grid, and move in opposite directions in upper and lower halves of the aperture, to maintain the balance of forces on a grid bearing member. This contribution will not be significant if shearing occurs only at the top (or bottom) surface of the reinforcement, which is the general mode of shearing in a typical direct shear test and also in an embankment slope. The effect the ratio (soil particle size)/(grid aperture) has on the location of the shear surface, illustrated in Figure 6.16, can also play a role in determining the significance of the second mechanism. The situation shown for silt size particles is the only case where this mechanism will be significant. The third mechanism, soil shearing over soil through the grid aperture (6.15c), contributes to the shear strength an amount that again depends on the relative particle size. This mechanism can be reproduced in a typical direct shear test of soil alone.

Takasumi and others (1991) reviewed the types of direct shear tests that had been performed to-date. Three configurations of direct shear (soil-grid) tests were identified: a) a test where the geosynthetic is completely fixed to one half of the shear box; b) where the geosynthetic is only partially fixed (as shown in 3.9b);

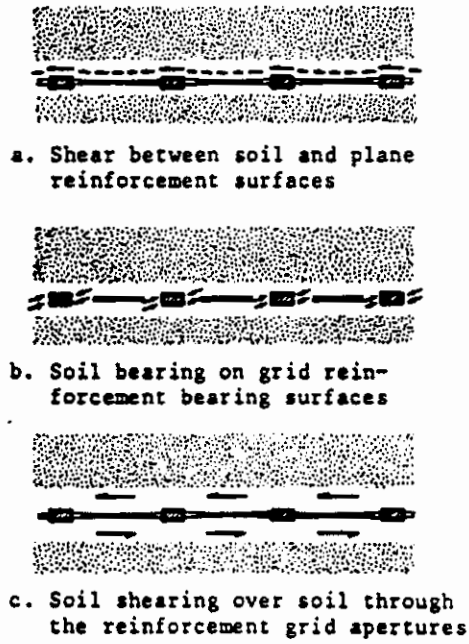


Figure 6.15 Three mechanisms resisting direct sliding over a geogrid (from Jewell and others, 1984)

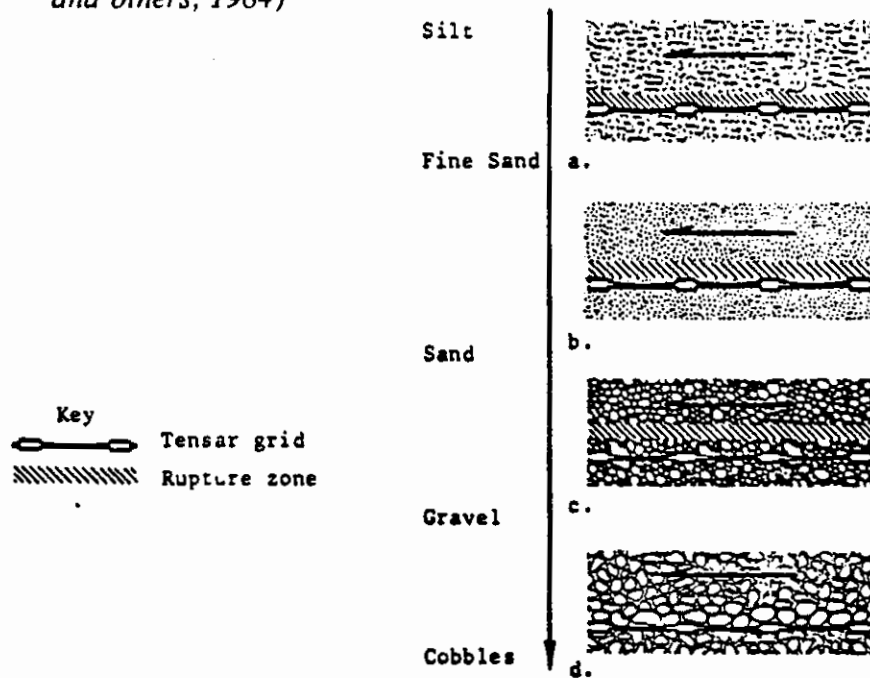


Figure 6.16 Effect of particle size on direct sliding over a geogrid (from Jewell and others, 1984)

and c) where the geosynthetic is kept free to move between the box halves. The case where the geosynthetic is only partially fixed commonly gave the greatest ϕ value compared to the other two. It is also the case that most closely resembles the condition of a geogrid in a sloping embankment.

In a 100+ m high embankment, as the one proposed for SH299, the major concerns regarding the interface shear strength are the variation of the peak ϕ value under increasing normal stress and the difference between peak and residual ϕ values. In several investigations where cohesionless soils were sheared over smooth geomembranes, reviewed by Takasumi and others (1991), no apparent curvature in the strength envelope was noted within a normal pressure range between 30 to 1000 kPa. Makiuchi and Miyamori (1988) noted that in single face shear box tests on sand over a geotextile, the density affected the peak ϕ value but not the residual value. Both Eigenbrod and Locker (1987) and Miyamori and others (1986) reported that the residual friction angle for concrete sand in contact with geosynthetics did not change with significant changes in density. Al-Omari and others (1988) reasoned that, if the normal stress level is high and the stiffness of the reinforcement is low, then the bond between reinforcement and soil may be strong enough to extend the reinforcement, and the composite mass may follow the failure pattern of the soil. However, if the reinforcement is relatively stiff, they postulate that sliding will occur at the interface accompanied with particle crushing and overriding. In such a case, there will be no significant dilation and no significant difference between the peak and the residual strength values. The effect of saturation on residual friction angle for cohesionless soil produced mixed results, and Takasumi and others (1991) reported that, for geotextiles, saturated condition produced strength values less than or equal to the values under dry condition.

The results of direct shear (soil-grid) tests conducted in this study are shown in Figure 6.17. All the test specimens were compacted at 95 percent relative compaction at about 8 percent water content, and the tests were conducted under a soaked condition. The geogrid used in these tests was Matrex 240, a woven grid with an average aperture of 90 mm x 8 mm. At the lowest normal

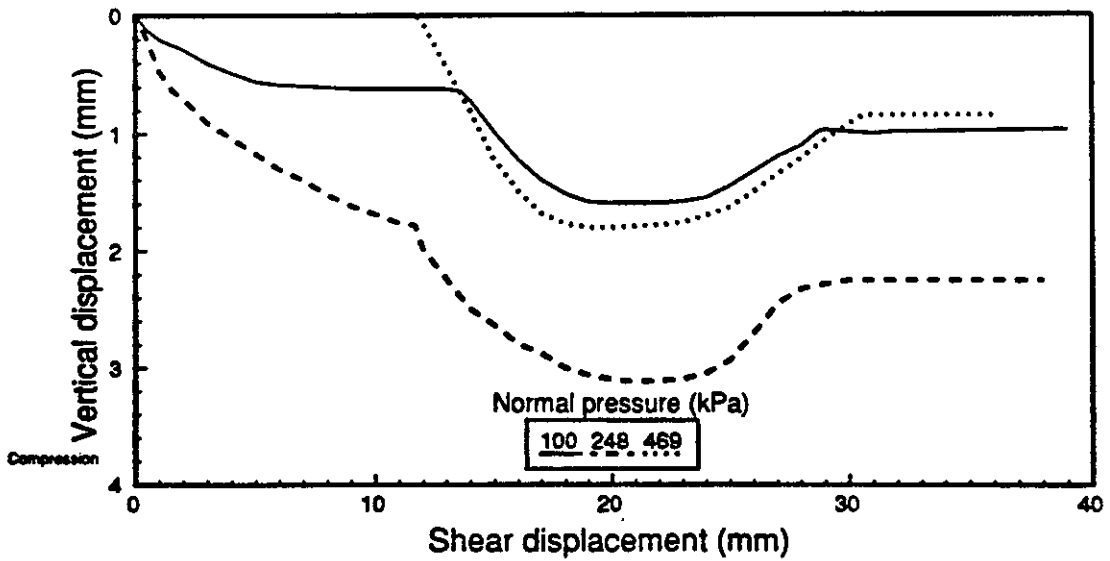
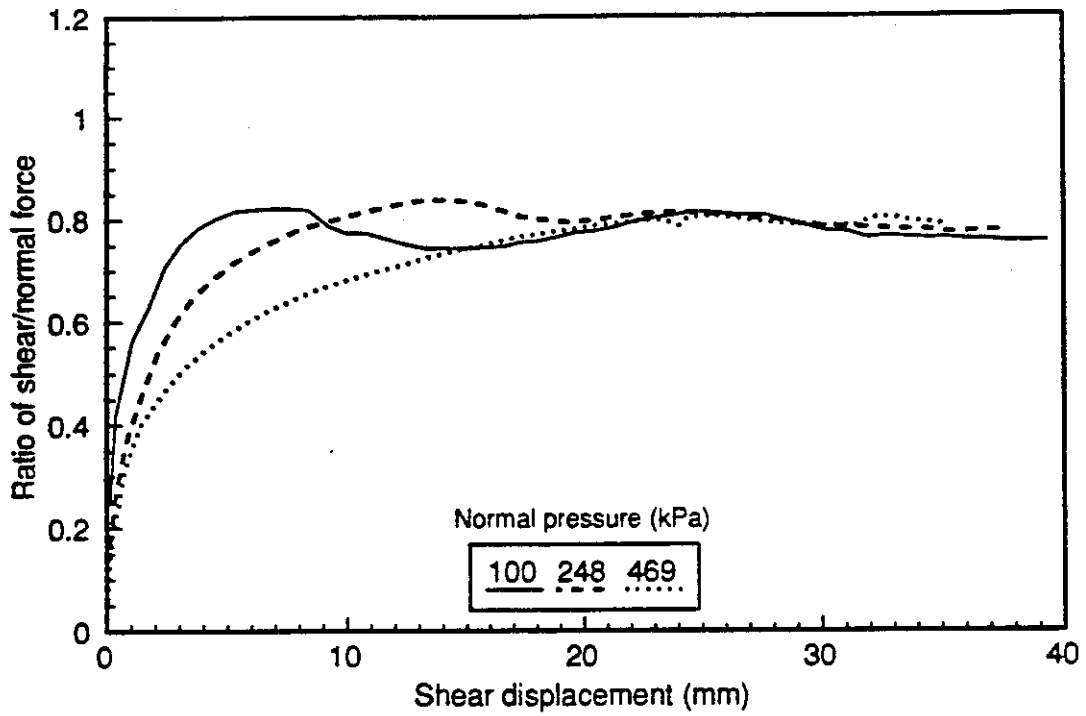


Figure 6.17 Results of direct shear interface strength tests on decomposed granite under different normal pressures

pressure, the (shear force)/(normal force) ratio shows a wavy pattern, which is less in other specimens under higher normal pressures. The exact reason for this behavior could not be ascertained. Some possible reasons are the dilatation pressures that decrease with increasing normal pressure, and possible soil accumulations near a grid bearing member before the back edge of the shear box moves over it. Another possibility, a wavy geogrid produced by the compaction process, was ruled out after examining a specimen dismantled before shearing. The vertical displacements during shearing were only compressive, but were very small. The sudden upward shifts recorded after about 25 mm of shearing may be due to slight tilting of the moving upper box. Vertical displacements measured in this direct shear apparatus are not very accurate and are used to make only qualitative judgements. The peak and the residual ϕ values obtained from these tests are plotted against the average normal pressure in Figure 6.18. They do not differ much, and the variation with increasing pressure is also insignificant. On the average, the interface shear strength is about 38° .

The direct shear (soil-soil) test results from the tests on decomposed granite from the Shasta Bally batholith are shown in Figure 6.19. Unlike in soil-grid tests, in these tests there were significant shear strength peaks and dilatation tendencies. It should be noted that in tests under the average normal pressures of 137, 270 and 479 KPa, the pressure was not maintained constant manually as in the other two tests, and the given values were averaged over the entire range of shear displacement. Yet, all peak ϕ values follow the same trend (as shown in Figure 6.20), and all residual shear strength values are very close (about 39°) except for the test under the lowest normal pressure.

6.4 Pullout tests

The increase in stability of a reinforced slope is realized by anchoring the reinforcement layer deep in the stable soil mass, beyond the anticipated failure surface. Jewell and others (1984) discussed the mechanisms that provide the anchoring effect. The main contribution is from soil shearing on plane surface areas of the reinforcement, as illustrated in Figure 6.21a, which in this case acts on

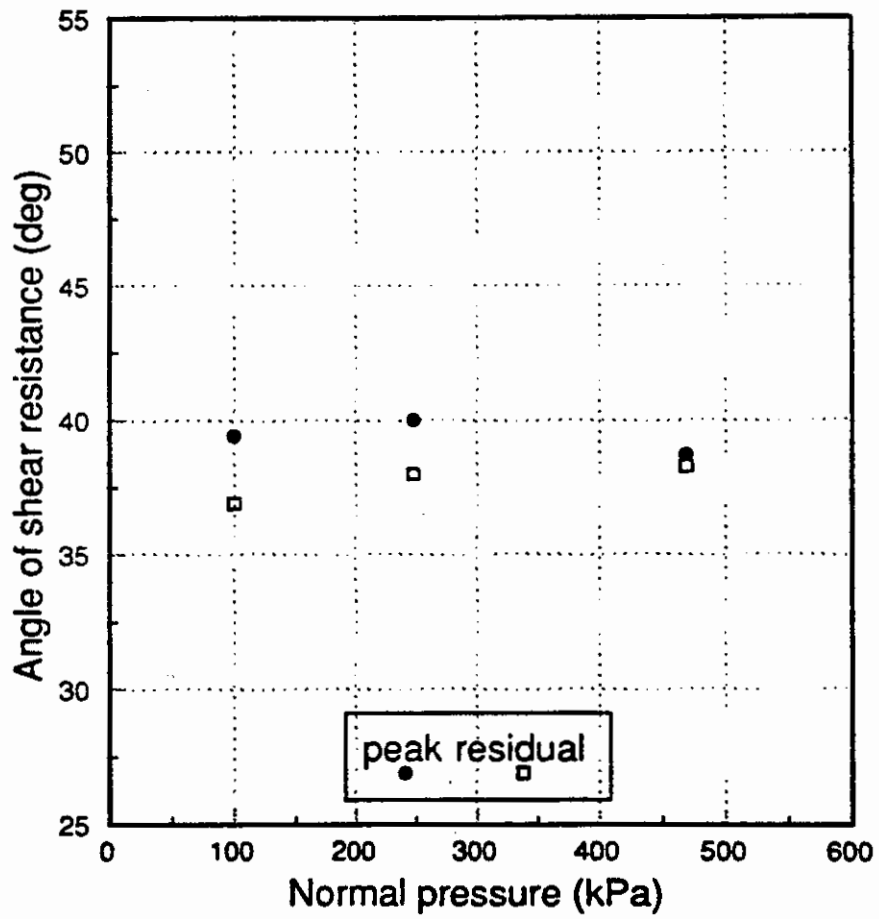


Figure 6.18 Variation of decomposed granite-geogrid interface shear strength with normal pressure

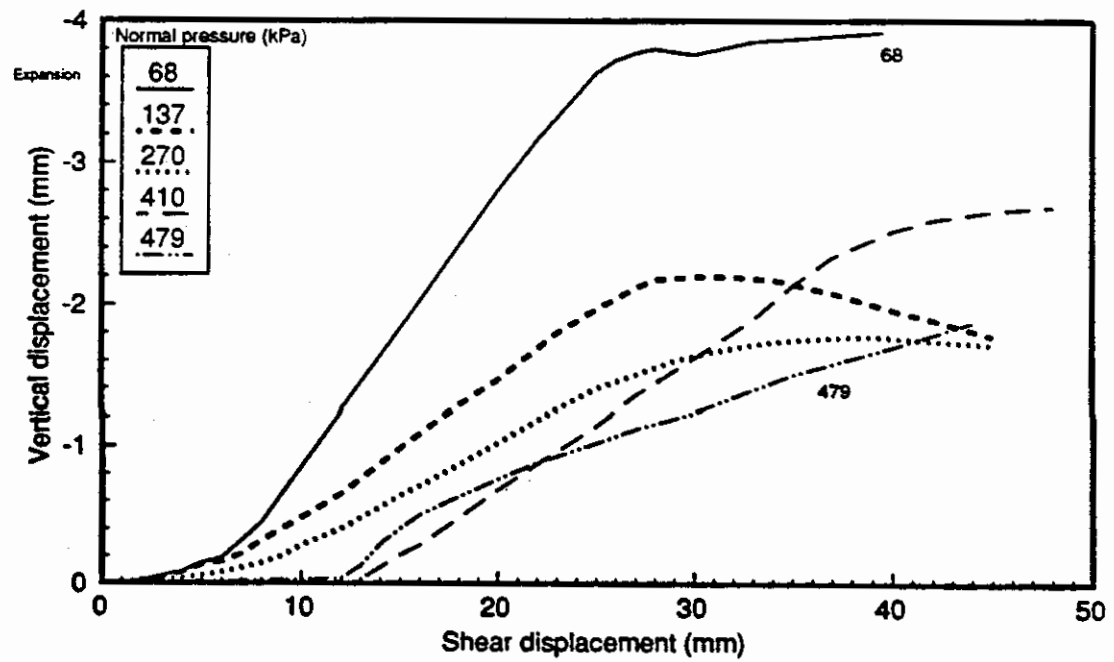
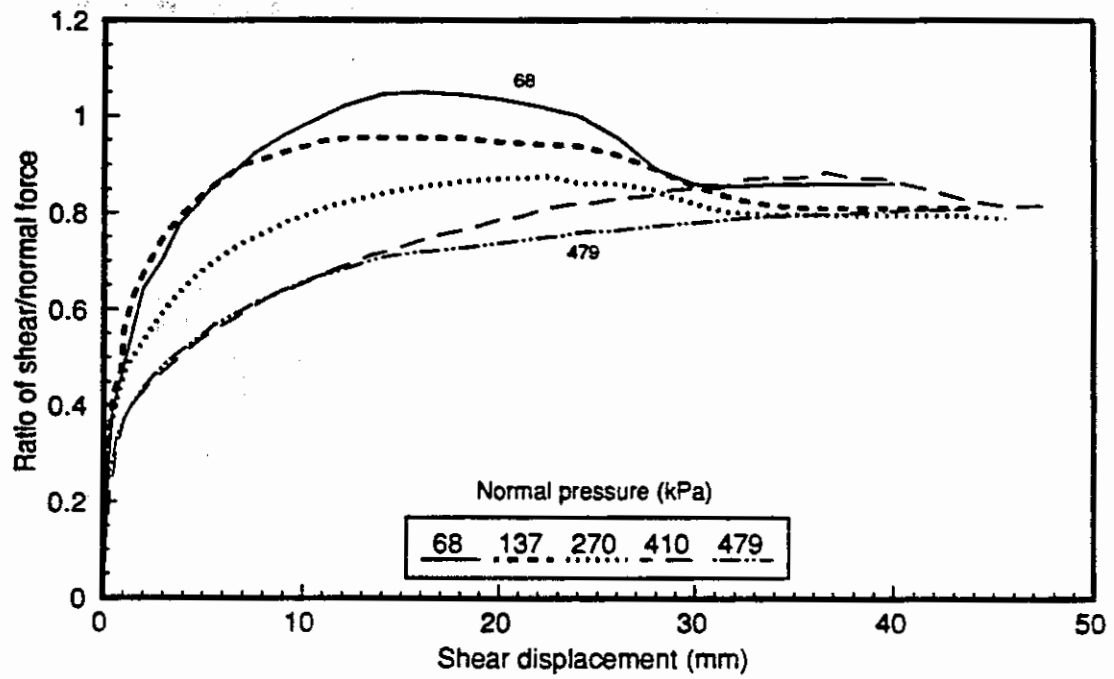


Figure 6.19 Results of direct shear tests on decomposed granite under different normal pressures

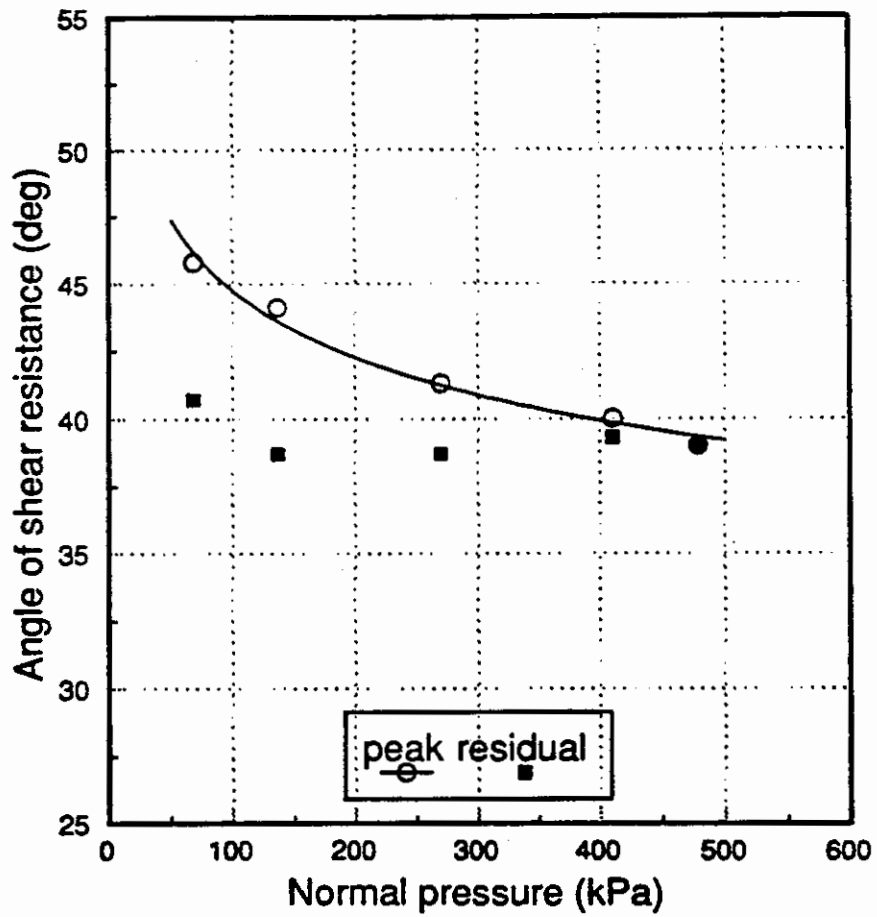
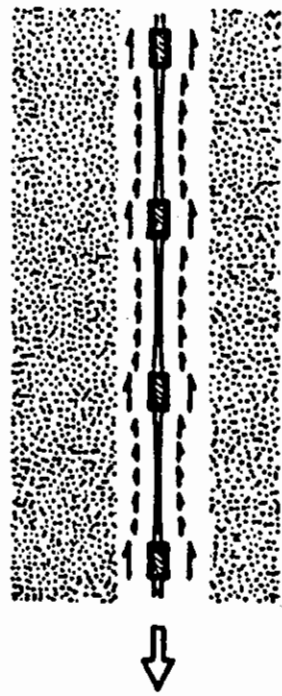
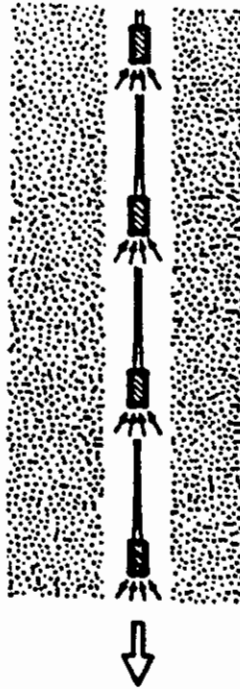


Figure 6.20 Variation of ϕ with normal pressure in direct shear tests on decomposed granite



a. Shear between soil and plane surfaces



b. Soil bearing on reinforcement surfaces

Figure 6.21 Mechanisms of bond strength development between a grid and soil (from Jewell and others, 1984)

both sides of the reinforcement layer. This is the same skin friction effect discussed before regarding the direct shear test, and is significantly dependent on the particle size if the reinforcement is a grid. Jewell and others (1984) suggest, from laboratory experience, that the effect of particle size can be conservatively ignored when;

$$\frac{\text{Minimum aperture dimension}}{\text{Average particle size}} \geq 3 \quad (6.4)$$

The other contribution to anchoring comes from soil bearing on cross-wise reinforcement members, as shown in 6.21b. This bearing pressure is somewhat similar to base pressure on deep foundations in soil, and is dependent on the soil density, the depth of embedment and the size of bearing area, in addition to the shear strength of the soil. However, the ultimate resistance depends only on the relative density, as reported by Vesic (1963) after laboratory tests on sand.

The type of reinforcement and its stiffness, or the level of extensibility, could influence pullout test results. Since the test procedure is not standardized yet, the testing techniques (some of which were discussed in detail in Chapter 3) could also be of concern in analyzing the results. In pullout tests of inextensible and extensible rods through dense medium sand, Jewell (1980), using photographic techniques, observed a significant influence of reinforcement stiffness on pullout. Jewell (1980) postulated that soil in a pullout test is "at rest" and has a low principal stress ratio until pullout occurs. With pullout, the soil adjacent to the reinforcement experiences an increasing stress ratio. When the critical stress ratio is exceeded, the soil yields, leaving behind a large mass of unyielding soil. For the extensible rod, the surrounding zone of yielding soil was small, only about 5 grains thick (about 18 mm). The peak pullout force was also much less than for the stiff rod, and a greater displacement was required to mobilize it. The normal pressures used were in the range of 40 to 115 kPa. Palmeira performed pullout tests on different types of grids under conditions similar to Jewell (Palmeira, 1987; Palmeira and Milligan, 1989 and 1990). In tests with small aperture grids, failure occurred in the soil, and the pullout force showed a significant peak. As the grid aperture is increased, the peak disappeared.

Palmeira and Milligan (1990) postulated that progressive failure occurs along the reinforcement, citing as evidence: a) a peak in horizontal thrust on the front wall that occur much before the pullout force peaks; and b) an initially non-linear tensile strain distribution in the grid (with much higher strains at the front end) that becomes linear only near pullout.

Several elaborate models have been developed to describe the bond or pullout strength: for example, the use of the grid geometry to account for the contribution from bearing pressure (Jewell and others, 1984); and the use of displacement compatibility conditions, widely used in analyzing friction pile foundations (Salomone and others, 1978; Beech, 1987). The simplest and the most reliable means of estimating the pullout strength is by conducting a pullout test. The parameter "Coefficient of Interaction" (C_i), obtained from pullout test data, can be used in a fashion similar to a ϕ value obtained from a shear test. It is defined as:

$$C_i = \frac{P}{2 L \sigma_n \tan \phi_r} \quad (6.5)$$

where, L = the embedded length of the geogrid, P = the maximum pullout force per unit width of the geogrid, σ_n = normal pressure, and ϕ_r = the residual angle of shear resistance of soil. One disadvantage of the parameter C_i is that it ignores the aperture size of a grid, and treats a grid and a sheet reinforcement the same way. Therefore, in comparing the effectiveness of different types of reinforcements, C_i may not be the most appropriate parameter. However, for the current study, the use of C_i is justified, as the emphasis is on evaluating the performance of decomposed granite rather than of the grid.

In the current test series, some of the major concerns regarding the design of a reinforced embankment were addressed. They were: a) the variation of C_i with the expected overburden pressure; b) the effect of compaction density on C_i ; and c) the effect of saturation on C_i . Pullout test results from the test series P200 (Table 3.3) are presented in Figure 6.22. The pullout force (per unit width) is plotted against the displacement at the back end of the grid, as measured by gage

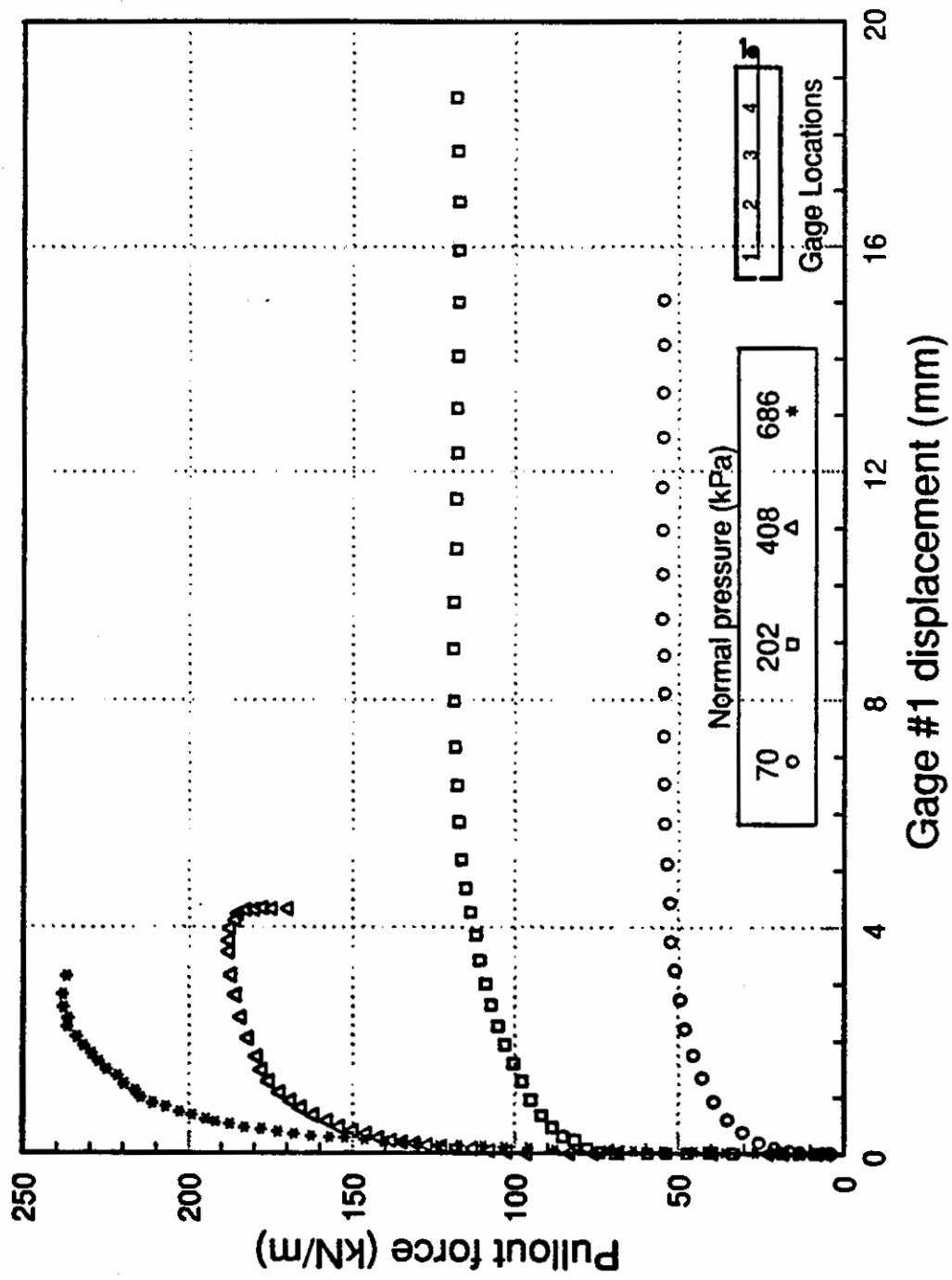


Figure 6.22 Variation of pullout force with normal pressure in decomposed granite, RC = 95%, soil thickness = 150 mm

#1. The pullout force increased by a factor of about 5 for an increase in normal pressure by a factor of about 10. The value of C_i decreased correspondingly from about 1.4 to about 0.6, as shown in Figure 6.23. In calculating C_i , an average residual ϕ value of 39° , obtained from direct shear tests discussed above, was used. It should be noted that the final displacement at the front end of the grid (at the clamp) was about 45 mm in each test shown in Figure 6.22, except in the test at 70 kPa in which the final pull was only 25 mm (because of a technical problem). As the normal pressure increases, the pull required to mobilize maximum pullout force increased significantly. In Figure 6.24, the development of the pullout force is plotted against the displacement of the gages as well as that of the clamp. The extension of the exposed portion of the grid (at the front), calculated using unconfined stress-strain characteristics of the grid, roughly accounted for the difference in displacements between gage #4 and the clamp.

To qualitatively investigate the extent of the zone of shearing due to pullout, a few pullout test specimens were provided with flexible markers in the middle, following the technique adopted by Gilbert and others (1992). Once soil was compacted, four vertical holes (about 4 mm in diameter) were drilled through the full soil thickness along the long centerline of the pullout box at a spacing of about 75 mm, and a flexible cord (caulking cord) of almost the same diameter was inserted in each hole. Any gaps remaining were filled with white uniform sand, poured around the cord. The holes were located so as not to destroy the integrity of the geogrid buried in the middle. Pullout resistance will not be influenced, it was assumed, by this arrangement because of the high flexibility of the cord chosen and its small diameter. At the end of pullout, one half of the specimen was excavated to expose the cords. 6.25 shows two of the specimens that were provided with these cords, one tested under 70 kPa average normal pressure and the other under 686 kPa. In the first, only the top half of the cords are exposed, while in the second test the cords are exposed completely by carefully removing half of the grid. As the grid was pulled out, the cords were sheared-off at the grid. There was no change in the verticality of the cords, except within about 5 mm above and below the grid. The disturbance within this zone could be either

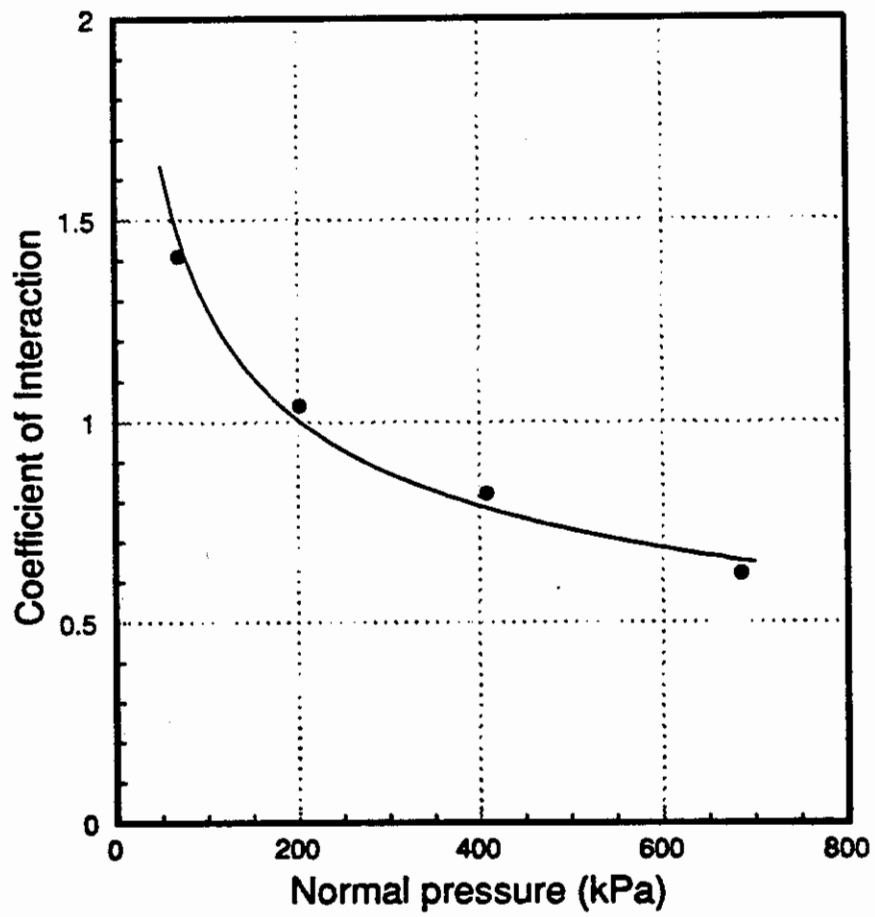


Figure 6.23 Variation of C_i with normal pressure in pullout tests on decomposed granite, RC = 95%

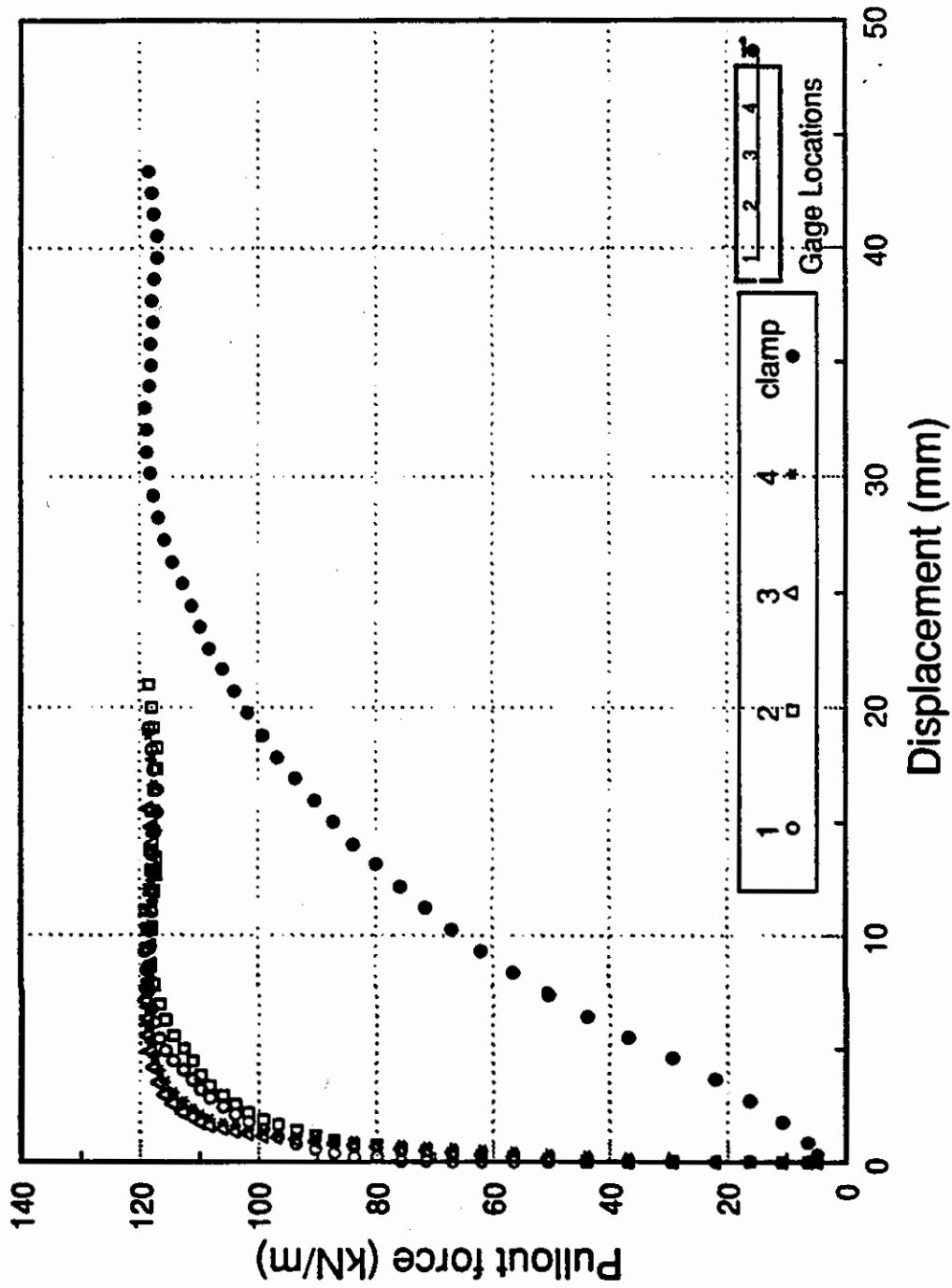
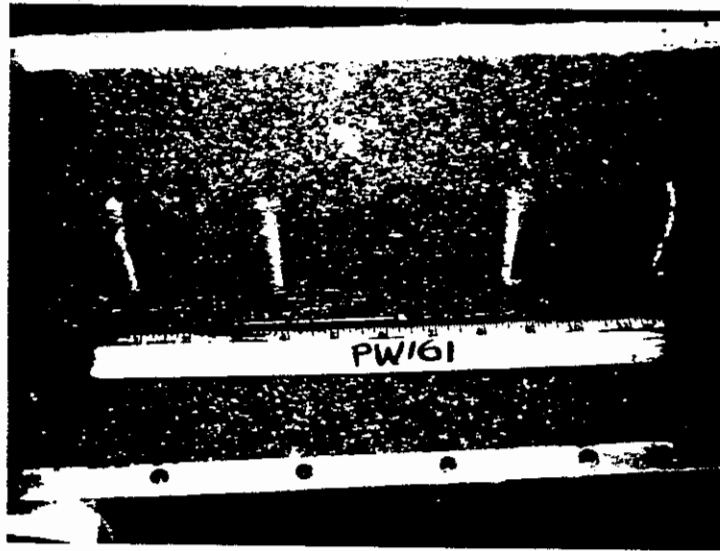


Figure 6.24 Comparison of gage displacements with that of the clamp in a pullout test, $RC = 95\%$, $\sigma_N = 200$ kPa, soil thickness = 150 mm



a) $\sigma_N = 70$ kPa



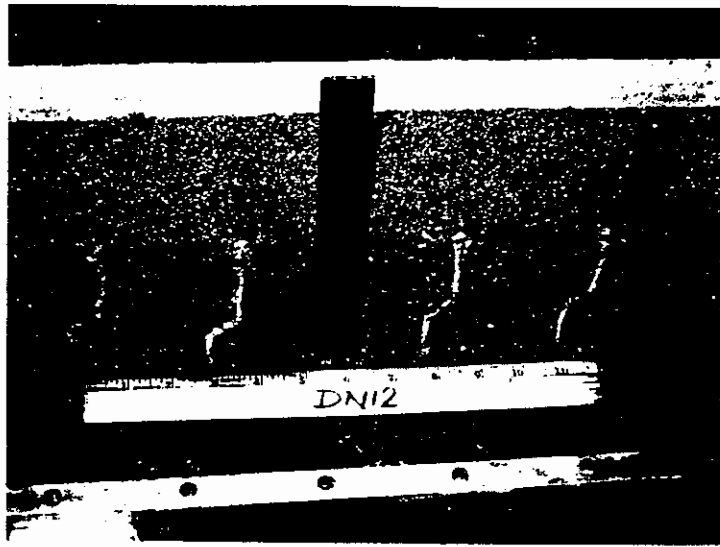
b) $\sigma_N = 686$ kPa

Figure 6.25 The extent of shear zone in pullout tests

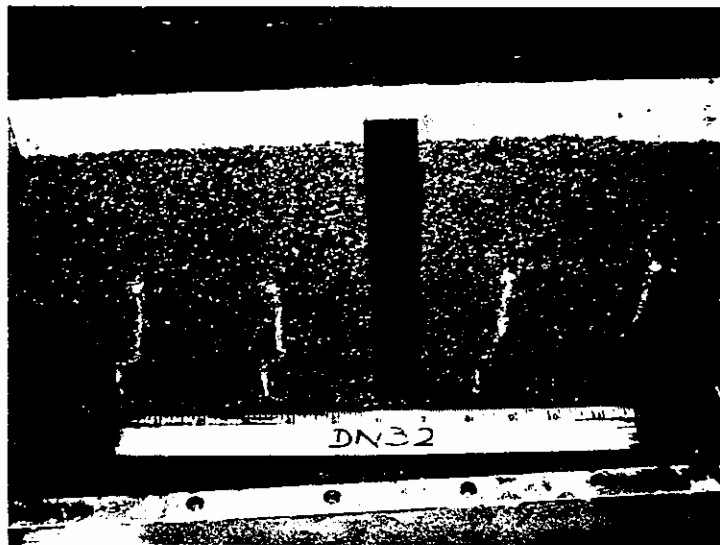
due to the shearing of soil and/or due to shearing of the cord. There was no noticeable change in the width of this zone between the two tests where the normal pressure difference was almost 10 times. The nearly zero vertical movements of the normal load platform observed during pullout tests could also be a result of this very thin shear zone.

A similar arrangement was used in a few direct shear (soil-soil) tests also. Two of those are shown in Figure 6.26, one under an average normal pressure of 68 kPa and the other under 410 kPa. The shear displacement at this stage was about 40 mm. The cord at the front end could be affected by the rigid wall of the bottom box. Rough measurements made on the other three cords indicate that the average width of the shear zone is about 12 mm in the test under 68 kPa pressure and about 5 mm in the other. For comparison, in direct shear tests the initial gap between the top and bottom boxes was about 6 mm.

All the previously described tests were performed on specimens prepared at 95 percent relative compaction. Test results from a specimen compacted at 90 percent relative compaction is compared in Figure 6.27 to the results from the corresponding denser specimen (at 200 kPa normal pressure). The pullout force in the loose specimen is about 25 percent less. Therefore, in designing a reinforced embankment, this reduction in pullout capacity should also be considered before finalizing the compaction density. The effect of saturation on the development of pullout force is illustrated in Figure 6.28. This series of tests used only a 100 mm soil thickness, and the final pull at the clamp was only 25 mm. The break in the data points of the as-compacted specimen represents a sudden slippage in the grid. Although both specimens developed about the same pullout force at the same amount of pull, it is clear that the as-compacted specimen is stiffer and could have developed a larger ultimate pullout force at a greater pull. Nevertheless, it is conservative to use the soaked pullout strength for design purposes, as the soaked condition provides the most critical situation for embankment stability.



a) $\sigma_N = 68 \text{ kPa}$



b) $\sigma_N = 410 \text{ kPa}$

Figure 6.25 The extent of shear zone in pullout tests

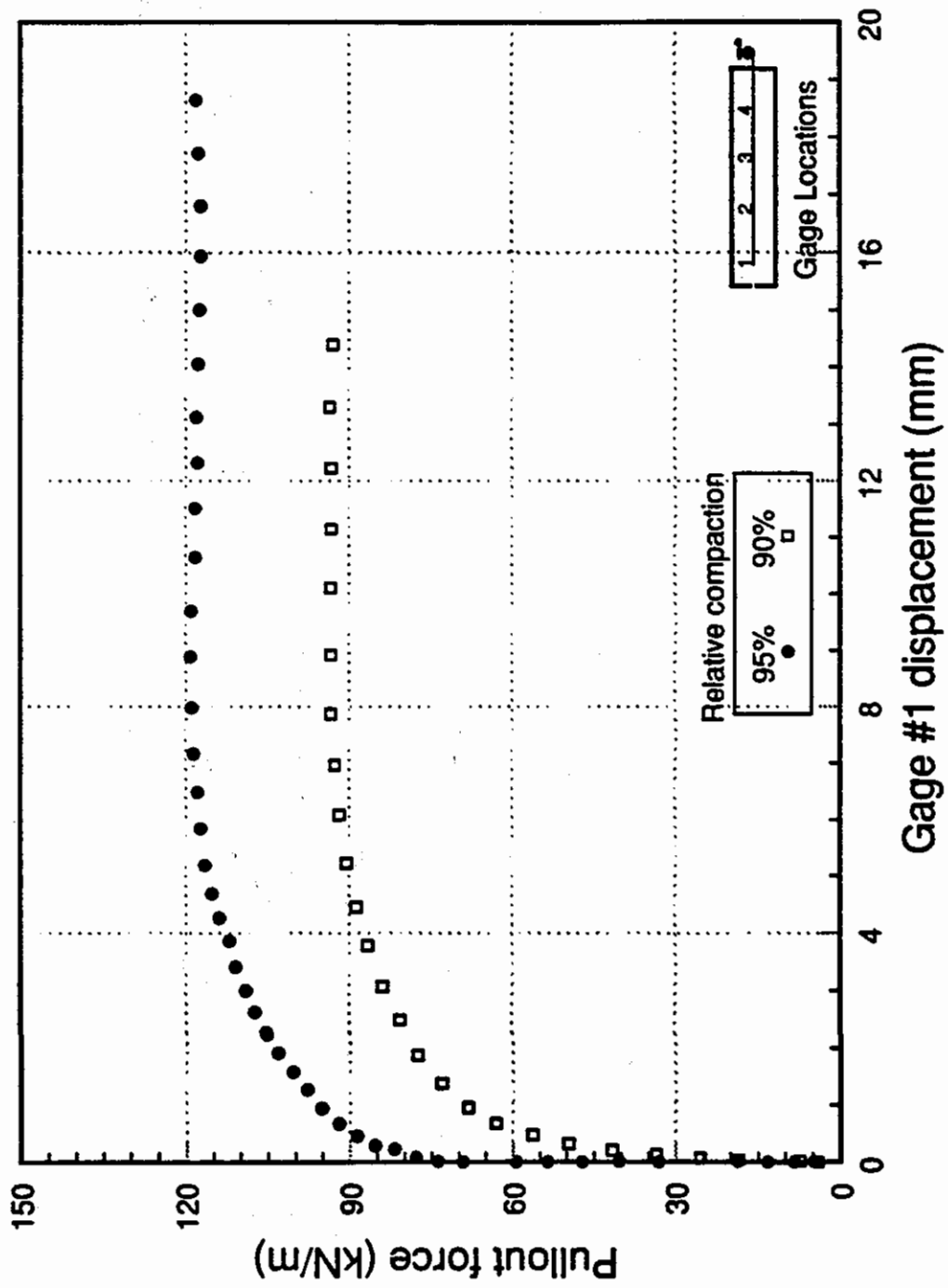


Figure 6.27 Variation of pullout force with relative compaction, $\sigma_N = 200 \text{ kPa}$, soil thickness = 150 mm

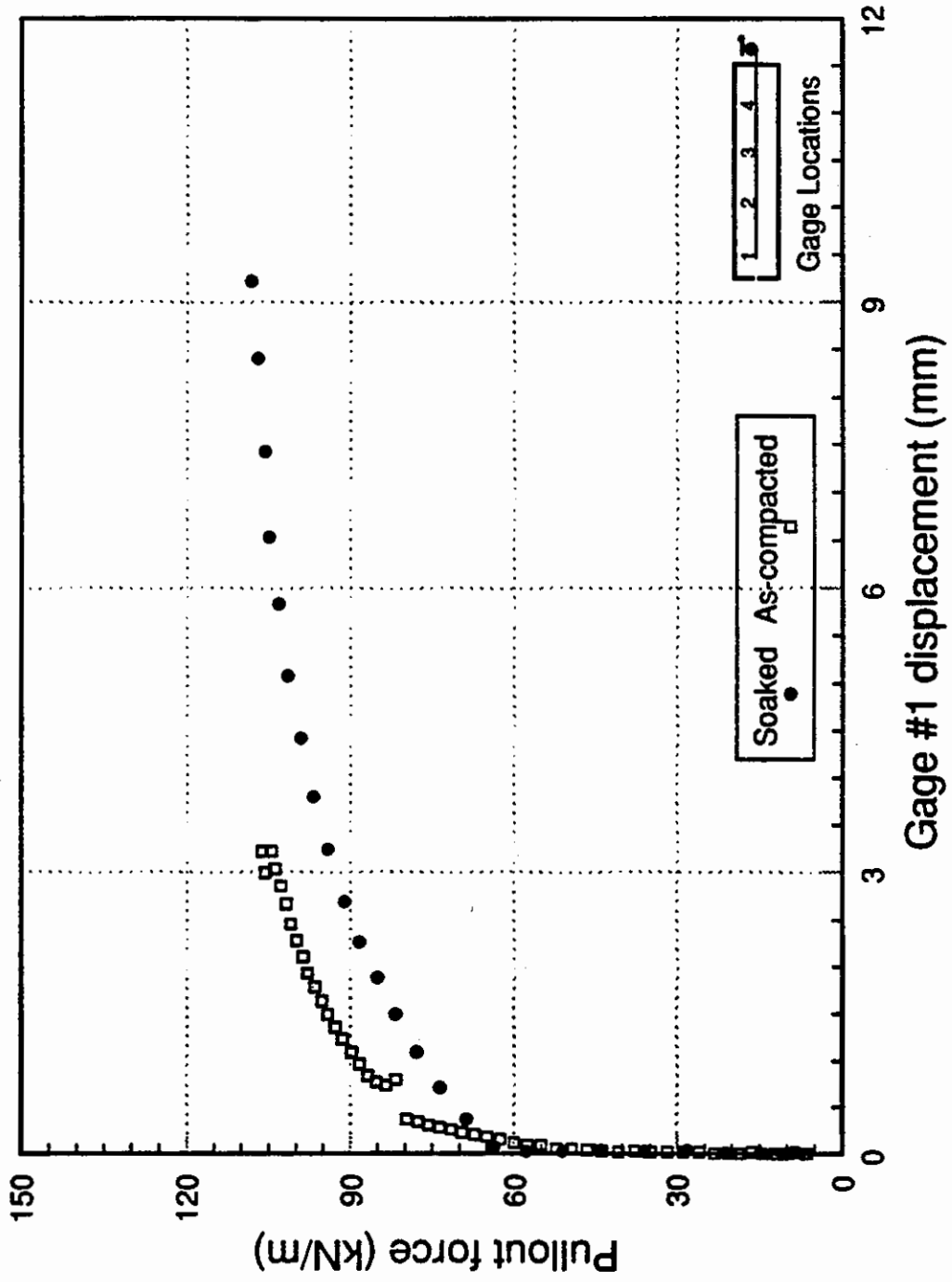


Figure 6.28 Variation of pullout force with saturation, $RC = 95\%$, $\sigma_N = 200 \text{ kPa}$, soil thickness = 150 mm

6.5 Past practices in some decomposed granite embankments

In Table 6.2, some mechanical properties used in designing a few important earth structures built using decomposed granite are presented, along with details on material placement conditions. All the structures listed are embankment dams. Most were built around 1960's, and hence the compaction densities, and consequently the strength parameters, seem to be low compared to current practices. Another reason for the choice of low strength parameters could be the serious concerns the engineers had regarding the fragility of the material. However, the design values in Table 6.2 could still be used as a guide in future embankment designs.

Table 6.2 Construction details and design parameters used in some decomposed granite embankments

Ref	Embankment	Ht (m)	Material Type	Zone Used	Top Size (cm)	R.C. (%)	W.C. wrt Wopt	Method of Compaction	Cohes. (kPa)	Friction (deg)	Slope (H:V)	K (1E-7) (cm/s)
1	Plover Core, Hongkong	40	ML	shell		85	+3 (avg)	30 cm - Tracked Dozer	0	30	3:1	0.1
2	Challawa, Nigeria		SP	shell	2.0	90	0:+2	20 cm - 6 p. SFR	6-13	28-32	3:1	
3	Buckhorn, CA	24	SM	shell	4.0	90		30 cm - 8 p. SFR/VSDR	0	37	2.25:1	1-15
4	Spring Creek, CA	58	CL-SM	shell	13.0				73	29		2.6
5	N.L. Arrowhead, CA	61	SM	homog.	15.0	92	-2:+2		20	35	2:1	
6	Mammoth Pool, CA	124	coarse	shell	0.6	92	-3:0	20 cm - 10 p. RTR		34	2:1	40
			fine	core	1.0					34		4
7	Union Valley, CA	122	coarse	shell		92	-1:+1.5	30 cm - 8 p. RTR	0	31	2.5:1	5-530
8	Antelope, CA	34	fine	core	0.4	90	-1.5:+1.5	20 cm - 12 p. SFR	0	33		0.4-360
9	Anthony House, CA	23	coarse	shell	15.0	92	-1.5:+1.5	15 cm - 12 p. SDR	0	32		
10	Cherry Valley, CA	96	fine	core	11.0	95		15 cm - 12 p. SFR	0	27		720
11	Dixon, CA	35	sand	transit.	15.0	90	-1:+2.5	15 cm - 12 p. SDR	40	37		10
12	Ponderosa, CA	50		shell		90	+0 (avg)	20 cm - 12 p. SFR		35	2.25:1	590
13	Poway, CA	47	coarse	shell	23.0	90	-1:+3	30 cm - 4 p. RTR	0	38	2.75:1	100
14	Turner, CA	34		core	15.0	94	-1:+1	20 cm - 12 p. SFR	0	34		

R.C. - Relative compaction with respect to Modified AASHTO

W.C. - Water content with respect to optimum water content

Method of Compaction - Layer thickness (in cm) and # of passes of Sheep Foot (SFR), Rubber-Tired (RTR), Steel Drum (SDR) or Vibratory Steel Drum Roller (VSDR)

Cohesion - Effective cohesion

Friction - Effective angle of shear resistance

Slope - Steepest side slope of embankment (horizontal : vertical)

K - Hydraulic conductivity

References:

- 1 Gaifford & Chan (1969)
- 2 Lazanyi (1986)
- 3 Solbos (1990)
- 4 USBR (1960)
- 5 Wu (1977)
- 6 CDWR (1973)
- 7 CDWR (1973)
- 8 CDWR (1973)
- 9 CDWR (1973)
- 10 CDWR (1973)
- 11 CDWR (1973)
- 12 CDWR (1973)
- 13 CDWR (1973)
- 14 CDWR (1973)

CHAPTER 7

SUMMARY, CONCLUSIONS AND RECOMMENDATIONS

The suitability of decomposed granite as an embankment fill material has been investigated with a view of modifying the practice of earthwork design and construction to accommodate the special character of the material. The physical characteristics of decomposed granite were examined through a review of literature on deposits worldwide and through common classification tests on a particular sample, obtained from the Shasta Bally batholith in northern California. Important mechanical properties of the compacted material were studied using oedometer and triaxial tests. In addition, the feasibility of using geogrid reinforcements in decomposed granite embankment fills to enable steepening of the side slopes was investigated through direct shear and pullout tests. The important findings from the literature review and the laboratory tests are given below, followed by recommendations on material placement conditions and on design parameters. The recommendations are specifically for the preliminary design and analysis of 100+ m high embankments, proposed by CALTRANS as a part of the realignment of the highway SH299 in Shasta County, CA.

Physical characteristics and classification

The term "decomposed granite" is used to identify a broad range of materials, from slightly weathered but intact rocks and boulders, to sand and even clay. The in situ fabric of decomposed granite typically contains relatively coarse grained aggregates of minerals, predominantly quartz, weathered feldspar and mica, and a relatively small proportion of fines. In the particular sample under investigation, the fines contain clay minerals such as kaolinite, smectite and vermiculite.

Difficulties arise in using conventional classification tests such as sieve analysis and Atterberg Limits for decomposed granite, since the particle aggregates may undergo breakage during sieving, and the presence of mica may affect the Atterberg Limits of the material passing the #40 sieve. The granitic

rock classification scheme proposed by Lee and de Freitas (1989) seems appropriate in classifying decomposed granite for embankment fills because of its emphasis on the classification of rock materials. Embankment fill materials, classified into six grades using this system, can be classified further into subgroups based on the Unified Soil Classification system. The material from the Shasta Bally batholith used in this investigation can thus be identified as a Grade VI (residual soil) SW-SM (well graded sand/silty sand) material.

Particle breakage

The grain aggregates and weathered minerals, primarily feldspar, in decomposed granite undergo substantial breakage under relatively low loads. Qualitatively, breakage is greatest in materials that are coarse and uniformly graded, or that have particles of high angularity or high intragranular void content. Laboratory tests showed that increasing the compactive effort increases particle breakage, but no significant increase in breakage was evident with increasing compaction water content.

Shear-induced breakage under conventional triaxial conditions is significantly greater than that under oedometer conditions, probably because of the greater shear stress/strain component under triaxial conditions. Loosely compacted specimens exhibit greater shear-induced breakage than dense specimens. In laboratory triaxial specimens, post-failure particle breakage estimates depend on whether a specimen dilates or compresses. In a dilative specimen, breakage mostly occurs in a narrow zone along the slip plane, whereas in a compressive (bulging) specimen, breakage occurs over a much larger volume. Breakage is primarily controlled by the applied strain level rather than the stress level. When triaxially sheared to the same strain level, particle breakage in compressive specimens increases with increasing stress level.

Volume change characteristics

Because oedometer specimens did not produce significant breakage, at least within the range of stresses used in this test program, the influence of particle breakage on volume change characteristics was not significantly high.

- 1) The settlement in loose specimens (90 percent compaction relative to Modified Proctor) was about twice as large as in dense specimens (95 percent relative compaction) at the highest normal pressure applied (about 1600 kPa). At this pressure, the loose specimens seem to have reached "virgin compression" (a steeply dipping stage in the compression curve), but the dense specimens seem not. A change in compaction water content did not significantly change the level of settlement.
- 2) When compacted near the optimum water content, hydrocompression, i.e., settlement due to soaking under load, exhibited by both dense and loose specimens was minimal. However, decreasing the compaction water content significantly increased the hydrocompression.
- 3) The "secondary compression index" in both loose and dense oedometer specimens was observed to increase with increasing normal pressure, in the range from 400 to 1600 kPa. Owing to delayed grain crushing and wetting effects, the time-dependent settlement of decomposed granite may be higher than that of conventional granular earthfill materials.
- 4) Under triaxial conditions, volumetric strain in consolidation was not directly controlled by the applied maximum principal stress, contradicting a postulate by some previous investigators. The reason may be that, in the range of pressures used in the triaxial test program, particle breakage was not the dominant cause for consolidation strains.
- 5) The rate of volume change, or the rate of dilatancy, at failure increased from negative (dilatant) values to zero with increasing confining pressure, a behavior exhibited by many other granular materials. However, the rate of volume change did not increase further and show positive (compressive) values, but remained at zero with further increase in pressure, in contrast to the reported behavior by other materials.

Shear strength characteristics

In contrast to the volume change characteristics, the influence of breakage on shear strength was quite significant:

- 1) In dense specimens subjected to confining pressures in the range 100 to 1500 kPa, the angle of shear resistance at failure, ϕ_f , decreased by about 25 percent and in loose specimens by about 15 percent. At the highest confining pressure, both the dense and the loose specimens exhibited almost the same ϕ_f value, which was nearly equal to the average residual ϕ value of the material.
- 2) In direct shear tests, decomposed granite exhibited a reduction in the peak ϕ value similar to that observed in triaxial shear. The residual ϕ value remained almost the same within a normal pressure range of 70 to 475 kPa.
- 3) The direct shear interface strength tests between a geogrid and decomposed granite, prepared at 95 percent relative compaction, produced residual ϕ values nearly equal to the residual ϕ value from direct shear tests of the soil alone. However, the peak ϕ values in the tests with geogrids were much less than those of the soil alone.
- 4) The coefficient of interaction, which is used to measure pullout strength, of a geogrid embedded in densely compacted (95 percent relative compaction) decomposed granite decreased by more than 50 percent when normal pressure was increased from 70 to 700 kPa. A decrease in compaction density from 95 percent to 90 percent resulted in about 25 percent reduction in pullout strength.
- 5) All triaxial, direct shear and pullout tests mentioned above were conducted under saturated or soaked conditions. The results may not differ significantly for specimens tested as-compacted.

Recommendations and suggestions

These findings have an important bearing on the use of decomposed granite as an embankment fill material. Based on these findings, the following recommendations and suggestions can be made:

- 1) The compaction water content must be controlled during placement, and should be kept near the optimum water content; for the particular material investigated, not less than about ($w_{opt} - 1\%$). This would keep the level of hydrocompression low.
- 2) The compaction density should be above 90 percent relative compaction (relative to Modified Proctor), and the actual value should be determined based on a number of other criteria such as: the steepness of the side slope; the utility of geosynthetics; the acceptable settlement level; and the comparative economy of each alternative.
- 3) Geogrids can be employed to steepen the slopes of decomposed granite embankments, but the advantages may be small if the soil placement density is low.

Several alternative configurations for the embankment side slope can be evaluated to minimize costs and optimize performance. For example, the slope could be designed to have a steeper top portion compacted at a high density and reinforced with geogrids, and a less steep bottom portion, with or without reinforcements. Such an approach takes advantage of both high soil friction angle and high geogrid pullout coefficient of interaction at low overburden stresses. When the bottom portion is made flatter, the overburden stresses near the sloping edge would not be as high, so that using geogrids may still be economical. Moreover, such a bi-linear slope configuration would require less total soil volume than a configuration with a single intermediate slope angle.

Once preliminary design of the embankment is completed, it is recommended that further laboratory studies be made on the particular geosynthetic material to be used, under the particular placement and stress conditions. If a substantial volume of the embankment includes geosynthetics, the deformations estimated from the current laboratory test program may be too conservative, because geosynthetics tend to provide some vertical deformation restraint as well. A numerical study may be employed to obtain better predictions on settlement in such a situation.

In the past, unwarranted conservatism seems to have made using decomposed granite in embankment fills uneconomical. In the face of such conservatism, economies can be realized mainly through innovative designs that make the full use of comprehensive studies on material properties.

REFERENCES:

- Adesunloye, M.O. (1985), "Sampling and Testing of Residual Soils in Nigeria", in Sampling and Testing of Residual Soils, Ed: Brand, E.W. and Phillipson, H.B., South Asian Geot. Soc., Hong Kong, pp 127-131, May.
- Albers, J.P. (1964), "Geology of the French Gulch Quadrangle, Shasta and Trinity Counties, California", USGS Bull., 1141-J, p 69.
- Al-Omari, R.R., Mahmood, A.K. and Hamodi, F.J. (1988), "Dilatancy and Failure of Reinforced Sand", Proc. International Geotechnical Symposium on Theory and Practice of Earth Reinforcement, Fukuoka, Japan, pp 57-62, Oct.
- Anwar, H.A. (1989), "Membrane Compliance Effects in Undrained Testing of Saturated Cohesionless Soils", Ph.D. Thesis, Stanford Univ., CA, Nov.
- Becker, E. (1972), "Strength and Deformation Characteristics of Rockfill Materials Under Plain Strain Conditions", Ph.D. Thesis, Univ. of Calif., Berkeley, CA, Sept.
- Beech, J.F. (1987), "Importance of Stress-Strain Relationships in Reinforced Soil System Designs", Proc. Geosynthetics'87 Conference, New Orleans, LA, pp 133-144.
- Billam, J. (1971), "Some Aspects of the Behavior of Granular Materials at High Pressures", Proc. Roscoe Memorial Symposium, Cambridge, England, pp.69-80, Mar.
- Bisdorn, E.B.A. (1967), "The Role of Micro-Crack Systems in the Spheroidal Weathering of an Intrusive Granite in Galicia (NW Spain)", *Geologie En Mijnbouw*, vol 46, pp 333-340, Sept.
- Brandon, T.L., Duncan, J.M. and Gardner, W.S. (1990), "Hydrocompression Settlement of Deep Fills", *Jou. Geotech. Eng., ASCE*, vol 116, n 10, pp 1536-1548, Oct.
- CDWR (1973), "Embankment Sections for Existing Earth and Rockfill Dams under State Jurisdiction", Division on Safety of Dams, California Department of Water Resources, Sacramento, CA, Jan.

- Colliat-Dangus, J.L., Desrues, J. and Foray, P. (1988), "Triaxial Testing of Granular Soil under Elevated Cell Pressures", in *Advanced Testing of Soil and Rock*, ASTM STP 977, pp 290-310.
- DallaValle, J.M. (1943), "Micromeritics", Pitman Publishing Corporation, New York, NY.
- Dearman, W.R., Baynes, F.J. and Irfan, T.Y. (1978), "Engineering Grading of Weathered Granite", *Eng. Geol.*, vol 12, pp 345-374.
- Duffy, J. (1990), Personal communication, CALTRANS, Sacramento, CA.
- Eggler, D.H., Larson, E.E. and Bradley, W.C. (1969), "Granites, Grusses, and the Sherman Erosion Surface, Southern Laramie Range, Colorado-Wyoming", *Amer. Jou. Sci.*, vol 267, pp 510-522, Apr.
- Eigenbrod, K.D. and Locker, J.G. (1987), "Determination of Friction Values for the Design of Side Slopes Lined or Protected with Geosynthetics", *Canadian Geot. Jou.*, vol 24, no 4, pp 509-519.
- Eubank, D.W. (1990), Personal communication, USBR, Sacramento, CA.
- Farrag, K, Acar, Y.B. and Juran, I. (1993), "Pull-out Resistance of Geogrid Reinforcements", *Geotextiles and Geomembranes*, vol 12, pp 133-159.
- Feda, J. (1971), "The Effect of Grain Crushing on the Peak Angle of Internal Friction of a Sand", *Proc. 4th Budapest Conf. on Soil Mechanics*, pp 79-93.
- Feda, J. (1977), "High Pressure Triaxial Tests of a Highly Decomposed Granite", *Proc. Symposium on the Geotechnics of Structurally Complex Formations*, Capri, Italy, pp 239-244.
- Feda, J. (1992), "Creep of Soils and Related Phenomena", Elsevier, Amsterdam, Netherlands.
- Fukumoto, T. (1979), "Fundamental Study on the Compactability and Permeability of Decomposed Granite Soil", Ph.D. Thesis, Kyoto University, Japan. (in Japanese)
- Furukawa, Y. and Fujita, T. (1990), "Properties of Decomposed Granite Soil Distributed in the Abukuma Mountains, Northeastern Japan", in *Residual Soils in Japan*, Research Committee on Physical and Mechanical Properties of Residual Soil Ground, JSSMFE, pp 89-96.

- Gidigasu, M.D. (1985), "Sampling and Testing of Residual Soils in Ghana", in Sampling and Testing of Residual Soils, Ed: Brand, E.W. and Phillipson, H.B., South Asian Geot. Soc., Hong Kong, pp 65-74, May.
- Gilbert, P.A, Oldham, J.C. and Coffing, L.R., Jr. (1992), "Laboratory Measurement of Pullout Resistance of Geotextiles Against Cohesive Soils", Tech. Rept. GL-92-6, USAE Waterways Experiment Station, Vicksburg, MS 39180, June.
- Goodman, R.E. (1980), "Introduction to Rock Mechanics", John Wiley & Sons, New York, NY.
- Goodman, R.E. (1992), "Engineering Geology: Rocks in Engineering Construction", John Wiley & Sons, New York, NY, in press.
- Goswami, S.C. (1984), "Influence of Geological Factors on Soundness and Abrasion Resistance of Road Surface Aggregates: A Case Study", Bulletin, International Assoc. of Eng. Geol., n 30, pp. 59-61.
- Guilford, C. M. and Chan, H.C. (1969), "Some Soil Aspects of the Plover Cove Marine Dam", Proc. 7th Int. Conf. Soil Mech. and Found. Eng., Mexico City, vol 2, pp 291-299.
- Hale, B.C., Lovell, C.W. and Wood, L.E. (1981), "Development of a Laboratory Compaction-Degradation Test for Shales", Transportation Research Report 790, Transportation Research Board, Washington, D.C., pp 45-52.
- Hencher, S. R. and Martin, R.P. (1982), "The Description and Classification of Weathered Rocks in Hong Kong for Engineering Purposes", Proc. 7th Southeast Asian Geot. Eng. Conf., Hong Kong, Nov., pp 125-142.
- Hendron, A.J. Jr. (1963), "The Behavior of Sand in One Dimensional Compression", Ph.D. Thesis, Univ. of Illinois, Urbana, IL.
- Hendron, A.J. Jr., Fulton, R.E. and Mohraz, B. (1963), "The Energy Absorption Capacity of Granular Materials in One Dimensional Compression", Rpt to Air Force Special Weapons Center, Kirkland Air Base, NM.
- Hilf, J.W. (1975), "Compacted Fill", in Foundation Engineering Handbook, Ed: Winterkorn, H.F. and Fang, H-Y., 4th ed., Van Nostrand Reinhold, New York, NY, pp 244-311.

- Huntington, G.L. (1954), "The Effect of Vertical Zonality on Clay Content in Residual Granitic Soils of the Sierra Nevada Mountains", M.S. Thesis, Univ. of Calif., Berkeley, CA.
- Isherwood, D. and Street, A. (1976), "Biotite Induced Grussification of the Boulder Creek Granodiorite, Boulder County, Colorado", *Geol. Soc. Amer. Bull.*, vol 87, pp 366-370, Mar.
- Ito, T., Kujime, A. and Sincho, S. (1990), "Classification of Decomposed Granitic Soil and Engineering Properties", in *Residual Soils in Japan*, Research Committee on Physical and Mechanical Properties of Residual Soil Ground, JSSMFE, pp 63-66.
- Jewell, R.A. (1980), "Some Effects of Reinforcement in Soils", Ph.D. Thesis, University of Cambridge, U.K.
- Jewell, R.A., Milligan, G.W.E, Sarsby, R.W. and Dubois, D. (1984), "Interaction between Soil and Geogrids", *Proc. Conf. on Polymer Grid Reinforcement*, Thomas Telford Ltd, London, U.K.
- Kitamura, R. and Haruyama, M. (1988), "Compression and Shear Deformation of Soil under Wide Ranging Confining Pressure", in *Advanced Triaxial Testing of Soil and Rock*, ASTM STP 977, pp 501-511.
- Krank, K.D. and Watters, R.J. (1983), "Geotechnical Properties of Weathered Sierra Nevada Granodiorite", *Bull. Assoc. of Eng. Geol.*, vol 20, n 2, pp 173-184.
- Kulhawy, F.H. and Mayne, P.W. (1990), "Manual on Estimating Soil Properties for Foundation Design", Final Report EL-6800, Prepared for Electric Power Research Institute, Palo Alto, CA.
- Ladanyi, B. (1967), in discussion of Lee, K.L. and Farhoomand, I. (1967), *Canadian Geot. Jou.*, vol 9, n 1, pp 87-88.
- Lambe, T.W. (1951), "Soil Testing for Engineers", J. Wiley & Sons, New York, NY.
- Lanphere, M.A. and Irwin, W.P. (1965), "Carboniferous Isotopic Age of the Metamorphism of the Salmon Hornblende Schist and Abrams Mica Schist, Southern Klamath Mountains, CA", *USGS Prof. paper 525-D*, pp 27-31.

- Lavery, B.R. and Langner, L.L. (1958), "Mammoth Pool Shear Tests", Rpt to Southern California Edison Co., in Archives of Division of Safety of Dams, California Department of Water Resources, Sacramento, CA, May.
- Lazanyi, I. (1986), "The use of Decomposed Granite Rock for Dam Construction", Water Power and Dam Construction, July, pp 25-28.
- Lee, I-K. (1991), "Mechanical Behavior of Compacted Decomposed Granite Soil", Ph.D. Thesis, City University, London, U.K.
- Lee, K.L. and Farhoomand, I. (1967), "Compressibility and Crushing of Granular Soil in Anisotropic Triaxial Compression", Canadian Geot. Jou., vol 9, no 1, pp 68-99.
- Lee, K.L. and Seed, H.B. (1967), "Drained Strength Characteristics of Sands", Jou. Soil Mech. Found. Eng., ASCE, vol 93, no 6, pp 117-142, Nov.
- Lee, K.L., Seed, H.B. and Dunlop, P. (1967), "Effect of Moisture on the Strength of a Clean Sand", Jou. Soil Mech. Found. Eng., ASCE, vol 93, no 6, pp 17-40, Nov.
- Lee, S.G. (1987), "Weathering and Geotechnical Characterization of Korean Granites", Ph.D. Thesis, Imperial College, Univ. of London, United Kingdom.
- Lee, S.G. and de Freitas, M.H. (1989), "A Revision of the Description and Classification of Weathered Granite and its Application to Granites in Korea", Qua. Jou. Eng. Geol., vol 22, no 1, pp 31-48.
- Leslie, D.D. (1963), "Large Scale Triaxial Testing on Gravelly Soils", Proc. 2nd Pan American Conf. on Soil Mech. Found. Eng., Sao Paulo, vol II, pp 537-560, July.
- Li, C.Y. and Mejia, V. (1967), "Building Earth Dams in a Region of Residual Soil in Colombia", Proc. 3rd Pan American Conf. on Soil Mech. and Found. Eng., Caracas, vol 2, pp 65-76.
- Lo, K.Y. and Roy, M. (1973), "Response of Particulate Materials at High Pressures", Soils and Foundations, JSSMFE, vol 13, no 1, pp 61-76, Mar.
- Macfarland, J. (1990), Personal communication, CALTRANS, Sacramento, CA.

- Makiuchi, K. and Miyamori, T. (1988), "Mobilization of Soil-Geofabric Interface Friction", Proc. International Geotechnical Symposium on Theory and Practice of Earth Reinforcement, Fukuoka, Japan, pp 129-134, Oct.
- Marachi, N.D. (1969), "Strength and Deformation Characteristics of Rockfill Materials", Ph.D.Thesis, Univ. of Calif., Berkeley, CA, Jun.
- Marsal, R.J. (1965), "Stochastic Processes in the Grain Skeleton of Soils", in Proceedings of 6th Int. Conf. on Soil Mech. and Found. Eng., Montreal, vol 1, pp 303-307.
- Marsal, R.J. (1967), "Large Scale Testing of Rockfill Materials", Jou. Soil Mech. Found. Eng., ASCE, vol 93, n 2, pp 27-43, Mar.
- Marsal, R.J. (1973), "Mechanical Properties of Rock Fill", in Embankment-Dam Engineering, Ed: Hirschfield, R.C. and Poulos, S.J., John Wiley & Sons, NY, pp 110-199.
- Matsuo, S. and Nishida, K. (1968), "Physical and Chemical Properties of Decomposed Granite Soil Grains", Soils and Foundations, JSSMFE, vol 8, no 4, pp 10-20.
- Matsuo, S. and Nishida, K. (1970), "The Properties of Decomposed Granite Soils and Their Influence on Permeability", Soils and Foundations, JSSMFE, vol 10, no 1, pp 93-105.
- Matsuo, S., Fukuta, M. and Nishida, K. (1970), "Consistency of Decomposed Granite Soils and Its Relation to Engineering Properties", Soils and Foundations, JSSMFE, vol 10, no 4, pp 1-9.
- Mejia, C.A., Vaid, Y.P. and Negussey, D. (1988), "Time Dependent Behavior of Sand", Proc. International Conf. on Rheology and Soil Mechanics, Ed: Keedwell, M.T., Coventry, U.K., pp 312-326, Sept.
- Mitchell, J.K. (1993), "Fundamentals of Soil Behavior", 2nd Ed., John Wiley & Sons, New York, NY.
- Mitchell, J.K. and Sitar, N. (1982), "Engineering Properties of Tropical Residual Soils", in Engineering and Construction in Tropical and Residual Soils, Proc. ASCE Specialty Conf., Honolulu, Hawaii, pp 30-57, Jan.

- Miura, N., Murata, H. and Harada, A. (1983), "Effect of Water on the Shear Characteristics of Sandy Soils Consisted of Breakable Particles", Transactions of JSCE, Tokyo, vol 15, pp 377-380.
- Miura, N. and O-Hara, S. (1979), "Particle Crushing of a Decomposed Granite Soil under Shear Stresses", Soils and Foundations, JSSMFE, vol 19, no 3, pp 1-14, Sept.
- Miura, N. and Yamanouchi, T. (1973), "Compressibility and Drained Shear Characteristics of a Sand under High Confining Pressures", Technology Reports of Yamaguchi Univ., vol 1, no 2, pp 271-290.
- Miura, N. and Yamanouchi, T. (1975), "Effect of Water on the Behavior of a Quartz-Rich Sand under High Stresses", Soils and Foundations, JSSMFE, vol 15, no 4, pp 23-34, Dec.
- Miura, N. and Yamanouchi, T. (1977), "Effect of Particle Crushing on the Shear Characteristics of a Quartz-Rich Sand", Transactions of JSCE, Tokyo, vol 9, pp 198-202.
- Miyamori, T., Iwai, S. and Makiuchi, K. (1986), "Frictional Characteristics of Non Woven Fabrics", Proc. Third International Conf. on Geotextiles, Vienna, Austria, pp 701-705.
- Moore, I.C. (1979), "Granitic Weathering in NE Scotland and Its Effects upon Aggregate Properties", Ph.D. Thesis, Univ. of Glasgow, United Kingdom.
- Mori, H. (1985), "Sampling and Testing of Granitic Residual Soils in Japan", in Sampling and Testing of Residual Soils, Ed: Brand, E.W. and Phillipson, H.B., South Asian Geot. Soc., Hong Kong, pp 99-108, May.
- Moye, D.G. (1955), "Engineering Geology for the Snowy Mountains Scheme", Jou. Inst. Eng., Australia, vol 27, pp 281-299.
- Murphy, D.J. (1987), "Stress, Degradation and Shear Strength of Granular Material", in Geotechnical Modeling and Applications, Ed: Sayed, S.M., Gulf Publishing Co., Houston, TX, pp 181-211.
- Newbery, J. (1971), "Engineering Geology in the Investigation and Construction of the Batang Padang Hydroelectric Scheme, Malaysia", Quar. Jou. Eng. Geol., vol 3, pp 151-181.

- Nishida, K. and Kagawa, M. (1972), "Shear Strength Properties of Weathered Residual Soil", Technology Reports of Kansai University, no 13, pp 139-148, Mar.
- Nishida, K., Sasaki, S. and Aoyama, C. (1979), "Water Adsorption on Decomposed Granite Soil Particles and Its Influence on Permeability", Technology Reports of Kansai Univ., no 20, Osaka, Japan, pp 153-160, Mar.
- Nobari, E.S. (1971), "Effect of Reservoir Filling on Stresses and Movements in Earth and Rockfill Dams", Ph.D. Thesis, Univ. of Calif., Berkeley, CA, Sept.
- Oda, M. (1972), "Initial Fabrics and Their Relation to Mechanical Properties of Granitic Material", Soils and Foundations, JSSMFE, vol 12, no 1, pp 17-36, Mar.
- O-Hara, S. and Matsuda, H. (1984), "Creep Deformation of Compacted Decomposed Granite Soils", Technology Reports of Yamaguchi University, vol 3, no 3, pp 239-247, Dec.
- Onitsuka, K. and Yoshitake, S. (1990), "Engineering Properties of Decomposed Granite Soils as Backfill Materials", in Residual Soils in Japan, Research Committee on Physical and Mechanical Properties of Residual Soil Ground, JSSMFE, pp 63-66.
- Onitsuka, K., Yoshitake, S. and Nanri, M. (1985), "Mechanical Properties and Strength Anisotropy of Decomposed Granite Soil", Soils and Foundations, JSSMFE, vol 25, no 2, pp 14-30.
- Onodera, T., Oda, M. and Minami, K. (1976), "Shear Strength of Undisturbed Sample of Decomposed Granite Soil", Soils and Foundations, JSSMFE, vol 16, no 1, pp 17-26, Mar.
- Onodera, T.F., Yoshinaka, R. and Oda, M. (1974), "Weathering and Its Relation to Mechanical Properties of Granite", Proc. 3rd Int. Cong. Soc. Rock Mechanics, Denver, vol II-A, pp 71-78.
- Palmeira, E.M. (1987), "The Study of Soil Reinforcement Interaction by means of Large Scale Laboratory Tests", Ph.D. Thesis, University of Oxford, U.K.

- Palmeira, E.M. and Milligan, G.W.E. (1989), "Scale and Other Factors Affecting the Results of Pull-out Tests of Grids Buried in Sand", *Geotechnique*, vol 39, no 3, pp 511-524.
- Palmeira, E.M. and Milligan, G.W.E. (1990), "Large Scale Pull-out Tests on Geotextiles and Geogrids", *Proc. Conf. on Geotextiles, Geomembranes and Related Products*, Ed: Den Hoedt, Balkema, Rotterdam, Netherlands, pp 743-746.
- Phillipson, H.B. and Brand, E.W. (1985), "Sampling and Testing of Residual Soils in Hongkong", in *Sampling and Testing of Residual Soils*, Ed: Brand, E.W. and Phillipson, H.B., South Asian Geot. Soc., Hong Kong, pp 75-82, May.
- Prysock, R.H. (1979), "Triaxial Testing of Large Diameter Compacted Soil Specimens", Rpt FHWA/CA/TL-79/19, CALTRANS, Sacramento, CA, Oct.
- Rowe, P.W. (1962), "The Stress Dilatancy Relations for Static Equilibrium of an Assembly of Particles in Contact", *Proc. Royal Soc., London, Series A*, vol 269, pp 500-527.
- Ruxton, B.P. and Berry, L. (1957), "Weathering of Granite and Associated Erosional Features in Hong Kong", *Bull. Geol. Soc. Amer.*, vol 68, pp 1263-1292, Oct.
- Salomone, W.G., Holtz, R.D. and Kovacs, W.D. (1978), "A New Soil-Reinforcement Interaction Model", *Proc. Symposium on Earth Reinforcement*, Pittsburg, PA, pp 714-734.
- Sandroni, S.S. (1985), "Sampling and Testing of Residual Soils in Brazil", in *Sampling and Testing of Residual Soils*, Ed: Brand, E.W. and Phillipson, H.B., South Asian Geot. Soc., Hong Kong, pp 31-50, May.
- Seed, H.B. and Lee, K.L. (1967), "Undrained Strength Characteristics of Cohesionless Soils", *Jou. Soil Mech. Found. Eng., ASCE*, vol 93, no 6, pp 333-360, Nov.
- Shannon and Wilson (1957), "Shear Strength Investigation of Proposed Borrow Materials for Mammoth Pool Dam", Rpt. to Southern California Edison Co., Seattle, WA, Aug.

- Siddiqi, F.H., Seed, R.B., Chan, C.K., Seed, H.B. and Pyke, R.M. (1987), "Strength Evaluation of Coarse-Grained Soils", Rpt UCB/EERC-87/22, Univ. of Calif., Berkeley, CA, Dec.
- Solbos, E.J. Jr. (1990), Personal communication, US Bureau of Reclamation, Weaverville, CA.
- Sousa, J.B. and Chan, C.K. (1991), "Computer Applications in the University of California, Berkeley Geotechnical Laboratories", Proc. Geotechnical Engineering Congress, Boulder, CO, Geotechnical Special Publication 27, vol 1, pp 531-541, July.
- Sowers, G.F. and Richardson, T.L. (1983), "Residual Soils of Piedmont and Blue Ridge", Transportation Research Record 919, TRB, pp 10-16.
- Sowers, G.F., Williams, R.C. and Wallace, T.S. (1965), "Compressibility of Broken Rock and the Settlement of Rockfills", Proc. 6th Int. Conf. on Soil Mech. Found. Eng., Montreal, vol II, pp 561-565.
- Sueoka, T. (1990), "Granitic Residual Soils: Their Global and Local Geotechnical Properties", in Residual Soils in Japan, Research Committee on Physical and Mechanical Properties of Residual Soil Ground, JSSMFE, pp 55-61.
- Takasumi, D.L., Green, K.R. and Holtz, R.D. (1991), "Soil-Geosynthetics Interface Strength Characteristics: A Review of State-of-the-Art Testing Procedures", Proc. Geosynthetics'91 conference, Atlanta, GA, pp 87-100.
- Terzaghi, K. (1960), "Discussion on Settlement of Salt Springs and Lower Bear River Concrete Face Dams", Transactions of ASCE, vol 125, part II, pp 139-148.
- Trollope, D.H. and Chan, C.K. (1960), "Soil Structure and the Step-Strain Phenomenon", Jou. Soil Mech. Found. Eng., ASCE, vol 86, no 2, pp 1-39, Apr.
- Uchida, I., Matsumoto, R. and Onitsuka, K. (1968), "Shear Characteristics of Compacted Partially Saturated Soils", Soils and Foundations, JSSMFE, vol 8, no 3, pp 32-45.

- USBR (1960), "Laboratory Tests on Proposed Embankment Materials - Spring Creek Debris Dam", Earth Laboratory Report EM-590, Division of Engineering Laboratories, US Bureau of Reclamation, Denver, CO, Aug.
- USBR (1965), "Trinity River Diversion Features of the Central Valley Project: Technical Record of Design and Construction", vol I & II, US Bureau of Reclamation, Denver, CO.
- USBR (1987), "Laboratory Results - Soil Samples from Proposed Borrow Areas - Buckhorn Dam, Central Valley Project, CA", memorandum to Chief, Embankment Dams Branch, US Bureau of Reclamation, Denver, CO, April 7.
- USBR (1988), "Petrographic Identification and Freeze Thaw Test of Rip-Rap - Buckhorn Dam, Central Valley Project, CA", memorandum to Head, Concrete Division, US Bureau of Reclamation, Denver, CO, March 30.
- Vesic, A.B. (1963), "Bearing Capacity of Deep Foundations in Sand", Highway Research Record, no 39, National Research Council, Washington, D.C.
- Vesic, A.S. and Barksdale, R.D. (1963), Discussion of Test Methods and New Equipment, Symposium on Laboratory Shear Testing of Soils, ASTM STP 361, pp 301-305.
- Vesic, A.S. and Clough, G.W. (1968), "Behavior of Granular Materials under High Stress", Jou. Soil Mech. Found. Eng., ASCE, vol 94, no 3, pp 661-688.
- Wahrhaftig, C. (1965), "Stepped Topography of the Southern Sierra Nevada, California", Bull. Geol. Soc. Amer., vol 76, pp 1165-1190, Oct.
- Wu, G.Y. (1977), "Cyclic Strength of New Lake Arrowhead Dam, Decomposed Granite Soil", M.S. Thesis, Univ. of Calif., Los Angeles, CA.
- Yatsu, E. (1988), "The Nature of Weathering: An Introduction", Sozoshia, Tokyo.
- Yoshitake, S. and Onitsuka, K. (1990), "Factors Influencing Strength Parameters' Behavior of Decomposed Granite Soil", in Residual Soils in Japan, Research Committee on Physical and Mechanical Properties of Residual Soil Ground, JSSMFE, pp 105-110.
- Zaruba, Q. and Mencl, V. (1976), "Engineering Geology", Elsevier Scientific Publishing Co, New York, NY.

APPENDIX A

SUMMARY OF LABORATORY TEST RESULTS

Table A.1 Oedometer specimen data and post-test breakage results (initial and final percentage passing and IC value)

a) Relative Compaction - 90%

Sieve Open (mm)	Initial gradation	Specimen label									
		C101a	C102a	C102b	C102c	C103a	C104a	C105a	C201a	C202a	C203a
12.700	100.0	100.0	100.0	100.0	100.0	100.0	100.0	100.0	100.0	100.0	100.0
4.760	96.4	98.4	97.6	97.8	98.2	97.7	98.5	97.8	96.9	97.5	97.5
2.380	79.2	87.0	86.4	85.6	85.0	87.0	86.9	84.4	84.7	84.2	84.5
1.190	54.5	63.5	62.9	60.6	59.8	63.4	62.7	59.8	60.7	59.9	59.5
0.590	35.9	43.8	42.9	41.1	40.2	43.6	44.0	40.8	41.0	40.7	39.8
0.297	23.0	30.1	29.2	28.0	26.5	29.1	29.7	27.3	27.4	27.4	26.9
0.149	14.9	20.4	19.7	19.0	17.5	19.6	20.1	18.2	18.4	18.5	18.3
0.074	10.2	14.8	13.2	14.0	12.1	13.6	13.6	12.7	12.9	12.9	13.0
IC =		23.7	19.6	17.5	17.0	21.1	23.4	15.4	13.5	14.3	14.1
Density(kN/cu.m.) =		18.5	18.3	18.2	18.2	18.2	18.2	18.3	18.2	18.2	18.1
Wc - initial (%) =		7.6	8.6	8.0	7.9	7.8	8.1	7.9	7.8	8.0	8.5
Wc - final (%) =		12.7	12.0	13.2	13.0	12.1	9.5	12.5	12.5	12.7	12.3

b) Relative Compaction - 95%

Sieve Open (mm)	Initial gradation	Specimen label						
		C151a	C153b	C154a	C155a	C251a	C252a	C253a
12.700	100.0	100.0	100.0	100.0	100.0	100.0	100.0	100.0
4.760	93.4	98.3	97.5	98.5	97.6	97.7	98.1	98.2
2.380	71.0	85.7	84.9	87.0	84.7	85.2	84.8	85.5
1.190	45.4	62.0	60.7	64.3	59.3	61.2	60.1	61.5
0.590	28.5	42.7	41.6	45.5	41.1	42.3	40.9	42.8
0.297	17.2	29.4	28.1	31.0	27.9	28.6	28.1	29.5
0.149	10.3	20.1	18.9	21.1	19.0	19.3	19.2	20.4
0.074	6.4	14.1	13.1	14.8	13.5	13.5	13.7	15.5
IC =		37.5	33.8	41.0	33.1	35.0	34.8	37.0
Density(kN/cu.m.) =		19.3	19.2	19.2	19.1	19.2	19.1	19.3
Wc - initial (%) =		7.9	7.9	8.2	8.0	7.9	8.1	7.6
Wc - final (%) =		9.7	9.3	8.5	10.9	10.8	9.7	9.8

Table A.2 Triaxial specimen data (initial and post-consolidation)

Specimen #	Initial		Water content		Compaction density (kN/cm.m.)	Post consolidation	
	Height (cm)	Diameter (cm)	Initial (%)	Final (%)		Height (cm)	Diameter (cm)
T101a	15.02	7.16	7.93	17.34	114.96	15.02	7.16
T102b	15.06	7.17	8.03	16.73	114.88	14.91	7.18
T103a	15.00	7.15	8.24	16.19	115.93	14.98	7.11
T104a	15.03	7.17	8.04	16.88	114.48	14.81	7.17
T105a	15.04	7.18	8.15	14.90	114.67	14.57	7.22
T105b	15.03	7.17	8.00	-	115.54	-	-
T105c	15.03	7.14	8.30	14.14	115.90	14.98	7.07
T105d	15.08	7.13	7.47	14.40	116.52	14.97	7.06
T106a	14.87	7.15	7.73	13.11	117.06	14.80	7.07
T106b	15.02	7.16	7.57	13.67	116.22	14.94	7.08
T107a	15.01	7.16	7.36	13.02	116.35	14.88	7.05
T108b	15.03	7.16	8.06	15.02	115.05	14.92	7.02
T151a	15.01	7.16	8.23	16.61	121.25	14.99	7.16
T152a	15.08	7.18	8.11	15.89	120.93	14.96	7.17
T153a	15.01	7.15	8.56	16.38	121.89	14.99	7.13
T154a	15.15	7.18	7.89	14.20	120.59	15.12	7.15
T155a	15.33	7.19	7.04	13.84	119.63	15.29	7.15
T155b	15.18	7.16	7.87	14.19	120.66	15.10	7.11
T155c	14.93	7.17	7.11	13.41	123.60	14.88	7.13
T156b	15.01	7.17	7.74	12.66	121.86	14.97	7.17
T157a	15.02	7.15	7.52	12.84	122.38	14.96	7.08
T158a	15.04	7.14	8.40	12.37	122.63	14.96	7.06
T159a	15.03	7.14	7.44	13.75	123.20	14.99	7.09
T251a	15.01	7.15	7.83	12.43	122.77	14.98	7.08
T252a	14.99	7.14	8.29	12.52	122.48	14.95	7.08
T253a	15.03	7.16	7.38	13.18	122.74	14.99	7.10
T351a	15.01	7.14	7.72	-	123.35	14.86	7.10
T352a	15.02	7.15	7.56	13.58	-	14.79	7.13

Table A.3 Summary of triaxial test results (shear strength and volume change)

Specimen #	Max. csl. ppl stress (kPa)	Vol. strain in consol. (%)	Mean fail. ppl stress (kPa)	Friction angle (deg)	Vol. strain in shear (%)	Rate of vol. chang.	Remarks
T101a	100	0.16	255.00	44.40	-0.30	-0.46	
T102b	200	0.50	451.00	40.80	0.21	-0.12	
T103a	300	0.93	659.00	40.00	1.17	-0.09	
T104a	400	1.28	812.00	37.40	2.42	0.00	
T105a	600	1.73	1232.00	37.80	2.31	0.00	
T105b	600	-	-	-	-	-	
T105c	600	2.29	1282.00	39.10	2.79	0.00	
T105d	600	2.58	1286.00	39.20	3.37	0.00	
T106a	900	2.31	1842.00	37.70	3.69	0.00	
T106b	900	2.56	1851.00	37.80	4.42	0.00	
T107a	1200	3.61	2476.00	37.90	4.85	0.00	
T108b	1500	4.45	2955.00	36.30	5.60	0.00	
T151a	100	0.13	317.00	49.90	-0.83	-0.86	
T152a	200	0.44	534.00	45.60	-0.51	-0.50	
T153a	300	0.68	737.00	43.30	-0.39	-0.39	
T154a	400	0.82	927.00	41.60	-0.07	-0.18	
T155a	600	1.15	1290.00	39.30	1.10	-0.05	
T155b	600	1.72	-	-	-	-	
T155c	600	1.31	1358.00	40.90	0.17	-0.19	
T156b	900	1.70	1887.00	38.50	1.80	-0.05	
T157a	1200	2.18	2516.00	38.50	2.34	-0.03	
T158a	1500	2.49	3070.00	37.70	3.23	0.00	
T159a	900	1.67					Csl only
T251a	1000	1.83					ended before peak
T252a	900	1.72	1908.00	38.80	1.85	-0.06	
T253a	900	1.57	1905.00	38.80	1.80	-0.05	
T351a	1620	1.75	1929.00	39.20	1.28	-0.07	Kc=1.8
T352a	2250	1.94	1935.00	39.30	0.98	-0.06	Kc=2.5
T353a	1620	2.20					Kc=1.8, Csl only
T354a	2250	2.29					Kc=2.5, Csl only
T354b	2250	2.13					Kc=2.5, Csl only

Max. csl ppl stress - Maximum consolidation principal stress

Vol strain in consol - Volumetric strain in consolidation alone (compression +ve)

Mean fail. ppl stress - Mean principal stress at failure

Friction angle - angle of shear resistance at failure

Vol strain in shear - Volumetric strain in shear alone at failure (compression +ve)

Rate of vol chang. - Rate of volume change at failure (compression +ve)

Table A.4 Summary of triaxial post-test breakage results (initial and final percentage passing and IC value)

a) Relative Compaction - 90%

Sieve Open (mm)	Initial gradation	Specimen label														
		T101a	T102a	T102b	T103a	T104a	T105a	T105b	T105c	T105d	T106a	T106b	T107a	T108b		
12.700	100.0	100.0	100.0	100.0	100.0	100.0	100.0	100.0	100.0	100.0	100.0	100.0	100.0	100.0	100.0	100.0
4.760	93.4	96.4	97.5	97.4	97.1	97.5	97.5	96.9	97.4	98.3	97.6	97.7	98.3	97.9	98.3	97.9
2.380	71.0	82.6	82.6	79.0	81.7	83.7	80.2	80.8	84.9	81.9	83.4	84.1	83.4	83.4	84.1	83.4
1.190	45.4	53.6	58.7	58.9	54.8	57.5	61.3	55.0	57.2	63.1	58.8	60.3	61.6	62.1	62.1	62.1
0.590	28.5	35.5	39.8	39.5	37.1	39.0	42.8	36.8	40.3	44.4	41.7	42.6	43.8	44.3	44.3	44.3
0.297	17.2	23.2	26.2	25.8	24.2	25.9	28.6	23.1	27.3	29.7	28.2	28.2	29.6	30.1	30.1	30.1
0.149	10.3	14.8	16.6	16.1	15.2	16.3	18.0	14.3	18.2	18.8	18.3	18.4	19.1	19.2	19.1	19.2
0.074	6.4	9.0	10.2	9.7	9.7	9.9	10.9	8.8	12.5	12.3	12.7	12	12.3	12.4	12	12.4
IC =		20.6	30.1	29.7	23.3	28.5	33.2	23.7	28.0	37.5	30.6	32.9	36.1	34.9	36.1	34.9

a) Relative Compaction - 95%

Sieve Open (mm)	Initial gradation	Specimen label																		
		T151a	T152a	T153a	T154a	T155a	T155b	T155c	T156b	T157a	T158a	T159a	T251a	T252a	T253a	T351a	T352a	T353a	T354a	T354b
12.700	100.0	100.0	100.0	100.0	100.0	100.0	100.0	100.0	100.0	100.0	100.0	100.0	100.0	100.0	100.0	100.0	100.0	100.0	100.0	100.0
4.760	93.4	97.7	97.4	97.8	98.3	97.8	97.8	98.4	98.2	97.3	97.7	96	97.5	97.4	98.3	97.7	97.8	97.7	97.2	97.6
2.380	71.0	83.1	81.7	80.9	82.9	82.8	82.8	83.8	84.0	82.5	83.3	79.2	80.2	81.7	85.2	81.6	82.3	80.5	81.5	79.3
1.190	45.4	59.9	57.8	56.5	59.8	62.5	60.2	60.4	61.3	60.9	60.9	55.2	55.6	58.0	62.9	58.8	58.5	56.3	57.6	53.6
0.590	28.5	41.0	39.7	39.3	41.1	44.1	42.0	41.8	43.8	43.4	43.9	37.2	37.8	40.6	44.2	41.0	41.2	38.1	39.5	36
0.297	17.2	27.2	26.4	26.0	27.6	30.0	27.7	27.7	29.7	29.7	29.9	24.3	24.8	27.3	29.7	27.7	27.6	25	26.2	23.5
0.149	10.3	17.2	16.9	16.8	17.4	19.4	17.3	17.7	18.9	19.5	19.5	15.5	15.7	17.9	19.3	17.9	18	15.9	16.7	15.2
0.074	6.4	10.5	10.3	11.2	10.4	12.4	11.0	11.5	12.1	13.1	12.7	10.1	10.1	12.1	12.8	11.6	12	10.6	11.1	10.5
IC =		31.9	28.7	28.3	32.0	37.6	32.3	34.8	35.6	31.8	33.7	21.0	26.0	29.2	37.7	30.3	31.1	27.2	27.8	24.0

Table A.5 Summary of direct shear and pullout test results (shear strength)

a) Direct shear test results

Soil - Soil				Soil - Grid			
Sp. #	σ_N kPa	ϕ (deg)		Sp. #	σ_N kPa	ϕ (deg)	
		Peak	Residual			Peak	Residual
D101b	68	45.8	40.7	D201c	100	39.4	36.9
D101a	137	44.1	38.7	D202a	248	40.0	38.0
D102b	270	41.3	38.7	D203a	469	38.7	38.3
D103b	410	40.0	39.3				
D103a	479	39.0	39.0				

b) Pullout test results

Specimen #	Normal Pressure σ_N (kPa)	Pullout Force P (kN/m)	Coefficient of interaction (C_i)
P201a	70	55.3	1.41
P202a	200	116.8	1.04
P203b	400	189.0	0.82
P204a	700	240.0	0.62

Note:

1. $C_i = P / (2 L \sigma_N \tan\phi_r)$; where L = embedded length of the geogrid
2. C_i values were calculated using the average soil residual friction angle of 39 degrees.

Table A.6 Summary of direct shear and pullout post-test breakage results (initial and final percentage passing and IC value)

a) Direct shear tests of soil alone

Sieve Open (mm)	Initial gradation	Specimen label					
		D101a	D101b	D102a	D102b	D103a	D103b
12.700	100.0	100.0	100.0	100.0	100.0	100.0	100.0
4.760	97.6	98.5	98.2	97.8	99.0	98.2	98.0
2.380	80.6	85.3	85.7	83.1	88.5	84.0	83.8
1.190	53.1	61.2	59.7	58.8	64.6	58.5	57.7
0.590	32.4	40.5	38.9	39.0	43.5	37.4	37.7
0.297	18.7	25.9	24.5	25.1	28.0	23.5	24.3
0.149	10.4	15.5	14.5	15.7	17.4	13.9	14.4
0.074	5.8	9.9	9.2	9.9	10.7	8.6	9.1
IC =		16.7	14.6	10.0	25.2	11.3	10.3

b) Direct shear interface strength tests

Sieve Open (mm)	Initial gradation	Specimen label				
		D201a	D201b	D201c	D202a	D203a
12.700	100.0	100.0	100.0	100.0	100.0	100.0
4.760	97.6	98.1	97.9	98.3	97.6	98.0
2.380	80.6	82.1	82.8	83.4	80.1	81.8
1.190	53.1	57.8	56.7	58.2	54.5	56.5
0.590	32.4	37.8	35.6	37.9	35.3	36.8
0.297	18.7	23.9	22.3	24.0	22.6	23.3
0.149	10.4	14.3	13.3	14.5	13.7	13.9
0.074	5.8	9.0	8.7	9.4	9.3	8.8
IC =		8.7	7.3	11.1	2.0	6.9

c) Pullout tests

Sieve Open (mm)	Initial gradation	Specimen label							
		P102a	P103a	P201a	P202a	P203b	P204a	P301a	P401a
12.700	100.0	100.0	100.0	100.0	100.0	100.0	100.0	100.0	100
4.760	97.6	97.5	97.9	98.3	98.0	98.4	98.4	98.3	98.1
2.380	80.5	82.8	83.2	83.7	83.1	84.9	85.1	83.6	82.2
1.190	52.9	57.5	57.6	56.9	57.2	58.7	59.2	57.1	56.1
0.590	32.1	37.3	37.3	36.5	37.5	38.4	38.4	36.6	36.3
0.297	18.4	23.5	23.4	22.9	24.1	24.4	24.3	22.8	23.2
0.149	10.0	13.9	13.9	13.4	14.7	14.7	14.2	13.2	13.9
0.074	5.4	8.7	8.7	8.6	9.3	8.6	8.9	8.3	9.4
IC =		7.5	9.3	10.4	9.5	13.9	14.4	10.4	7.7

